Case Studies in the Absorption of Low Frequency Sound in Music Rooms

Douglas John Shearer

Student ID: 3229091

A thesis submitted in partial fulfilment of the requirements of London South Bank University for the degree of Doctor of Philosophy

July 18th 2021

First Supervisor: Professor Stephen Dance, London South Bank University
Second Supervisor: Dr Luis Gomez Agustina, London South Bank University
Third Supervisor: Justin Randell, London South Bank University

Abstract

Room design for music is a special and highly valued skill. The spectrum, timbre and dynamics of music, coupled with our keen sense for musical sounds make these rooms a particular challenge for the acoustician. The goal is to create an acoustic environment whereby the sound field within the space supports the instruments and enhances their tone, with unfavourable colourations and effects minimised. Room dimensions, construction materials and specialised treatments must be chosen carefully to achieve the perfect musical balance for the performance.

Architectural Acoustics is the field which brings together art and science to address the challenge of creating an environment suitable for music. The most challenging aspect is to achieve the required spectral balance, particularly at low frequency. This thesis presents a literature review of current knowledge of architectural acoustics for music and traditional acoustics treatments. This is followed by three case studies which each investigate a novel solution to improve the acoustic environment for musicians.

The first case study investigated room boundaries as potential absorbers. The study arose at a music college who wanted an evaluation of a beautiful new recital hall. Professional musicians had expressed concern about the unusual acoustic in the hall. A room acoustic assessment is described, and results analysed and compared to standards and guidance. Multiple studies including modal analysis, physical experiments and wave-based computer simulation were undertaken to investigate the mechanism for the low frequency dip in the room response. It was determined that the false walls in the hall were acting as quarter wavelength resonators but for multiple low frequencies thus creating an effective absorber. This absorber design could be repurposed to reduce the boom commonly found in modern music venues.

The second case study explored pneumatic absorbers. This investigation arose when a London orchestral rehearsal space wanted an inexpensive, quick to deploy, flexible acoustic which would reduce the low frequency boom in the space thereby balancing the room response. A variety of airbeds were selected for the study and tested in the laboratory with different levels of inflation. Finally, the position and number of the airbeds was investigated for optimisation purposes. The airbeds were installed in Henry Wood Hall and the room response measured. It was found the room response was flattened thus improving the acoustic quality. Conductors from world leading orchestras responded positively to the new condition of the hall.

The third case study focused on the Targeted Energy Transfer method as a means of creating a novel low frequency absorber. This approach transferred knowledge from the field of vibration control to architectural acoustics. A test rig was built to measure the vibrational damping in two types of hyperelastic latex materials using a laser vibrometer. A small low frequency non-linear response was found but there was not enough evidence to pursue the research further.

Acknowledgements

I would like to express my appreciation for the support and happy collaboration with the Royal Academy of Music.

I would like to thank my lead supervisor Professor Stephen Dance for the direction, support and coffee that helped me through countless hours of data collation. I would also like to thank supervisors: Dr Luis Gomez Agustina and Mr Justin Randell for your advice and input. Also, the technical staff at LSBU, Richard White, Paul Elsdon, Chris Grey, Joe Cheney, Nick Duggan, John and Andy in the workshop.

My gratitude goes to my fellow acoustics researchers; Eric Ballestero, without whose quick humour and enthusiasm this thesis would certainly never have been finished; MSc student Paula Menin who helped enormously with field measurements; Rodrigo Sanchez Pizani; Suzana Zekic, and LSBU colleagues Mubarak Elnour, Di Wang and Dr Wahid Oseni. I'd like to express my sincere appreciation to Dr Brian Hamilton of the University of Edinburgh for his computer simulations. Others too numerous to mention; Thank you.

Sanity during the PhD journey has more or less been maintained, mostly through the mediums of music and cricket, so thanks must go to my colleagues in Scow, The West Midlands and Paddington Rabbits CC; as well as to the FFJU quiz team (especially the much-missed John Sparrowhawk).

Special thanks to old friends and confidants Andrea Kerr, Jared Hawkes and Helen Jahn.

Finally, very special thanks to my parents Ima and Douglas Shearer for supporting and encouraging me in so many ways, for making me curious and showing me the value in education.

Declaration

This thesis is submitted to London South Bank University in support of my application for the degree of Doctor of Philosophy.

I, Douglas John Shearer, declare that the work, research and results presented within this thesis are my own having been generated by myself as a result of my own original investigation and research and has not been submitted in any previous application for any degree at any institution.

Douglas John Shearer
18th July 2021

Papers by the author

Journal Papers

D Shearer, S Dance, L Gomez Agustina, Justin Randell, *'Flexible control of acoustic conditions in a music rehearsal space using airbeds'* Applied Acoustics 173, 2021

Conference Papers

S. Dance, D. Shearer, *Measurement of absorption coefficients to ISO354 using tall sources and microphones*, Proc. InterNoise 2020, Seoul

S. Dance, G. Zepidou, D. Shearer, *Face the music: A 12-year study of the sound of performance and hearing of classical music students*, Proc. International Congress on Acoustics 2019, Aachen

D. Shearer, L. Gomez Agustina, E. Ballestero, S. Dance. *Henry Wood Hall – The creation of a flexible acoustic using airbeds*, Proc. Inter-Noise 2019, Madrid

E. Ballestero, S. Dance, D. Shearer, H. Aygun, *Acoustic conditions in orchestra pits: Can metadiffusers be a potential solution?* Proc. IoA, 2018

D. Shearer, S. Dance, L. Gomez Agustina, J. Randell, *Towards a novel acoustic absorber using a magnetically induced geometric nonlinearity in an elastic membrane*, Proc. Euronoise 2018, Crete

S. Dance, D Shearer, *Facing the music: A before and after study of the hearing acuity of classical music students*, Proc. International congress on Sound and Vibration, 24, July 2017, London

D. Shearer, S. Dance, *Measuring absorption below 100Hz with a particle velocity-pressure sensor*, Proc. Inter-Noise 2016, Hamburg.

Symbols Used

A	Equivalent absorption area (m^2)
c, c_0	Speed of sound, in air (ms^{-1})
C	Number of decay curves evaluated
d	Cavity depth (m)
EDT	Early Decay Time (s)
f	Frequency (Hz)
H	Total energy (J)
h	Panel thickness (m)
k	Wavenumber ($cyc.m^{-1}$)
L	Mean free path (m), Length (m), Cavity depth (m)
m	Mass (kg), Air intensity attenuation coefficient (m^{-1})
N	Number of modes
N_R	Number of reflections
p	Pressure (Pa)
R	Reflection factor
RT	Reverberation time (s)
S	Surface Area (m^2)
t	Boundary layer thickness (m)
V	Room volume (m^3)
V	Potential energy (J)
v, v_0	Kinematic viscosity, of air (m^2s^{-1})
Z	Wall impedance ($N\ sm^{-1}$)
α	Absorption coefficient
δ	End correction (m)
γ	Adiabatic constant
ζ	Specific Impedance ($Pa.sm^{-1}$)
η	Dynamic viscosity (Pl)
θ	Angle of incidence (°)
λ	Wavelength (m)
ρ, ρ_0	Density, of air (kgm^{-3})
φ	Phase angle (rads)
ω	Angular frequency ($rads.s^{-1}$)

Table of Figures

Table of Figures

Table of Contents

1 Introduction

Humans are uniquely attuned to the sound of instruments and voices in a music context. Most music draws upon a documented culture which has developed over one thousand years. Music is built upon adherence to, and deviation from, this familiarity and expectation. Timbre comes from the instrument, but unless sounded in an anechoic chamber, the space in which the instrument is played contributes too, through the action and interaction of sound reflected around the room. Timbre is an ephemeral term; Donnadieu [1] defines it as the perceptual attribute by which the listener can distinguish instruments even if they play the same note with the same dynamics, and that it conveys the identity of the sound source.

In the context of "Western" acoustic classical music, there is a clear cultural and experiential expectation of the timbre of orchestral instruments. Therefore, shortcomings in instrumental timbre presented in music rooms will be noticed, not just by the musician, sound engineer or connoisseur, but by everyone, whether consciously or not. One of the main challenges at the start of a project is to establish whether the acoustic issues are clearly defined and understood – this is an especial challenge as not everyone has the language to describe or diagnose what is "wrong". Luckily, acoustic performance in music rooms is a key attribute so designers working in this field have an understanding of the context of their use. This is not always the case with architects, surveyors etc who may not understand the acoustic implications of design compromises; remedial works are always more expensive than dealing with the issue during the initial build.
This thesis will confine itself to measurable quantities in room acoustics, on the understanding that a perceptually even tonal presentation best suits acoustic music.

Within this context, low frequencies are a special case with disproportionate weight in music perception, due to the ear: our reduced sensitivity to them, and to masking effects over higher frequency sounds; due to the response of many

rooms at low frequencies; due to the necessity for larger size (and hence more expensive) building elements designed for control of low frequencies.

The rationale of this thesis is to add to the study of music spaces at low frequencies. Despite much attention, this remains a common problem area, one with no affordable, easily designed and deployed, flexible control solutions.

1.1 Aim

There were several specific research aims of the project

- Work empirically in the context of room acoustics.
- Review the existing room acoustics literature pertinent to the scope of the thesis. In this is included:
    - A brief overview of room acoustics and common acoustic control measures, and the standards and guidance documents to which the acoustic designer must refer.
    - An overview of pneumatic structures, including the small amount of acoustics research in this field.
    - An overview of quarter wave resonators, and their previous uses.
- Present two case studies of classical music spaces.
- Evaluate these music spaces using standard measurement methodology, with reference to the latest and most comprehensive standards for music rooms.
- Identify new and novel absorption and control measures.
- Assess their strengths and weaknesses
- Evaluating their wider suitability, both in the context of music rooms and beyond.
- Evaluate Targeted Energy Transfer (TET), a novel loss mechanism for use in the context of architectural acoustics, including a brief review of background literature in TET.

1.2 The Thesis

The acoustic designer has a number of tools at their disposal when designing for good sound. Most of these are not new; they were available, in some cases in less refined form at least, to the designer of almost one hundred years ago. This thesis presents three case studies relating to this problem, focused on low frequencies. It is structured as follows.

Chapter 2 is a wide-ranging literature review covering the established theories of sound in rooms, both that of reverberation (2.2) and the modal approach (2.3). Section 2.4 concerns sound absorption and its measurement, covering the strengths and shortcomings of the various methods; firstly, the standardised methods of reverberation room, and of impedance tubes; then discussing lesser used methods such as free field and intensity methods, and discussing why low frequencies present an especially difficult challenge for measuring absorption. Section 2.5 discusses the design of music rooms and the special problems which can be encountered. It reviews guidance documents and standards pertinent to music room design, whether performance, rehearsal, recording or critical listening spaces.

Classical acoustic control approaches are discussed in section 2.6, comprising porous absorbent panels, resonant absorbers (resonators and plates) and active control techniques (although these will be discussed only briefly in this thesis). Section 2.7 covers further acoustic control measures which will be pertinent later in the thesis, but which are nonetheless strictly classical in nature, while Section 2.8 looks at nonlinear behaviour and at Targeted Energy Transfer, a more recent loss mechanism which will be explored in Chapter 5.
A summary of finds and gaps in knowledge is included in 2.9.

Chapter 3 is a case study of a music recital room which had been recently completed. The room was assessed for suitability for purpose using standardised measurement procedures. Several aspects of room design for this purpose are discussed in the context of their ability to negatively impact the tonal balance of

music. One unusual resonant structure is considered in more detail and remedial actions which could be taken are discussed.

Chapter 4 considers a classical rehearsal space which required a low frequency lightweight absorption solution to tame a “boomy” response. An easily sourced modular treatment with a low footprint was created. Its effect was tested in laboratory conditions and in situ.

Chapter 5 reports on tentative experiments with a nonlinear membrane and attempts to observe and assess the Targeted Energy Transfer (TET) mechanism in the architectural acoustics context. These first steps were not followed to completion but are presented here in the name of completeness. This work is presented in Chapter 5.

Chapters 6 and 7 summarise and discuss the results of the previous chapters. References are listed in Chapter 8, and there are some extra graphical results in the appendix, Chapter 9.

2 Literature Review

This chapter looks at the historical background to Architectural Acoustics, focussing on music rooms and low frequency problems found in that context. The review starts with the fertile period triggered by Sabine's work on reverberation time, the key move into applied science that founded Architectural Acoustics as a subject, then considers the special case of low frequencies in rooms. The following sections discuss the absorbing effects of different materials and constructions, and this is followed by discussion of how the acoustic designer brings all these elements together, with reference to guidance documents and standards, to formulate a design goal and, deploying appropriate classical control measures, achieve suitable spaces for music.

2.1 Low Frequencies in Rooms for Music

Rooms designed for music are a special and valued case in Architectural Acoustics. The spectrum, timbre and dynamics of music, coupled with our keen sense for musical sounds makes these rooms a special challenge for the acoustician. The acoustician's goal is to create an acoustic environment whereby the sound field within the space supports the instruments and enhances their tone, with unfavourable colourations and effects minimised. Room dimensions, construction materials and specialised treatments must be chosen carefully to achieve a suitable acoustic for practice, rehearsal and performance.

The sound field within a music space can be thought of as a combination of direct sound, together with early and late reflections. The direct sound travels from the instruments (sources) to the listener or microphone (receiver) in a straight line. Sound also propagates in other directions and this sound will eventually reach the room envelope or fittings and some proportion of this energy will be reflected by these surfaces, depending on the material's properties. Some of this reflected energy will also eventually reach the receiver, whether by simple or complex routes, having undergone many or few reflections, but always at some time after the direct sound, having travelled further. These many reflections build up to

form a reverberant field which modifies the timbre of instruments either for good or ill.

In all but very large spaces such as auditoria, low frequencies present a special case due to modal effects. Room modes are caused by standing waves, whose wavelength is related to the distance between (especially parallel) surfaces in that room. Practically, this results in a greatly uneven frequency response at any given listening position as different modal frequencies reinforce or cancel each other. This reinforcement causes the levels of modal frequencies to vary greatly throughout the space, gaining up to 6dB at room boundaries, while cancellations can cause “dead” spots within the space, where that frequency’s energy can appear near to zero.

In music rooms, the result can be uncertainty for the musician or sound engineer, as certain bass notes will resonate strongly and unmusically, while others, only a few semitones away, might be barely audible due to cancellation. The balance of frequencies also varies spatially in complex ways, confusing things further; thus, critical evaluation of the frequency content of the instrument or recording becomes very difficult. If the space is used for music performance, the audience may not be consciously aware of modality, but the power of the music performed there will be compromised. Controlling these modal frequencies to the benefit of our perception of music is the aim of low frequency acoustic treatments.

2.1.1 Context and Scope

The principles of reflection control are applicable to any low frequency sound, whether modal, as in small rooms, or not, as in large rooms where the lowest modal frequencies are below our auditory range and thus of no concern and the modal density is much higher.

This project has in mind rooms for music with the following scope.
-Practice rooms for classical or amplified music

-Small performance rooms for classical music
-Recording "live" rooms for classical or amplified music

The control methods discussed are also relevant to "dead" spaces; critical listening spaces such as control rooms, mixing and mastering rooms, these being the most demanding case in terms of acoustic performance, and indeed to any space where low frequency sources are present. In spaces for amplified music, however, it must be noted that low frequencies are playing an increasing role in contemporary popular musical styles. Duarte Pestana *et al* give an overview of this trend [2].

2.2 The Sound Field in a Room

2.2.1 Reverberation

Room acoustics is the study of the movement of sound within an enclosure and its interaction with the boundaries of that space. Historically, the classical method for quantifying that interaction is through Wallace Sabine's foundational study [3] of Reverberation Time. Sabine performed a series of experiments in the lecture theatre of the Fogg Art Museum on the campus of Harvard University, changing the amount of absorbent material (using cushions) in the room and measuring, with a stopwatch, the decay time of the room, excited with an organ pipe. From these experiments, he derived an expression linking the time for a sound field to decay by 60dB. This time he called Reverberation Time (RT) or T_{60}.

$$RT = \frac{0.161V}{S\alpha} \qquad \text{Eq 1}$$

where V is volume in m^3, S is the surface area of the room in m^2 and α is the average absorption coefficient of the room surfaces.

If sufficient signal to noise ratio cannot be established, a 20 or 30dB portion of the decay can be taken and extrapolated to represent the 60dB equivalent; giving measures referred to as T_{20} and T_{30} respectively. Measurements are taken from 5dB below the start of the decay. Many rooms have near-linear decays (when

plotted logarithmically) and so give a straight-line decay. In these cases, T_{20}, T_{30} and T_{60} should be the same value.

The dependent variables in the RT calculation are the room's volume (V) and its total equivalent absorption area, that is the equivalent area of a hypothetical perfect absorber. This is dependent on the surface area (S) of the room boundaries and the sound absorbing qualities of those boundaries such that $A = S\alpha$ where $\propto$ is the absorption coefficient, with 1 being perfectly absorbing and 0 being perfectly reflecting.

This relationship was confirmed analytically by Norris [4] and Eyring [5] by considering the *mean free path* (L) of the sound, the average distance it travels between reflections at the boundary, where $L = 4V/S$. Thus, the average number of reflections per second (N) is $N = c_0 S/4V$ where c_0 is the speed of sound in ms^{-1}. With each reflection, the sound is reduced in energy by the factor $(1 - \overline{\alpha_E})$ where $\overline{\alpha_E}$ is the area-averaged energy absorbent coefficient at random incidence. Therefore, the total energy attenuated during one RT is $(1 - \overline{\alpha_E})^{NT}$. This results in the Eyring-Norris Equation, which is preferred when highly absorbent rooms are considered as Sabine's version breaks down when $\propto \rightarrow 1$ as it tends to $0.161V/S$ instead of zero. [6]

$$RT_{EN} = \frac{0.161V}{-Sln(1 - \overline{\alpha_E})} \qquad \text{Eq 2}$$

where α_E represents statistical absorption coefficients, which must be used in the Eyring-Norris equation. Those measured in the reverberation chamber [7] should only be used with the Sabine equation.

However, as noted by Millington [8], and Sette [9], in practice, the Eyring equation can result in too great a coefficient, sometimes exceeding 1, due to the use of a single averaged absorption coefficient for the whole space. The reason being the assumption that after a certain amount of energy is absorbed at a

boundary, the remainder spreads by scattering or by propagation in all directions and is absorbed at the next reflection at all boundaries equally. In practice, even in reverberation rooms, this diffuse assumption does not always hold, and some sounds incident in a directional manner may well be reflected into one boundary alone at the next reflection and be subject to the absorption characteristics of that surface alone. To correct this, in their formula, absorption areas are summed and averaged geometrically rather than arithmetically. This gives the Millington-Sette equation.

$$RT_{MS} = \frac{0.161V}{-\sum S_n ln\,(1-\alpha_n)} \qquad \text{Eq 3}$$

where S_n is the surface area of surface n within the room in m² and α_n is its absorption coefficient.

Dance and Shield [10] provided a conversion chart between Sabine and Millington absorption coefficients. The latter must be used with the Millington-Sette equation for good results and Dance and Shield improved the results of computer geometrical model results by using them instead of Sabine coefficients, which must be limited to the 0-1 range, although they often lie outside it in measured data. Jeong [11] summarised three models based on porous absorbers to convert from Sabine to true random incidence coefficients.

Above, the true path lengths involved in the energy decay are replaced by a mean free path, an averaged value which is strictly only true if each path is exactly equal to it, i.e. in a one-dimensional room. Kutruff instead expressed the path lengths by using a probability function, ultimately re-expressing Eyring's absorption coefficient in terms of the squared variance of the path length, γ^2, giving

$$RT_{Kutt} = \frac{0.161\mathrm{V}}{-\mathrm{S}\alpha''} \text{ where} \qquad \text{Eq 4}$$

$$\alpha'' = -\ln\left(1-\bar{\alpha}\right).\left[1+\frac{\gamma^2}{2}\ln\left(1-\bar{\alpha}\right)\right]$$

when $\gamma^2 > 0,\ \alpha'' < \bar{\alpha}$ and therefore RT is longer than Eyring.

Fitzroy [12] considered rooms where absorption was non-uniformly distributed, such as the case when floor and ceiling are heavily damped while walls remain reflective. His formulation treated sets of opposing boundaries completely separately and then summed their contributions to the whole RT.

$$RT_{Fitz} = \left(\frac{S_x}{S}\right)\left(\frac{0.161V}{-Sln(1-\alpha_x)}\right) + \left(\frac{S_y}{S}\right)\left(\frac{0.161V}{-Sln(1-\alpha_y)}\right) + \left(\frac{S_x}{S}\right)\left(\frac{0.161V}{-Sln(1-\alpha_z)}\right) \quad \text{Eq 5}$$

where $S_{x,y,z}$ is surface area of opposing surfaces in the *x, y* and *z* directions in m^2. and $\alpha_{x,y,z}$ are their corresponding absorption coefficients. Arau-Puchades [13] considered Fitzroy's equation mainly suitable for rooms with an RT around 0.5 and applied geometric averaging instead, and Neubauer [14] applied Kutruff's correction to Fitzroy's formula.

2.2.2 Early Decay Time

Another metric, Early Decay Time (EDT) is also useful. EDT, rather than measuring from 5dB into the decay, measures the first 10dB from the start of the decay, then multiplies by six to facilitate comparison to RT measurements. The metric was defined by Jordan [15] to be an indication of running reverberation, or the perceived sensation of reverberation. In music spaces, the latter part of the decay is only heard at the end of a piece, while in running music, subsequent notes mask it. The metric is widely used and considered as being a better measure of reverberation's influence on how music sounds to listeners than reverberation time, but in practice, they are used side-by-side.

Barron discusses possible effects of the early part of the decay in performance spaces in [16]. He defines three decay types based on the appearance of the decay slope. Firstly the "cliff" type where the initial decay drops quickly; direct sound and early reflections dominate and EDT will be shorter than RT. Secondly, the "plateau" type where direct sound and early reflections have a small effect and EDT will be longer than RT. Thirdly, the "Sagging" type which Barron ascribes to Cremer & Müller [16] where an absorptive floor and vertical walls are described, which allow a two-dimensional reverberation to occur separate from the floor area. Again, in this case, EDT would be shorter than RT. The EDT-RT

ratio can be used as a comparison metric, for example as an indicator of diffuseness. Barron made a comparison of British concert halls using this metric, with most halls having a ratio of between 0.8 and 1. Barron also relates that for perception of running reverberation, some acousticians still favour the earlier Initial Reverberation Time (IRT) metric of Atal *et al* which evaluates the first 15dB of the decay [16].

More recent work on reverberance has sought to relate the measured parameters to a more refined psychoacoustic model. Lee *et al* give a review of recent approaches in [17].

2.2.3 Reflections at a Boundary

The diffuse sound field is influenced by what happens to sound as it encounters the room envelope and fittings, and these interactions are key, especially at low frequencies. As a plane wave is incident upon a plane boundary (which is assumed infinite) at normal incidence, some proportion of the incident energy will be reflected, depending on the material and construction of the boundary. Kutruff [18] quantifies this change in energy and phase due to a reflection using the complex reflection factor.

$$R = |R| exp\,(i\varphi) \qquad \text{Eq 6}$$

where R is the complex reflection factor and φ is the phase angle in radians. The intensity of a plane wave is proportional to the square of pressure, so the intensity of the reflected wave is given by

$$\alpha = 1 - |R|^2 \qquad \text{Eq 7}$$

where α is the *absorption coefficient*. If $R = 0$, the wall is perfectly absorptive and the absorption coefficient is therefore 1, its maximum.

The acoustic properties of boundary materials are generally defined using the ratio of pressure at the boundary face and the particle velocity generated by the incident wave at the material surface.

This is known as the Wall Impedance.

$$Z = \left(\frac{p}{v_n}\right)_{surface} \quad \text{Eq 8}$$

where p is pressure at boundary in Pa, v_n is particle velocity normal to the boundary at the boundary surface in ms^{-1} and Z is wall impedance in $Pa.sm^{-3}$. Like the reflection factor, it is generally a complex quantity and dependent on angle of incidence. It is frequently expressed as *specific acoustic impedance* by ratio with the *characteristic acoustic impedance* of air

$$\zeta = \frac{Z}{\rho_0 c} \quad \text{Eq 9}$$

where ρ_0 is the density of air in kgm^{-3}, c is the speed of sound in air in ms^{-1} and ζ is the specific acoustic impedance of the wall in $Pa.sm^{-1}$.

For normal incidence, the pressure of the incident wave, which comes from the negative x direction is

$$p_i(x,t) = \hat{p}_0 exp\,(i[\omega t - kx]) \quad \text{Eq 10}$$

where p_i is the incident pressure in Pa, $\hat{p}_0$ is the peak magnitude of pressure in Pa, ω is the angular frequency in rads/second and k is wavenumber ($k = \frac{\omega}{c_0}$) in $rads.s^{-1}$.

Its particle velocity is

$$v_i(x,t) = \frac{\hat{p}_0}{\rho_0 c} exp\,(i[\omega t - kx]) \quad \text{Eq 11}$$

where v_i is incident velocity in ms^{-1}

The reflected wave is attenuated and of reversed direction and hence velocity and wavenumber are of opposite sign.

$$p_r(x,t) = R\hat{p}_0 e^{(i[\omega t + kx])} \quad \text{Eq 12}$$

$$v_r(x,t) = -R\frac{\hat{p}_0}{\rho_0 c} e^{(i[\omega t + kx])} \quad \text{Eq 13}$$

Adding these expressions for $x = 0$ gives the total pressure and velocity at the boundary.

$$p(0,t) = \hat{p}_0(1+R)e^{(i\omega t)} \quad \text{Eq 14}$$

$$v(0,t) = \frac{\hat{p}_0}{\rho_0 c}(1-R)e^{(i\omega t)} \quad \text{Eq 15}$$

Therefore, the wall impedance is

$$Z = \rho_0 c \, \frac{1+R}{1-R} \quad \text{Eq 16}$$

and therefore

$$R = \frac{Z-\rho_0 c}{Z+\rho_0 c} = \frac{\zeta - 1}{\zeta + 1} \quad \text{Eq 17}$$

Inserting into Eq 7 gives

$$\alpha = \frac{4Re(\zeta)}{|\zeta|^2 + 2Re(\zeta) + 1} \quad \text{Eq 18}$$

At oblique incidence, a dependence on incident angle is introduced into the previous equations such that x previously is replaced by x' such that

$$x' = xcos\theta + ysin\,\theta \quad \text{Eq 19}$$

Following the same procedure above with this angular dependency gives

$$Z = \frac{\rho_0 c}{cos\theta}\left(\frac{1+R}{1-R}\right) \quad \text{Eq 20}$$

and

$$R = \frac{Zcos\theta - \rho_0 c}{Zcos\theta + \rho_0 c} = \frac{\zeta cos\theta - 1}{\zeta cos\theta + 1} \quad \text{Eq 21}$$

One of three assumptions are made about reflections at boundaries [19].

1. That the absorption occurs at the point of incidence only, so the response of any point on the surface is independent of the rest of the surface. This is known as the locally reactive assumption. It enables the use of the simplification of a specific acoustic impedance with no dependence on incidence angle.

2. Modal reactivity, whereby the response of each point on the surface depends on all other points on the surface. This assumption is applied, for instance to membranes and plates.
3. Extensive reaction, for materials which cause attenuation over a region of internal propagation, where the absorption at a point depends only on neighbouring points within a given area surrounding it, called non-locally reacting absorption.

In addition, a phase change of reflections occurs due to the slower sound speed within the material. This is generally ignored in room acoustic simulations as phase information of reflections is hard to measure in practice, and not often provided for in geometrical acoustics modelling software. Jeong *et al* [20] used a Phased Beam Tracing method to model phase shifts at the boundaries of a medium sized room in simulation. The effect on room acoustic metrics (RT and Early Decay Time (EDT)) was a difference of up to ±5% compared to the 0° phase shifted condition. Level changes due to phase change were most pronounced at lower frequencies. Using binaural impulse responses, a listening test was conducted which showed that such changes were also noticeable perceptually. The authors ultimately suggested that such errors were, in most practical situations, a small source of error, and the zero-phase change assumption was generally justified.

2.3 Rooms in the Low Frequency Range

2.3.1 Room Modes

Statistical analyses of a room such as those of Sabine and Eyring do not provide a complete analysis; the diffuse field assumption does not hold for lower frequencies in small and medium sized rooms [21]. Instead, standing waves at frequencies related to room dimensions dominate. As boundaries are generally poor absorbers at low frequencies, when sound propagates within the room, paths which double back on themselves tend to resonate and the frequencies whose wavelengths are equal in length to these paths interfere constructively or

destructively depending on location, leading to peaks and dips in pressure within the space.

To correctly analyse this behaviour, a wave-based approach is required. The linearised 3d acoustic lossless wave equation is as follows

$$\nabla^2 p = \frac{1}{c^2}\frac{\partial^2 p}{\partial t^2} \qquad \text{Eq 22}$$

where p is pressure in Pa, c is the speed of sound in ms^{-1} and t is time in seconds. The wave equation can be solved for parallelepiped enclosures.

Kinsler [6] takes a room of dimensions L_x by L_y by L_z m, and assumes all boundaries are rigid, then $\hat{n}.\vec{u} = 0$ at all boundaries where $\hat{n}$ is a unit vector and $\vec{u}$ is particle velocity. Also $\hat{n}.\nabla p = 0$ there and thus

$$\left(\frac{\partial p}{\partial x}\right)_{x=0} = \left(\frac{\partial p}{\partial x}\right)_{x=L_x} = 0$$

$$\left(\frac{\partial p}{\partial x}\right)_{y=0} = \left(\frac{\partial p}{\partial x}\right)_{y=L_y} = 0 \qquad \text{Eq 23}$$

$$\left(\frac{\partial p}{\partial x}\right)_{z=0} = \left(\frac{\partial p}{\partial x}\right)_{z=L_z} = 0$$

Since energy cannot escape from the cavity, solutions to the wave equation are standing waves. Substituting

$$\boldsymbol{p}(x, y, z, t) = \boldsymbol{X}(x)\boldsymbol{Y}(y)\boldsymbol{Z}(z)e^{j\omega t} \qquad \text{Eq 24}$$

into the wave equation and separating variables gives

$$\left(\frac{d^2}{dx^2} + k_x^2\right)\boldsymbol{X} = 0$$

$$\left(\frac{d^2}{dy^2} + k_y^2\right)\boldsymbol{Y} = 0 \qquad \text{Eq 25}$$

$$\left(\frac{d^2}{dz^2} + k_z^2\right)\boldsymbol{Z} = 0$$

where constants of separation must be equal

$$\left(\frac{\omega^2}{c^2}\right) = k^2 = k_x^2 + k_y^2 + k_z^2 \qquad \text{Eq 26}$$

The boundary conditions indicate that cosines are the appropriate form for solutions. Therefore:

$$\boldsymbol{p_{lmn}} = \boldsymbol{A}_{lmn}(cosk_{xl}x)\,(cos\,k_{ym}y)\,(cos\,k_{zn}z)\,e^{j\omega t} \qquad \text{Eq 27}$$

where

$$k_{xl} = \frac{l\pi}{L_x} \quad l = 0,1,2\ldots$$

$$k_{ym} = \frac{l\pi}{L_y} \quad l = 0,1,2\ldots \qquad \text{Eq 28}$$

$$k_{zn} = \frac{l\pi}{L_z} \quad l = 0,1,2\ldots$$

Thus, the Eigen-frequencies are given by

$$\omega_{lmn} = c\sqrt{\left(\frac{l\pi}{L_x}\right)^2 + \left(\frac{m\pi}{L_y}\right)^2 + \left(\frac{n\pi}{L_z}\right)^2} \qquad \text{Eq 29}$$

or converting to linear frequency:

$$f_n = \frac{c}{2}\sqrt{\left(\frac{l}{L_x}\right)^2 + \left(\frac{m}{L_y}\right)^2 + \left(\frac{n}{L_z}\right)^2} \qquad \text{Eq 30}$$

There are three types of modal path.

- Axial modes (see Figure 1)with paths between two parallel boundaries along an axis of the room, for example the (n_x, 0, 0) modes. Thus, sound absorption on the other two walls would have little or no effect on this mode. Axial modes dominate in the lower frequency range and are the most troublesome from a sound control point of view as modal density is low in this range. Modal spacing is sufficient that each mode which coincides with a musical note is likely to be surrounded by notes where no such modal reinforcement is present, so musical lines in this range are susceptible to unevenness. This can be unmusical, as it affects balance between instruments. Also, bass instruments tend to mask those of higher frequency so when they play, they have the power to "lift" the whole ensemble. If

this happens in an uneven way, the emotional impact of the whole piece can be negatively affected.

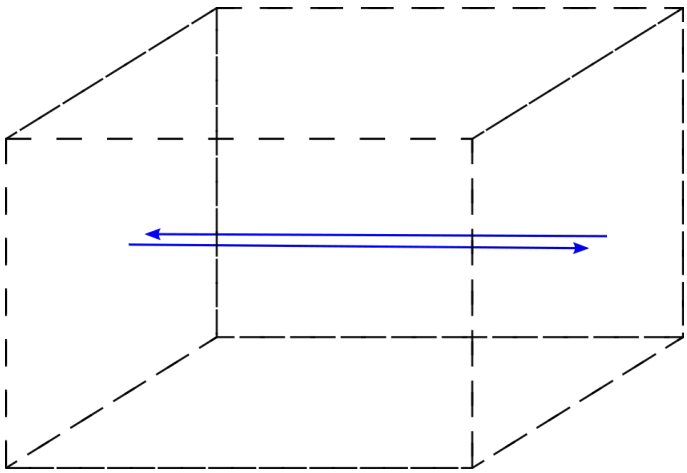

Figure 1: Axial mode shapes involve standing waves between two walls.

- Tangential modes (see Figure 2) have a path travelling parallel to a set of opposite walls around the four other walls. These only have half the sound energy of the axial modes. However, there are of the order n^2 tangential modes compared to n axial modes.

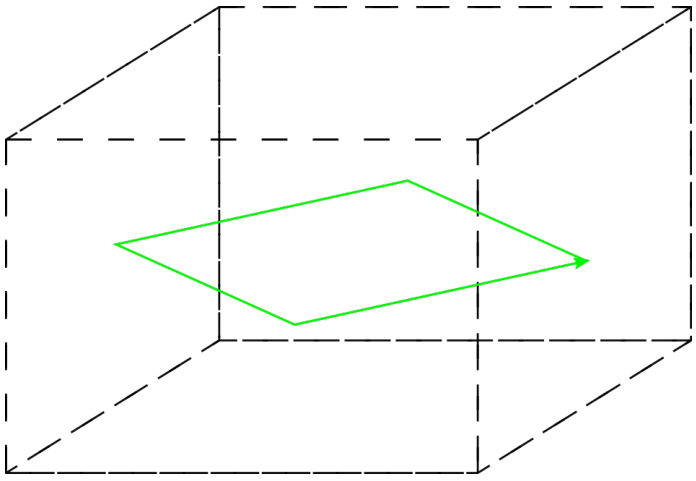

Figure 2: Tangential mode shapes involve standing waves around four walls.

- Oblique modes (see Figure 3) resonate along paths taking in all six room surfaces. These have half the sound energy of the tangential modes. However, there are of the order n^3 oblique modes compared to n, the number of axial modes.

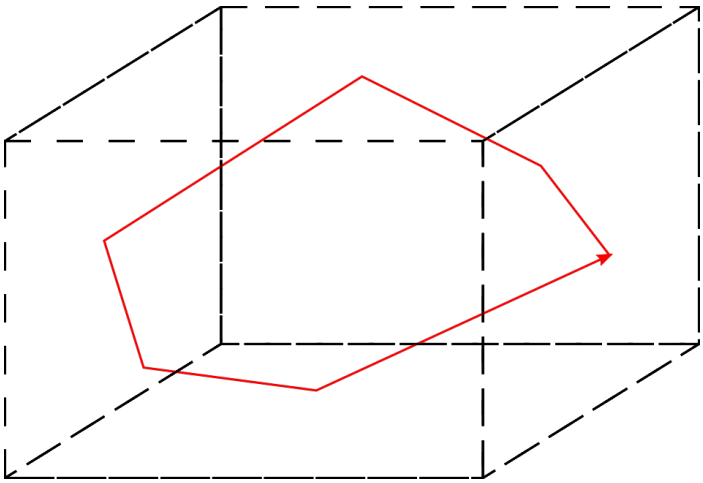

Figure 3: Oblique modes around all six room boundaries.

These latter two mode types dominate as frequency increases

Frequency (Hz)	Wavelength (m)	x	y	z	Type
23	14.97	1	0	0	Axial
27.1	12.71	0	1	0	Axial
35.5	9.7	1	1	0	Tangential
40	8.61	0	0	1	Axial
45.9	7.5	2	0	0	Axial
46.2	7.46	1	0	1	Tangential
48.4	7.12	0	1	1	Tangential
53.3	6.46	2	1	0	Tangential
53.5	6.44	1	1	1	Oblique
54.2	6.35	0	2	0	Axial

Table 1: First ten modes for LSBU Reverberation Chamber (7.5 x 6.35 x 4.3m, volume 202m³) showing order and type of modes.

Frequency (Hz)	Wavelength (m)	x	y	z	Mode
5.6	61.5	1	0	0	Axial
9.1	37.85	0	1	0	Axial
10.6	32.49	1	1	0	Tangential
11.1	31.03	2	0	0	Axial
14.3	24.09	2	1	0	Tangential
16.7	20.62	3	0	0	Axial
17.2	20.02	0	0	1	Axial
18.1	19.03	0	2	0	Axial
18.1	19.03	1	0	1	Tangential
19	18.13	1	2	0	Tangential

Table 2: The first ten modes for Henry Wood Hall [22] (see 4.1) (31 x 19 x 10m, Volume = 6000m³). Modes are lower and modal wavelengths longer due to greater dimensions.

2.3.1.1 The Pressure Chamber Mode

Below the lowest modal frequency, the space acts as a pressure chamber and pressure is evenly distributed throughout the space. Although it is assigned the designation (0,0,0), this is not a true mode, being neither axial or tangential but closest to the family of oblique modes of form (n,n,n). True resonance cannot take place, however it does represent a physical state with a damping constant [23]. In practice, this is of little concern in a normal or music performance room.

2.3.1.2 Modal Density and Energy

Morse and Bolt [24] gave the following expression for the number of modes N from zero to f Hz in a rectangular room

$$N = \frac{4\pi f^3 V}{3c^3} + \frac{\pi f^2 S}{4c^2} + \frac{fL}{8c} \qquad \text{Eq 31}$$

Differentiating this gives the modal density within a given frequency band [19]

$$\frac{dN}{df} = \frac{4\pi f^2 V}{c^3} + \frac{\pi f S}{2c^2} + \frac{L}{8c} \qquad \text{Eq 32}$$

Rindel [23] outlines how the energy of a given mode can be measured by considering a *representative wave* i.e. a propagating wave which is reflected between the surfaces implied by its mode number, with the absorption coefficients of those surfaces the only contributor to its decay. A number of reflections N_R must be considered for a meaningful calculation where

$$N_R = 2\,(l + m + n) \qquad \text{Eq 33}$$

and l, m and n are mode numbers in the x, y and z directions. The total length of propagation of the representative wave experiencing N_R reflections is

$$L_{R,lmn} = 2\sqrt{(L_x l)^2 + (L_y m)^2 + (L_z n)^2} \qquad \text{Eq 34}$$

where $L_{x,y,z}$ are room dimensions in those directions in m, and l, m, n are mode numbers 1,2,3….

The energy of the wave is reduced by one minus the absorption coefficient at each boundary, so the energy after N_R reflections is

$$E_{N_R,lmn} = E_0\left[(1-\alpha_{x1})(1-\alpha_{x2})\right]^l.\left[\left(1-\alpha_{y1}\right)\left(1-\alpha_{y2}\right)\right]^m.\left[(1-\alpha_{z1})(1-\alpha_{z2})\right]^n \qquad \text{Eq 35}$$

where α_{ij} is the absorption coefficient of surface j (of two parallel) facing the i direction. Reverberation time of a mode h is calculated in similar fashion to Eyring's equation, but the total path of N_R reflections is used instead of mean free path and absorption coefficients of particular surfaces are used instead of an average absorption coefficient.

$$T_h = \frac{13.8 l_{N_R,h}}{-cln\left(E_{N,h}/E_0\right)} \qquad \text{Eq 36}$$

Combining the above gives the reverberation time of a particular mode l,m,n

$$T_h = 13.8 \cdot 2\sqrt{(L_x l)^2 + \left(L_y m\right)^2 + (L_z n)^2} \cdot \left[-cln\left(\left[(1-\alpha_{x1})(1-\alpha_{x2})\right]^l.\left[\left(1-\alpha_{y1}\right)\left(1-\alpha_{y2}\right)\right]^m.\left[(1-\alpha_{z1})(1-\alpha_{z2})\right]^n\right)\right]^{-1} \qquad \text{Eq 37}$$

2.3.1.3 The Limit of Modality

The Schroeder frequency is the name given to that frequency above which a sufficient number of modes overlap, and hence no one mode dominates at a given frequency, meaning the use of statistical methods becomes valid. It is defined as that frequency at which modal overlap exceeds three modes within the half power bandwidth of a given resonance. The Schroeder frequency as given by Schroeder's revised paper [25] is given by

$$f_s = 2000\sqrt{\frac{RT_{mid}}{V}} \qquad \text{Eq 38}$$

where V is volume in m^3 and RT_{mid} is the midrange reverberation time in s. Of course, there is a continuum from widely spaced modes through increasing modal density to true diffuse conditions, rather than a cut-off at a single frequency. Schroeder initially used 4000 as the multiplier for the equation, but qualified this as a "conservative" estimate, which he later revised to 2000. There is still discussion about whether his earlier conservatism might be justified or not. This was recently studied by Dance and van Buuren using a new analytical

solution to the wave equation [26] and they found that Schroeder's original German paper [27] (where 4000 was used instead of 2000 as the multiplier of Eq 38) was a more accurate test of the diffuse assumption in assuming 10 modal overlaps rather than the 3 assumed in Eq 38.

2.3.2 Perception of Modality

Humans do not perceive all frequencies equally, Fletcher and Munson, in a series of papers culminating with [28], empirically measured this nonlinearity, which varies with sound level and is presented as a series of equal loudness contours for sound levels from 0 phon (threshold of hearing) to 120 phon (onset of pain response). Measured using pure tones, these equal loudness contours show that in general, humans are less sensitive to sound at low frequencies, especially when the sound level is low. This is important as there must be more sound energy at low frequencies for it to be equally perceived and raises questions about what the correct tonal balance for a room response is (see Chapter 3).

Experience shows that the Schroeder frequency is sufficient to give some guide to the frequency at which a statistical approach is justified for modelling in large rooms, but perceptual studies such as that of Fazenda and Wankling have shown that its real-world efficacy decreases with room size when measured against listeners' preference [29].

Sabine's work was carried out in large, reflective rooms, where modal effects were so low in frequency as to not be a factor. However, in small and medium sized rooms, modal effects can be perceptible and colour music unfavourably.

To measure to what extent this is audible, Olive *et al* [30] introduced spectral dips and peaks of various Q values into pink noise and into pulse trains to measure subjects' thresholds to such coloration using the Up Down Transformed Response Rule (UDTR). In this method, the parameter being tested is moved up or down from the previous value depending on the response of the subject, that is, if they can hear the parameter then it is reduced by a fixed amount

downwards until they can no longer hear it. By iterating this process, a threshold is arrived at. Results of 70.7% thresholds showed that thresholds increased by around 3.2dB per doubling of Q for pink noise, that detection was reduced by 0.5-2dB per octave decrease below 500Hz, except for lower Q which remained constant. For low Q, resonances and anti-resonances were equally discerned, but for medium and high Q, detection of anti-resonances was much reduced. Temporal aspects for perception proved to be important; with pulse train sources, resonances and anti-resonances proved to be equally detectable for a given magnitude and Q, and detection thresholds reduced at higher Q.

Fazenda *et al* [31] followed up this work by testing perceptual thresholds of modes from 32 to 250Hz as a function of modal decay, using both artificial (sine) sources to establish an absolute threshold and music sources to provide an *ecologically valid* situation. In the latter test the colouration of modality was added to the signal derived from an auralisation of an actual room.

The test signals were reproduced over headphones and the test methodology was by Parameter Estimation through Sequential Testing (PEST) modified with an ABX test, a methodology originating from Bell Labs work in the 1950s and still common in audio testing, where two options A and B are presented to the subject, followed by a third, X, which the subject is asked to assign as being either A or B. Over a series of such tests, a given confidence level can be established that the subject can indeed perceive a difference between A and B.

Each run of Fazenda's test comprised a series of responses which converge upon a threshold for the given parameter. Results were plotted on a perceptual map showing that longer modal decays were tolerated for music sources and thresholds of acceptability for music generally increased as frequency decreased until a large increase below 63Hz. Thresholds derived from artificial stimuli represent a worst-case perceptual scenario.

2.4 Measurement of Absorption

There are several standards associated with measurement of sound absorbing materials, generally with absorption coefficients at octave or third-octave bands as an output. Those pertinent to materials used in music rooms are as follows.

2.4.1 Impedance Tube Methods

ISO 10534 deals with impedance tube-based methods for determining normal incidence absorption coefficients, reflection factor and surface impedance.

Part 1: 2001 [32] defines the method of the standing wave ratio of the tube, that is by the evaluation of the standing wave pattern within it, generated by the superposition of incident and reflected waves. Since the absorbing qualities of the test specimen will change the magnitude and phase of the reflected wave, so the location of nodes and antinodes within the tube will change accordingly.

Part 2: 2001 [33] details the transfer function method where two microphone measurements are taken close to the surface of the sample and absorption coefficients and impedances are determined by comparison between the two.

Tube methods are a useful method for basic research but have several limitations; the sample must fit snugly in the tube, and some materials can prove difficult to mount effectively; mounting of some types, such as panel, membrane or Helmholtz-type absorbers can be especially problematic as they are not locally reactive and are scale-dependent. The methods also give only normal-incidence coefficients, which is not representative of behaviour in a real room, where incidence is considered random or "field" incidence, where near oblique incidence is weighted to be of lesser importance.

The lower limit of the frequency range of operation for an impedance tube is limited by its size. To allow two pressure minima to be measured, the distance between sample and loudspeaker should be at least

$$L_{tube} \geq \frac{3\lambda}{4}$$

where L_{tube} is the tube length in m and λ is the wavelength in m. Furthermore, the loudspeaker will also produce higher order non-plane waves which will die out within 3 wavelengths of the source.
To avoid these areas, the following relation defines the required length of the tube [32].

$$L_{tube} \geq \frac{250}{f} + 3d$$

So, for 100Hz, if the diameter is 100mm, the tube must be

$$L_{tube,100Hz} = \frac{250}{100} + 3(0.1) = 2.8m$$

This figure increases to 4.27m at 63Hz, thus a low frequency impedance tube is a large and expensive piece of equipment.

2.4.2 Reverberation Room Tests

ISO354 [7] defines the method for testing absorption coefficients in a reverberation chamber. This common test is still, despite some shortcomings, the benchmark for measuring absorbing materials (and their geometries') behaviour in rooms.

The standard defines appropriate dimensions for the chamber, and for diffusers to be added such that an optimally diffuse sound field is achieved. This optimum condition is achieved by adding a successively greater area of diffusers until the measured absorption coefficient no longer changes with the addition of the most recent diffuser. Walls should be of heavyweight construction and brick and concrete surfaces should be painted to reduce absorption within.

The test comprises measurement of reverberation decay time in the chamber both with and without the presence of the sample using either the interrupted noise or integrated impulse methods. Measurements should be spatially

averaged using at least six receiver positions and two source positions, totalling 12 measurements in one-third octave bands between 100 and 5000Hz.

From these reverberation measurements, the total equivalent sound absorption area is calculated by

$$A_n = \frac{55.3V}{cT_n} - 4Vm_n \qquad \text{Eq 39}$$

where A_n is the total equivalent sound absorption area of the test room under condition n which is either empty or with sample, V is the volume of the room in m^3. T_n is the reverberation time in seconds under condition n. $4Vm_n$ is the correction for air attenuation which is considered negligible at the frequencies of interest here with m measured in $NPam^{-1}$.

The equivalent absorption area of the sample is then calculated as

$$A_T = A_E - A_S \qquad \text{Eq 40}$$

where A_T is the total equivalent absorption area of the sample, A_E is the equivalent area of the empty chamber, and A_S is the equivalent area of the chamber with the sample present, all three measured in m^2.

From this, the absorption coefficient of the test sample is given by

$$\alpha_S = \frac{A_T}{S} \qquad \text{Eq 41}$$

where S is the area covered by the test sample in m^2. This should be at least $10m^2$ in a standard $200m^3$ reverberation chamber.

The relative standard deviation of the T_{20} measurements can be estimated as follows.

$$\frac{\varepsilon_{20}(T)}{T} = \sqrt{\frac{2.42 + 3.59/C}{fT}} \qquad \text{Eq 42}$$

where $\varepsilon_{20}(T)$ is the standard deviation of the reverberation time T_{20}. f is the centre frequency of the one-third octave band, and C is the number of decay curves evaluated.

Results are presented as a table and as a graph, for absorption coefficients for plane absorbers and arrays of objects, and as the equivalent sound absorption area per object for a single object.

2.4.3 Limitations of Reverberation Room Tests

Although ISO354 tests are the most widely used for measuring acoustic performance of materials, since the beginning of their use, there have been problems and inconsistencies with the method [34]. The coefficients produced by this method are referred to as Sabine coefficients as, due to edge effects and the finite size of the sample, coefficients greater than 1 are common, which, by definition, are impossible. However, due to the universal and standardised nature of the test these are used as is without comment.

Sample size and placement of absorbers has a significant effect on absorption performance. As sample size decreases, apparent absorption increases for the same material. Morse and Bolt [24] showed analytically that this was due to diffraction at sample edges. This can be expressed as

$$\alpha_{apparent} = \alpha_0 + \beta E \qquad \text{Eq 43}$$

where α_0 is the true absorption coefficient, β is a constant and E is the ratio of sample perimeter to sample area. Bartel [35] showed that arrangements of a given area of absorbent with a different perimeter (and therefore a different ratio E), results in a difference of measured absorption coefficient of several percent, but not consistently between materials. In addition, he showed a linear relation between E and absorption coefficient, although in this relation, the value β, was different for different materials.

Warnock reviews several mechanisms by which errors can occur in reverberation room tests, including spatial averaging, diffuseness, and notably mounting condition, where he notes that the latter affects low frequency results disproportionately and recommends that test methods should require measurements with different specimen conditions when low frequency absorption is significant [36].

2.4.4 Impulse Methods

ISO 1793-5 [37] defines a standard test for assessing the *reflection index* of materials and structures designed to reduce road traffic noise. The standard is one of several absorption methods generally used outdoors for determining absorption of soils and other ground materials. The principle is that an impulsive sound is reproduced some distance in front of the sample, and a single or an array of microphones mounted close to the sample records the incident and reflected pressure waves. By the addition of a phase-inverted free-field incident wave measured previously, and by removal of parasitic reflections from extraneous objects by time-windowing, these two can be separated and analysed. Thus, reflection and diffraction indices can be determined. Similar arrangements can be used for oblique or grazing incidence measurements.

Attenborough *et al* [38] summarise several such techniques used by researchers and practitioners, but none are standardised. This family of measurements are generally limited to the frequency range above 200Hz due to the requirements of the time windowing algorithm.
Bolen & Bass made similar measurements outdoors down to 40Hz [39]. However, to achieve near-point source conditions their source-receiver distance was of the order of 15-300m.

One such method, that of Mommertz [40] is devised for indoor use, as an engineering rather than scientific method. The incident wave (subjected to pre-emphasis to improve signal to noise ratio) is cancelled by inversion with a free field response, allowing positioning of the microphone close to the sample, allowing oblique incidence measurement. Mommertz advocates conversion of the calculated absorption coefficients to random incidence using the Paris formula

$$\alpha_{ran}(f) = \int_0^{\frac{\pi}{2}} \alpha(f,\theta)\, sin2\theta\, d\theta \qquad \text{Eq 44}$$

where θ is the angle of incidence. Alternatively, a measurement can be made at 60 degrees to the normal, as advocated by Thomasson [41], as this is the most representative incidence angle in rooms.

2.4.5 Intensity Methods

Absorption coefficient can be deduced from intensity measurements at the face of a surface. The portability of P-P and P-U probes mean that the method promises the possibility of in-situ measurement of small elements such as individual acoustic panels in a studio.

The limitations, as summarised by Fahy [42], ar e that absorption or reflection factors are deduced by comparing incident with reflected energy. However, it is not possible to simply measure the incident energy alone, but the net energy flow at the surface. Incident power must be inferred from sound pressure measurements, which require assumptions about the nature of the propagation from the source.

Since the first commercially available instrumentation reached the market in the 1980s, great progress has been made, notably with the introduction of the Microflown P-U sensor, a micro-machined dual hot-wire anemometer based velocity sensor paired with a conventional pressure microphone in a small housing. This sensor has been incorporated into several products for intensity measurement and acoustic holography. For in-situ absorption measurement the sensor is paired with a small spherical calibrated sound source. A propagation model is used to separate reflected and incident sound, although no account is taken of sample thickness and absorption is assumed to happen at the surface of the sample (a Type 1 assumption as given in 2.2.3). Absorption calculations can be derived either from intensity or impedance. This setup can measure absorption coefficient at arbitrary incidence above around 300Hz [43]. Results are strongly dependent on sample size and location. Tijs found that intensity-based measurements were more robust than impedance–based ones at oblique angles [44].

2.4.6 The Low Frequency Measurement Problem

Reverberation room tests remain the most common measurement method for absorption of commercial absorbing panels. However, problems still arise when low frequencies are considered. The underlying theory of reverberation tests assumes a diffuse field, but at low frequencies, room modes dominate, and diffusivity is no longer a valid assumption. ISO 354 mentions that, although measurements below 100Hz may be taken, these may be problematic due to the low modal density of the test room in that frequency range.

Fuchs *et al* [21] studied how to extend the useful low frequency range of reverberation chambers by placing low frequency Compound Baffle Absorbers (CBA) at the room boundaries to damp modes as much as possible. The same team, in Zha *et al* [45], also proposed an extended version of the standardised technique by splitting the measurement into three ranges by frequency.

1. The range where each one-third octave band has at least 20 modes within it: here the standardised test is used.
2. The range where each one-third octave band has between five and 20 modes present: here the source and receiver positions used are in the room corners where all modes may be engaged. Measurements are again taken with the empty room and with the sample present, and pseudo-absorption coefficients are calculated using the standard formula.
3. The range where each one-third octave band has fewer than five modes present: here each individual modal frequency shall be generated by a loudspeaker in the corner of the room, then measured at a location in the room appropriate to that mode, that is, a location where it alone is expected to be present in that one-third octave band. Pseudo-absorption coefficients are calculated using the standard formula.

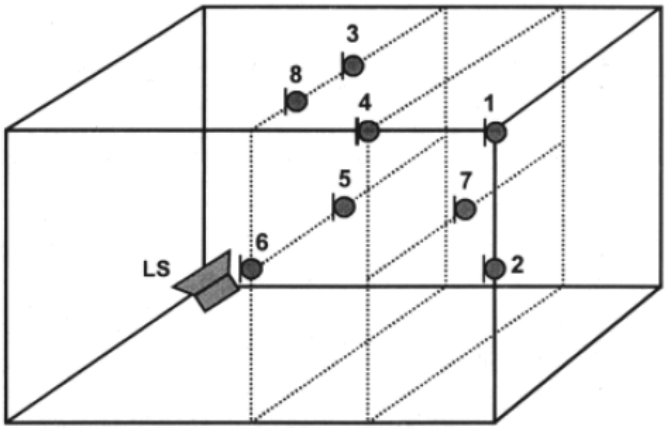

Microphone position	Mode (x,y,z)
1	1,0,0
1	0,1,0
2	1,1,0
3	0,0,1
4	1,0,1
5	2,0,0
4	0,1,1
1	1,1,1
6	2,1,0
7	0,2,0
8	2,0,1

Figure 4: Microphone positions used for sounding of individual room modes. From Zha et al. Reproduced with permission [45].

This method has the advantage of giving some indication of absorption performance at low frequencies, but the results still depend strongly on the placement of the sample within the room. The diffuse assumption used in absorption measurement holds that the test signal falls equally on the whole area of the sample equally, but as modal frequencies are not distributed evenly spatially this is not the case when measuring modal decays.

Also, only modal frequencies of the test room being used are available for the third range of tests at the extreme low frequencies, and if the test is repeated in a chamber of different dimensions, then different frequencies will be present, so cross-validation between test facilities may be difficult, if not impossible, or meaningless.

Jacobsen [46] notes that, although an exponential decay is assumed for ISO 354 measurements, at low frequencies the sound field is comprised of relatively few

modal decays, which may have significantly differing decay rates, thus the exponential decay assumption is not valid. The early part of the decay had been suggested as more representative in this case and it was shown that systematic error in measurements using early part of the decay were around two thirds those for measurement between -5 and -35dB.

Daniel [47] showed the dependence of absorption coefficient on the size of the sample compared with the size of the room, which is a near-linear relation, although different for each material.

Harwood *et al* [48] followed up this work by measuring absorption coefficients of randomly distributed absorbers in situ in the rooms in which they which they were to be used or in scale models thereof. They noted that the resulting absorption coefficients at mid and low frequencies were higher than those measured in the reverberation chamber by a factor of up to three.

The effect is more pronounced as frequency decreases, and although, as Harwood *et al* concede, the data is insufficient to draw a precise relation, there is a strong trend for significantly higher absorption coefficients measured in larger rooms.

Wavelength-related effects are also in play close to room boundaries, Waterhouse [49] [50] observed interference patterns in pressure close to chamber walls and so accurate measurements should be taken at least half a wavelength from a boundary. Below 100Hz this distance would become significantly large as to compromise spatial averaging.

2.4.6.1 Sound Sources at Low Frequency

Prato *et al* [51] worked on measurement of reverberation time at low frequency and noted that exciting individual modes with sinusoidal sources *a la* Zha *et al* can be problematic, with the motion of the loudspeaker driver impeded by the pressure caused by modality in the room.

Instead, they used either pink noise (which suffers from exciting multiple modes, resulting in highly nonlinear decay at this frequency range) or non-modal sine tones where at the cessation of the tone, only energy distributed to adjacent modes continues to decay and can be more easily measured.

Further complications occur with low frequency sources, where in any practical setup, the measurement position would be in the near field of the sound source. The problem remains difficult, although several approaches have been tried, Zhang *et al* [52] used a planar array of loudspeakers to create a plane wave propagation and reported good results down to 100Hz. Castagnede *et al* [53] used a parametric array of ultrasound sources, utilising an ultrasound carrier signal which is demodulated by propagation in the air leaving the plane-wave low frequency signal remaining. Again, good results above 100Hz were reported.

2.5 Design of Music Rooms

Several standards and other documents are used to guide acousticians in the design of music rooms. In the UK and Europe, some of these are discussed below including EBU Tech 3276 for critical listening rooms, BB93 for music facilities in schools, and the more recent Norwegian standard for music rehearsal and performance spaces.

The interaction of musicians and the acoustics of their playing environment is complex and has been subject to much study, with some clear themes becoming apparent, but much still not understood, and with wide variation between individuals. Reverberation time is the main metric in most cases, but Early Decay Time (EDT) better reflects the listeners' perception of reverberance. Bass Ratio gives an idea of the 'warmth' of the space. It is usually given by

$$BR = \frac{Average\ (RT_{125}, RT_{250})}{Average\ (RT_{500}, RT_{1000})} \qquad \text{Eq 45}$$

where BR is bass ratio (dimensionless) and RT_n is the reverberation time in the nHz octave band. Sometimes just the 125Hz band is used as the numerator, and sometimes the 2000Hz band is also included in the average in the denominator [54]. It has been noted that some halls are perceived as having poor bass

response while having longer bass RTs, and alternative bass ratios have been used which are calculated similarly, but with EDT or Strength (G) measurements instead of RT.

For performance spaces, the presence of strong, unmasked early lateral reflections has been shown to be extremely important subjectively, with this spatial impression being associated with warmth i.e. low frequencies. If these early reflections are masked by adjacent ceiling reflections, then low frequencies are disproportionately masked by their interaction. And as Marshall points out in his consideration of this phenomenon, the two most famous performance halls of all, the Concertgebouw in Amsterdam and the Grosser Musikvereinsaal in Vienna are also noted for their warmth. [55]

2.5.1 Musicians and Acoustics

It has been empirically clear that musicians perform somewhat differently from space to space. This has been confirmed empirically under laboratory conditions and continues to be an active area of research. Schaerer-Kalkandjev *et al* measured the performance of a cellist in an anechoic chamber who was playing with acoustic feedback replayed via headphones of several modelled spaces [56]. All room acoustic parameters were shown to affect playing; RT had a strong correlation with tempo, tempo variations and absolute loudness. Reverberant energy (ST_{Late}, Early Support (G_{Early}) and Bass Ratio all had an impact on the timbre of playing, with high G_{Early} causing softer (in terms of level and tonally) playing and strong ST_{Late} the opposite.

2.5.2 Music Rooms in Schools

For teaching and solo practice, a generally shorter reverberation time is required. As long ago as 1967, Patrick & Boner identified low frequencies as problematic, stating that the warmth valued in performance is disturbing in rehearsal and recommended RTs of 0.3s for 100-250Hz and 0.5s for 500Hz and above, shorter than generally recommended for music spaces of the time, as they note [57].

More recently, Osman gives a more up to date synopsis of guidelines for several types of music teaching spaces, summarizing guidance from several source documents from the UK, USA and Australia/New Zealand [58]. His advice begins with room ratio choice, preferring Walker's BBC ratios [59] as a definitive source.

He then comments that there is some difference in acoustic preference between instrument groups, citing his own research in which percussion players preferred slightly shorter RTs to bowed string players, with woodwinds preferring an intermediate acoustic. This seems logical as percussion can generate higher peak levels, yet are more dynamic, allowing reverberation to be perceived more easily between notes. String instruments can be somewhat "raspy" in very dry acoustic and need more support.

Osman continues by specifying allowable tolerances for RTs as ±10% of target RT in the 250-2kHz octave bands. For lower frequencies, he recommends RT be longer than the target RT, hence reflecting the traditional tolerance for bass rise and seeing bass dip as less desirable [58].

Building Bulletins 86 and 93 [60] [61] *(part 5)*
These documents provide guidance for the acoustic design of school buildings, including music classrooms, practice, performance and recording rooms. Guidance is given for size, midrange RT, construction etc. of these spaces. Their only guidance for low frequencies is to note that an increase in low frequency RT (below 500Hz) is "permissible and indeed preferred".

2.5.3 Norwegian Standard NS8178:2014

The Norwegian Standard NS8178:2014 [62] is a more recent document focusing on music rehearsal and performance spaces, splitting this definition into three classes: spaces for amplified music, loud acoustic (brass bands, jazz big bands, orchestras etc.) and soft acoustic music (voice, choral, folk and chamber

ensembles). Within each of these divisions, guidance is given in terms of room volume, geometry, background noise level and sound insulation for four size classes: individual practice rooms and small, medium and large ensemble rooms.

For performance spaces, guidance for room volume is given in terms of volume per person, including performers and audience. This guidance is summarised graphically as a room volume vs RT plot in which preferred zones for the different classes of space are indicated (see Figure 5 over).

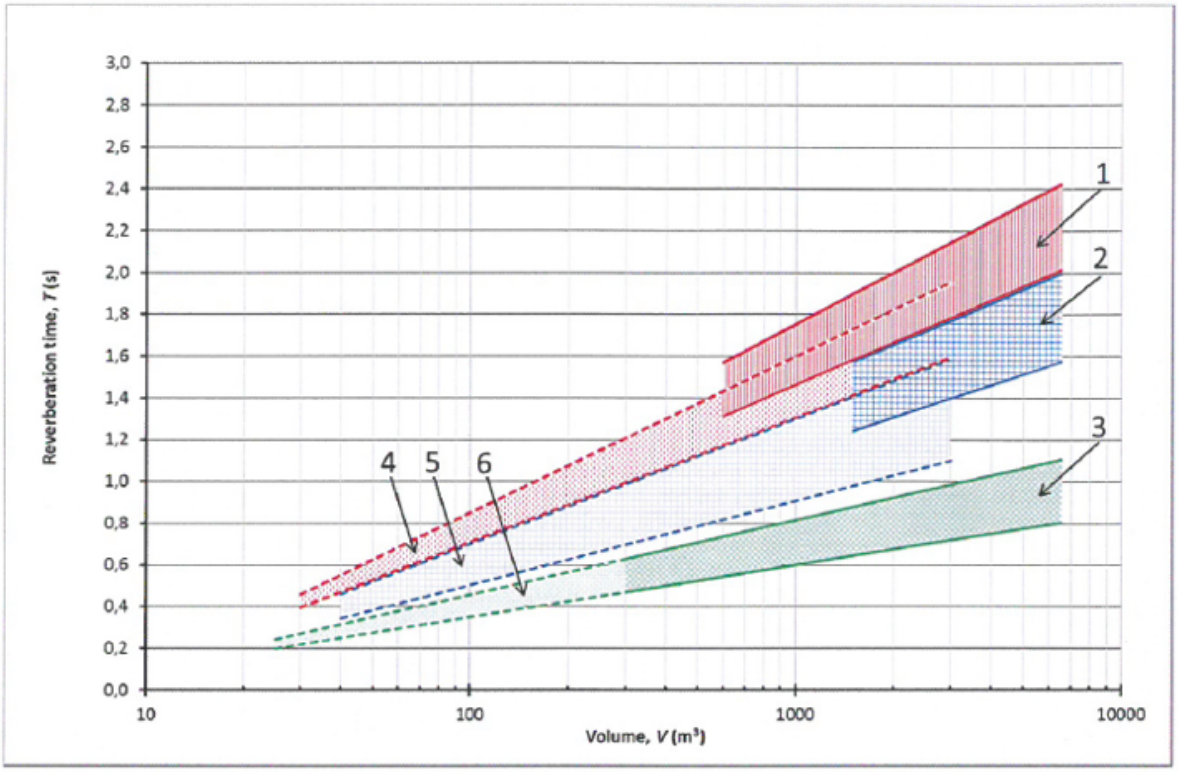

Key

1 upper and lower limit for quiet music in performance halls (solid lines)
2 upper and lower limit for loud music in performance halls (solid lines)
3 upper and lower limit for amplified music in performance halls (solid lines)
4 upper and lower limit for quiet music in rehearsal rooms (dotted lines)
5 upper and lower limit for loud music in rehearsal rooms (dotted lines)
6 upper and lower limit for amplified music in rehearsal rooms (dotted lines)

Figure 5: Volume vs RT recommendations from NS8178. Reproduced with permission [62].

Frequency dependence of RT is indicated within upper and lower limits for each sound source type (see Figure 6).

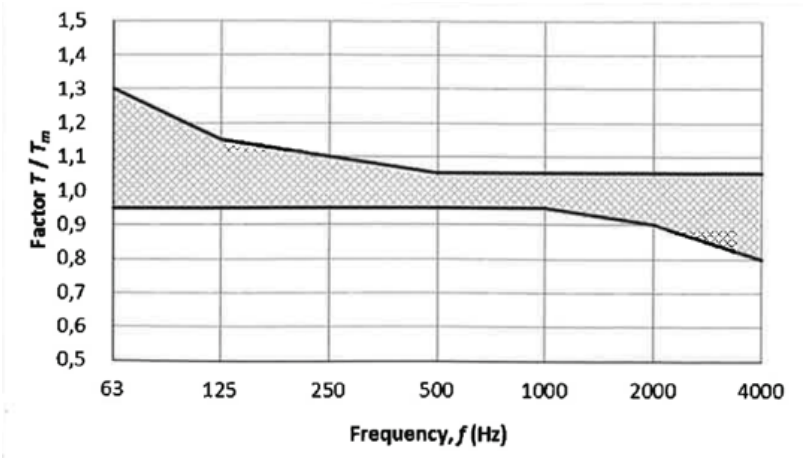

Figure 6: Frequency dependence range of RT in acoustic (loud) performance and rehearsal spaces (from NS8178 – reproduced with permission) [62].

A method for estimating the *forte* sound level for any given ensemble of I instruments is outlined. Each instrument is given a power factor based on solo sound power measurements. These factors are summed for an arbitrary ensemble. Sound strength G is then estimated from given RT/Room volume curves and overall *forte* sound power of the ensemble is calculated by

$$L_P = G + 59 + 10log \sum_{i=1}^{I} n_i k_i \qquad \text{Eq 46}$$

where L_p is forte sound level in dB SPL, G is sound strength, n_i is the nth instrument and k_i is the power factor of that instrument. For a forte passage, L_p should lie within the 85-90dB range (perhaps slightly higher for large ensembles). The standard provides a chart to allow estimation of G based on RT and volume, if a measurement is not available.

2.5.4 Acoustic Measurement of Performance Spaces:

ISO BS 3382-1:2009 [63] defines a standard method of measuring the acoustics of music performance spaces.

The Space Under Measurement

Firstly, the degree of occupation of the space under test is noted, as various factors impact the measurement process:

- Unoccupied state, where the room is prepared for use by speakers or performers, but without them being present. Preferably, equipment such as music stands and chairs should be present.
- Studio state, where the room is prepared for speakers of performers, who are present, but in the absence of an audience. This represents the state at rehearsal or recording, with an appropriate number of technical staff also present.
- Occupied state, where an audience of 80-100% capacity is present.
  If components for adjusting the acoustic, such as curtains, are present, a separate test should be carried out with them in each of their normal settings. In theatres, note should be made of whether the safety curtain is up or down, or whether the orchestra pit is open or closed. If artificial reverberation systems are in operation (see 3.7.4), it is noted that they can create non-time-stationary effects and that spatial averaging such as used in the standard may not be appropriate.

2.5.4.1 Measurement Setup.

An omnidirectional sound source should be used, and acceptable deviations from this are specified.

A signal strength sufficient to produce a sound pressure level at least 45dB above background noise is required. If only T_{20} is to be measured, then 35dB is sufficient. If a pseudorandom noise source such as maximum length sequence (MLS) is used, this can be reduced. Microphones should be omnidirectional and of small diameter, ideally no more than 13mm. Measurement equipment should be calibrated, and equivalent quality of a Class 1 Sound Level Meter as defined in ISO61672-1. Octave or 1/3 octave filters should conform to ISO61260.

The initial decay is measured by a digital recording device such as a laptop. The test duration should be enough to capture the whole decay of the room, with five seconds plus the expected reverberation time being a guide figure. Frequency response should be flat within ±3dB over the range of measurement and dynamic range at least 50dB; which is now no problem with modern digital systems.

2.5.4.2 Test Procedure

Sound sources should be placed where natural sound sources in the room may be located. At least two source positions should be used, and their height should be 1.5m. Microphone positions should be at positions representative of listener positions, and be at 1.2m height, that of a seated listener. Microphone positions should be placed to spatially sample the room and represent any inherent variations within the room such as stalls, balconies, seats closer to walls etc. Judgement should be exercised on how to best sample the space and how diffuse it is by noting location of absorbing surfaces etc. Larger spaces should receive a greater number of microphone positions to give a representative spatially averaged result. Microphone positions should be at least half a wavelength apart (around 2m for normal frequency range) and at least a quarter wavelength (normally 1m) from the nearest reflective surface such as a wall. No microphone position should be too close to a source position to avoid strong influence of direct sound.

Two methods can be used to excite the room

- *Interrupted Noise Method*: a broadband sound source such as pink noise or pseudo-random electrical noise shall be used. It shall be sounded continuously for a duration more than the RT and sufficient to ensure a diffuse response within the space. The noise is then interrupted and the decay measured.

- *Integrated Impulse Method*: the impulse response from source to receiver can be measured by pistol shot, spark gap noise, Maximum Length Sequence noise or sine sweep. Dynamic range requirements are significantly lower in the latter two methods, which both require significant post processing of the recorded signal to derive the room impulse response.

The impulse response thus obtained is squared and backward-integrated

$$E(t) = \int_t^{\infty} p^2(\tau)d\tau = \int_{\infty}^{t} p^2(\tau)d(-\tau) \quad \text{Eq 47}$$

where p is the sound pressure of the impulse response as a function of time, E is the energy of the decay curve as a function of time and t is the time.
This is often achieved by performing two integrations

$$\int_t^{\infty} p^2(\tau)d\tau = \int_0^{\infty} p^2(\tau)d\tau - \int_0^{t} p^2(\tau)d\tau \quad \text{Eq 48}$$

2.5.4.3 Evaluation of Decays

For determination of T_{30}, the evaluated range is 5dB to 35dB below the steady state level, which in the integrated impulse response method is the total level of the integrated impulse. A least squares fit shall be calculated within this range and the slope of this line gives the decay rate, d in decibels per second, from which the T_{30} is calculated by

$$T_{30} = \frac{60}{d} \quad \text{Eq 49}$$

For calculation of T_{20}, the range used is from -5dB to -25dB.

For interrupted noise measurements, multiple soundings of the room are necessary to allow for the random nature of the source sound. Integrated impulse response measurements do not require this.

Spatial averaging between source/receiver combinations shall be done as an arithmetic average of reverberation times, typically 12 to 18 combinations.

Results should be presented in table and graph form. A single figure T_{30mid} can be presented as the arithmetic average of 500Hz and 1000Hz T_{30} times.

2.5.4.4 Auditorium Measures

In Annex A of the standard, a series of subjectively derived metrics is defined, and this gives some framework for extension of guidance documents, at least for performance spaces. Most commonly used are Sound Strength G, expressing the subjective level of the space, and Early Decay Time EDT expressing perceived

reverberance, based on the first 10dB of the decay. Two of these metrics concern low frequencies and are measured using averaging from 125 to 1000Hz [63].

2.5.4.5 Stage Measures

Two metrics are defined to assess conditions for the musicians on the stand. Early support ST_{Early} is the ratio of the reflected energy within 0.1s from source onset to the direct sound energy; measured at 1m from an omnidirectional source. It relates to the sense of ensemble, that is, of hearing other players. Late support ST_{Late} is the ratio of the reflected energy after 0.1s from source onset to the direct sound, measured at 1m from an omnidirectional source. It relates to the musicians' sense of the reverberance in the hall.
Gade notes, however that most research has failed to correlate ST measurements to subjective experience of musicians [64].

2.5.5 Background Noise

Music spaces must have strict background noise ratings to ensure that extraneous noises do not distract the engineers or audience during quiet passages in the music.

For critical listening spaces, EBU3276:1998 [65] specifies preferably NR10, and no more than NR15.

For performance spaces, Barron [66] suggests NR15 for large concert halls, NR20 for Opera Houses and Theatres, and NR25 for smaller auditoria.

Large audiences create noise themselves, Barron recounts that Kleiner measured their contribution to be up to NR25 [66]. However, as he later notes, even large audiences can be extremely quiet during critical passages of music, and with this in mind, some designs have pursued the reduction of background noise beyond NR15, giving the example of Birmingham Symphony Hall, which has a background level of NR10. Audiences have been noted to have responded by being quieter than elsewhere.

Norwegian Standard NS8178:2014 [62] refers to another Norwegian standard NS8175 which quotes guidance in RC28 for lecture halls as generally being applicable to music rooms. RC28 is harder to achieve than NR28, as Room Criteria are much more stringent particularly at lower frequencies.

2.5.6 Critical Listening Rooms:

EBU Tech 3276 1998 [65] *and Supplement 1 2004* [67]

This document provides target reverberation time and frequency responses for reference listening rooms and studio control rooms, which require a dead acoustic.

The standard gives a reference RT given by

$$T_m = 0.25 \left(\frac{V}{V_0} \right)^{\frac{1}{3}} \qquad \text{Eq 50}$$

where T_m is nominal RT, V is room volume in m^3 and V_0 is the volume of a reference room ($100m^3$)

T_m is recommended to lie between 0.2 and 0.4s between 200Hz and 4kHz in 1/3 octave bands. A slightly longer RT is tolerated at low frequencies, e.g. up to an additional 0.3 seconds for the 63Hz 1/3-octave band than for the average midrange RT. Likewise, frequency response tolerances are set at ±3dB from the mean midrange level (measured from 200Hz to 4kHz 1/3-octave bands) down to 50Hz. Overall, as one might expect, these requirements are rather strict, and as the standard notes, possibly difficult to comply with, especially in smaller rooms. This document assumes stereo sound sources, and Supplement 1, from 2004 focuses on the design of critical listening rooms for surround sound studios.

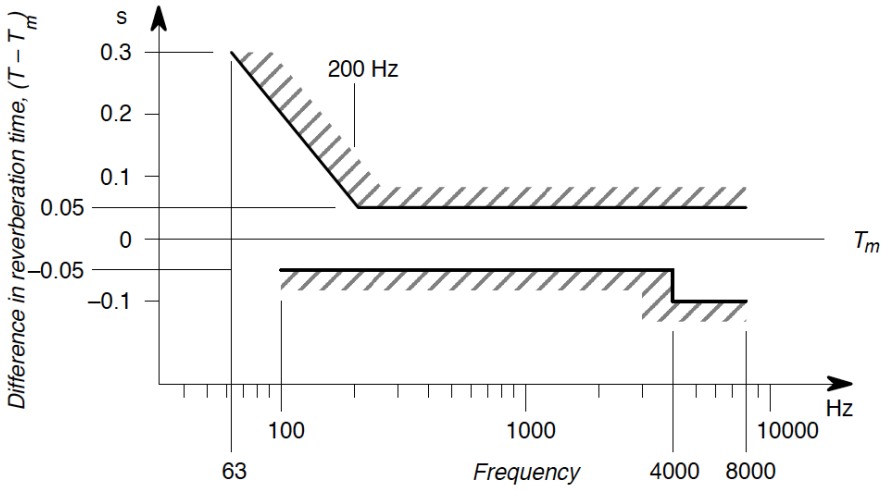

Figure 7: Guidance for frequency dependence in reverberation time from EBU 3276: 1998 [65]and EBU 3276-E: 2004 [67] . RT is expressed as T-$T_{midrange}$. Reproduced with permission of the European Broadcast Union.

Several other organisations carry out research in this field, notably broadcasters such as the BBC who prepare technical white papers on acoustic treatment and studio design, for example WHP021 [68], which provides similar recommendations for control rooms as EBU3276.

2.6 Classical Control Approaches

There are two main categories of treatment available to the acoustic designer hoping to control the sound field in a room: porous and resonant absorbers. The former is cheap and ubiquitous but is less appropriate for low frequencies. The latter can be highly effective at lower frequencies but may need to be designed to order for a particular end use. The pros and cons of each are discussed below.

2.6.1 Porous Absorber

Acoustic materials deployed to control the sound field normally consist of porous materials, typically foam or mineral fibre, which present a large internal surface area to the incident sound, resulting in dissipative losses. However, the effectiveness of porous treatments depends on particle velocity and at the room boundary, where space is available for acoustic treatment, the particle velocity is near zero except at high frequencies. Thus, porous absorbers must be deployed in great depth to attenuate low frequencies, doubling the thickness of absorber reducing the onset frequency by an octave. Optimally the depth of absorber

should be one-quarter of a wavelength, to be placed at the position of maximum particle velocity: so, to absorb 100Hz, a depth of at least 0.86m is required. In practice, an absorber is considered to begin absorbing at around 1/10th wavelength [69]. This doubling of thickness often precludes their effective use for low frequency application for reasons of space.

Given the wide variety of material types, the performance of porous absorber materials can be predicted using empirical models, such as those of Delany and Bazley [70] and of Miki [71].

Some efforts have been made to extend the capability of porous absorbers. The simplest being to mount the absorber in front of an air gap. This places the material away from the wall, where particle velocity is near zero. A more developed example is in the recording studio designs of Tom Hidley and Phillip Newell. Their *Total Environment* concept [72] called for near-anechoic conditions in critical listening rooms and to achieve this they deployed arrays of hanging panels lined with porous absorber in large and deep cavities at the room boundaries.

These were empirically designed but have been subsequently analysed by Torres-Guijarro *et al* [73] (among others) using intensity measurements in situ in a Newell-designed control room and by Finite Element Method (FEM) simulation. They found that the panels, when turned partially away from the sound sources, (with 40 degrees to the source found to be optimum subjectively), acted as low frequency waveguides, thus allowing the incident sound to be exposed to a greater area of absorber for a given depth from the wall.

In addition, transverse modes were present higher in the frequency range, and the balancing of these two mechanisms led to this arrangement providing very strong absorption from below 100Hz to over 1000Hz. Wincentz *et al* [74] measured an experimental cavity of similar design and made FEM models and concluded that, although a good low frequency design, performance was no better

than the normal incidence condition, when the absorber panel (this time with no rigid mount) was mounted as a facing for the same cavity. However, in this case, absorption at normal incidence was more uneven than at other angles, as all the absorber was concentrated at one distance from the back wall. For a music room, even absorption should be considered desirable and, in addition, the angling of absorber vanes facilitated a shallower cavity than the normal condition tested by Wincentz *et al,* and thus saved space.

In another strategy, Dunn & Davern [75] proposed layering of multiple materials with differing flow resistivities, and later Xu *et al* [76] used a generative algorithm to optimise the depth and properties of these layers and created a construction in which absorption was effective at one-sixth of a wavelength, rather than ¼ of the wavelength and hence for 100 Hz only 0.57m was required.

2.6.2 Resonant Absorbers

Conventional lower frequency treatments tend to use resonance as a mechanism and comprise either Helmholtz resonators or panel and membrane absorbers.

- Helmholtz resonators, in which the volume of air within a cavity connected to the room via a neck or aperture is set into resonance, where the motion of the air through the neck gives rise to viscous losses, while the spring action of the trapped volume of air also contributes. Microperforated panels (MPP) are a special case of this type.

- Panel or membrane absorbers, in which a plate or membrane, normally backed by a cavity, is set into motion by the incident sound, with losses incurred due to the compressibility of the trapped volume of air and sometimes due to the plate stiffness.

  In both cases, energy around the resonant frequency is lost from the room to drive this mechanism [69] [77].

  Damping materials can spread the frequency range of such resonators, but, in essence, they are targeted at a specific frequency so must be designed in a

bespoke manner for each project as each room has different dimensions and hence modal frequencies. To cover a wide frequency range, an array of such resonators would be required. Their construction is not trivial and they can be heavy, cumbersome and expensive, often being incorporated into the structure of walls and ceilings. For this reason, light-weight alternatives and designs which, if they must be bulky, are well optimised, are of ongoing concern in acoustics.

2.6.2.1 General Design Considerations

Cox and D'Antonio [69] show how the general impedance expression for a cavity fronted by a panel, which could be a membrane or a perforated sheet,

$$z = -jz_i cot\,(kd) \qquad \text{Eq 51}$$

can be modified to add acoustic mass $j\omega m$ and resistance r_m terms, giving the surface impedance of a resonant system,

$$z = r_m + j[\omega m - \rho_0 c_0\, cot(kd)] \qquad \text{Eq 52}$$

where wavenumber $k = 2\pi/\lambda$, d is the cavity depth in m, m is the mass per unit area of the panel in kgm^{-2}, ω is the angular frequency in rads^{-1}, ρ_0 the density of air and c_0 the speed of sound in air.

If we ignore the porous component, the resonant system resonates when the imaginary part of Eq 52 is zero. If the cavity depth is much smaller than the acoustic wavelength so cot (kd) → 1/kd, the resonant frequency can be given by

$$f_{res} = \frac{c_0}{2\pi}\sqrt{\frac{\rho_0}{md}} \qquad \text{Eq 53}$$

This is the general form for resonant absorbers and can be modified for specific types.

2.6.3 Helmholtz Resonators

Helmholtz resonators, an arrangement of a rigid-walled volume of air coupled to a room via one or more openings, are the oldest form of acoustic control. They were mentioned by Vitruvius [78] and have been used since, notably in some mediaeval churches where vessels were embedded within the walls, with small amounts of sand placed inside to tune the resonant frequency. They were

formally analysed by Hermann von Helmholtz and subsequently took his name [79].

In the case of a pure Helmholtz resonator, within the volume itself, away from the aperture, pressure is assumed to be spatially constant as the enclosed air acts simply as a spring and the air within the neck of the aperture oscillates as a moving mass. If there is no aperture at the mouth of the volume then the volume will resonate as a quarter wave resonator, in the manner of an organ pipe (see 2.7.1)

2.6.3.1 Design

Cox and D'Antonio analyse Helmoltz resonators by first considering a perforated panel of thickness h with perforations of radius a spaced D apart and repeating on orthogonal directions, in front of a cavity of depth d. This arrangement comprises a series of air masses within the perforations, with a shared mass of air acting as a spring behind. A porous absorber could be used to back the panel but was omitted initially.

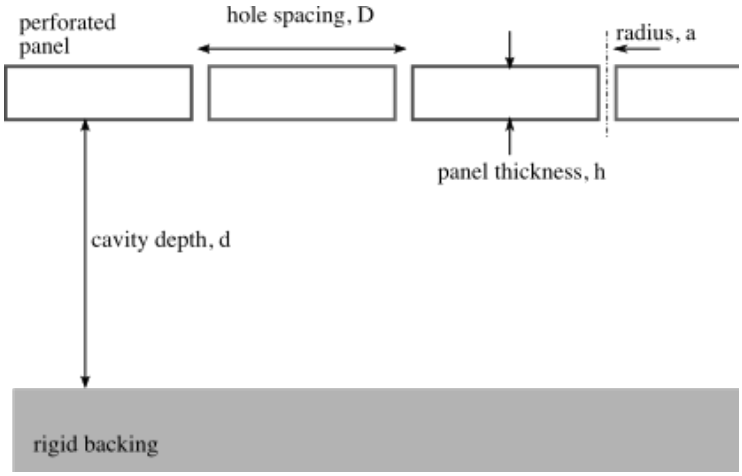

Figure 8: Section of a perforated panel in front of a cavity. D is hole spacing, d is cavity depth, a is hole radius, t is panel thickness and t_a is absorber thickness.

We can consider this panel as being divided into individual, independent cells. In practice, this assumption does not hold at low frequencies and physical subdivision of the cavity can improve performance [80]. The hole spacing should be large compared with diameter.

The resonant frequency can be expressed in terms of ε the open proportion of the panel

$$f_{res} = \frac{c}{2\pi}\sqrt{\frac{\varepsilon}{h'd}} \qquad \text{Eq 54}$$

where

$$\varepsilon = \frac{\pi a^2}{D^2}$$

This is used when considering arrays of resonators and perforated panels.

Taking the general form which is in the form of the general equation above. For a single resonator, the above relation can be expressed as

$$f_{res} = \frac{c_0}{2\pi}\sqrt{\frac{S_n}{Vh'}} \qquad \text{Eq 55}$$

where f_{res} is resonant frequency in Hz, c_0 is the speed of sound in air in ms^{-1}, S_n is the cross-sectional area of the neck in m^2, V is the volume of the cavity in m^3 and h' is the effective length of the neck in m, comprising the physical length plus an end correction to correct for the radiation of the particular geometry of the opening. Assumptions are that all dimensions are small compared to wavelength, $ka \ll 1$ where k is wavenumber and a is a dimension of the geometry. Thus, it is assumed that only one resonant frequency can be supported, unlike a quarter wave resonator, in which multiple harmonics can be supported.

2.6.3.2 End Corrections

The vibrating plugs of air within the neck of the apertures provide the mass in the previous expression. Calculating it is complicated by the effect of radiation impedance, including interaction between adjacent holes. Thus, the length of the holes is the physical length h plus an end correction, which is influenced by the shape of the orifice and the space available for the sound wave behind it. The full expression for the perforated panel is

$$m = \frac{\rho_0}{\varepsilon}\left[h + 2\delta a + \sqrt{\frac{8\upsilon_0}{\omega}\left(1 + \frac{h}{2a}\right)}\right] \qquad \text{Eq 56}$$

where the last term is the effect of boundary layer losses, where υ_0 is the kinematic viscosity of the air in m^2s^{-1}. This last term may be negligible unless the holes are very small (<1mm). δ is the end correction for radiation impedance; a value of 0.85 is taken as a first estimate (by considering the radiation of a

baffled piston), which is accurate for the archetypal single orifice in an infinite baffle. For arrays of orifices, and for other geometries, other corrections exist. e.g. for more open structures, including ε = 1

$$\delta = 0.8\,(1 - 1.47\varepsilon^{\frac{1}{2}} + 0.47\varepsilon^{\frac{3}{2}}) \qquad \text{Eq 57}$$

for a square aperture, with $\varepsilon < 0.16$

$$\delta = 0.85\,(1 - 1.25\varepsilon^{\frac{1}{2}}) \qquad \text{Eq 58}$$

Other conditions can affect the acoustic mass. Grazing incidence can increase resistance; high amplitude sound can create turbulent flows which reduce effective mass.

2.6.3.3 Losses

For the resistance term above, for Helmholtz resonators without additional absorbent material, and assuming holes are not sub-millimetre, Cox and D'Antonio [69] present the following.

$$r_m = \frac{\rho}{\varepsilon}\sqrt{8\nu_0\omega}\left(1 + \frac{h}{2a}\right) \qquad \text{Eq 59}$$

where ν_0 is the kinematic viscosity of the air in m^2s^{-1}.

They also relate a simplified version from Ingard.

$$r_m = \frac{\sqrt{2\rho\eta\omega}}{2\varepsilon} \qquad \text{Eq 60}$$

where η is the dynamic viscosity of air, 1.85 x 10^{-5} $kgm^{-1}s^{-1}$.

The latter is commonly used, but does not allow for burrs and other inconsistencies, which for most absorbers are negligible.

2.6.3.4 Practicality

Helmholtz resonators can be problematic to implement. Size and weight both increase with lower resonant frequency, and they in all cases have very narrow bandwidth of absorption and thus need much damping material to broaden this, which can alter the resonant frequency as the resistance term r_m and apparent length in the above equations will change. Their interaction with room modes and thus their siting is difficult to predict. The BBC Guide to acoustic practice from 1990 [81] sums up these limitations.

"These absorbers are seldom specified for BBC studios due to the problem of siting them precisely where they are required, but when they are, a special detail will be supplied. Dimensions and construction of these units are critical to one millimetre and particular care must be observed in their erection and location"

2.6.3.5 Micro-Perforated Panels

Originally developed in the 1960s by Maa [82], micro-perforated panels (MPPs) offer the main advantage of the possibility of clear construction, which is very attractive in some applications. Damping materials can be dispensed with through the use of extremely small (sub-millimetre) perforations; these, being not much larger than the acoustic boundary layer, cause large viscous losses to occur. This offers the possibility of creating fire resistant designs. Devices using this principle comprise a micro-perforated panel mounted in front of a non-perforated panel. The space in-between can be open, as the mechanism does not depend on the spring action of an enclosed volume of air. MPPs have become quite common but remain somewhat difficult and expensive to manufacture so have remained a niche product.

2.6.4 Plates and Membranes as Absorbers

A plate (depending on material stiffness for its shape) or membrane (depending on tension for shape) can present to the incident sound wave a mass which is large compared with that of the air it moves. The plate can only react with the sound field when part of a resonance system, thus it is placed in front of a sealed cavity where the enclosed volume of air acts as a spring in a mass-spring resonant system. The cavity should be neither too deep nor too shallow compared with wavelength to be absorbed, with Fuchs [83] relating Fasold and Veres' recommendation that

$$\frac{\lambda}{100} < L < \frac{\lambda}{12} \qquad \text{Eq 61}$$

where L is the cavity depth in m.

If a plate or membrane is clamped around its edges in front of a sealed cavity containing air and optionally further porous damping material, it is assumed to

act as an inertial mass and its bending stiffness is generally considered negligible compared to the stiffness of the spring force of the enclosed air. The frequency of peak resonance can be predicted using

$$f_{res} = \frac{1}{2\pi}\sqrt{\frac{\rho_0 c_0^2}{mL}} \approx \sqrt{\frac{60}{mL}} \qquad \text{Eq 62}$$

where f_{res} is the frequency of peak resonance in Hz, ρ_0 is the density of air in kgm^{-3}, c_0 is the speed of sound in air in ms^{-1}, m is the surface mass of the panel in kgm^{-2}.

Sendra's modified formula incorporates the geometry of the panel [19].

$$f_{res} = \frac{1}{2\pi}\sqrt{\frac{\rho_0 c_0^2}{mL + 0.6L\sqrt{ab}}} \qquad \text{Eq 63}$$

where a and b are the dimensions of the panel in m.

Whether this assumption that panel losses are negligible has concerned researchers for some time. A notable early study was by Ford & McCormick [84] who used the virtual work principle and electrical analogies to analyse a clamped square plate in front of a cavity. They concluded that absorption due to the plate stiffness can only occur at the resonant frequency of the plate and not elsewhere.

Sakagami *et al* [85] [86] in a series of papers made an analytic and numerical study of panel absorbers of infinite extent backed with a cavity and concluded that the mass-spring effect of the absorber is indeed the dominant mechanism, as strong absorption is shown only at the resonant frequency and close to the coincidence frequency of the panel.

Their numerical parametric study is summarised in Figure 9. The key findings (expressed in terms of reflection coefficient) relate to plate thickness Figure 9b where the lightest weight panel studied (h=0.003m) caused a peak in absorption around 150-180Hz, i.e., in the low mid/high bass region. Thicker panels cause the resonant peak to occur lower and to broaden. In Figure 9d, increased absorption

coefficient of the back wall of the cavity is shown to also lower and broaden resonance. In Figure 9e, increasing angle of incidence from the normal is shown to broaden absorption.

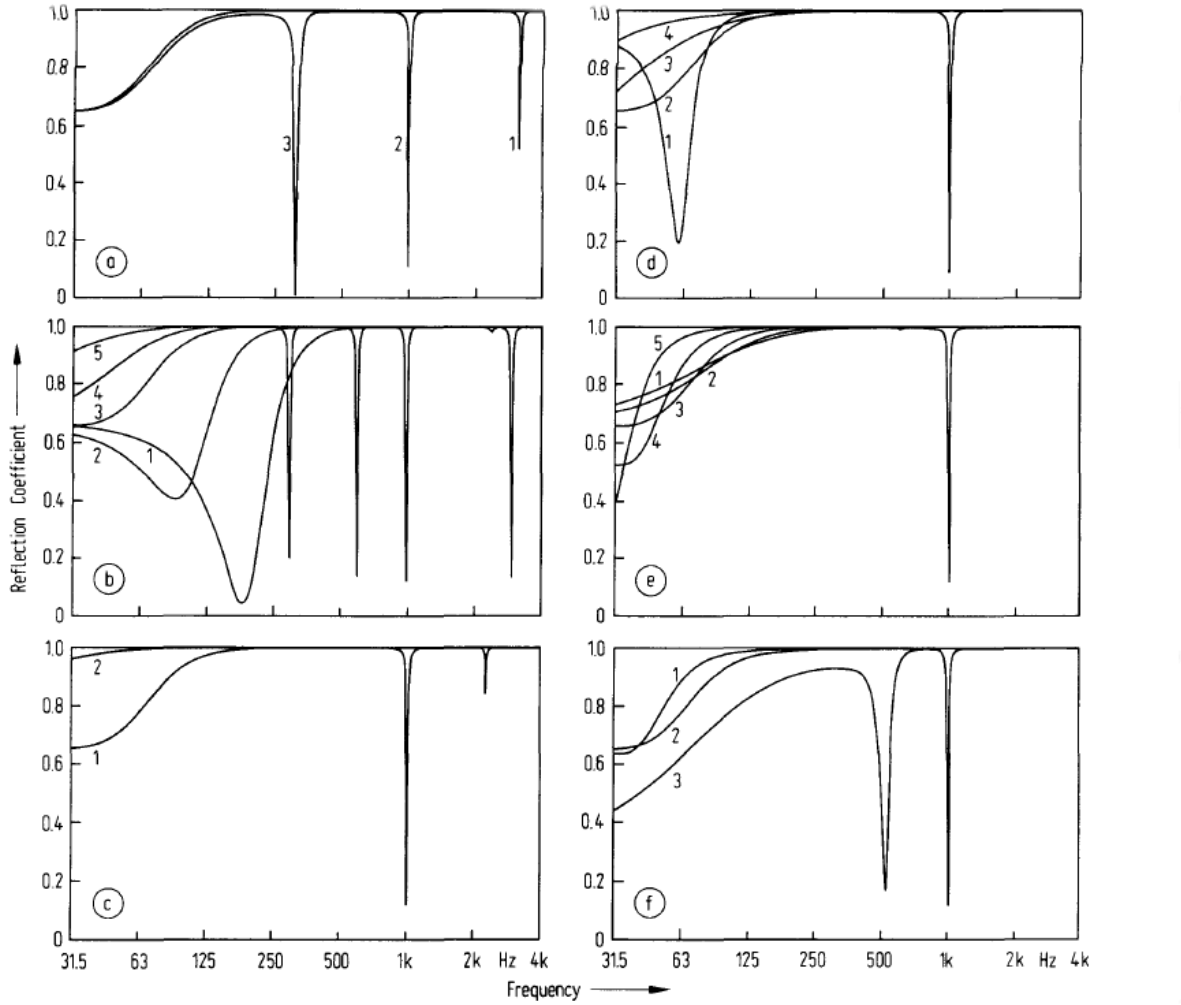

Figure 9: Sakagami's numerical simulation of the effects of the properties of an infinite elastic plate with a back cavity [86]. α is the absorption coefficient of the back wall, z is the depth of the air back cavity in m*, E is the Young's Modulus of the membrane material in* Nm^{-2}*, σ is the density of the membrane material in* kgm^{-3}*, t is the panel thickness in* m*, η is the panel loss coefficient, θ is the angle of incidence in degrees and z is the cavity depth in* m*. Reproduced with the permission of the author.*

a) Effect of Young's Modulus: E=109 (1), 1010 (2) 1011 (3) Nm-2, where σ = 600kgm-3, h=0.03m, η = 0.01*, θ =* 45°*, z = 0.1m, α = 0.25.*

b) Effect of panel thickness: h=0.003 (1), h=0.01 (2), h=0.03 (3), h=0.05 (4), h=0.1 (5) m, where E=109 (1), 1010 (2) 1011 (3) Nm-2, where σ = 600kgm-3, η = 0.01*, θ =* 45°*, z = 0.1m, α = 0.25.*

c) Effect of panel density: σ = 600 (1), σ = 3000 (2) kgm-3, where E=1010 Nm-2, h=0.03m, η = 0.01*, θ =* 45°*, z = 0.1m, α = 0.25.*

d) Effect of back wall absorption coefficient: α = 0.05, α = 0.1, α = 0.2, α = 0.4, where E = 1010 Nm-2 , σ = 600kgm-3, h=0.03m, η = 0.01*, θ =* 45°*, z = 0.1m.*

e) Effect of cavity depth: z = 0.025 (1), z = 0.05 (2), z = 0.1 (3), z = 0.2 (4), z = 0.4m (5) where E = 1010 Nm-2, σ = 600kgm-3, h=0.03m, η = 0.01*, θ =* 45 ° *, α = 0.25.*

f) Effect of angle of incidence: θ = 15° (1)*, θ =* 45° (2)*, θ =* 75° (3)*, where E = 1010 Nm-2, σ = 600kgm-3, h=0.03m, η =* 0.01*, z = 0.1m, α = 0.25.*

It is customary to assign a Sabine absorption coefficient to panel absorbers, but this is not strictly correct as they are non-locally reacting; a Type 2 absorption mechanism in 2.2.3. Their response is not due to local properties, but by those of panel as a whole, and to the coupling between it and the room.

All resonant absorbers depend on coupling with rooms modes, thus mounting and positioning are of critical importance. As they are not locally reacting, the sound field incident upon one part of the panel or membrane will affect its whole.

Cavity-backed panels have been noted as causing issues in music rooms. The Royal Festival Hall in London suffered from poor bass response due to a short reverberation time at low frequencies. When Kirkegaard Associates refurbished the hall in 2007, they targeted wood panelled sections as undesirable for bass response.

"For example, all the wood panelling that lined the interior of the hall was carefully removed, marked, restored, placed in storage until the substructure was completely modified to eliminate any hollowness behind the panels. Then the panels were carefully replaced." - Kirkegaard [87]

2.6.5 Absorption of Curtains

Curtains act as a hybrid absorber as there occurs a certain amount of low frequency absorption due to membrane action (see Eq 70) It is known that porous materials such as curtains tend to absorb mid and high frequencies. Kutruff gives the absorption coefficient for a thin, porous layer in front of a rigid plane surface as follows [18].

$$\alpha(f) = \frac{4r'_s}{\left(r'_s + 1\right)^2 + cot^2(2\pi fd/c)} \qquad \text{Eq 64}$$

where r'_s is a resistance term related to the porosity of the curtain, f is frequency, d is the gap between curtain and wall, and c is the speed of sound. This gives a frequency dependency of absorption whereby peak absorption is achieved with cavity distance of quarter or three quarters wavelength and integer multiples

thereof. Minimal absorption is observed with cavity depth of half wavelength and wavelength and integer multiples thereof.

2.6.6 Active and Shunt Control

Another approach to the control of low frequencies in rooms is to exploit the linearity of superposition of sound at normal amplitudes [88]. When two in-phase waves meet, they will reinforce each other and a 6dB boost is achieved. If their phase difference is π radians or 180^{o}, or if their relative polarity is inverted, then complete cancellation occurs, and silence is the result. Active control measures seek to introduce an artificially generated source into the room with the opposite phase of the problem frequency.

The idea was initially proposed by Lueg in 1936 [89], and from the 1950's onward it began to be developed in earnest, initially by Conover [90] working with power transformer noise. He employed a feedforward control strategy where a sinusoidal source signal being played through a loudspeaker was manually adjusted in magnitude and phase until the operator considered optimum cancellation at the receiver position had been achieved. It must be noted that the effect is to create a quiet direction of propagation, and sound pressure can be increased in locations where waves emanating from the noise source and sound source constructively interfere. Multiple loudspeakers can be used to achieve attenuation over a larger angle of propagation. Further work automated the optimisation procedure, necessary for noise which changes continuously such as car engine noise. The development of Digital Signal Processing (DSP) in recent times has seen the feedforward technique improved by use of filtering and such methods are stable and common in practice [91].

The other type of active system incorporates a *feedback* approach, with the control signal coming from a closely coupled microphone near the loudspeaker, rather than being artificially generated. This type of system, first proposed in 1953 by Olson [92] is useful when the noise source is not known in advance or when it is non-constant, although it is frequency limited in terms of performance.

This type of control is only suitable for particular, low frequencies, and hence it is not suitable for classical music. At best this technique could be effective at removing easily separable modes, for instance the lowest axial modes in the room.

A more recent technique is the shunt absorber, proposed by Fleming *et al* [91], where an electrical impedance is connected across the terminals of a loudspeaker, and the dynamics of its motion can be modified to act as a resonator. A passive R/C shunt was used at low frequencies, with an inductor added at higher frequencies. More complex control elements including an error microphone were added in this case. As Fleming points out, active control strategies are often aimed at the relatively simple case of a duct, but in the case of an enclosure, more modes are present and are spatially distributed more extensively [91].

Generally, such systems are beyond the scope of this thesis, but as a mature technology they remain one of the acousticians' options in low frequency control and are not uncommon in music rooms for critical listening. For instance, Swiss company PSI make the AVAA active sound absorber, which is a development of the basic arrangement pioneered by Olson [93]. They extend the method to use the output of the microphone's pressure measurement to generate a volume velocity signal which projects through a porous baffle after band-limiting takes place to ensure stability at the frequency range of interest, which is between 50-200Hz.

The AVAA active absorber was tested in various rooms at LSBU [94]. These tests were to independently verify that the system was capable of reducing modal peaks and dips in the room response at frequencies below 150Hz, where distinct, widely spaced room modes reside. However, the effectiveness of the active absorber was found to be limited with up to four being required to make any significant difference to an averaged sized control room. With each unit costing several thousand pounds, they remain an expensive option which may be

considered where space does not allow for great depths of porous absorber, or a retrofit solution is required for a small room.

2.7 Beyond Classical Control I

The previous sections outline the most common control approaches in music rooms, in the next sections we discuss some less frequently used approaches, some of which, such as quarter wave resonators are old and well-studied, but not used so often. Also discussed is a newly developed loss mechanism which may be applied to music rooms in the future.

2.7.1 Quarter-Wave Resonators

Quarter wave resonators are a type of cavity resonator, differing somewhat from the better-known Helmholtz resonators. Field & Fricke in 1998 [95] noted that they were comparatively neglected in the literature and presented qualitative and quantitative expressions for their resonant frequencies. In their description, the archetypal quarter wave resonator is simply a pipe or tube, closed at one end and open at the other. Under certain conditions the body of air confined within can be brought to resonance (see Figure 10).

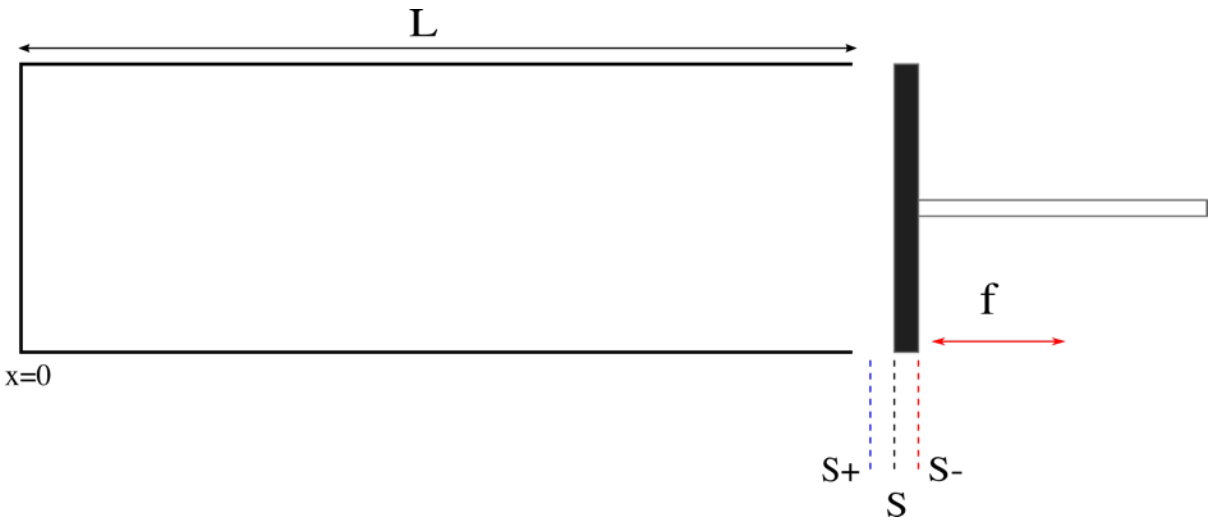

Figure 10: Basic arrangement of quarter wave resonator of length L. The piston source at the mouth oscillates at frequency f, between S_+ and S_-, with S being the equilibrium position. After Field & Fricke [95].

Under harmonic excitation, compressions and rarefactions of the source S travel down the tube, reflecting at the solid end x=0 and interacting with the next cycle of the source's motion at the mouth.

Motion of the source from S_0 to S_+ causes a compression to reflect and reach the mouth as the source begins its motion from S_0 to S_- when the wave has travelled twice the length of the tube, corresponding to half a wavelength. Thus,

$$2L = \frac{\lambda}{2} \; or$$

$$L = \frac{\lambda}{4}, \qquad \text{hence quarter wave resonance}$$

This also holds for any additional half wavelength of the source, so

$$L = \frac{(2n-1)\lambda}{4} \qquad \text{Eq 65}$$

where L is tube length in m, n = 1,2,3,…, λ is wavelength in m. Field and Fricke show this intuitive relation holds when derived from the wave equation.

Practically, quarter wave resonators are known in music as amplifiers for xylophone bars, and as organ pipes and woodwinds. Field & Fricke used them in a building acoustics context to mitigate fan noise in ducts. They summarise similar cases and review other industrial attempts, notably as enhancements to noise barriers.

2.7.2 Modal Coupling

A further assumption made when considering room acoustics is that the boundaries are either perfectly rigid or can be represented by a locally reacting impedance. In some lighter weight constructions, this is not the case, especially at low frequencies and the boundaries can exhibit plate modality of their own. These modes and those of the room or cavity couple to a greater or lesser degree, leading to energy exchange which can impact the room sound field.

Coupled mode theory was formalised for acoustics and vibration by Dowell & Voss [96], having previously been used in coupled transmission lines. Their formulation in acoustics expands the pressure in a series using the cavity modes and in-vacuo panel modes as basis functions for a system of ordinary differential equations.

Fahy [97] provided fundamental approaches to the problem, and Green's function and modal coupling approaches to the problem.

Later, Pan and Bies [98] [99] considered a concrete cavity, closed on five sides, with the sixth comprising an aluminium panel. The free modal frequencies of these elements are respectively

$$f_{l,m,n} = \frac{c_0}{2}\left[\left(\frac{l}{L_x}\right)^2 + \left(\frac{m}{L_y}\right)^2 + \left(\frac{n}{L_z}\right)^2\right]^{1/2} \quad \text{Eq 66}$$

$$f_{u,v} = 0.458 c_L h\left[\left(\frac{u}{L_x}\right)^2 + \left(\frac{v}{L_y}\right)^2\right] \quad \text{Eq 67}$$

where Eq 66 is the same as stated previously in Eq 30. c_L is the longitudinal wave speed of sound in the panel and h is the panel thickness in m.

The acoustical system is considered to be the combination of these two modal subsystems, with the proportion of energy on one or the other subsystem dictating whether a given mode is "panel controlled" or "cavity controlled". Most modes will be weakly coupled and can be ignored. There are two archetypal situations. Firstly, where a pair of modes are well coupled; in this case, the motion of the system is dominated by these modes. Alternatively, when no pair of modes is dominant, the energy of the system is distributed among many modes.

The panel modal density gives not only the number of panel modes in a given frequency band but also, together with mode shapes and boundary conditions, determines the resonance frequencies.

They summarise their findings thus.

- The degree of matching between the uncoupled mode-shapes of interacting elements determines energy exchange between the modes.
- If two modes are well matched, then the difference between their resonance frequencies determines the rate of energy exchange. On average, modal decay

times of low frequency cavity-controlled modes decrease as panel modal density increases.

- The resonance frequency of a cavity-controlled mode can be different to that of its corresponding uncoupled cavity mode, as panel modes can change the frequency of the cavity mode with which it interacts. (See [100])
- If the panel is thin and damping is low, then radiation through the panel can be an important source of losses.

Later, Davis [100] presented a simplified method for calculating system frequencies for coupled systems. In his scheme, a given geometry is analysed from the point of view of its mode shapes. A coupling parameter L_{jk} is calculated, which can be thought of as the spatial similarity of mode shapes in each subsystem. This, together with modal normalisation factors as defined previously by Dowell and Voss [96] and Fahy [97], enables calculation of a new parameter, ψ, which Davis describes as a measure of a structural mode's propensity to couple with an acoustic mode.

These two latter parameters are combined in a compound coupling parameter, β

$$\beta_{jk} = \frac{\rho_0 c_0^2}{\rho_p h L_{jk}} \psi_{jk} \qquad \text{Eq 68}$$

It can be seen that β_{jk} decreases with panel thickness, as might be expected, a thinner panel couples better with acoustic modes. This parameter may be used in Fahy's classical equation for system frequencies of coupled oscillators [97] .

$$\omega_{1,2} = \frac{1}{\sqrt{2}} \sqrt{\omega_j^2 + \omega_k^2 + \beta_{jk} \mp \sqrt{\left(\omega_j^2 + \omega_k^2 + \beta_{jk}\right)^2 - \left(2\omega_j \omega_k\right)^2}} \qquad \text{Eq 69}$$

Davis uses this method to discuss veering phenomena in coupled oscillators. This is illustrated by his example of the rectangular enclosure fronted by a flexible panel. The above methodology is used to create a parametric study for the interaction of the 1,1 mode of an aluminium simply supported plate with plate thicknesses from 0.1 to 6mm, and the 0,0,1 mode of an enclosure with dimensions 0.91x0.32x1.52m. When panel thickness is such that the in-vacuo panel modes and cavity modes are not well coupled, each system's natural

frequency is as predicted classically (see Eq 30). However, when their natural frequencies are close, their coupling causes them to "veer" away from their uncoupled frequencies.

Also, the resonant response in practice will be less than that predicted by an uncoupled analysis, as the latter fails to account for the fact the coupled system shares stored energy between subsystems. Thus, coupling produces two new coupled modes in which the oscillators either move in phase at a resonant frequency lower than, or in opposite phase at a resonant frequency higher than, either oscillator taken individually. This indicates the jump in the phase of the specific acoustical transfer impedance.

Lee, using a Finite Element approach, derived a model for the nonlinear coupling of a plate cavity system under large deformations. He noted that at certain frequencies a negative stiffness effect was observed due to the cavity's out of phase vibration of the enclosed air [101].

2.7.3 Pneumatic Structures

Pneumatic structures are a class of tensile structures which rely for structural integrity on the differential air pressure either side of an impervious membrane: this supporting pressure gives rise to loadbearing strength. While familiar in domestic settings as airbeds, bouncy castles and other leisure products, on a larger scale they have become common in the built environment, mostly for pavilions and other temporary structures. Such pressurised structures have interesting acoustic properties as noted from the early days of their use in architecture and which can be harnessed creatively.

2.7.3.1 Introduction

Chi *et al* [102] identify three basic arrangements for pneumatic structures.

Insufflated; where the building envelope is supported by a pressure differential with air pumped into the occupied part of the building creating an increased pressure within.
Aspirated; where the building envelope is supported by a pressure differential with air pumped out of the occupied part of the building, causing a lower pressure within.
Inflated; where the envelope of a building element is supported by a higher internal pressure, but the occupied part of the space is outside this element.

The first man-made pneumatic structures on a large scale were the early balloon experiments of the Montgolfier brothers in the late 1700s. The principle was first considered in an architectural context during World War 1 with a proposed design by Lanchester for an inflatable field hospital.

The earliest realised design was during World War 2 with the development of inflatable radomes designed to protect radar equipment from the elements, and with inflatable decoy tanks and trucks to confuse enemy reconnaissance efforts. After the war, they became a vogue strain in architecture, with, on the one hand the academic work of Frei Otto and on the other, radical and experimental movements such as the Utopie movement in France and Archigram in the UK, who appreciated their buoyancy and ephemerality [102].

This fitted into the broader trend of form-finding in architecture in which, starting in the late 19th century, architects such as Antoni Gaudi sought to move away from the pen and drawing board as generator of geometry. Rather he investigated novel and optimised structures through the associative relations between materials and shape; for example, his use of string and bead constructions or fabric constructions to create purely compressive vaulting [103].

The big moment for inflatables was the 1970 Expo in Tokyo where several pavilions used pneumatic construction.

While this type of architecture is especially suited to temporary structures, some subsequent large scale permanent uses included large span roofs for stadia such as Detroit's Pontiac Silverdome (1975) and the Minneapolis Metrodome (1982) but these proved costly to maintain and have fallen out of favour.

Tensile structures remain popular but large inflated and insufflated (supported by differential pressure from within the inhabited space) examples have generally given way to structures combining the concept with other structural elements such as cable-stayed domes; examples being the Millennium Dome (1999), the Eden Project (2000) and Barcelona's Media-ICT Building (2010). Smaller scale projects such as pavilions, art installations proliferate, and at least one insufflated concert hall, the Ark Nova has been built, to a design by Arata Isozaki and Anish Kapoor. This was designed to travel the regions of Japan devastated by the 2011 Tsunami and could accommodate 500 people for concerts and art exhibits [104].

2.7.3.2 Design

Design of pneumatic structures can be divided into three tasks

1) Form finding

Determining the equilibrium shape for a given stress distribution and boundary conditions. This gives a geometry in which only tension is present (see Figure 11).

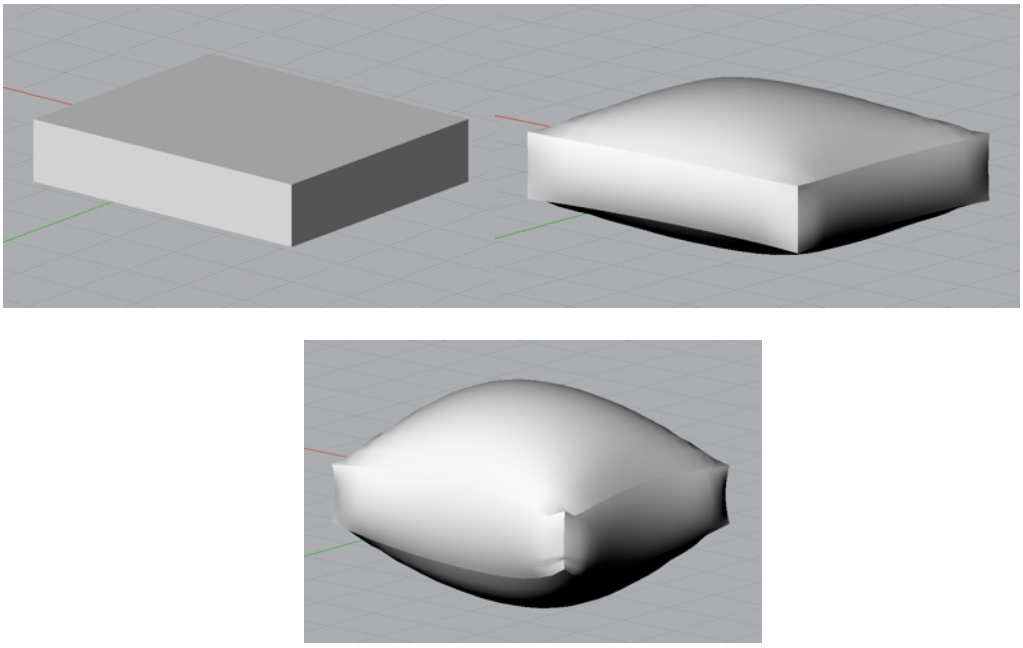

Figure 11: Basic airbed-like geometry uninflated (top L), subject to low inflation pressure (Top R) and high inflation pressure (bottom) – note nonlinearities at the edge in the latter.

This process sees the boundary deform to accommodate the increase in volume within. Strains within the material are generally small (highly inelastic materials such as Mylar are often used), and small nonlinearities such as wrinkles and folds will be an inevitable part of shape finding and these must be accounted for in structural or other analyses [105].

2) Static analysis

If required, structural analysis is performed numerically, with the aim being an even distribution of stress within membrane systems.

3) Cutting pattern

The geometry is divided into geodesic strips to create components from which the finished structure can be assembled [106].

2.7.3.3 Acoustics of Pneumatic Structures

Texts from the pioneering era of pneumatic structures make only brief mention of acoustic properties. Dent [107] notes (when referring to large, insufflated structures) that acoustic performance was poor, caused by the tendency of such structures to have concave internal geometry and hence create focusing effects and echoes. When considering small inflatable structures within conventional rooms, this drawback becomes a boon, with convex surfaces exposed to the room

providing naturally scattering tendency at higher frequencies. He also notes poor sound insulation properties due to low mass and stiffness. Herzog [108] echoes these comments but mentions that acoustic insulation behaviour was better than predicted. He also considers insufflated halls to be unsuitable for music and relates the experience of Brylka in creating a large (1900m^3) insufflated hall. This space had a measured 1.3s reverberation time from "100Hz to 1[k]Hz" (sic), lower than the desired 1.7s. In addition, bad flutter echoes were reported due to the concave internal geometry.

More recently, Kim *et al* [109], while trying to predict the acoustic performance of PTFE membrane roof structures, also found that low frequency absorption was greater than that suggested by impedance tube measurements of roof material samples.

2.7.3.4 Pneumatic Structures as Sound Absorbers

Generally, a pneumatic structure can be thought of as a membrane absorber, with the mass of the external envelope acting as an inertial mass, and the air within acting as a spring. However, there are certain differences between that idealised situation and the reality of inflatables. Firstly, a perfectly flat membrane can be built from rigid materials or conventionally supported membranes quite easily, but inflatables and other pneumatic structures are constructed with flexible materials which strive to take on an equilibrium shape which encloses the internal volume of air in the most tensile manner. Therefore, the simplest shapes for inflatables are a sphere or cylinder. Flat or panel-like shapes require constraining elements (yarns or drop-cords) to maintain their geometry, and these of course change the behaviour away from the archetypal flat membrane [110].

Adelman-Larsen *et al* has investigated the use of inflatables as low frequency absorbers in large rooms for amplified music [111]. This work has resulted in the FlexAcoustic series of commercial large-scale absorbers, generally of cylindrical shape – subject of a number of patents [112] [113] [114].

Early on in this work [111] [115] an analysis was made of commercial airbeds as a proof of concept. It was found that all airbeds displayed a peak in absorption around 300-400Hz and that low frequency performance varied considerably but increased greatly with airbed thickness (see Figure 12).

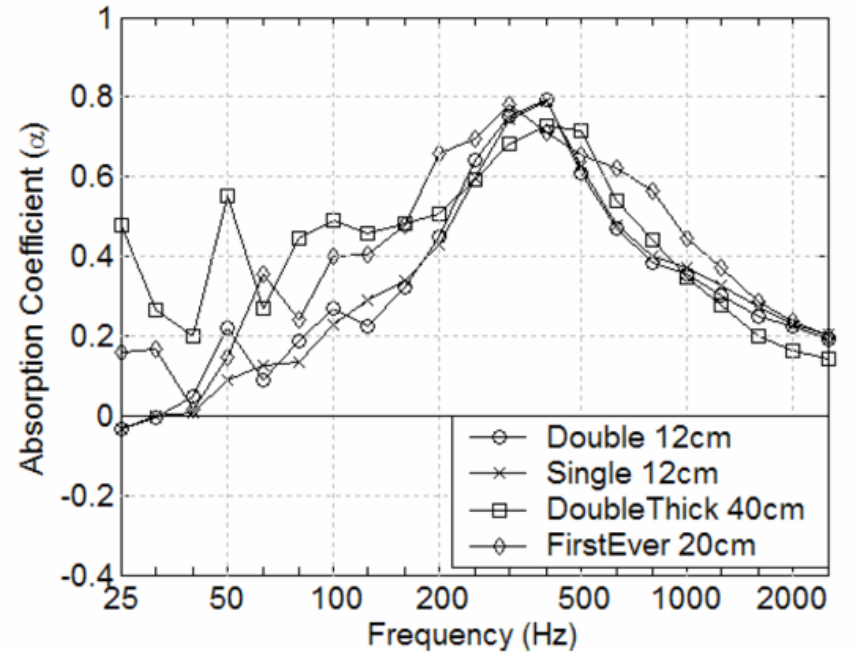

Figure 12: Larsen's experimental data comparing four brands of airbed using ISO354. Reproduced with the permission of the author [111].

2.7.3.5 Resonance Frequencies

Since pneumatic structures take on equilibrium shapes which are complex and curved, existing panel absorber analyses, based on panel mode shapes, will not be adequate for the whole surface. True shell resonances differ greatly from plane panel resonances due to curvature. For this reason, Soedel [116] warns that, even with complex numerical methods of analysis such as finite element analysis (FEM), inaccurate solutions can be produced, due to a lack of understanding of sensitivity to curvature.

2.7.3.6 Absorber Design

There is some research and practice showing that pneumatic structures are a suitable mid-to-low-frequency absorber [115]. In the most reductive analysis of an airbed, it will act as a membrane absorber, with the outer surface acting as a mass and the air trapped inside as a spring. The resonant frequency of a simple

membrane absorber in front of an air-filled cavity is generally predicted using the following relation.

$$f = \frac{60}{\sqrt{md}} \qquad \text{Eq 70}$$

where f is the resonant frequency in Hz, m is the unit mass of the membrane in kgm^{-2} and d the depth of the absorber in m.

It is known that this expression, a much-simplified analysis of membrane resonance itself, can give inaccurate predictions, even in simple membrane designs, especially where the nature of any damping materials can change the resonant frequency [69].

Adelman-Larsen *et al* tested air mattresses during the development of the Flex Acoustic inflatable absorbers used in large venues for amplified music [117]. They noted a very large divergence from classical membrane behaviour, noting the resonant frequency to be around four times that given by Eq 70 while recognising that the complexity of construction renders the concept of a single resonant frequency as being reductive [111].

The construction of air mattresses and airbeds can vary considerably, but generally comprises two flat membranes connected by a collar which connects them to complete the bed shape. Of course, being a pneumatic structure, when inflated, it seeks to take on a purely tensile shape. If the airbed shape was left as described, then upon inflation it would initially bulge at the edges, and as internal pressure increased it would approach a shape close to a sphere (see Figure 11). To prevent this deformation, the faces are constrained by arrays of drop cords or by plane members. These act as anchor points and the geometry often bulges between them, creating shell rather than truly box-like shapes.

These constraining elements, whether simple ties or plane elements, can also act to add extra moving mass or damping and lead the structure to be quite different from the archetype of simple membrane analysis, although it is assumed that in

low pressure inflatables like airbeds, mass inertia remains the dominant mechanism.

2.7.3.7 Inflation

In a conventional membrane absorber, the air within the cavity and outside the membrane is considered to have equal pressure. An inflatable structure has a higher pressure inside than out. The effect this has on absorber performance is considered here.

The impedance of air is given by

$$z = \rho_0 c_0 \qquad \text{Eq 71}$$

where z is the impedance in $kgm^{-2}s^{-1,}$ ρ_0 is the density in kgm^{-3}, and c_0 is the speed of sound in air in ms^{-1}. While the speed of sound - given (in $ms^{-1)}$ for air by $c_0 = 331.4 + 0.6T$ where T is temperature in Celsius - changes only due to changes in temperature; in the airbed, it is assumed that any increase in temperature due to inflation will dissipate to the environment over time and can be neglected in the time periods being considered. Density, however, changes in accordance with the molar form of the ideal gas law, expressed in terms of the specific gas constant R_S

$$\rho = \frac{P}{R_S T} \qquad \text{Eq 72}$$

Thus, density increases linearly with pressure, therefore, by Eq 71 the air inside an inflatable has a higher impedance than that at atmospheric pressure.

Neglecting material stiffness, a unit portion of the envelope of an inflatable is, although held in equilibrium by internal and external pressures and by the tension of the membrane, subject to the spring force of the air either side of it opposing its motion (see Figure 13).

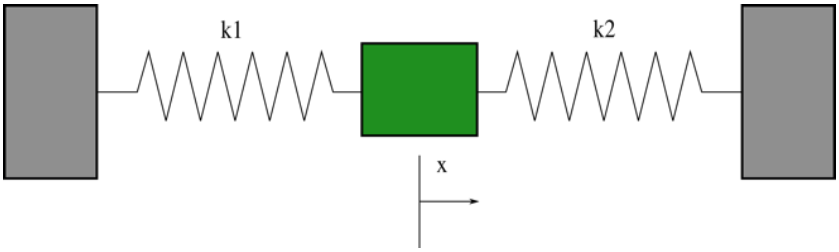

Figure 13: Mass/two-spring system.

Assuming mass inertia is the dominant mechanism in an inflated airbed, absorption, through resonance, comes with that mass forming part of a mass-spring system, with the enclosed air forming the spring of the system.

Air's "springiness" is defined by its bulk modulus, κ. This describes the volume strain of a unit volume of gas under a pressure load. Under Laplace's adiabatic assumption for an ideal gas, which is valid for air, the constant entropy modulus κ_S is used, given by

$$\kappa_S = \gamma p \qquad \text{Eq 73}$$

where γ is the ratio of specific heat capacities or adiabatic ratio, 1.4 for air. [118] The normalised impedance of a gas can thus be expressed as

$$Z_S = \frac{\sqrt{\kappa_S \rho_S}}{S} \qquad \text{Eq 74}$$

where S is the surface area and ρ_S is the density of the air. The relationship between density and pressure is expressed using the ideal gas law in the form [119]

$$\frac{p}{\rho T} = R = constant \qquad \text{Eq 75}$$

So, if pressure is doubled, and temperature is assumed to be constant, as it would be as any added heat due to inflation would eventually dissipate to the outside of the bed, then density would also increase by a factor of two.

So, the impedance in the airbed under inflation can be estimated as

$$Z_{airbed} = \frac{\sqrt{(Rp).(p^2(\frac{R}{T}))}}{S} = \frac{\sqrt{p^3\left(\frac{R^2}{T}\right)}}{S}$$

Therefore, a doubling of pressure gives an increase in Z of $2^{\frac{3}{2}}$. At higher pressures this can cause a very large increase in impedance, however, airbeds are fairly low-pressure structures and at low inflation, the increase in impedance is close to proportionate to pressure. In practice, the complex geometry of an airbed may cause some deviation from this general behaviour as the effect of cross members and geometrical effects also contribute to impedance. Thus, a

thorough analysis of a given structure is difficult and would require complex FEM modelling. Since this thesis is primarily concerned with experiment, such models are considered beyond its scope.

2.8 Beyond Classical Control II

Previously the use of resonant panels and membranes in the control of vibrations has been discussed. This comprises coupling a linear oscillating system of interest (such as the modes within a cavity or room) to a linear inertia attachment (such as a panel or membrane absorber). This system can be visualised as a mass-spring system with masses x and y, and a coupling term ε (see Figure 14).

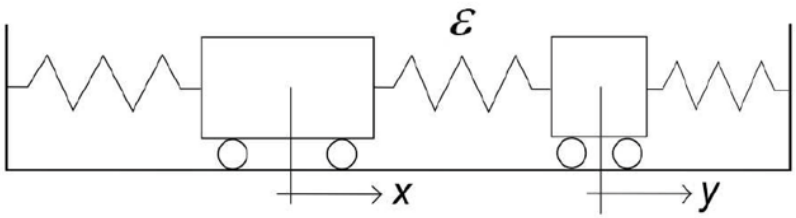

Figure 14: Linear 2 degree of freedom system. From Bellet [120]. Reproduced with permission.

This attachment inhibits oscillations of the main system by providing a reaction force equal and opposite to the driving force at the design frequency.

However, undamped linear attachments are not always desirable as their frequency range of operation is so narrow. Damping can broaden this at the expense of reducing absorbing efficiency and designing systems with accurate damping characteristics can be problematic. Over time attempts have been made to harness nonlinear behaviour to modify vibration characteristics.

2.8.1 Nonlinearity and Nonlinear Normal Modes

Linear normal modes have a number of properties which simplify their use.

- *Invariance:* If one mode alone is excited, all others remain quiescent (still) for all time.

- *Superposition*: All free and forced oscillations can be expressed as linear combinations of individual modes.

However, linearity is an ideal behaviour, an exception rather than the rule in nature, and many problems deviate from this ideal. In nonlinear systems, conventional analysis relying on the principles of invariance and superposition will not yield accurate results. Often, real world systems defy analytical approaches, and numerical or approximate methods are used, often to visualise complex behaviour, mainly using phase space (displacement-velocity in 2D or displacement 1-velocity 1 – displacement 2 in 3D) or configuration space (input – output) or the Frequency-Energy plot, which makes explicit the frequency-amplitude relationship apparent to the eye.

The concept of Nonlinear Normal Modes (NNMs) was coined by Rosenberg in the 1960s [121]. He proposed them as a framework for dealing with many nonlinear dynamic problems, but with a conceptual relationship to the familiar linear mode; he defined them as a vibration in unison, or synchronous oscillation of a system. They remained a curiosity until revived in the 1990s by Vakakis *et al* [122] and Shaw & Pierre [123], since when a sizeable literature has been created. Kerschen *et al* and Peeters *et al* provided a summary and a comprehensive explanation of nonlinear modes in 3D phase space in [124] and [125].

2.8.2 Nonlinear Frequency Response

A key characteristic of nonlinear oscillations is hence the frequency-amplitude interaction, whereby the resonance frequency is dependent on the amplitude of excitation. Figure 15 shows the influence of the nonlinear term in the equations of motion, α being a term which governs the direction and magnitude of the nonlinearity, where $\alpha = 0$ gives a linear spring (in green), $\alpha > 0$ gives a stiffening spring (in red) and $\alpha < 0$ gives a softening spring (in blue).

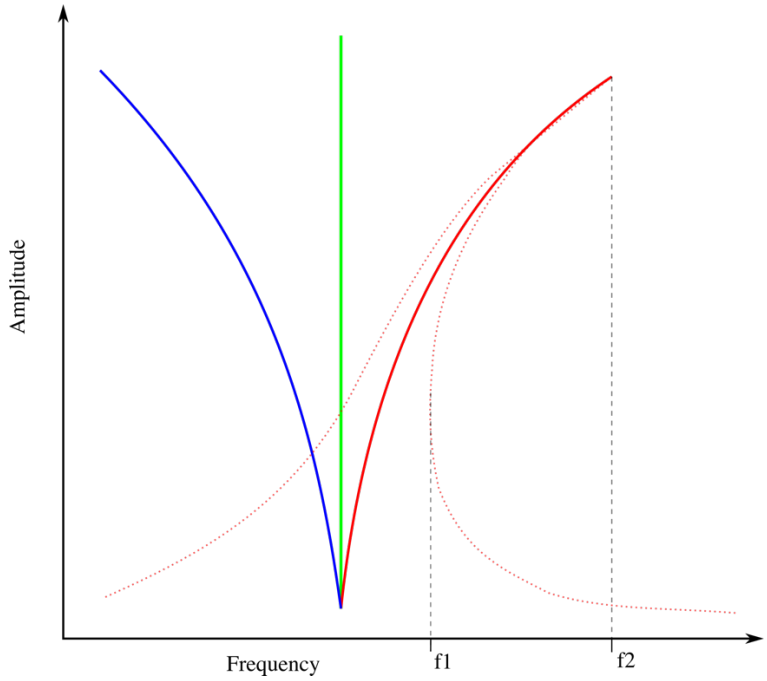

Figure 15: Amplitude vs frequency/driving frequency for nonlinear springs. Linear spring (green), stiffening nonlinear spring (red) and softening nonlinear spring (blue). The dotted red line shows a typical mode shape for the system with a stiffening spring. "Jump" phenomena are possible between frequencies f1 and f2 where two system states exist for a given frequency.

The bending of the frequency response curve to the right for a stiffening spring and to the left for a softening spring give rise to "jump" phenomena, whereby at certain frequencies, two states of resonance are possible, and where if the exciting frequency is slowly increased, the response "jumps" e.g., between higher and lower amplitude states in Figure 15.

Practically, then, one consequence of nonlinearity is that unicity is lost, and a number of solutions may exist for a given condition, raising the question of which solution is relevant under a given condition, and whether a solution is stable or unstable. Mathematically, this means that closed form solutions are the exception, and numerical methods must be used. Unlike in LNMs the dependency on the total energy of the system prevents the separation of time and space in the equations which complicates NNM analysis.

Neither are jump phenomena the only curiosity of nonlinearity, with other complex behaviours including, bifurcations, saturation, subharmonic and superharmonic resonance, resonance captures, limit cycles, modal interactions and chaos.

In nonlinear systems, several researchers have noted modal interactions which differ from that predicted by classical theory. Nayfeh & Chin report energy transfers from high frequency modes to a low frequency mode in a flexible structure in which large deformations can occur [126]. This is caused by the excitation frequency being close to the sum or difference of two linear system modes, and the nonlinearity of the system causes closely spaced modes to interact. They also report the experiment of Haddow & Hasan who, when parametrically exciting a flexible cantilever beam near twice the frequency of its fourth mode, observed the mode losing stability and the beam's motion becoming chaotic, and as a result, energy "seemed to cascade" down the modes, ending up in a very low frequency component [127].

2.8.3 Nonlinear Frequency Analysis

Since superposition is lost in nonlinear systems, Fourier analysis is no longer a valid approach. Various methods exist to replace it, with the Harmonic Balance Method being commonly used analytically, where nonlinear terms of ODEs are expanded in a series into a series of simultaneous harmonic equations. [128]. Experimentally, Wavelet or Hilbert space methods are preferred to replace FFT imaging, which relies on superposition. Of the latter, the Hilbert-Huang Transform is the most robust. The time series is decomposed using the Empirical Mode Decomposition method (EMD) into a series of Intrinsic Mode Functions (IMF) plus a residual (trend) function, which can be Hilbert transformed for spectral content. The EMD method identifies empirically the intrinsic modalities within the data based on their characteristic time scales within the data [129]. Debauchies *et al* developed the Synchrosqueezed Continuous Wavelet Transform which uses a reallocation method to "sharpen" the time-frequency response of the Continuous Wavelet Transform method to give a fidelity comparable with the Hilbert-Huang method [130].

2.8.4 Targeted Energy Transfer

In 2001, Gendelman *et al* and Vakakis & Gendelman produced three papers presenting a new loss mechanism utilising nonlinear oscillators. Christened Energy Pumping or Targeted Energy Transfer (TET) in [131] and [132], they define the dynamics of the problem in Hamiltonian terms and identify the mechanism of the interaction as Resonant Capture in [133].

Resonant capture can be thought of as a passing resonance, indeed it is most commonly discussed in the context of orbital mechanics, when celestial bodies come close enough to be within each other's gravitational influence. Likewise, when two oscillatory elements of a dynamical system come close in phase space, they interact, and under certain instances they can be locked into a close resonance for a while, before moving away from each other. The key is that energy exchanged by a short resonant interaction can be carried away from the site of that interaction [134].

Under such conditions, a nonlinear attachment to a linear master system could, under certain excitation conditions, be made to act as a Nonlinear Energy Sink (NES) and thus damp the master system over a wide frequency range. Kerschen *et al* analysed the phenomenon in terms of NNM's in 2005 [135].

In real-world vibration problems, it is normally undesirable to excite nonlinear normal modes for safety reasons, but a localised NNM in an attachment could absorb dangerous vibrations of the linear system and prevent them propagating in the system.

Bellet introduced TET by first describing a pair of undamped linear oscillators x and y (mass/spring pairs) coupled by a coupling coefficient ε, (where 0 is no coupling and 1 is perfect coupling) as seen in Figure 14. If $\varepsilon = 0$ then there is no coupling, and if the two subsystems have differing resonant frequencies; giving x an initial velocity of 1, the response is that x oscillates uniformly indefinitely, and almost no energy is transferred to y.

Setting the resonant frequencies of the subsystems close to one another ($\omega_1 = 1, \omega_2 = 0.98$ rads/s) and adding a small amount of coupling to this system ($\varepsilon = 0.05$) causes an exchange of energy to take place by beating (see Figure 16).

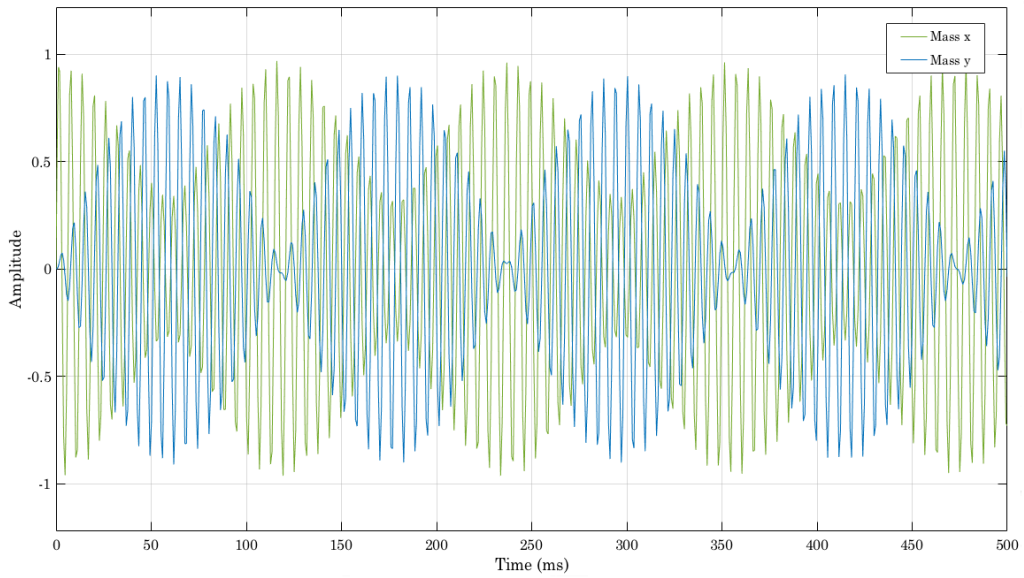

Figure 16: Lightly coupled linear mass-spring system. Equal exchange of energy through beating. (After Bellet [120]. Reproduced with permission).

If damping is added to the system, then we again observe a strong exchange of energy, but now the damping of the system causes the amplitude of oscillation to progressively reduce, and with it the beating frequency (see Figure 17).

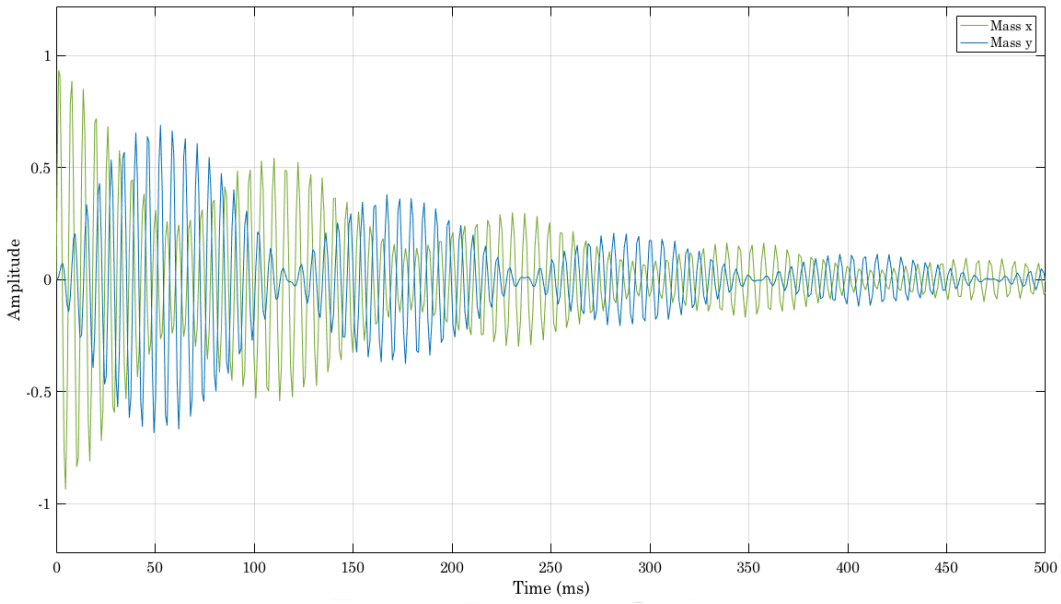

Figure 17: Damped linear mass spring system. (After Bellet [120]. Reproduced with permission).

So, resonance is required for energy exchange. The goal of TET is to create a targeted exchange of energy, then stop it, localising the energy away from the

primary system. For this to happen, the exchange of energy which occurs under resonance must be stopped in one direction. For a linear oscillator, frequency does not depend on amplitude (see Figure 18).

Figure 18: Linear oscillator, frequency does not depend on amplitude; the resonant frequency ω_0 is unchanged by system amplitude. (From Bellet [120]. Reproduced with permission).

In the presence of a strong nonlinearity, frequency increases with amplitude (in the case of a hardening nonlinearity) (see Figure 19).

Figure 19: Nonlinear spring; frequency-amplitude dependency. (From Bellet [120]. Reproduced with permission).

So, in the complete system, the linear and nonlinear subsystems interact at an elevated operating amplitude at which energy exchange can occur through resonant capture (see initial beating region at 0-120ms in Figure 21) but instead of the energy dissipating at that operating frequency as it would in a purely linear system, the presence of damping in the nonlinear system causes the energy to dissipate through decreasing frequency to zero (see 200ms onwards (blue line) in Figure 21).

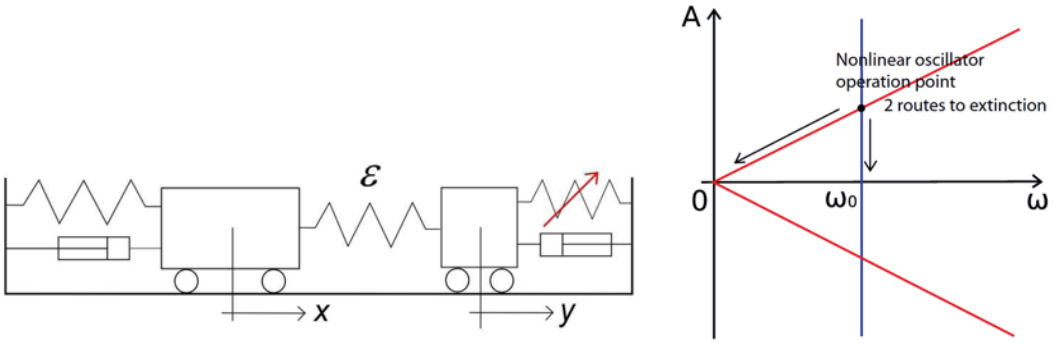

Figure 20: Combined system. (From Bellet [120]. Reproduced with permission).

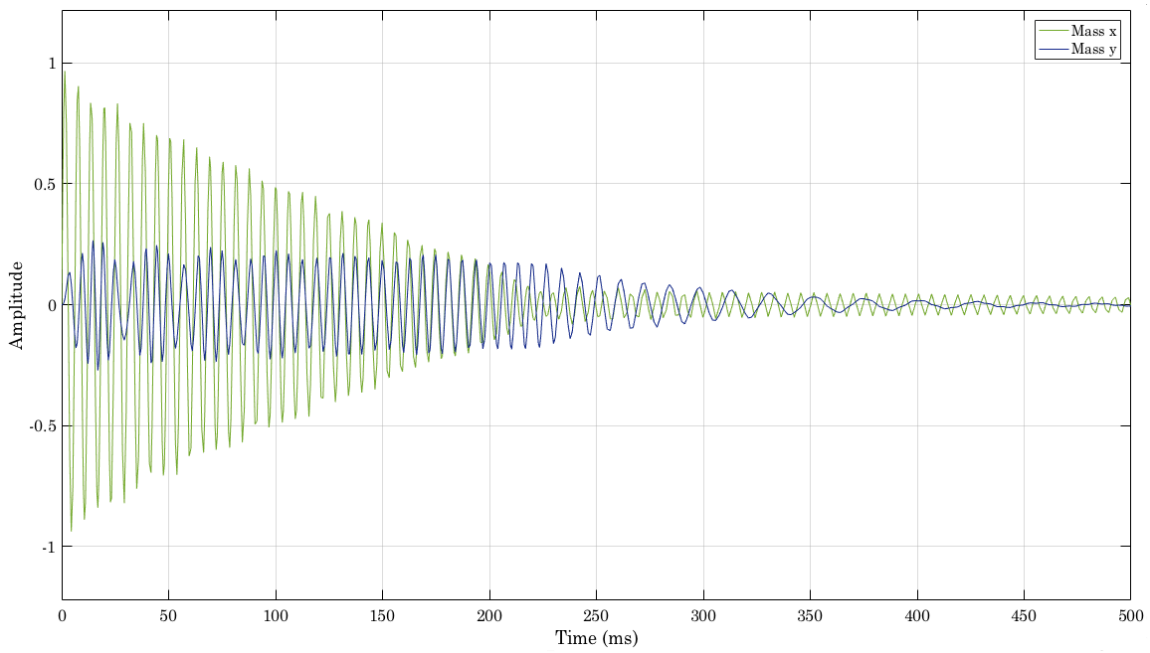

Figure 21: Complete system response; energy pumping. (After Bellet [120]. Reproduced with permission).

Fundamentally, TET is about localising energy in attachment, and breaking the exchange of energy between elements. This can only happen within a certain energy range, known as the operational plateau, and this is a characteristic feature of TET.

In a numerical and analytical study, Kerschen *et al.* identified three dynamic regimes in which resonant capture and hence energy pumping can occur.

1. Fundamental energy pumping, where the linear system and the attachment are in a 1:1 in-phase resonance at frequencies lower than the natural frequency of the linear system (ω_0).

2. Subharmonic – similar to 1) but along lower branches of the NMM.

3. Nonlinear beat pumping, where strong pumping is initiated above ω_0 by nonlinear beating [135].

McFarland *et al* demonstrated the phenomenon experimentally in the context of vibration mitigation, with a spring array acting as a near-cubic nonlinear spring [136].

2.8.5 Targeted Energy Transfer in Acoustics

In 2006, Cochelin *et al* [137] published a note on the observation of TET in an acoustic system. It comprised a circular duct with a sound source mounted at one end, an elastic membrane sample mounted via a coupling box at the other.

Pressure was measured at the centre of the pipe, as was the motion of the membrane. In addition, the signal being relayed to the loudspeaker was measured for a timing reference. His results show that, at a lower excitation level, the primary, linear system, in this case the acoustic mode of the pipe, decayed exponentially over more than two seconds. At an excitation level above the TET threshold, the nonlinear attachment makes large motions, sinking energy away from the primary system, which decays linearly to near zero energy in 1.6 seconds.

Bellet *et al* followed this work up with a more systematic exploration of acoustic TET, using a refinement of Cochelin *et al's* rig.
Using a specially constructed apparatus, they confirmed the cubic nonlinear stiffness of the hyperelastic membrane. They observed several regimes depending on excitation level.

1. Below a lower energy threshold S1, energy is stored in the acoustic mode and the membrane makes small oscillations close to NNM S11-.

2. Above a second threshold (S2>S1), the vibration is concentrated in the membrane as NNM S11+

3. In between these thresholds the motion is modulated, but with strong irreversible flow of energy into the membrane – known as the "strongly modulated response" indicating efficient energy pumping.

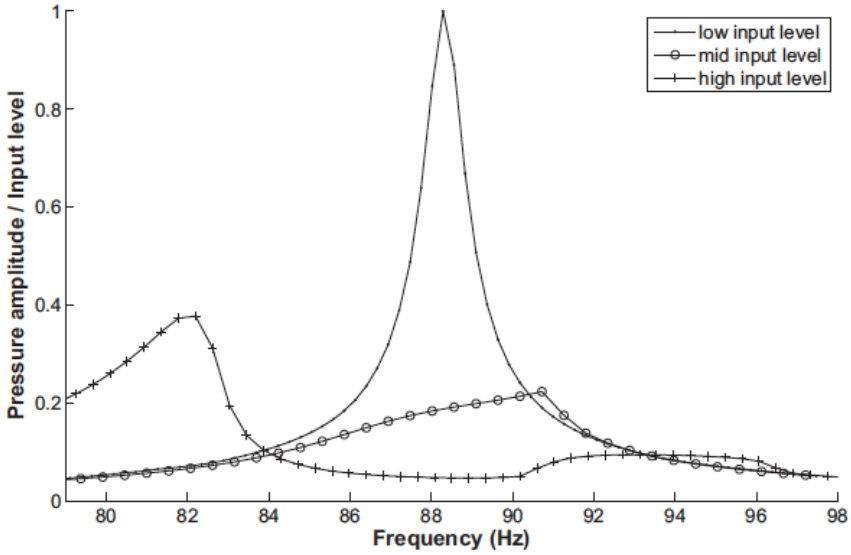

Figure 22: The three excitation regimes: Energy pumping maximised at mid input level [138]. Reproduced with permission.

Bellet *et al* then successfully extended the operational plateau of the system by using several membranes in parallel, with identical membranes serving to extend the useful pumping region most [139].

Shao & Cochelin, in [140] developed an analytical solution for the design operating point for a membrane mounted within a parallelepiped enclosure, and a numerical solution for the upper threshold where periodic responses begin to undermine energy pumping. In [141], Shao & Wu perform a parametric analysis of the system and determined that such energy sinks are best placed in corners to efficiently couple with room modes. This parametric analysis also showed that there was a linear relation between operating range and membrane thickness.

More recently Iurasov has moved away from "classical" TET and developed an attachment with a bistable dynamic response for vibration mitigation [142].

2.9 Summary of Finds and Gaps in Knowledge

Standards and guidance documents for the design of music rooms all agree that the low frequency range is critical for a favourable perception of music within a space.

There are three broad categories of treatment available to the acoustic designer concerned with the low frequency problem. Porous absorbers excel at higher frequencies unless used in great depth, which is impractical in most spaces. Also, since they tend to absorb all frequencies above a certain cut-off frequency, their utility at correcting a low/high frequency balance issue is moot. Membrane absorbers are efficient at low frequencies, but unless heavily damped, their absorption occupies a very narrow frequency range which is rarely what is required. For wide band application, an array of such membranes must be designed. This design is complicated by the fact that performance has proved difficult to predict for highly damped or thick membranes. Resonant absorbers such as Helmholtz and Quarter Wave Resonators, can be used to target low midrange frequencies if of moderate size, but again absorption is in a narrow frequency band and likewise damping and the use of arrays can widen the effective frequency range.

Newer designs such as perforated and micro-perforated panels are only applicable to higher frequency ranges, most metamaterial solutions to date are likewise for higher frequencies and often only within a very narrow frequency range. Inflatable absorbers have shown promise in the low frequency range but those tested so far are for very large-scale venues. Nonlinear materials again show promise but are yet to be tested in practice.
Together these form the designer's palette for control of sound in music rooms. Options are limited at low frequencies, especially lightweight solutions and this remains a key knowledge gap.

3 Case Study A: Room Boundaries

This chapter investigates the absorbing qualities of the fittings and construction of a music room. The chapter starts with a description of the hall, gives an acoustic assessment and determines the suitability of the hall. This is followed by an investigation to reproduce the effect of room geometry using both physical means and a modal model. Explanations are offered in the final section with comparison to a wave-based computer simulation; solutions are then discussed.

3.1 Introduction

A recital hall was assessed for suitability for chamber rehearsal and performance. This was a beautifully finished new hall, which was receiving complaints from professional musicians concerning an unusual acoustic. The author was asked to undertake measurements in the hall and to carry out an acoustic assessment. The professional musicians who had used the hall related that the hall became more usable when curtains were drawn but this ruined the aesthetic. Prof Steve Dance and two MSc Acoustics students assisted with logistics during measurement sessions.

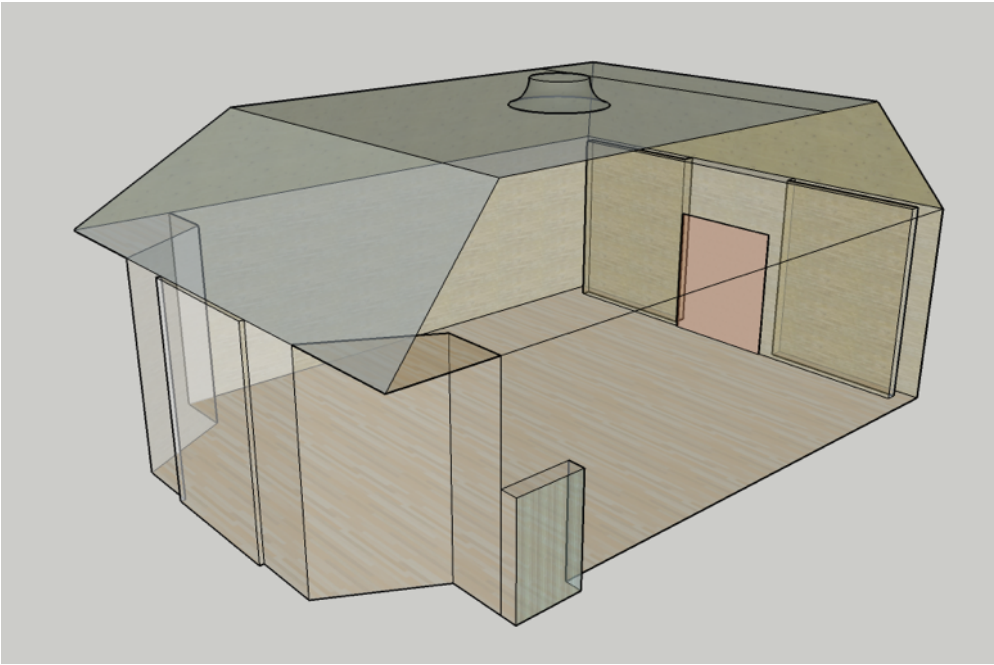

Figure 23: Basic arrangement of the recital hall.

3.2 Measurement of the Hall

A newly built recital hall was measured by the author; it was found to have a volume of approximately 690m^3. It could accommodate around 100 people in temporary seating using steel framed chairs with shallow padding on the seat and back (see Figure 24). The hall is used for performances, rehearsals and occasionally for lectures. The interior is oak-panelled with the behind cavity filled with mineral wool, the oak being perforated in some parts of the hall around the stage and ribbed throughout in a quasi-random diffuser type pattern with 5cm deep ribs spaced between 2 and 5 cm apart. The roof is 6m high and had a recessed skylight; the upper 2m are canted inwards. The canted part above the stage is angled inwards more acutely to act as a reflector to help projection to the back of the hall and was necessary to meet planning considerations concerning the skyline of the building. The 11.3m length is reduced at the edges of the room flanking the stage by angled doorways leading to a green room, a studio control room and storage areas for seating. The width is 9.6m (see Figure 24).

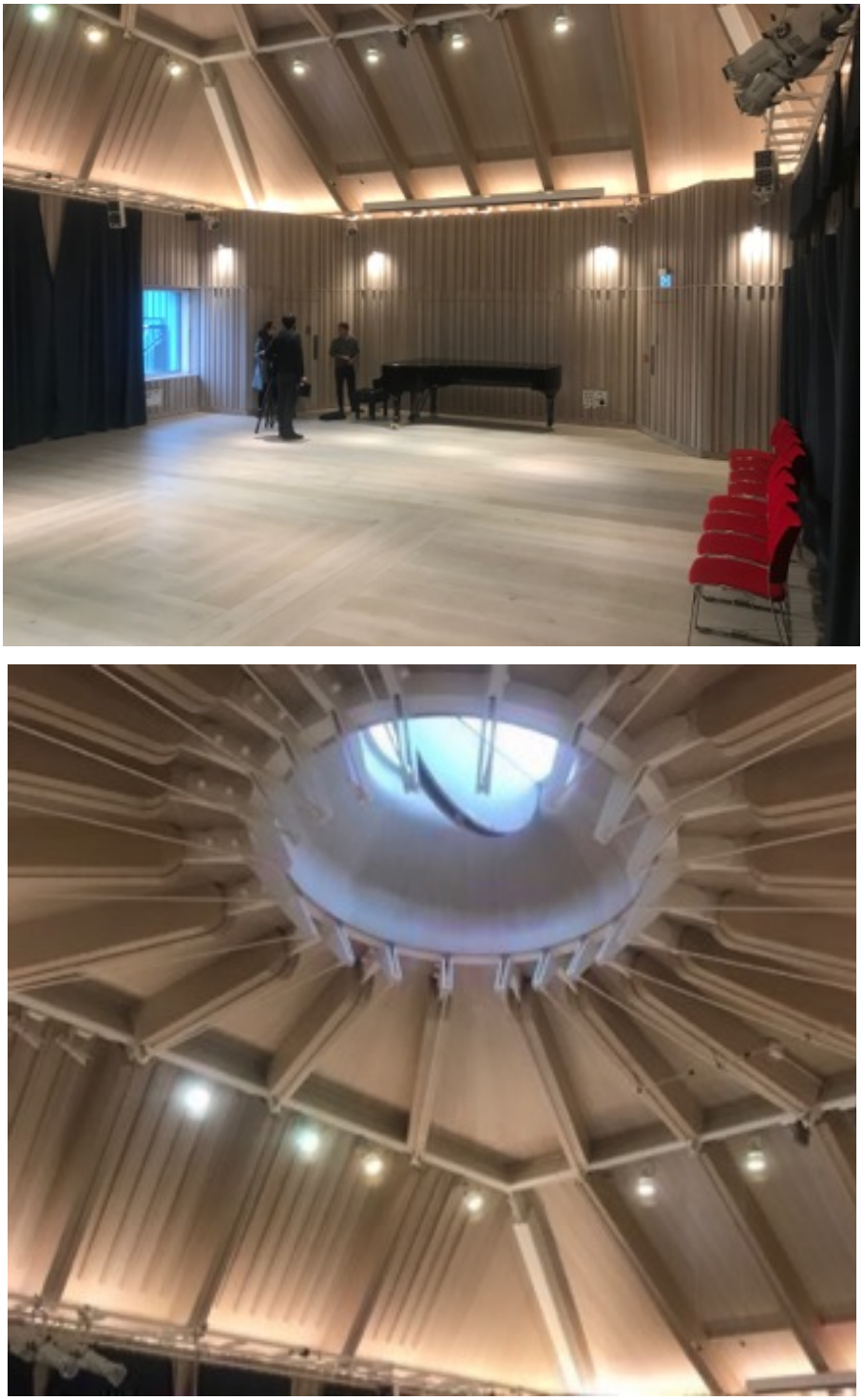

Figure 24: Interior of recital hall looking from the rear of the hall, and detail of the skylight.

The acoustic response is adjustable by moving the curtains along rails installed at the back and sides of the room. When not in use, the curtains are stored at the back of the room behind two false walls 4m high by 3m wide each side of the entrance doors (see Figure 25).

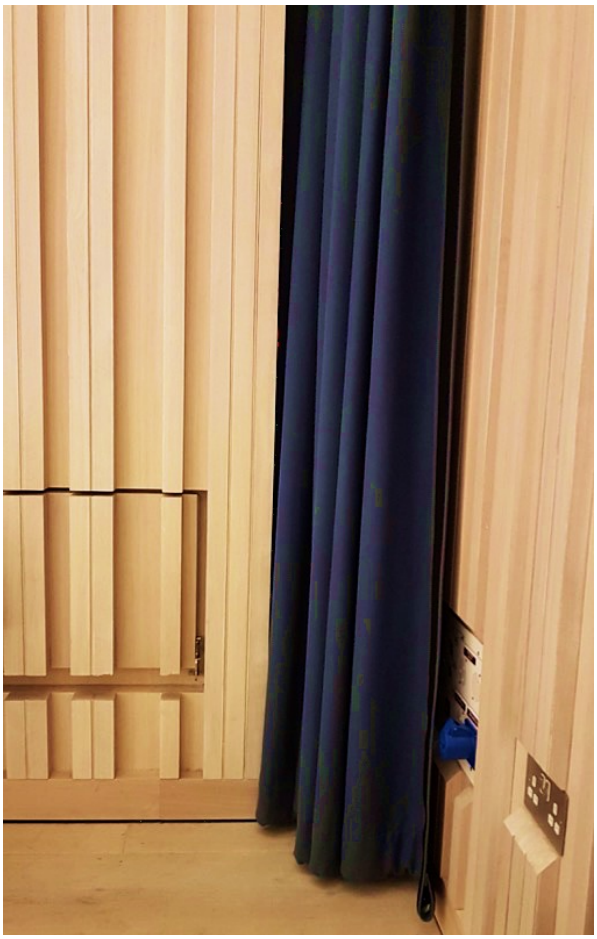

Figure 25: Curtains emerging from their storage position behind the false wall.

The gap behind the wall was 0.26m and the thickness of the wall is 0.203m including studwork on the inside of the cavity. The gap to the side wall was 0.365m on each side. There is a small access door on each fake wall (see Figure 26).

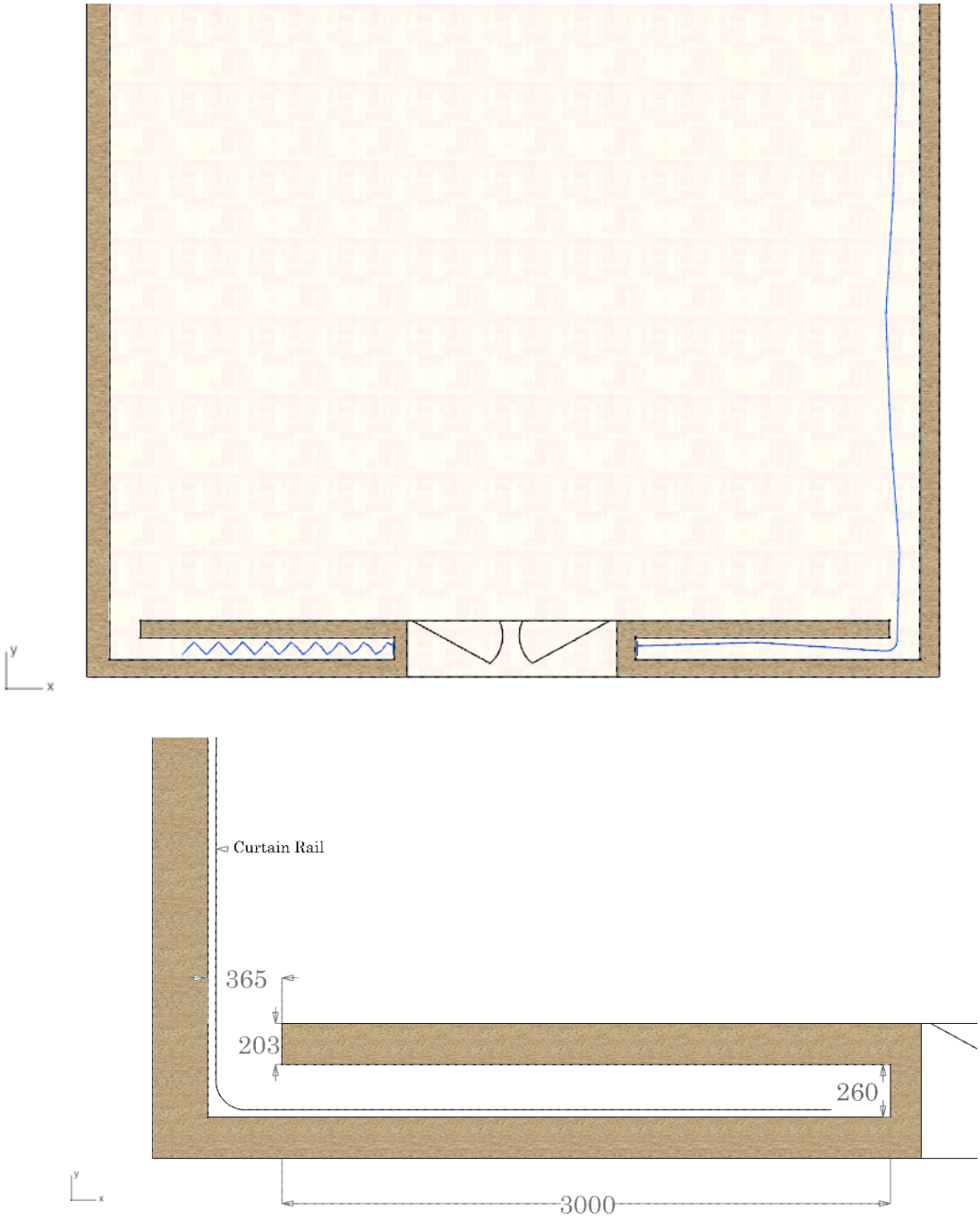

Figure 26: Top view of the recital hall false wall, showing (top) position of curtains, stowed at left, deployed at right, (bottom) dimensions of cavity in mm and the path of the curtain rail.

3.2.1 ISO 3382-1 Room Measurements

Acoustic measurements were undertaken in the hall to establish baseline acoustic room responses in different usage conditions and to confirm the hall's suitability for purpose.

Reverberation time (T_{20}) measurements were undertaken in accordance with ISO 3382-1 [143] using the integrated swept sine method measuring from 40Hz to 8kHz, with measurement positions as shown in Figure 27.

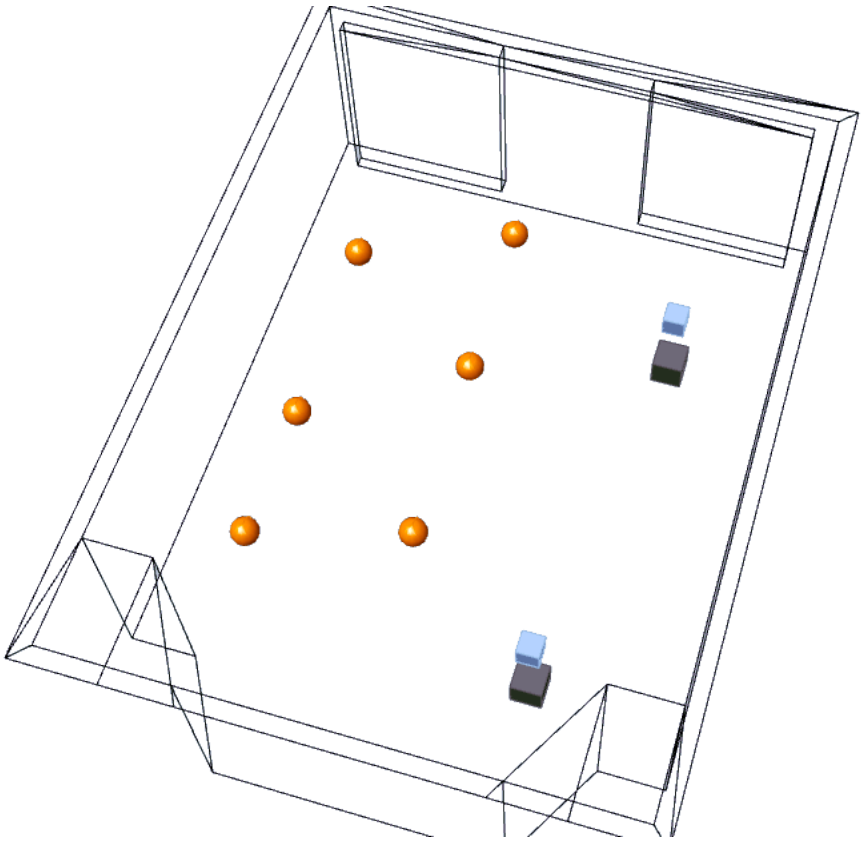

Figure 27: General arrangement of the recital hall showing dodecahedral and subwoofer source positions (blue and grey squares respectively) and receiver positions (orange spheres).

Background noise was measured as NR26 using a Norsonic 140 sound level meter and is presented in Table 3: and Figure 28. This is slightly (1dB) over the guidance given by Barron [66] for recital halls with audience size under 500. The dominant sound source was at its maximum in the 2000Hz octave band and came primarily from turbulent airflow from air conditioning outlets which line one long wall.

Frequency (Hz)	31.5	63	125	250	500	1000	2000	4000	8000
BG (SPL)	51.50	41.86	31.19	25.82	26.49	23.49	22.45	18.36	15.12
NR Band	-2	9	10	14	22	23	26	24	22

Table 3: NR data for background sound levels in the recital hall.

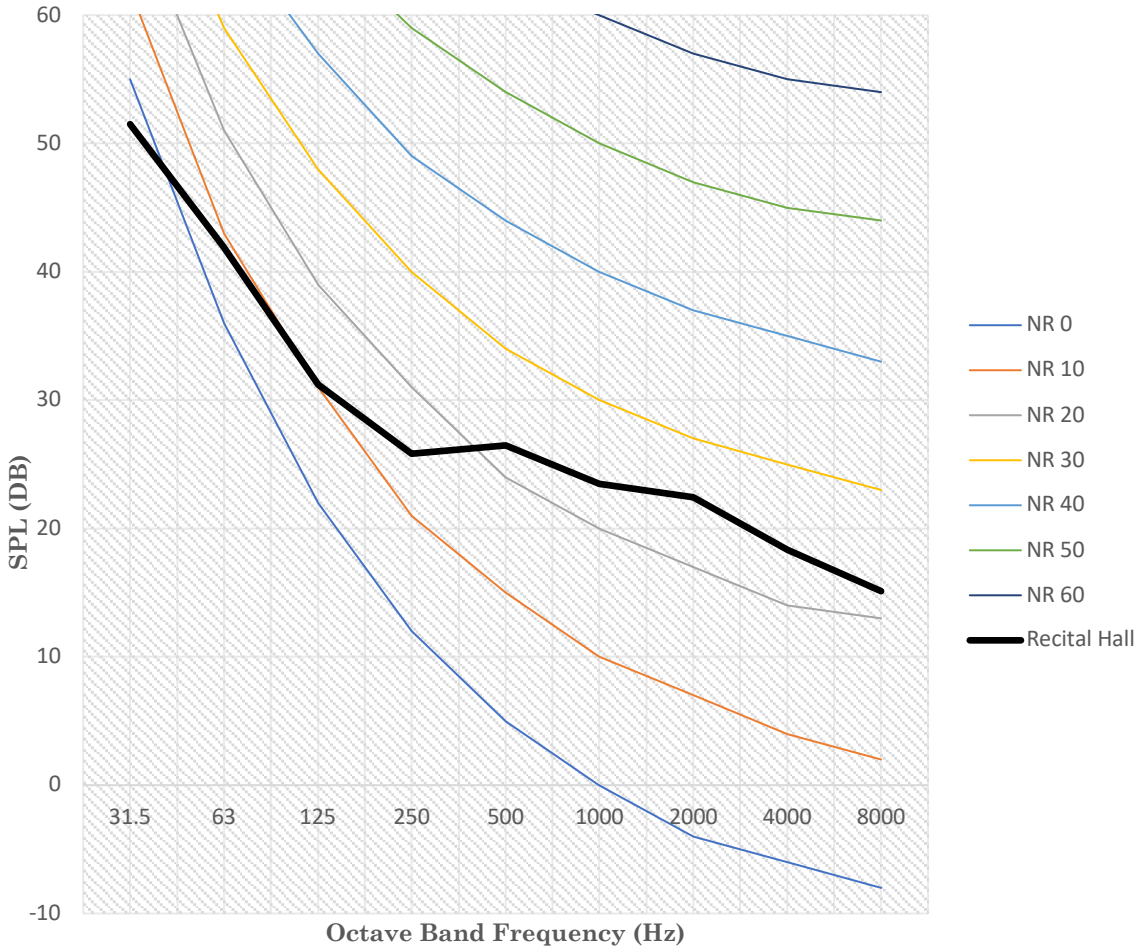

Figure 28: NR Curve for the recital hall.

Two source positions and six receiver positions were tested, each with both a dodec loudspeaker mounted 1.5m above floor level (see Figure 29) and a JBL subwoofer placed on the floor. The microphone was an Earthworks M30/BX, a Norsonic NOR 280 Power amplifier was used with the dodec and a Devine D-600 hi-fi amp was used with the subwoofer due to its unfiltered low frequency reproduction. Measurements were captured on a PC laptop running WinMLS software and analysis conducted in both octave and 1/3 octave bands, with averaging and graphing taking place in Microsoft Excel.

Figure 29: Measurements being undertaken in the hall.

The hall was initially tested in the condition as found upon arrival, with curtains fully deployed. This is the condition preferred by professional musicians who use the room. Fittings were minimal, with around 18 chairs around the perimeter of the room and a Steinway grand piano the only fittings, with four people present. This agreed with the stated typical usage condition. The measurement was then repeated with curtains stowed. Reverberation time results are shown with standard deviations (SD) in Figure 30 using the dodec sound source and in Figure 31 using the Subwoofer only for the curtains stowed condition.

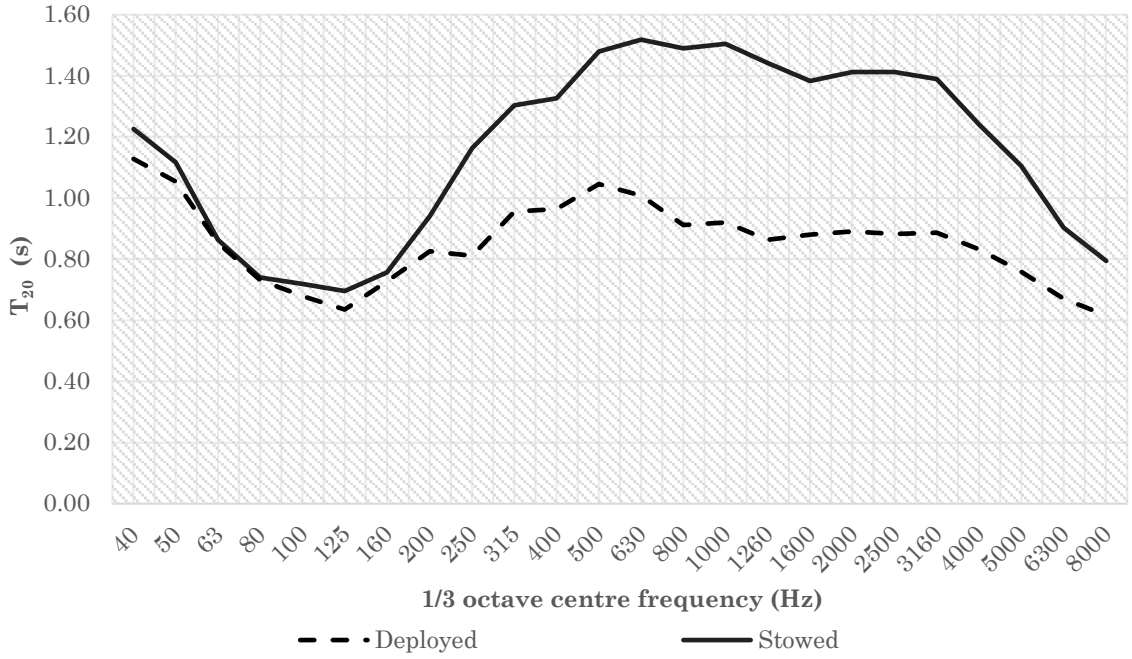

Figure 30: T_{20} in the recital hall, showing the dependence on curtain position.

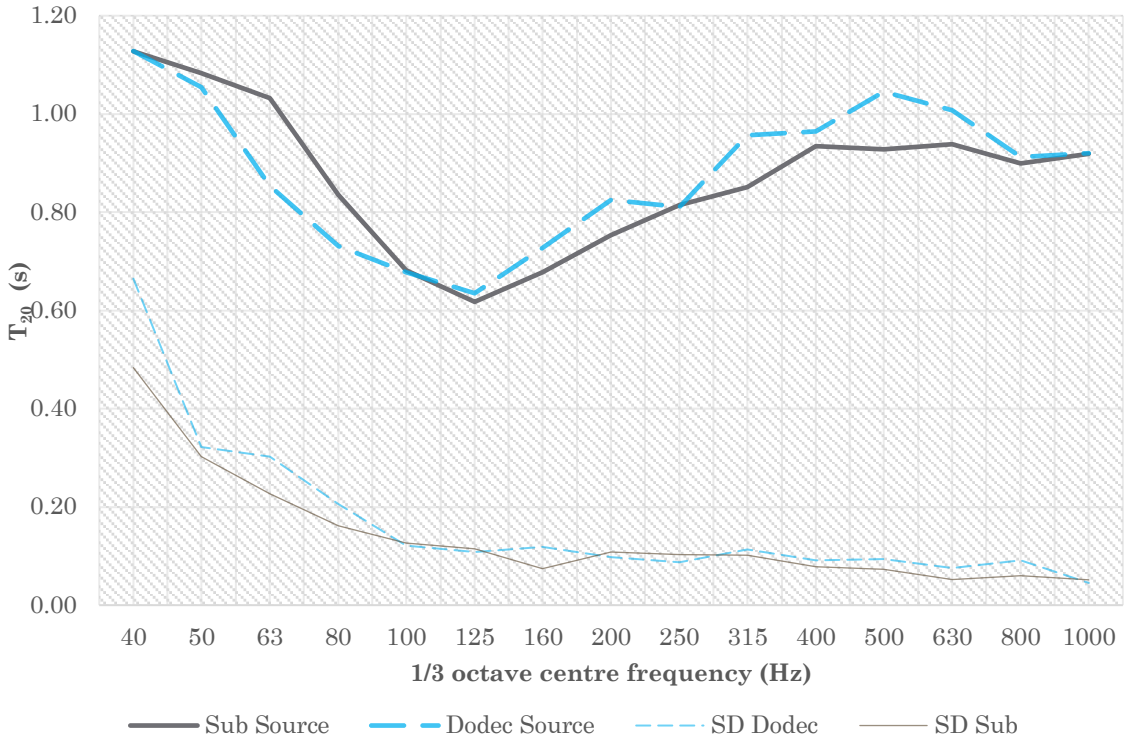

Figure 31: Subwoofer vs Dodec source for the curtains stowed condition.

The measurements using the subwoofer, although showing a better standard deviation (which indicates the spread of the individual measurements which make up the spatial average), were very similar to those for the dodecahedral source above 50Hz, and both showed a marked dip in the T_{20} in the hall between around 80Hz and 400Hz (see Figure 30).

It was considered that the Norsonic amp/dodec combination may lack the required low frequency response, so the measurements were repeated with the subwoofer system. The measurements using the subwoofer differed only in small respects from those with the dodec, with the dip characteristic being very slightly higher in frequency. This could be an effect of coupling with the floor, as the sub source was positioned directly on the floor, while the dodec was on a stand. As seen in Figure 31 this measurement verified the correctness of the initial measurement.

This dip was clearly the source of discontent among users of the hall, as to any listener therein, the low frequencies, across a relatively large range, across two octave bands, were significantly attenuated, by up to 20dB. This imbalance, in a

range which humans are less sensitive anyway, (see 2.3.2), and hence "bass rise" is often seen as desirable, we here observed the opposite, causing a drastic timbral shift in musical instruments sounded in the space, resulting in a "harsh" or "cold" perception, and a dissatisfying musical experience.

To establish the diffuse field in the hall the Schroeder frequency was calculated based on the measurements.

The Schroeder frequency of the hall is estimated using the volume of 690m^3 and the midrange RT (averaged between 500 and 1000Hz octave bands, being 0.98 and 0.9s respectively, giving an average of 0.94) with the curtains deployed.

$$f_{Sch2000} = 2000\sqrt{\frac{RT_{mid}}{V}} = 2000\sqrt{\frac{0.94}{690}} = 73.82\text{Hz} \qquad \text{Eq 76}$$

Or, using Schroeder's original multiplier

$$f_{Sch4000} = 4000\sqrt{\frac{RT_{mid}}{V}} = 4000\sqrt{\frac{0.94}{690}} = 147.63\text{Hz} \qquad \text{Eq 77}$$

Jacobsen [144] gives the modal density at frequency $f = 125$ as

$$n(f) = \frac{4\pi V f^2}{c_0^3} = \frac{4\pi V . 125^2}{343^3} = 3.35 \text{ modes/Hz} \qquad \text{Eq 78}$$

Modal density in the hall at the frequency of the dip is 3.35 modes/Hz (see Eq 78 and Figure 32).

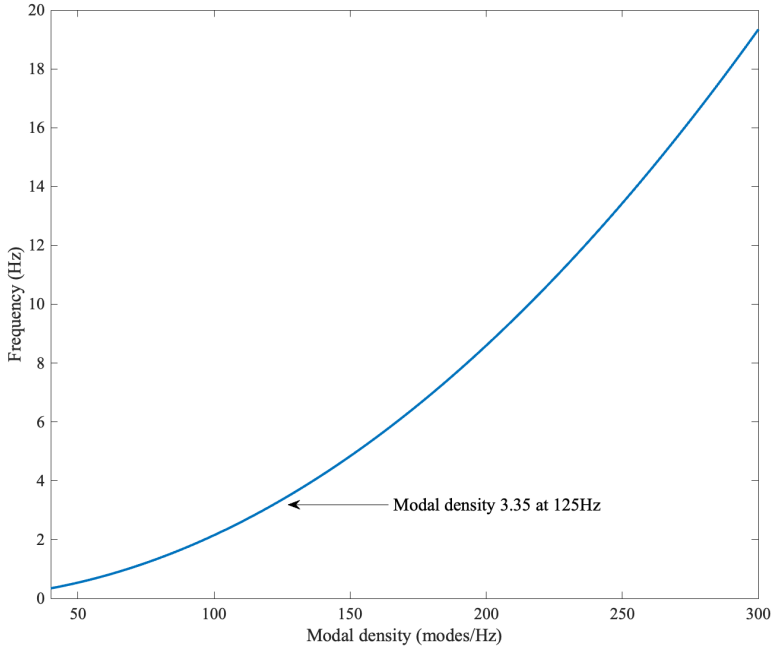

Figure 32: Estimated modal density in the hall, calculated using Eq 78.

This means that while the centre of the dip is strictly in the frequency zone where geometric acoustics can be justified within the room, the whole of the dip is not, so at best it was considered a marginal case. However, local modalities, such as within the rear wall, may play a role. In addition, bearing in mind Fazenda and Wankling's work on the perception of modality [29], it should be noted that the perceptual onset of diffusivity in the recital hall could be closer to 180Hz.

3.2.2 Suitability of the Hall

The Norwegian Standard NS8178: 2014 [62] is the most recent guidance document for music rooms. The midrange RT of 0.94s (with curtains deployed) vs the room volume criteria in that standard, places the hall as having a shorter than optimum RT_{mid} for purposes of performance, with 1.3s being the lower level stipulated by the standard for this volume of space, but not for rehearsal. With curtains stowed, the midrange T_{20} was found to be 1.46s, which per the standard is acceptable for the dual performance/rehearsal usage of the room (see Figure 33). However, since the usage was mixed, by the guidance in this particular graph, the hall could, with curtains used to adjust the acoustic, be said to be well suited for use,

However, when considering the frequency dependence, things are different and the low frequency dip comes into play. To investigate this frequency dependence the Bass Ratio was calculated under the two measurement conditions, and was found to be 0.78 with curtains deployed, and 0.60 with curtains stowed. These results are well below the ideal condition for a performance space with 1.0-1.2 being the recommended Bass Ratio [66]. However, this does explain objectively why the professional musicians preferred the hall when the curtains were deployed. To study frequency dependence further, the NS8178 standard was used to assess the acoustic in the hall.

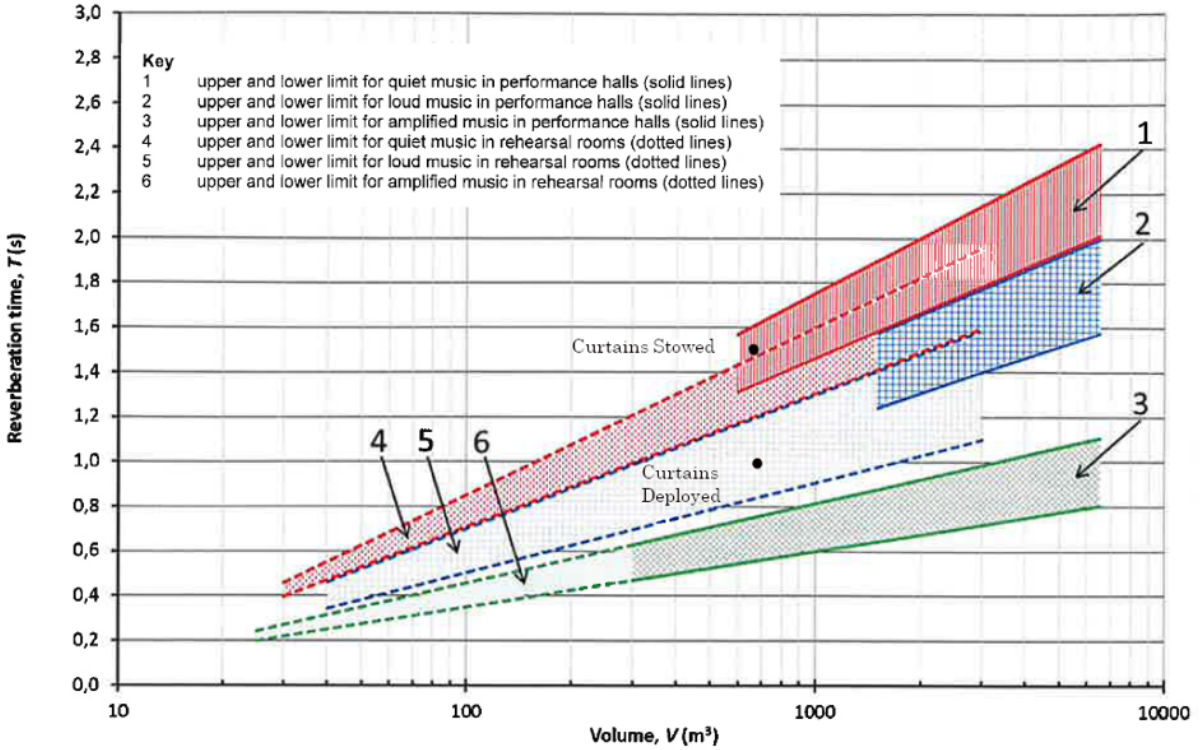

Figure 33: Room volume vs RT dependence (curtains deployed) guidance from NS8178 for recital hall (black dots), which should, as a small performance space, reside in zone 1 [62] Reproduced with permission.

NS8178 provides guidance limits for frequency dependency in music rooms. This is expressed in octave bands in terms of the $T_{20,f}$ / T_{mid} ratio, with maximum and values minimum being provided between 63 and 4000Hz in octave bands as can be seen in pink and green respectively in Figure 34 [62]. The maximum guidance permits higher *RT* at lower frequencies, allowing for bass rise. In addition, lower values for *RT* at high frequencies are permitted, a natural occurrence in large rooms as a result of air attenuation.

As could be foreseen from the room *RT* measurements, the hall deviates significantly from the guidance below 500Hz as shown in Figure 34. When curtains were deployed, the response was better, but at the expense of the overall *RT* being on the short side (see Figure 33). So, there is a trade-off between reverberance and frequency balance. Most users of the room generally have the curtains deployed, but their use is detrimental to the aesthetics of the hall, especially for performances. The frequency dependency response remains outside the guidance limits below 300Hz, even with curtains deployed (see Figure 34).

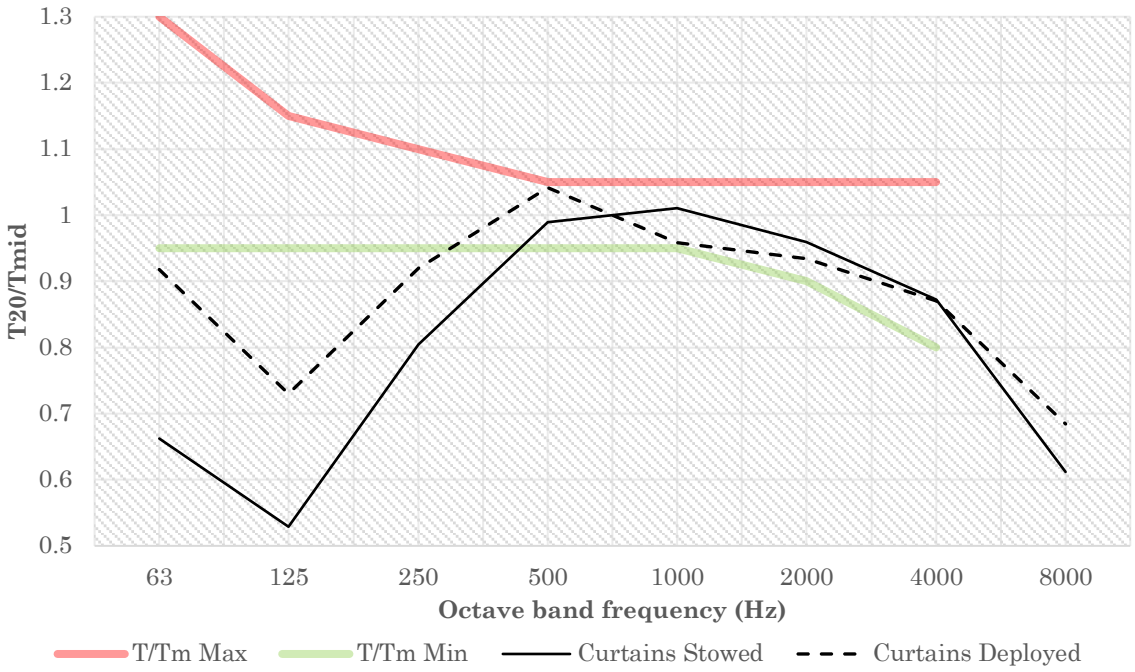

Figure 34: Frequency dependence limits for recital hall, expressed as defined in NS8178 in terms of RT/RT_{mid} between minimum and maximum limits. Curtains deployed and stowed conditions. [62] NS8178 guidance reproduced with permission.

3.3 Analysis.

To explain the dip in the room response, we must investigate the construction of the space, both the room envelope but also its fittings.

Since the curtains are very close to the wall surface, they can only have an effect in this manner at high frequencies so cannot be contributing to the low frequency dip, but, when deployed, absorb higher frequencies which mitigates it somewhat as seen in Figure 30. Curtains aside, there was very little porous absorber present in the hall.

3.3.1 Walls

The hall was lined with oak panelling fronting a 50mm cavity, which, by means of panel resonance, could be acting as a low frequency absorber, causing the dip in the room response. However, reference to Sakagami's parametric study in [86] shows that the only arrangement which would produce such a high resonance frequency would be an extremely thin panel (Figure 9b) or an extremely reflective back wall of the cavity (Figure 9d). The latter is not possible as the

cavity was filled with mineral wool. Neither were the oak panels used in the hall especially thin. However, given that all surfaces of the room are essentially wood panel, then any panel absorption effect could have a large impact overall. In addition, the hall is sited above a larger building, so the choice of materials may have been affected by weight concerns, and construction would be expected to be lighter weight than most.

3.3.2 Resonant Structures

A resonator could cause such a dip by acting as a Helmholtz resonator or a Quarter Wavelength Resonator (QWR). However, such a wide bandwidth would normally be associated with an array of resonators, as the latter usually have a very narrow bandwidth.

However, this seemed to be a possibility worth investigating. Resonators are often used in this frequency range and, indeed, such a cavity existed in the hall in the form of the false wall where curtains are stowed, and the working hypothesis was that the semi open cavity behind the wall and/or the wood panelling was a contributor to the dip in the room response, although the curtains, when stowed would be expected to damp this mechanism somewhat. This was, according to Field and Fricke, a neglected area of acoustics [95].

3.4 Reverberation Room Test

To try to reproduce the effect of the false wall, a test was undertaken in the LSBU reverberation chamber in which similar false walls were constructed either side of an existing doorway in the chamber. This test, although undertaken in a room of different dimensions and construction, would show whether the geometry of the false wall was resonating and causing a dip in the room response. Given the difference in dimensions of the room and the false wall, it was expected that the dip in frequency response would be centred on a different frequency than that of the recital hall, but the presence of that characteristic dip would show that the shape and geometry of the false wall was the cause of the irregularity.

The experiment could be considered a modified ISO 354 measurement. In the manner of that standard, reverberation times (T_{30}) were measured in five test conditions.

- Empty room.
- With an ad-hoc wooden false wall in place, of similar arrangement to the recital hall.
- With the sides of the false walls blocked off with wood panels.
- With both the sides and tops of the false walls blocked off.
- With false wall materials placed in the centre of the room in the manner of a standard ISO354 measurement.

Figure 35: False walls constructed in LSBU reverberation chamber. In "closed" condition

Six receiver locations and two source locations were used in the measurements. The JBL subwoofer driven by the Devine hi-fi amp was used for its flat frequency response, as previously in the recital hall measurements. A Norsonic 121 real time acoustic analyser was used to measure reverberation using two Norsonic

microphones simultaneously measuring in 1/3 octave bands using the interrupted pink noise method.

The false walls were constructed, one either side of the doorway (as in the hall) although the reverberation room dimensions prevented them from being exactly symmetrical as is the case in the recital hall. The inner side of the false walls were constructed from a thin layer of Class A porous absorbing material and the outer surface was made from plasterboard. Each panel weighed 60 kg (see Figure 35).

The results of the test are presented in Figure 36. The open cavity exhibits similar behaviour as observed in the recital hall, with an area of absorption, this time centred around 225Hz, and with a resonant reverberation boost around 125Hz.

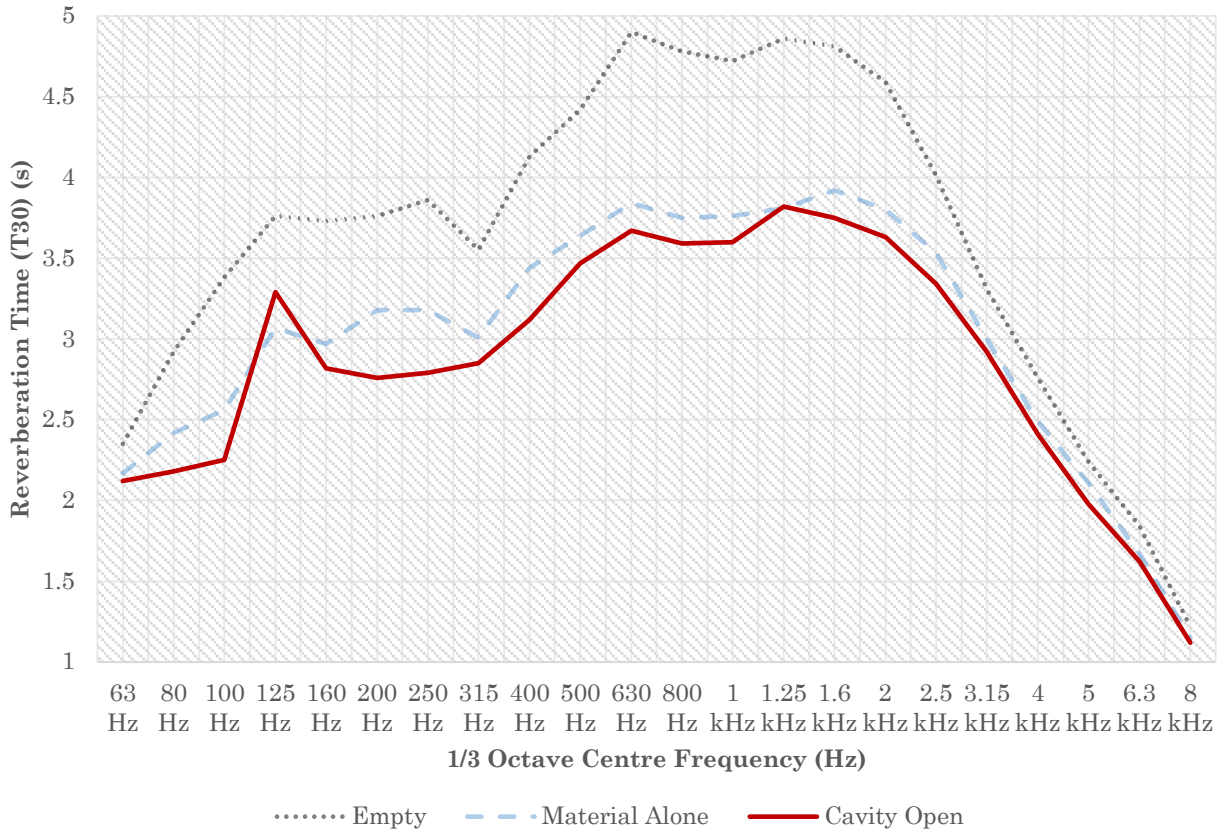

Figure 36: Effect of false wall cavity on reverberation time in the reverberation room measured in accordance with ISO 354.

Figure 36 shows the effect on *RT* of the false wall/cavity arrangement. It shows reverberation time over a very wide range, which may seem to not support the hypothesis, however, the material used in the false wall construction also, of course has absorbing qualities which must be allowed for. The blue dotted line in Figure 36 shows the reverberation time when the materials used for the wall construction were laid on the reverberation room floor in accordance with ISO354. Thus, the portions of absorption attributable to material and to the geometry of construction could be separated. Although, not perfectly, as only one side of the material was exposed to the room in this configuration, whereas in the case of the cavity wall, both sides are accessible to the sound field, albeit with the inner surface statistically much less likely to be hit.

The 'cavity open' configuration result shows a broad reduction in T_{30} above 300Hz which was consistent with the material properties of the wall, the T_{30} material alone configuration shown in Figure 36. Below this frequency there were two excess reductions in reverberation time in the ranges, 150 to 300Hz and below 100Hz. Between these areas, centred on the 125Hz 1/3 octave band, there was a peak, giving a result actually higher than the material-only measurement. These characteristics are consistent with the results seen in the recital hall (see Figure 30). Thus, it appears that the geometry of the wall is contributing to the uneven room response, and therefore that response could be improved by removing the effect of the wall.

A further experiment was undertaken to investigate possible remedial action, again in accordance with the standard approach given in ISO 354. This involved covering off the open cavity configuration.

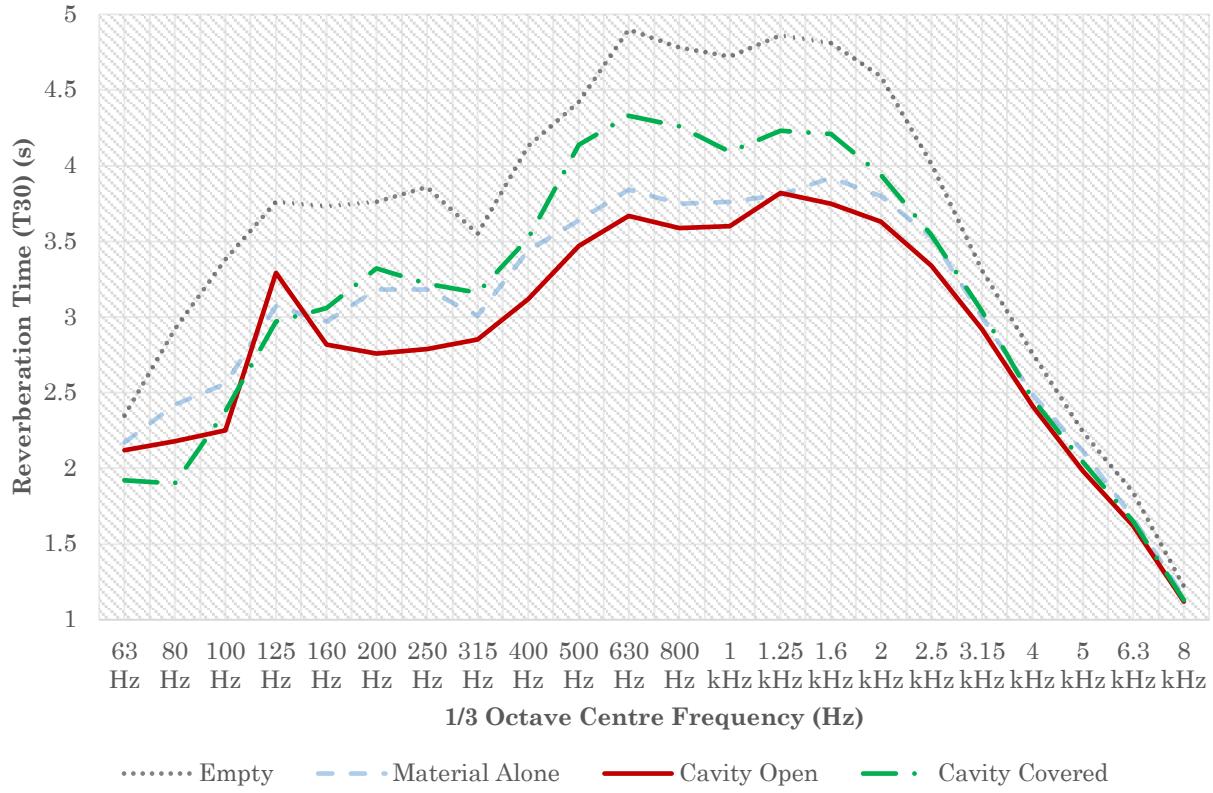

Figure 37: Reverberation times, with false wall in "open" and "covered" and just laid on the floor.

Adding the result for the closed-off cavity shows that covering the openings of the cavity with wood greatly reduces the dip in the room response at the frequency range of interest. This configuration also increased reverberation time between 400 and 2kHz due to a net increase in surface area which can reflect sound into the open space of the room. This shows a potential remedial action which could be undertaken to correct the room response at low frequencies, although the increase in higher frequency T_{30} would serve to maintain the lopsided balance between low and high frequencies. However, these higher frequencies could more easily be dealt with by the addition of a perforated panel absorber to target this frequency range.

To clarify the results presented in Figure 37, the reverberation times were normalised to the result for the material alone, in standard ISO 354 configuration, giving $T_{f,norm}$.

$$T_{f,norm} = T_f - T_{f,ref} \qquad \text{Eq 79}$$

where $T_{f,norm}$ is the normalised reverberation time in s at 1/3 octave band centre frequency f, T_f is the reverberation time in s at 1/3 octave band centre frequency f for a given condition and $T_{f,ref}$ is the reverberation time in s at 1/3 octave band f for the ISO354 mounting condition with wall construction materials placed in the centre of the room.

The resulting coefficient in seconds indicates the change in reverberation time attributable to the given geometry of the wall. In addition, a third "topless" condition, where only the side part of the wall was blocked off, is included in Figure 38 below.

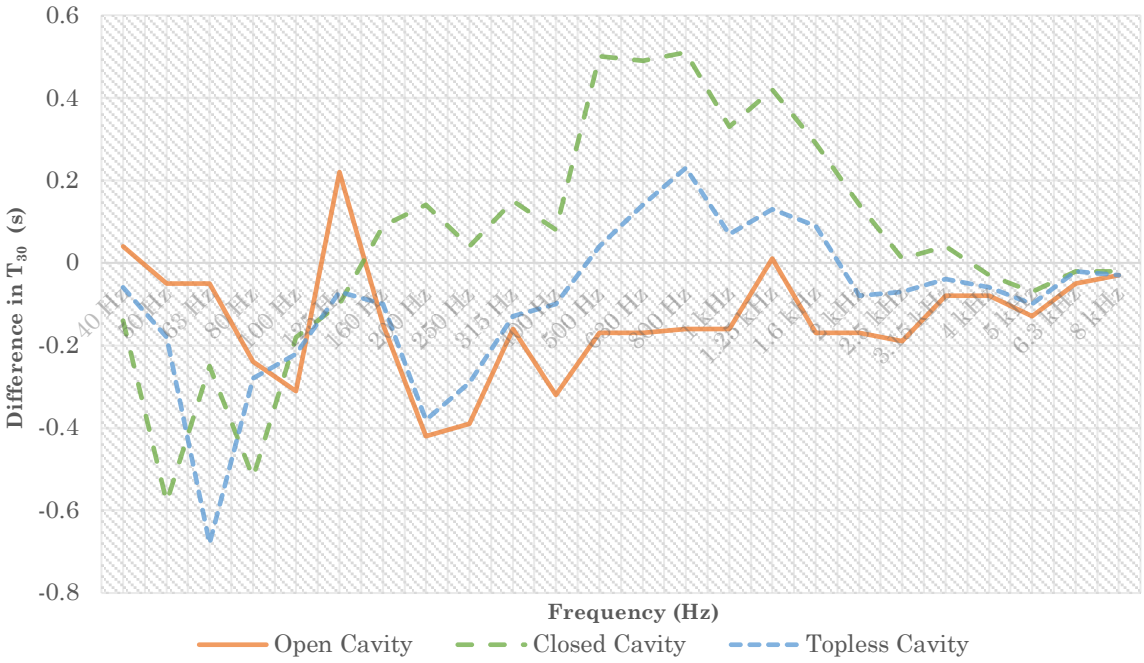

Figure 38: Effect on T_{30} of different configurations of false wall. Normalised to response of wall materials mounted in the centre of the reverberation chamber as per ISO 354.

Figure 37 and Figure 38 show that the false wall causes absorption across a broad range, and especially so between 160 and 400Hz, close in frequency range and similar in nature to the dip in the recital hall. Its second effect is that of adding a resonant peak at 125Hz. Reference to Figure 30 shows that the recital hall displays a large peak in reverberation time around 63Hz, and this combination of peak then dip suggested that the false wall was indeed causing this characteristic in the recital hall. The in-between "topless" condition still showed a little of these characteristics but somewhat reduced. The full "closed"

condition in which both top and side entries to the cavity behind the wall were closed off, showed that the resonant mechanism had been stopped, as the dip has been all but removed. In the case of the recital hall, this remedial treatment would balance that portion of the frequency spectrum somewhat. The "closed" condition did, however, by adding extra (largely) reflective material to the room, increase the T_{20} significantly between 400 and 3kHz, which had the effect of maintaining the imbalance between these two frequency ranges. It is thus suggested that the cavity be closed off with porous absorbent material or with a perforated panel fronting perforated absorber.

3.5 Computer Simulation

This section firstly investigates the room response through eigenmode analysis using commercial software (see 3.5.1) and classical theory of quarter wavelength resonators (see 3.5.2), and finally by using an experimental wave based computer simulation through a collaboration with Edinburgh University (see 3.5.3).

3.5.1 Eigenmode Analysis

As stated previously, resonant absorbers such as Helmholtz resonators and quarter wave tubes tend to exhibit narrow peaks of absorption, and the behaviour exhibited in the recital hall had a much broader resonance.

To begin to understand this mechanism, a modal analysis of the room was undertaken using COMSOL, an industry-standard numerical modelling software package [145]. It can perform many acoustic simulations including raytracing, Boundary Element Method (BEM), Finite Difference Time Domain (FDTD), and Finite Element Method (FEM), and the latter was used in the eigenmode analysis. In this simulation, the room was discretised as a mesh, and the Helmholtz simplification of the acoustic wave equation was solved at each point in the mesh. Boundaries were assumed to be rigid. For this reason, this would reveal the influence of geometry rather than wall properties. Solutions were sought which satisfied these boundary conditions, that is to say, modal paths within the room where pressure is zero at all boundaries on that path [146].

To facilitate the testing of different configurations of walls in the room, a parametric model of the hall was built in Rhino/Grasshopper CAD software [147], [148]. This allowed for easy construction of 3D geometry to export (in .stl format) to COMSOL (see Figure 39). Initially, models of the recital hall in real-world condition and with the false walls (and doorway) completely removed were compared.

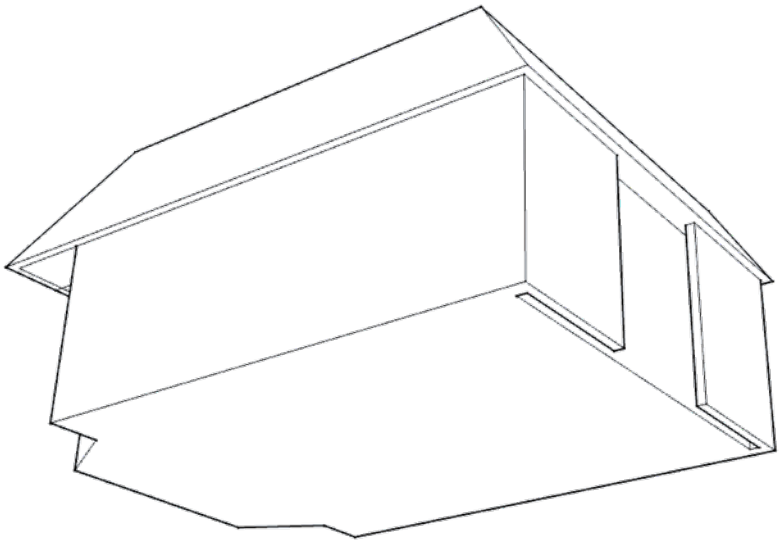

Figure 39: The 'baked' (i.e. rendered) geometry resulting from the above Grasshopper model.

A basic Eigenmode analysis was conducted in both room configurations with the aim of identifying resonant frequencies and mode shapes. The lowest modes observed within the cavity wall were at 23Hz (see Figure 40). This mode of the cavity seemed to couple with several room modes around this frequency.

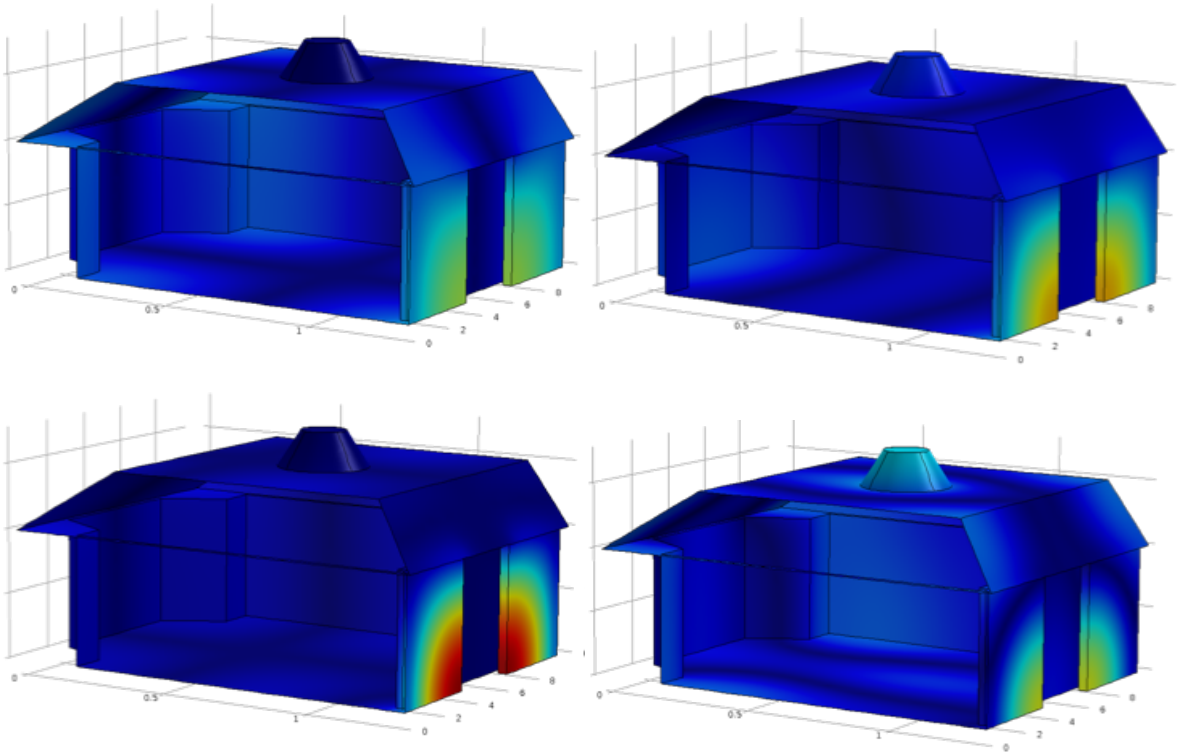

Figure 40: Modes shape within the cavity around 23-30Hz coupling with several room modes.

Comparing mode shapes with and without the false wall was difficult as the Eigen-frequencies tended to shift slightly due to the small change in length dimension and due to the different distribution of energy around the room in the two conditions. Attempts were made to match similar mode shapes like for like regardless of exact frequency match.

As can be seen from Figure 41, mode shapes exist which resemble mode shapes in a one-dimensional QWR, either in the x or z directions, (see left part of Figure 41). However, others exist which clearly involve both directions, and they take on a quadrant shape (see right part of Figure 41). These indicate that modal absorption was present, but the modal density at the frequency range of interest is such that the contribution of one, or even several modes was not enough to dominate.

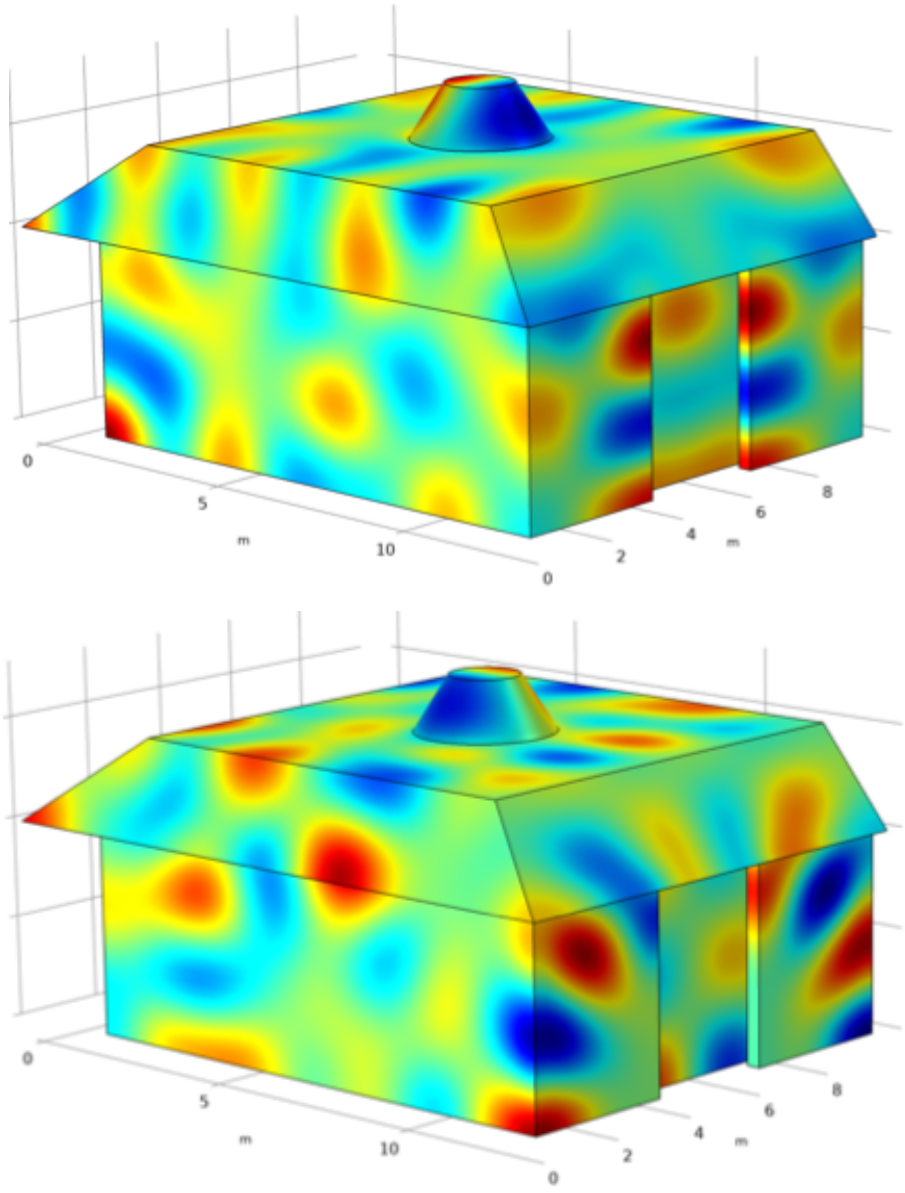

Figure 41: Mode shapes engaging one wall dimension (top) and both (bottom).

3.5.2 Classical Analysis as a Quarter Wave Resonator

As a starting point, Bies & Hansen [19] give the following equation for the impedance of a Quarter Wavelength Resonator.

$$Z_{QWR} = -\frac{j\rho c_0}{S} cot\left[kl_e\right] + R_{QWR} \qquad \text{Eq 80}$$

where S is the surface area of the aperture in m^2, k is the wavenumber in $radsm^{-1}$, l_e is the apparent length of the QWR in m, and R_{QWR} is a resistance term. To make a classical analysis of the recital hall false wall, since the dimensions of the wall and the properties of air were known, it was necessary to

calculate an end correction for the wall's radiation into the hall and to calculate the resistance term R_{QWR}.

3.5.2.1 The End Correction

The effective length l_e is usually a little more than the physical length of the cavity due to radiation effects from the orifice opening, with the correction δ applied depending on the geometry of the orifice and the space into which it radiates. Therefore

$$l_e = l + \delta$$

where l_e is the effective length, l is the physical length and δ is the correction, all in m. The literature contains reference to many end corrections for archetypal geometries, of which, the closest apparent match to the false wall geometry was chosen (see Figure 42).

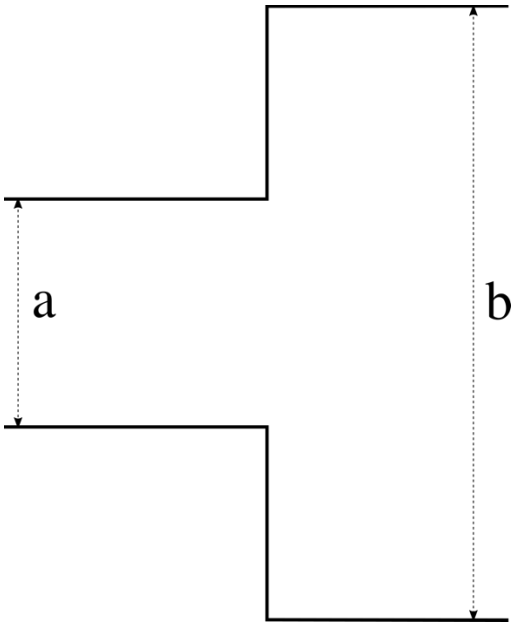

Figure 42: Expansion of a flat duct (side view).

Mechel [149] gives the following end correction for an expansion of a flat duct

$$\delta = \frac{a}{\pi}\left[\frac{(1-\beta)^2}{2\beta}\, ln\left(\frac{1+\beta}{1-\beta}\right) + ln\frac{(1+\beta)^2}{4\beta}\right] \quad where\ \beta = \frac{a}{b} \qquad \text{Eq 81}$$

where a is the dimension of the small duct and b is the dimension of the large duct (see Figure 42).

For cases such as the recital hall, where a ≪ b, this can be reduced to

$$\delta = \frac{a}{\pi}[1 - ln\,(4\beta)] \qquad \text{Eq 82}$$

For the false wall in the recital hall, the apparent length in the x (lateral) direction, small cavity width a=0.26m, large cavity (room) width b=9.58m, so

$\beta = {}^{0.26}/_{9.58} = 0.027$

So, from Eq 82 the end correction becomes

$$\delta_x = \frac{0.26}{\pi}[1 - \ln\,(4 \text{ x } 0.027)] = 0.267\text{m} \qquad \text{Eq 83}$$

So, the apparent length in the *x* direction is 3.267m.

In the *z* direction, the small cavity width *a*=0.26m, large cavity (room) width *b* = 6.04m so $\beta = {}^{0.26}/_{6.04} = 0.043$

So, from Eq 82 the end correction becomes

$$\delta_z = \frac{0.26}{\pi}[1 - \ln\,(4 \text{ x } 0.043)] = 0.228\text{m} \qquad \text{Eq 84}$$

and the apparent length in the *z* direction becomes 4.228m.

This end correction was a first approximation, although it didn't account for the true geometry, which, in the x direction also shows a 90-degree turn adjacent to a wall, and in the z direction, in which one wall is again adjacent to the side wall.

3.5.2.2 Resistance Term

From Bies & Hansen [19], the Acoustic Resistance R_A (kg m^{-4} s^{-1}) of an orifice of length w(m) and cross-sectional area S (m^2) and internal cross-section D (m).

$$R_{QWR} = \frac{\rho c_0}{S}\left[\frac{ktDw}{2S}\left[1 + (\gamma - 1)\sqrt{\frac{5}{3\gamma}}\right] + 0.288ktlog_{10}\left[\frac{4S}{\pi h^2}\right] + \epsilon\frac{Sk^2}{2\pi} + 0.7M\right] \qquad \text{Eq 85}$$

where

ρc_0 is the characteristic impedance of air,

γ is the ratio of specific heats (1.4 for air),

k is the wavenumber (ω/c_0) in rads.m^{-1},

M is the Mach number of any mean flow across the face of the orifice, so 0 in this case,

t is the viscous boundary layer thickness

$$t = \sqrt{2\mu/\rho\omega}$$

where μ is the dynamic viscosity of air (1.516×10^{-5} Nsm^{-1} at 20°C) and ρ is the density of air (1.204kgm^{-3} at 20°C).

The first term accounts for attenuation along the length of the orifice, which was considered negligible except for high frequencies and for very long or narrow orifices. The second term accounts for viscous losses at the orifice entry which is dependent on the parameter h which was the orifice edge radius.

The third term accounts for radiation loss at the orifice end. The parameter ϵ can, for an orifice which radiates into a near-free space from an unflanged, large plane wall or baffle should be 1 [19].

So, for the recital hall false wall, the parameters for the calculation were as follows and are shown parametrically in Figure 103:

Speed of sound in air at 20°C = 343.15ms^{-1}

For frequency range 63-315Hz, the angular frequency

$\omega_{min} = 2\pi f_{min} = 395.84\ rads^{-1}$; $\omega_{max} = 2\pi f_{max} = 1979.20$ rads^{-1}

Wavenumber k for the same frequency range:

$k_{min} = \omega_{min}/c_0 = 395.84/343.15 = 1.153$ m^{-1}; $k_{max} = 1979.20/343.15 = 5.768$ m^{-1}

Boundary layer thickness $t = \sqrt{2\mu/\rho\omega}$;

$t_{min} = \sqrt{2 \times 1.825 \times 10^{-5}/1.204 \times 395.84} = 2.52 \times 10^{-4}$m

$t_{max} = \sqrt{2 \times 1.825 \times 10^{-5}/1.204 \times 1979.20} = 1.13 \times 10^{-4}$m

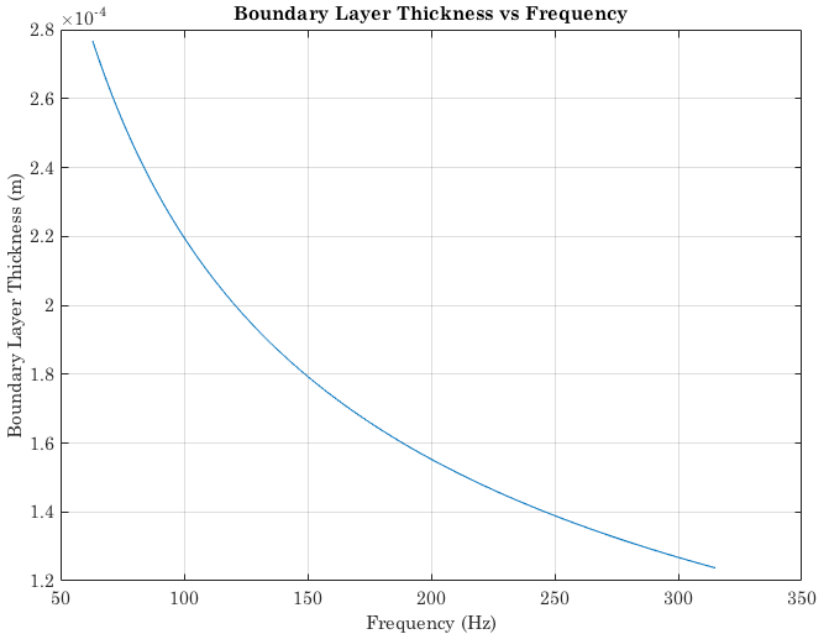

Figure 43: Boundary layer thickness t for the frequency range of interest.

The parameter h was taken to be the orifice edge radius $h = 0.203/2 = 0.106$ m

The parameter ϵ is set to 1, for an unflanged orifice radiating into free space, given that the hall is much larger than the false wall.

False wall properties

$S_x = 3 \times 0.26 = 0.78$ m^2

$S_z = 4 \times 0.26 = 1.04$ m^2

The resulting total impedance for the x and z directions are shown in Figure 44.

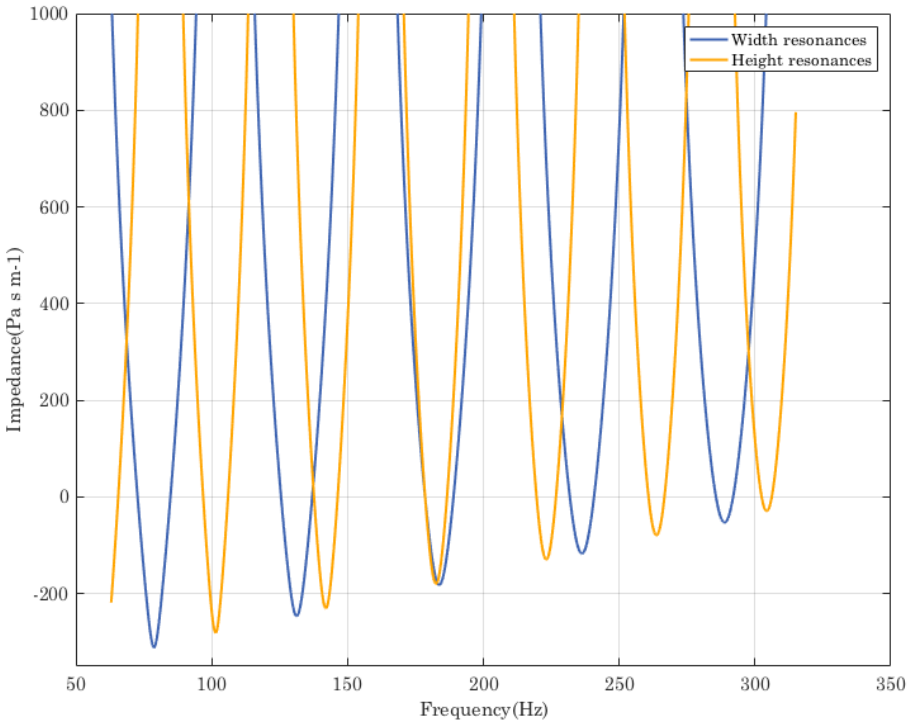

Figure 44: Impedance of Cavity in x direction (blue) and z direction (red).

3.5.2.3 Two Absorbers Acting in Parallel

The two cavities in the recital room were assumed to be acting in series so their impedances could be added. This neglects modal coupling effects and assumes spatial uniformity of function. For some mode shapes, those which share symmetry with the cavities, this was justified as a first assumption. As the COMSOL eigenmode analysis showed, there are additional mode shapes involving both dimensions together, and these were neglected in this analysis.

It was assumed that the action of each cavity in the x and z directions were separable and orthogonal and acting in parallel. Then they can be superposed in a combined impedance. Bies and Hansen calculate the resulting impedance from a Helmholtz resonator and a membrane absorber.

$$z_{combined} = -j\rho c_0 \cot(kd) + \frac{z_{mem} + z_{helm}}{z_{mem} z_{helm}} \qquad \text{Eq 86}$$

Using the same methodology, the impedances from the x and z directions were combined and normalised to the characteristic impedance of air as Z/Z_0, to give the result in Figure 45.

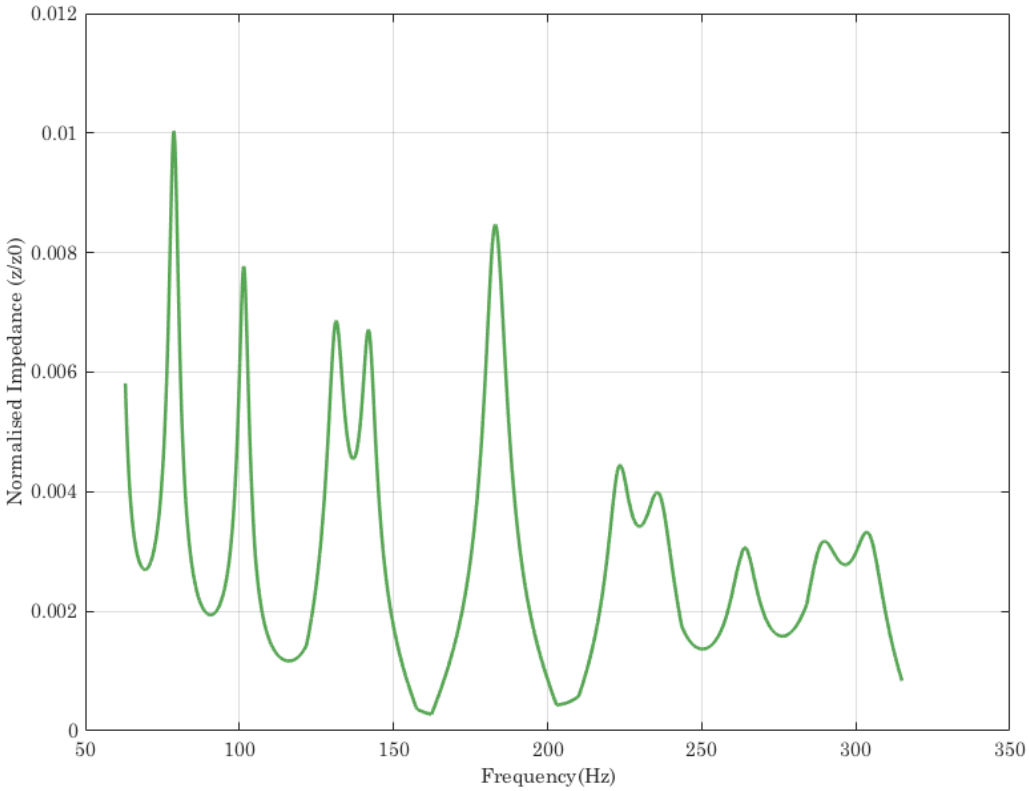

Figure 45: Combined normalised impedance of x and z directions.

Looking at our frequency range of particular interest for the recital hall, we see the lowest impedance at around 160Hz (see Figure 45). It can be seen from Figure 44 that the dips in impedance for height and width portions of the wall coincide at around this frequency. This shows that this accident of geometry results in additional absorption at this frequency range (see Figure 46, a detail view of part of Figure 45).

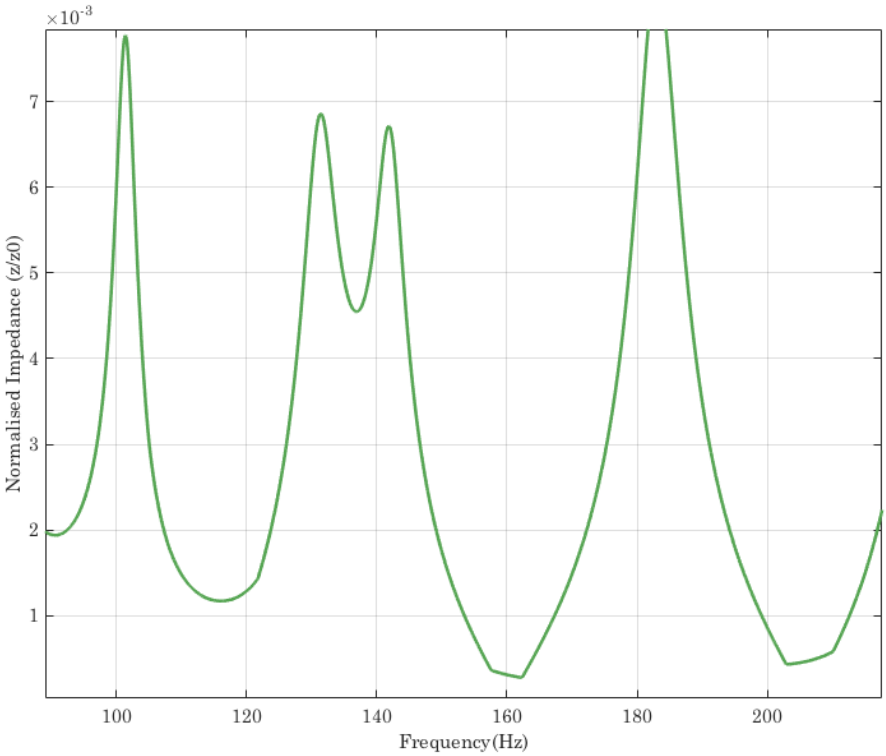

Figure 46: Detail of Figure 45 in frequency range of interest.

The MATLAB codes used to make this calculation can be found in the Appendix (see 9.3).

3.5.3 FDTD Model

A wave-based computer simulation was another method that was used to identify evidence for the acoustic mechanism that created the dip in the room response.

The author created 3D geometry in Rhino/Grasshopper software, for the hall in two conditions, firstly with the false wall in place, as in the real hall, and secondly with a hypothetical plain back wall with no cavity behind. These were supplied to Dr Brian Hamilton of Edinburgh University [150] and Roomerical [151], along with absorption data for oak panelling taken from Barron [66].
A Finite Difference Time Domain (FDTD) model of the hall was run by Dr Hamilton in each condition, with a single omnidirectional source and a 20x27 array of 540 receiver positions set up in his model under each condition. Source height was 1.7m and receiver heights were 1.5m, thus recreating the author's measurement condition, including dodec loudspeaker and microphone heights.

FDTD grid spacing was 17.5mm giving 8 data points per wavelength with a 5kHz cut-off frequency (see Figure 47).

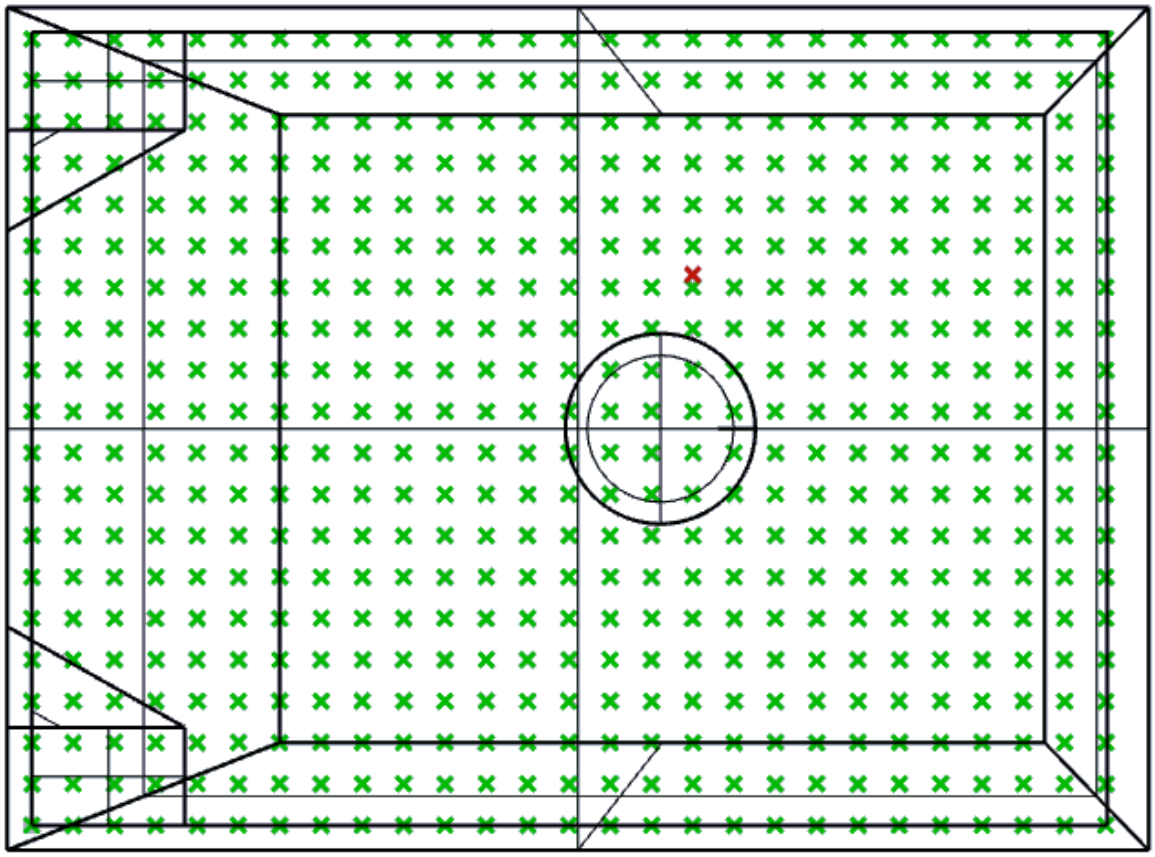

Figure 47: Top view of receiver array (green crosses) in FDTD model, source shown as red cross.

Dr Hamilton converted the oak panelling absorption data, expressed in 1/3 octave bands, to an impedance for use in the FDTD model (see Figure 48). The curves have a modulated nature due to his method for creating them from octave band data using a parallel resonance method. The results of the simulation were returned to the author for post processing and analysis. Firstly, results closer than 1.5m from the source or from room boundaries were rejected, leaving 333 valid receiver positions.

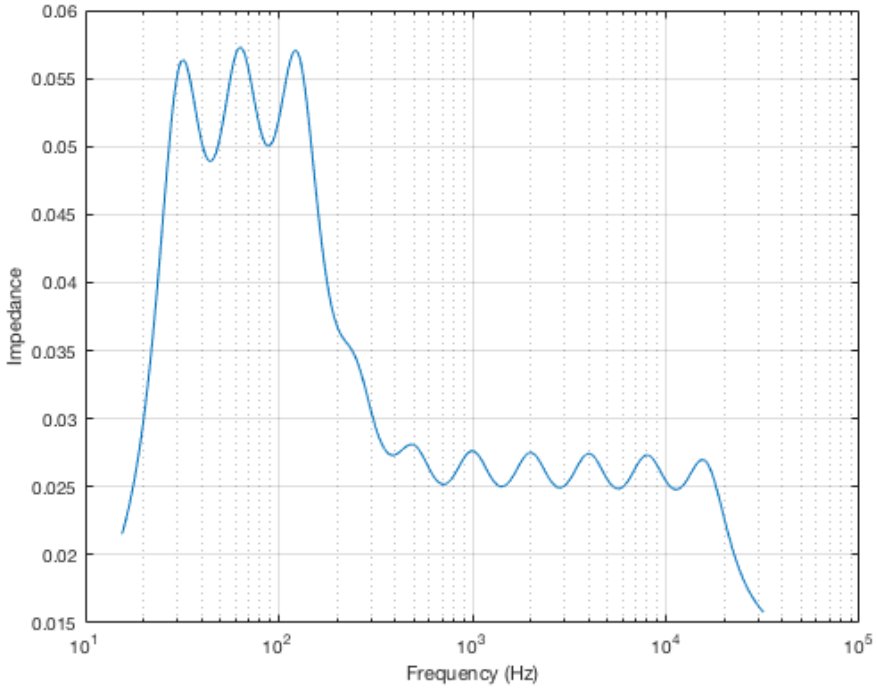

Figure 48: Impedance data derived from absorption coefficients for oak panelling in Barron [66], as applied by Dr Brian Hamilton to recital hall FDTD model.

Since absorption data was estimated rather than measured in the recital hall, T_{20} results were scaled by a factor of 1/2.5 to match measured curves at 1000Hz for comparison of their nature.

The raw results from the simulation (an impulse response for each receiver) were processed using a custom launch script (see Appendix, section 9.2) for ITA Toolbox from Aachen University [152] and averaged and plotted in Excel (see Figure 49). The model ran a single source position so 12 of the 333 receivers were selected to best enable comparison with the measurement, where two sources and six receivers were used.

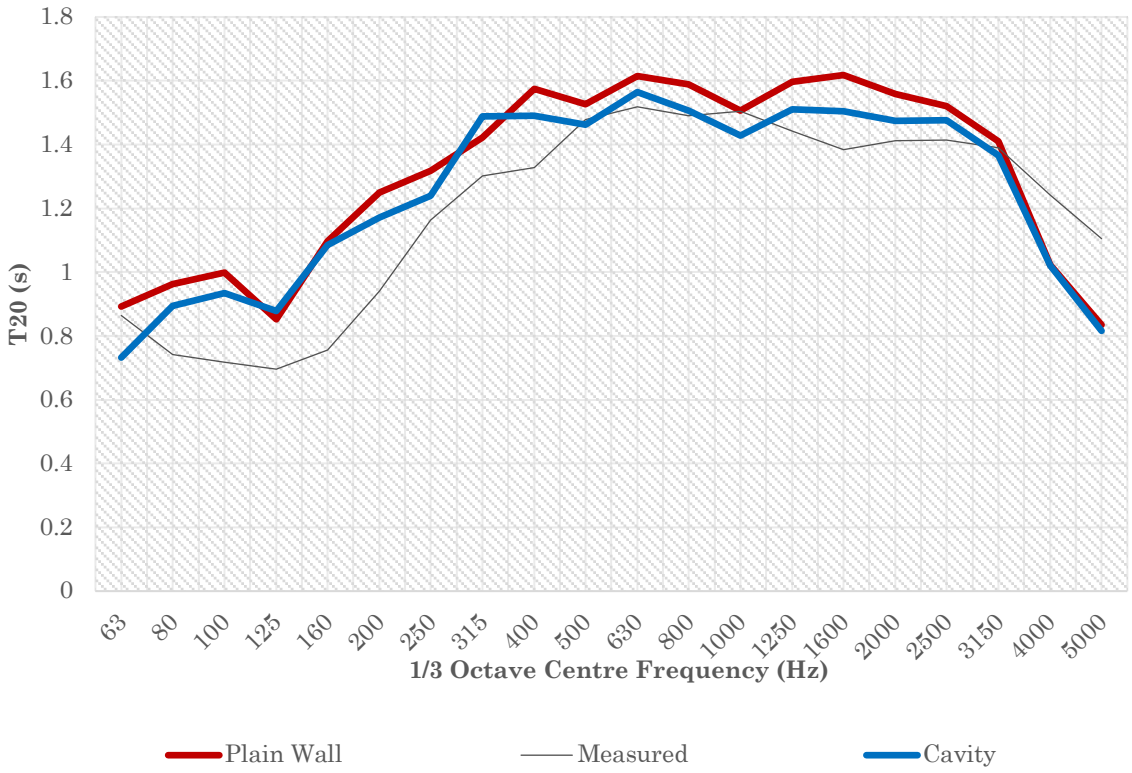

Figure 49: Spatially averaged, scaled T_{20} result for FDTD model with cavity wall and with a plain back wall. Measured values are shown for comparison.

T_{20} is generally a little lower for the cavity wall condition. This is to be expected as this configuration offers a larger surface area to the room, albeit within the cavity where not all sound paths can reach. There should be roughly the surface area of the panel (4x3m) - one of which on each side of the room and external and internal surfaces, so 4x3x2x2 = 48m² - extra plus a little for interior studwork.

Further excess absorption as observed in the hall was not seen in the model at the frequency of interest. In measured results, the dip is broader in nature, from 80 to 250Hz, whereas the model has a sharper dip at 125Hz. The modality in the reverberation times (small dips at 250, 500 and 1000Hz) is due to the nature of the impedance curve for the oak panel material (see Figure 48).

Some results from averaging fewer than all 333 receivers showed some difference between room conditions, so all data was plotted spatially for frequency bands of interest. At 125Hz the T_{20} was generally even across the space, but with some

hotspots, and distribution did change between wall conditions (see Figure 102 and Figure 103 in section 9 in the Appendix). The frequency dependency problem with the room was present across the whole room however (see Figure 30 for spatially averaged measurements), so this change in distribution was not considered a major contribution.

3.6 Other Absorption Mechanisms

This section investigates other possible absorption mechanisms, including panel resonance and audience absorption.

3.6.1 Geometrical Effects

As Marshall discovered, the warmth of a hall is adversely affected by near-simultaneous arrival of ceiling reflections and desirable lateral reflections from side walls, which can cause near cancellation of lower frequencies upon interaction [55]. The most favoured halls are mostly high compared to width (the classic "Shoebox" shape) and therefore do not suffer from this problem as ceiling reflections arrive later than lateral ones. The recital hall has a height just less than width so some interaction between ceiling and lateral reflections could be in play in this room with certain source-receiver combinations. As the low frequency problem was experienced throughout the room, this geometric mechanism was not considered as a key mechanism in this thesis.

3.6.2 Absorption due to Audience

Excess attenuation due to seating was first noticed at the opening of Philharmonic Hall in New York in 1962, whereby sound at grazing incidence interacts with that reflected through the audience and seating to cause attenuation in the bass range, normally between 100 and 300Hz. This can be overcome somewhat by ensuring strong early reflections are present. [54] [153]. While this mechanism is no doubt present to some degree during performances in this hall, the seating used by the hall is individual wire frame chairs, whose open sides tend to subvert the resonant mechanism somewhat. As a full

complement of chairs and an audience were unavailable for testing, and since the room was also tested without an audience, this avenue was considered outside the scope of the present study.

3.7 Potential Remedial Actions

This section investigates possible remedial actions including opening an existing door in the cavity wall, blocking off the cavity wall, and removing cavities behind the main walls of the room.

3.7.1 Opening Cavity Doors

The simplest remedial action was considered as the first call to action. The false walls each have an access door and it was hypothesised that leaving these doors open might subvert the resonance mechanism of the wall sufficiently to improve the room response. To test this hypothesis, the ISO3382-1 measurements were repeated using the curtain deployed first with doors open, and then with doors closed. The same equipment was used as in the first test, except that custom MATLAB scripts based on those by Novak *et al* [154] were used instead of WinMLS for performing swept sine measurements. Some analysis of these results was undertaken using the MATLAB ITA Toolbox by Aachen University [152]. Sweeps of 10 seconds were used.

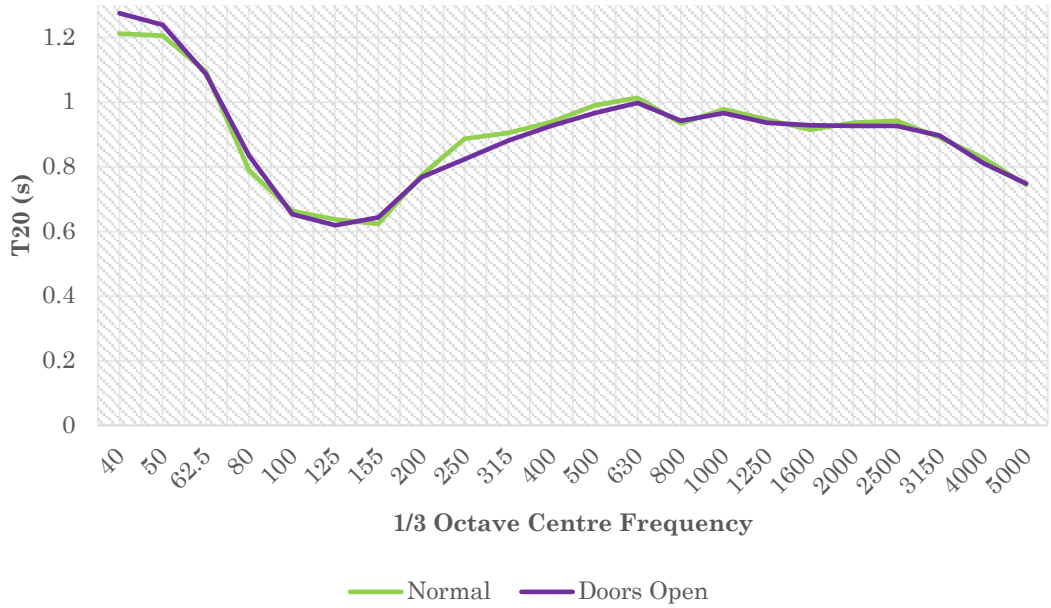

Figure 50: T_{20} dependence on door position.

The results (see Figure 50) show that there is no substantive difference between these conditions and the solution was rejected.

3.7.2 Blocking off Cavity Wall

As discussed previously, an option is to block off the openings to the cavity wall, thus removing the quarter wavelength resonance. As has been shown, this would also have the effect of adding a small amount of reflective surface area to the room and would remove the internal part of the cavity from access by high frequencies, thus, a marginal increase in high frequency reverberation would occur. Whilst an increase in reverberation might be considered desirable in the recital hall, it was most urgently required at lower frequencies, to redress the balance between low and high. Therefore, this option should not be undertaken without further compensating work to redress this imbalance. It could, however be achieved simply, although the improvement in bass response would be marginal rather than revelatory.

3.7.3 Removing Cavities Behind Walls

To remove the contribution of the rear cavity walls used for curtain storage, one solution would be to remove them altogether. This would remove the quarter wave action of the structure, which would mitigate somewhat against the low frequency dip in the response.

Kirkegaard, when undertaking the renovation of the Royal Festival Hall in 2007, removed the extensive 50mm cavity-backed wood panelling in the hall and re-mounted it, this time directly to the concrete structural walls behind, without a cavity. This was done to reduce attenuation at panel resonance and lower this resonance frequency (see Figure 9d [87]). This is a major undertaking, but this, or leaving brick or concrete structural wall enclosed, would improve bass response and increase *RT* across the spectrum. However, this may be undesirable architecturally, as the wood panelled aesthetic has clearly been enthusiastically embraced by the architect here. This would be the most productive corrective measure, but also the most disruptive.

3.7.4 Artificial Reverberation

For a recently built room that lacks bass response a strong candidate for remedial action would be to use a modern technical solution, an artificial reverberation system. Such systems have existed for some years, the Royal Festival Hall in London being an early example [155]. This system would be configured to boost low frequencies. However, this solution would introduce many loudspeakers, approximately 10, and microphones, approximately 10, into the room and thus also impair the aesthetic. However, no other technical solution currently available would improve the acoustic in the room. This has recently been implemented in the major refurbishment of the Royal Opera House Linbury Theatre with great success [156]. Välimäki *et al* provide a review of current progress in artificial reverberation systems in [157].

3.8 Discussion

A newly built recital hall has been measured both with and without curtains deployed along two long walls, these being used to modify the acoustic at mid and high frequencies. The hall was found to have insufficient reverberation time around 125Hz in a broad dip when compared with standards. Several causes of this shortcoming were investigated, with a combination of factors identified, including geometry, the resonant behaviour of the false wall used to store curtains, and the widespread use of relatively lightweight wood panelling. Remedial action which could be used to modify the existing hall could comprise two possibilities:

1. Blocking up or removing the false wall. The side effect of this would be to present more surface area to the room, and a subsequent increase in RT at higher frequencies although this could be accounted for by the addition of porous absorber.

2. Removing the cavity behind the wood panelling on the walls; however, this may have a detrimental effect on sound insulation properties, as there are classrooms and rehearsal spaces adjacent to the recital hall.

The leader in the field of architectural acoustics perhaps said it best regarding the acoustics of music venues when discussing the Royal Festival Hall in London:

"…secondly, they believed too much in this word "wood." They put a lot of wood in that hall. The result is there's no bass in it to speak of, because wood absorbs the bass. Any good hall — Boston, "Musik Vereinssaal", the old Gewanddhaus — were plaster, heavy walls, not thin wood. So, that hall is very deficient in bass"

- Leo Beranek, speaking of the Royal Festival Hall, London [158]

3.9 Conclusion

The sound field inside music rooms at mid to low audio frequencies is greatly dependent on both material properties and geometry of the building envelope. This case study has explored an unusual additional mechanism caused by a non-standard construction used to store curtains at the rear of a recital hall, showing that significant absorption has occurred due to a Quarter Wavelength Resonance. Further work could focus on harnessing such geometries to be used as acoustic treatments, whether permanent or flexible.

4 Case Study B: Pneumatic Absorbers

This case study describes a novel solution to a challenging brief for a mid and low frequency treatment for use in a classical rehearsal space. A successful space for some years, some concerns remained about a low frequency "boom" in the hall and, while seeking to expand the client base, the management sought to mitigate against this, and to prepare the space for operatic rehearsals. An affordable, portable ad-hoc acoustic solution was devised, tested in the lab, installed and further in-situ tests performed to confirm the lab data.

Figure 51: Henry Wood Hall in winter.

4.1 Henry Wood Hall

Holy Trinity Church in Borough, Central London was built in 1842, but suffered bomb damage during the Second World War and was subsequently abandoned. It was refurbished in the 1970s for use as a rehearsal and recording venue for the London Symphony Orchestra (LSO) and London Philharmonic Orchestra (LPO) and other ensembles. As Henry Wood Hall, it remains a busy venue in these roles, as well as for occasional public concerts (see Figure 51). The hall has a volume of approximately 6000m^3 and comprises a main area with four rostra of increasing

height, plus elevated choir stalls and an organ at the rear of the main space. The walls are made from Bath stone; the ceiling is lightly coffered with a plaster finish and the floor construction is wood parquet [22]. The recessed windows are covered by floor-to-ceiling curtains which can be used to adjust the acoustics in mid and high frequency ranges to the users' preference.

The condition with some or all curtains open is generally preferred by users of the hall. It is thought this choice is made mainly due to the preference for natural light while playing, rather than, or at least not wholly, for acoustic reasons (see Figure 52).

Figure 52: Henry Wood Hall.

4.2 The Acoustics of the Hall

The hall's room acoustic parameters have been measured by the author in accordance with ISO3382-1 [143] on several occasions and in several configurations, although access to this busy space was limited. Other members of the LSBU acoustics group provided assistance during these measurements in the form of practicalities such as moving and placing equipment and moving

microphones between measurements. This was in the interests of speed as limited time period were available for the measurements. Receiver positions were distributed around the performers' area, which was partly on the parquet floor and partly on risers, and source positions were also within these areas, usually one to the conductor's right, representing the usual location of double basses, and one in the centre of the top riser where percussion and timpani are usually set up; these being the dominant sources of low frequency sound in the orchestra.

4.2.1 Background Noise

The background noise (in worst case) was measured over 30 seconds using a Norsonic 140 meter mounted 1.5m above the conductor's position at the centre of the hall, giving a Noise Rating (NR) of 30. The main noise source in this case was a fan in the basement heating system which contributed a peak in background noise around 1-3kHz. This was only in use during the mornings in winter months so is considered the worst case but also a minority use case.

In terms of background noise, the space is considered suitable, although NR25 in all configurations would be desirable [66]. The latest guidance on music rehearsal and performance spaces comes from the Norwegian Standard NS8178:2014 [62]. Guidance for background noise in NS8178 endorses the recommendations of NS8175:2012 for teaching rooms. [159]. This standard uses Room Criteria (RC) and calls for RC28; the hall was rated at RC35 in this scheme (see Figure 53) which is considered suitable, as the offending fan is not often in use during rehearsals.

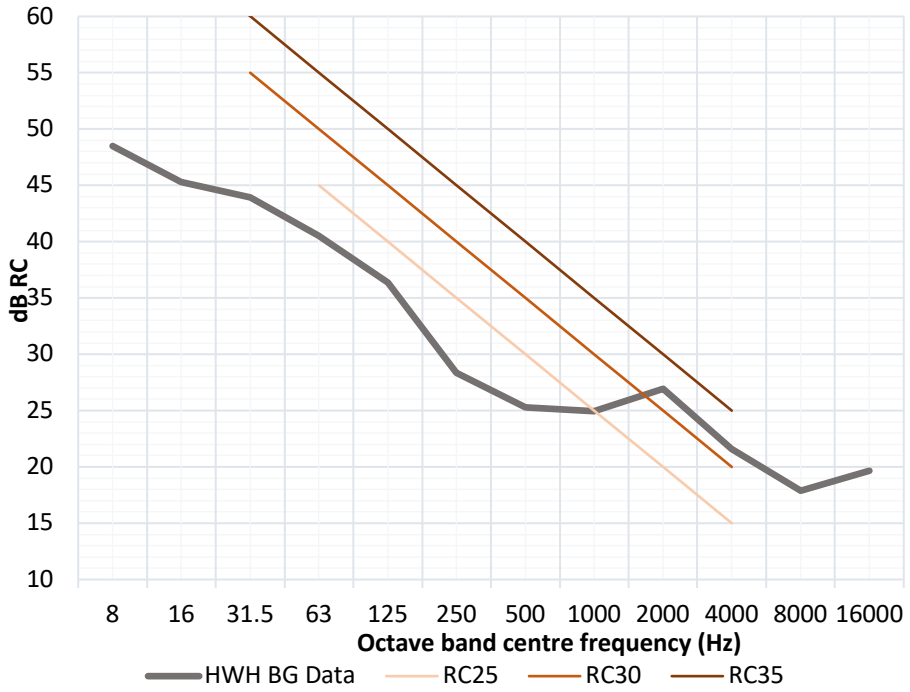

Figure 53: Background noise measurements in worst case in Room Criteria as specified by NS8175:2012. Henry Wood Hall is RC30.

4.2.2 Baseline Reverberation Time and the Effect of Curtains

The baseline Reverberation Time (*RT*) of the hall, the effect of closing all curtains and a condition where curtains are partially open (indicative of the most common usage condition) were measured in accordance with ISO3382-1 using two source positions (to the conductors right where contrabass normally sets up, and on the third level of the rostrum where percussion normally sets up, in order to reflect where low frequency sources were located in normal use) and six receiver positions, located around the playing area. The microphone used was an Earthworks M30BX, and the source a JBL Subwoofer powered by a Devine hi-fi amp, both selected for low frequency performance. WinMLS software running on a PC laptop was used to generate sine sweep excitation signal and capture and process results. A sine sweep between 40 and 8kHz was generated for each source-receiver position for each room condition. Reverberation time in 1/3 octave bands was derived for each position and spatially averaged and graphed (see Figure 56).

Figure 54: The absorption of the curtains in Henry Wood Hall being measured in-situ with the Microflown Impedance Gun [160].

The curtains in Henry Wood Hall are 3 metres wide and run the entire height of the main hall, 10 metres. The textile used in their construction had a surface density of 0.61kg/m^3, with a mass of 18kg on each curtain rail. Prof. Stephen Dance had performed an in-situ absorption measurement on the curtains in 2014 [161] using the Microflown Impedence Gun. This is an intensity-based method based around a P-U probe, which yields useful results above 250Hz [160].

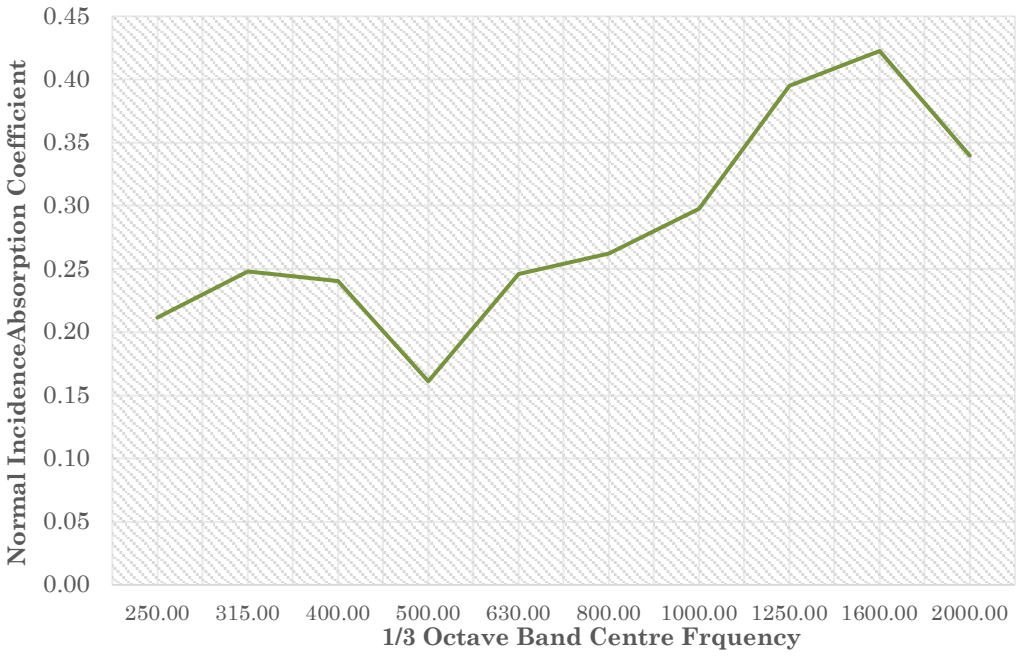

Figure 55: Normal incidence in-situ absorption coefficient for Henry Wood Hall curtains hung against the stone wall [161].

The results here show moderate absorption at 250Hz, which increases above 1kHz. Two mechanisms are at work here, with a membrane/cavity action at lower frequencies (see Eq 70) and absorption due to porosity of the curtain at higher frequencies (2.6.5).

Results are shown in Figure 56. This shows the curtains are a useful absorber in the mid and high frequency ranges and somewhat at low frequencies but only when all are closed, by which point high frequencies are attenuated substantially. Curtains and drapes can absorb sound well at lower frequencies (below 250Hz) but only if they are sealed around the edges and bottom to enclose a volume of air behind them [162]. This kind of approach was considered to be difficult to implement in the present scenario as hall staff would have to monitor the seal between curtain and wall closely, a task for which they have inadequate time.

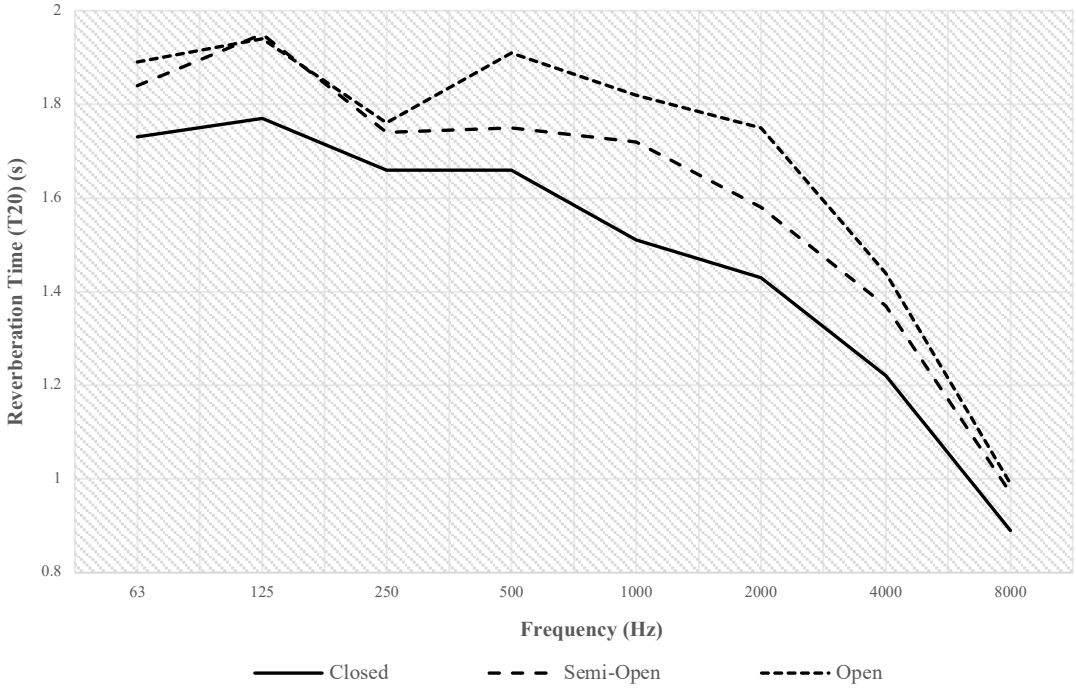

Figure 56: Baseline RT (T_{20}) showing dependence on curtains.

4.2.3 Comparison with Standards

NS8178 defines "loud" music as that performed on acoustic instruments that "produce a powerful sound", meaning large ensembles such as concert bands and orchestras, and jazz big bands. It also includes percussion and opera singing.

"Quiet" music includes quieter ensembles such as choirs, vocal ensembles, folk groups, string orchestras and unamplified guitar groups.

The guidance in NS8178 suggests that Henry Wood Hall is large for a rehearsal space, being more akin to a performance space by the standard's definition in terms of volume and midrange *RT*. However, extrapolating the standard's data to the larger volume suggests that the hall's midrange reverberation time is (for its size) suitable for both "Loud" and "Quiet" acoustic music. The hall is used mostly for the former, with most sessions hosting full symphony orchestra setups, although chamber and even solo sessions are not unusual. However, it is not known whether the authors intended such an extrapolation to be valid or whether such larger volumes are simply considered undesirable. The hall's location on this volume-*RT* graph can also change due to the configuration of the curtains, and it is possible for it to be placed from top to bottom of Zone 2 in Figure 57 by manipulation of the curtains.

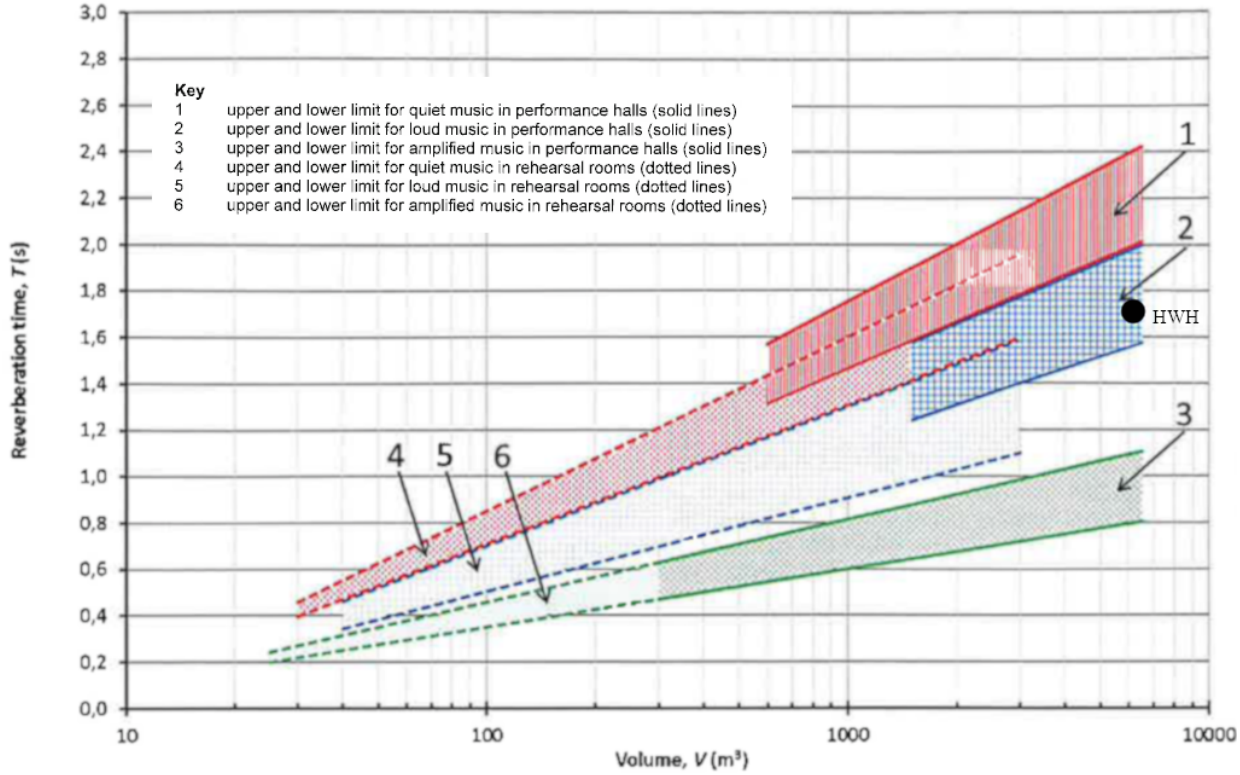

Figure 57: Midrange T_{20} of Henry Wood Hall's baseline measurement (in normal use condition with some curtains open) in relation to NS8178 ranges for "loud" and "quiet" acoustic music (Areas 4 and 5 above) [62] Reproduced with permission.

4.2.4 Frequency Dependency

NS8178 specifies that music rooms should have a "smooth reverberation time curve as a function of frequency". In addition, frequency dependency is expressed in terms of upper and lower boundaries of acceptable values of T/T_{mid} from 63Hz to 4kHz. The frequency dependency of Henry Wood Hall is within the guidance limits of the standard, although high frequencies are close to or at the lower acceptable limit depending on curtain deployment. This is to be expected in a larger volume space due to additional air absorption (see Figure 58). This could be the reason for NS8178's omission of spaces above 3000m^3 from the regions of optimum performance for rehearsal (see Figure 57).

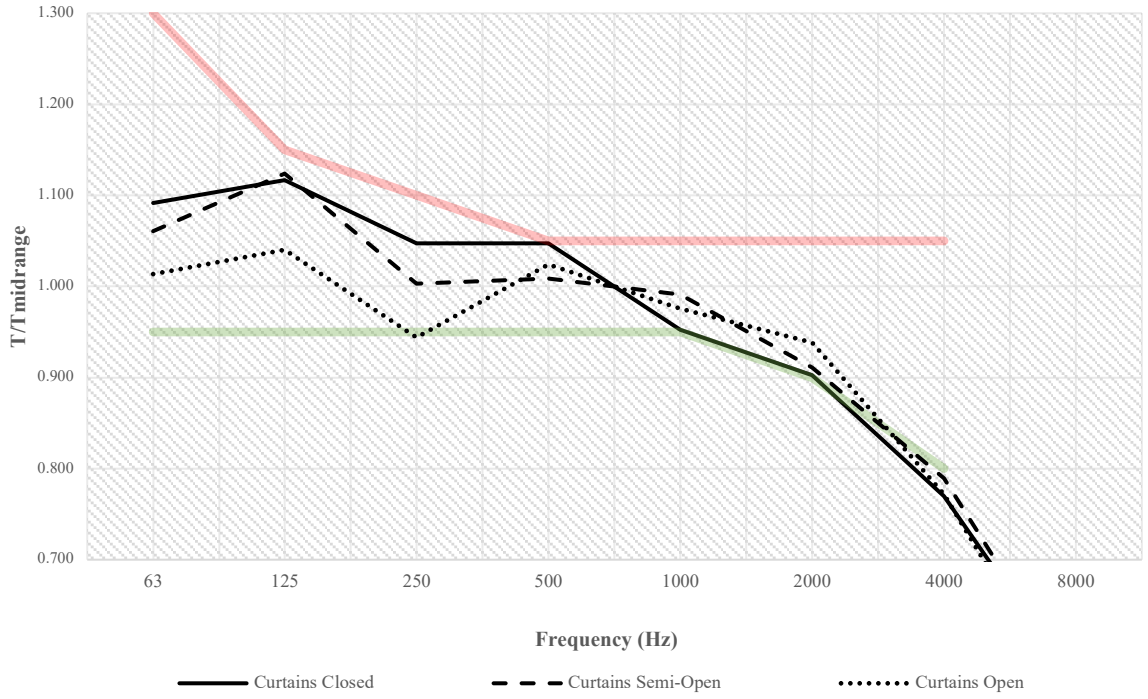

Figure 58: $T_{20}/T_{midrange}$ frequency dependency of Henry Wood Hall baseline measurements in relation to NS8178 minimum (green) and maximum (red) limits. [62] NS8178 guidance reproduced with permission.

4.3 Subjective Quality

A questionnaire had been prepared for musicians using the hall in order to quantify the subjective qualities of the hall. Unfortunately, for operational reasons within the hall, this could not be circulated. So, for an idea of how the space is perceived, brief conversations with management, and with a recording engineer familiar with the space had to suffice.

The acoustic of the hall is generally considered good, as its ongoing success testifies. It does, however, have a "warm" character which divides users, and there have been some complaints of "boominess", and indeed there is a distinct peak in the *RT* curve around 125Hz as shown in Figure 56. This has been of sufficient concern to the management that they have sought advice on mitigation measures several times over the past years.

A report was commissioned in 2010 for a firm of consultant acousticians to identify a solution to this problem. They recommended that up to 100 Helmholtz resonators be installed in the hall targeting the 80-150Hz range. Although acoustically a good solution, these would be intrusive, immobile due to their size and mass, and prohibitively expensive [163].

Other solutions had been suggested and assessed over subsequent years including the splitting of the space into two by an acoustic curtain, which was rejected as it would add too much high frequency absorption and may not have been structurally feasible. The same study group [164] performed a smaller-scale deployment of Helmholtz resonator arrays, targeted around key low-frequency instruments; the timpani, and contrabass; and although measured results were encouraging, the perceived difference by performers and conductors was insufficient to lead to the permanent deployment of this reduced, but still somewhat bulky solution.

Some remedial work had been carried out by the LSBU Acoustics Group to target the low frequency range several years previous to this study. This comprised Rockwool bales wrapped in plastic sheet placed under the rearmost three rostra (the first 'rostrum' is strictly a 'riser' as it has open sides). This had the effect firstly of damping any motion of the rostra and absorbing low frequency sound, and, secondly of removing the semi-enclosed (there are small openings on the ends) volume of air previously under the rostra. This treatment had significantly controlled the low frequency in general, but some concern remained (see Figure 60).

Figure 59: The plastic-wrapped porous absorber underneath the rostra in Henry Wood Hall.

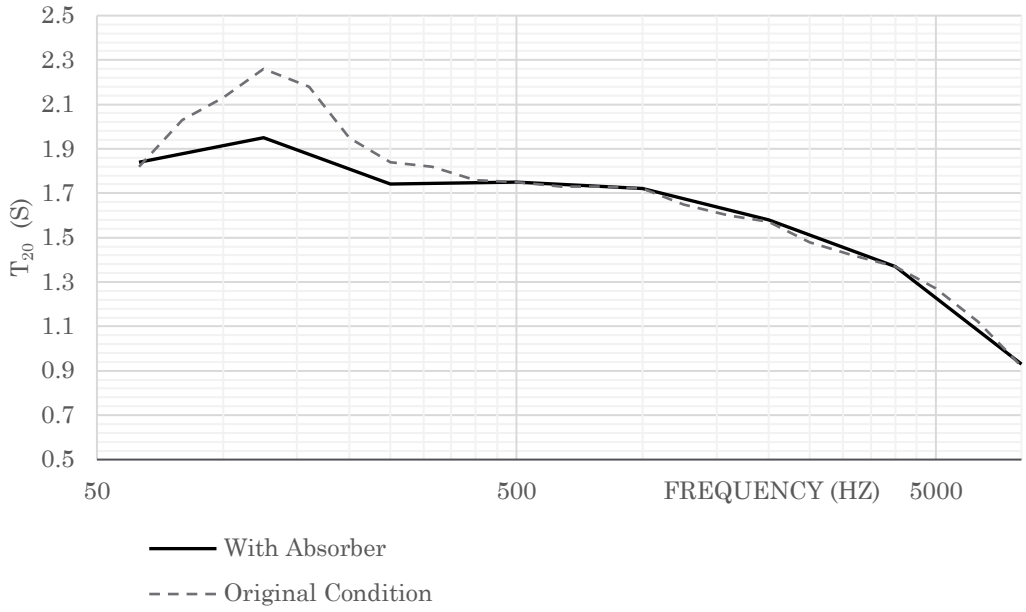

Figure 60: Dependence on under-rostra absorber.

4.4 The Brief

In 2018 the hall's management were looking to expand its use, notably for opera rehearsals, as the London Philharmonic Orchestra (LPO)'s summer residency is at Glyndebourne Opera House. As a result, the author was asked to provide an affordable, flexible solution to improve the hall's suitability for voice rehearsal, one which could be installed or removed within an hour, the changeover time between sessions at the hall, as a typical day's schedule could include vocal and orchestral sessions on the same day.

NS8178 lists operatic singing among "loud" acoustic sources, for which the hall is considered suitable, but the question of intelligibility arises when considering opera. Barron suggests midrange *RT* values intermediate between speech and music are appropriate, suggesting between 1.3 and 1.8s for performance spaces [66]. The hall again falls between these values in the midrange but has a significant bass rise at certain bass frequencies and these could cause significant masking in speech and singing.

4.4.1 Limitations and Challenges

The hall is a busy space and there was limited access time for measurement and installation, hence the demand for an easily portable solution. In addition, the hall is a Grade II listed historic building and as such, could not be changed structurally, neither could any fittings be attached to the walls. Guidance from the management also suggested that visual changes to the space were not desired, and as the space was sparsely fitted already, this was a significant constraint.

4.5 The Proposed Solution

The existing curtains in the hall were considered suitable for adjusting high and mid-range *RT*. In the case of the higher frequencies further absorption was not considered desirable, (see Figure 58), as it would make remaining "boominess" more noticeable, therefore it was decided to provide a complementary solution to target the latter.

Given the limitations in the brief, the only solution which could satisfy all its demands was to use pneumatic absorbers which could be inflated as required and easily stored when not. Although commercial pneumatic absorbers are available [117], to satisfy the cost demand, it was decided to select an ad hoc pneumatic structure in the form of airbeds and repurpose them as acoustic treatments.

In the case of Henry Wood Hall, airbeds were attractive for their cost (around £40 per bed for the chosen solution, with many cheaper alternatives), widespread availability in a number of types, light weight and ease and speed of deployment.

They are also suited to being placed in the hall without special fittings, vital due to the hall's Grade II listed status.

Using a number of airbeds also meant the solution was modular, so they could be located in a number of spaces around the room; in practice, there were two areas which lent themselves to the purpose, firstly propped against the wall behind the rostra at the edge of the rear of the room, where airbeds could easily be placed to have minimum visual impact, but maximum effectiveness; and secondly, laid flat on the choir stalls on the balcony where, again they are out of view of the main floor. Also, their modular nature handed some control of the acoustic to the management and users of the hall. In this context, this is a desirable outcome, as they are experienced critical listeners in their own performance culture and, while lacking formal acoustics knowledge, are well placed to critique a particular acoustic. To fully understand their acoustic properties, laboratory tests were organised.

4.6 Laboratory Tests

Standard ISO354 tests were undertaken in LSBU's Reverberation Chamber to measure the absorption performance of three available airbed types (see Figure 61), the first (the "thin" model) being one made by Bestway and being 0.22m thick and 1.9 by 1.37m. The second "thick" design made by Livivo measured 0.44m thick and 2 by 1.6m (see Figure 61). A third airbed, smaller than the rest, and in fact a lilo for use in the swimming pool was also tested. Each lilo measured 1.87 x 0.71 and was 0.12m thick. See Table 4 for a summary of dimensions. A dodecahedral sound source was used in two positions at a height of 1.5m and six receiver positions were selected for the Earthworks M30BX microphone. WinMLS software running on a PC laptop was used for processing results.

Airbed	*Length (m)*	*Width (m)*	*Depth (m)*	*Number Used*	*Area (m²)*	*Mass per Airbed (kg)*
lilo	1.87	0.71	0.12	6	7.9	1.2
Bestway "Thin"	1.9	1.37	0.22	4	10.4	2.8
Livivo "Thick"	2	1.6	0.44	4	12.8	6.2

Table 4: Basic dimensions of the three airbeds under consideration.

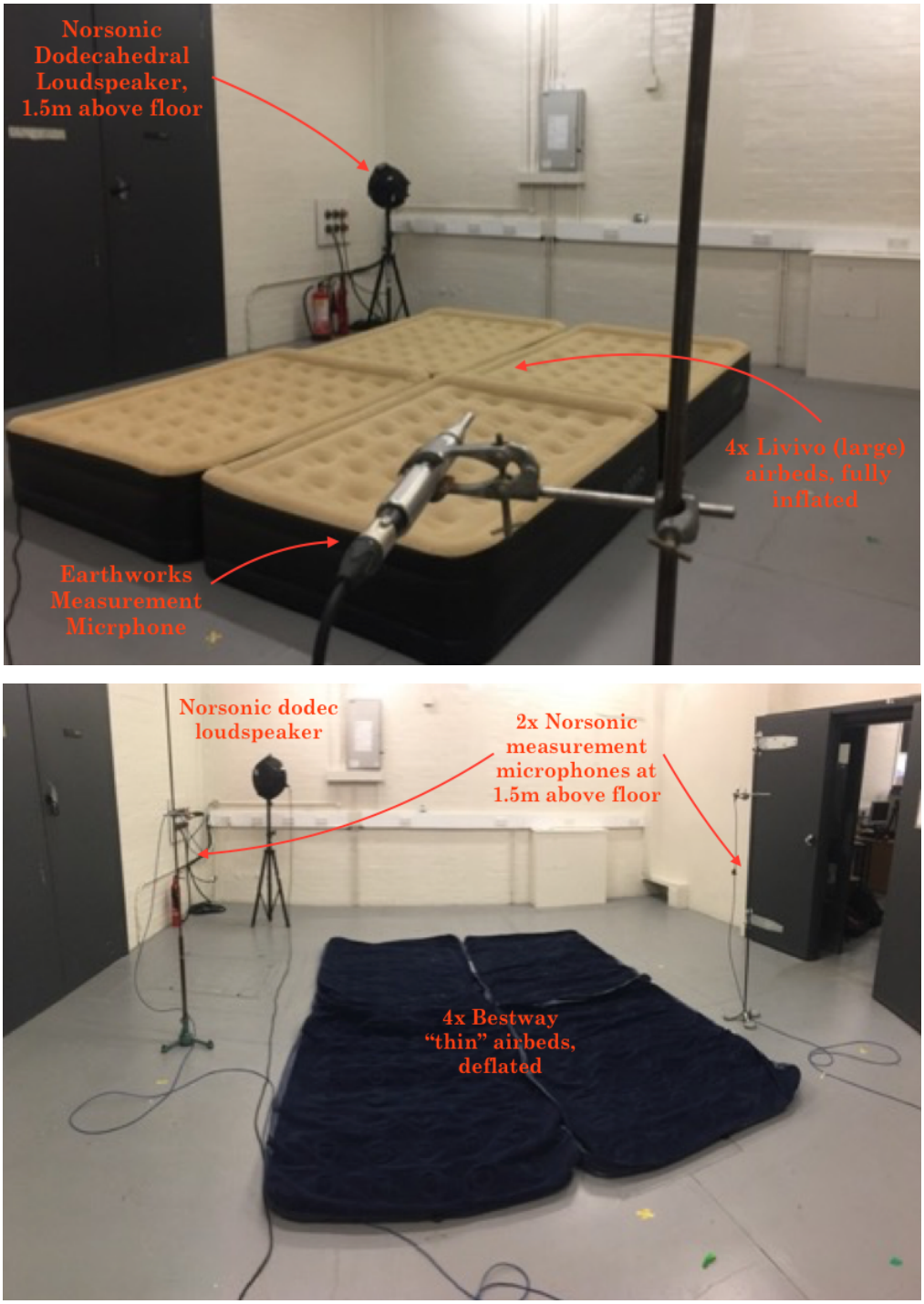

Figure 61: The two types of airbed undergoing testing in the LSBU reverberation chamber.

Absorption coefficient results in Figure 62 show that the airbeds' absorption were fairly broadband in the larger models (with only the lilo having a fairly narrow bandwidth of absorption) but with several resonant peaks, this is in line with Larsen's previous findings [111], with the higher frequency peak also being present when the airbeds were deflated, indicating that the material used in their construction was responsible for this particular feature of the response.

In a conventional membrane absorber, Eq 70 might be used to predict the lowest absorption frequency. In the case of inflatables, this equation does not hold, because rather than a simple infinite plane predicted by the equation, the airbed is supported by internal pressure and in-plane tension and tension pulling against internal drop cords. This causes bulging and wrinkling nonlinearities which will cause the equation to be in error, as shown by Larsen et al [115]. However, since no corresponding equation exists for airbeds, Eq 70 will be used as a comparison measure. The lowest peak was closer to that predicted by Eq 70, around 200Hz, but still far above the predicted 45Hz for the large airbed (based on an estimate of 40% of the overall mass being able to oscillate due to incident sound when placed on the floor). However, this is close to Larsen's estimate of four times the result from Eq 70 being accurate for airbeds.

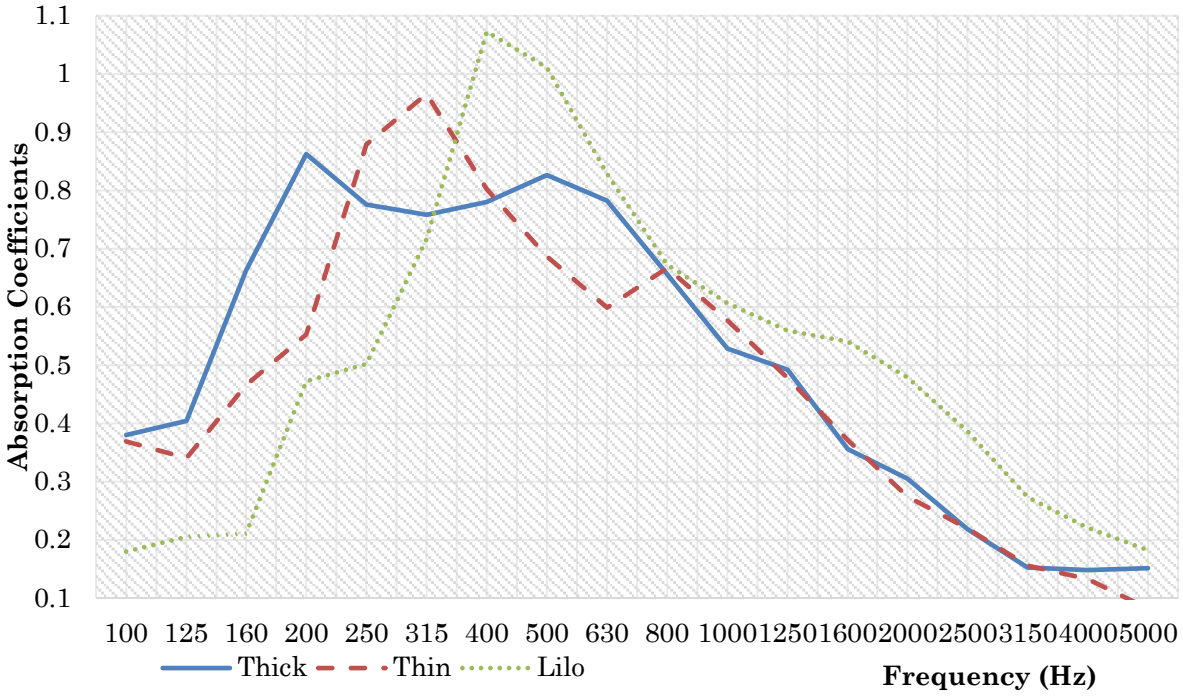

Figure 62: Comparison of Absorption Coefficients of thin, thick and lilo airbeds.

It must be noted that the lilo result displays an absorption coefficient above 1 which is of course impossible. This result is caused by a difference in scale of the edge effects of that sample compared to the thicker airbeds, due to the sample size used in the lilo test, where a test area of 7.9m^3 was used.

Bartel [35] showed that measured absorption coefficient is affected by the geometry of the sample. He defines the parameter E, the ratio of sample perimeter to sample area as a way of factoring in these edge effects in reverberation room tests. E is observed to have a linear relationship with measured absorption coefficient.

	Livivo	**Bestway**	**Lilo**
Perimeter	14.4	13.1	11.7
Area	12.8	10.4	8.0
E	1.13	1.26	1.47

Table 5: E (ratio of sample perimeter to area) for the three airbed types.

It can be seen that the test area comprising six lilos has a significantly larger E value than the other two airbed types, and corresponding higher absorption coefficients. Bartel also observes that the effect of edges is highly frequency dependent and different for each material.

The thicker of the two airbed designs was chosen for use in Henry Wood Hall as it displayed strong absorption at lower frequencies and a broader range of absorption, see Figure 62. The thick and thin designs show two main peaks of absorption. These might be expected to correspond to their dimensions, and taking the thick airbed first, this seems to be plausible, with (speed of sound in ms^{-1} divided by length in m)

$$f_{res} = \frac{343}{2} = 171.5\ Hz$$

This corresponds to the measured peak in absorption in the 200Hz 1/3 octave band. However, by the same reasoning, the other airbeds should have absorptive peaks at the near same frequency, as they are all similar in length (2m, 1.9m and 1.87m), however the thin bed has its main peak around 300Hz, and the lilo

around 450Hz. This indicates a dependence on thickness rather than width or length (see Figure 63). This appears to be because the edges of the beds are relatively unconstrained and free to vibrate, as opposed to the main face, whose surface is divided by drop cords and other constraints; hence longer wavelength waves are suppressed and those of the order of the wavelength of the unconstrained portions are favoured.

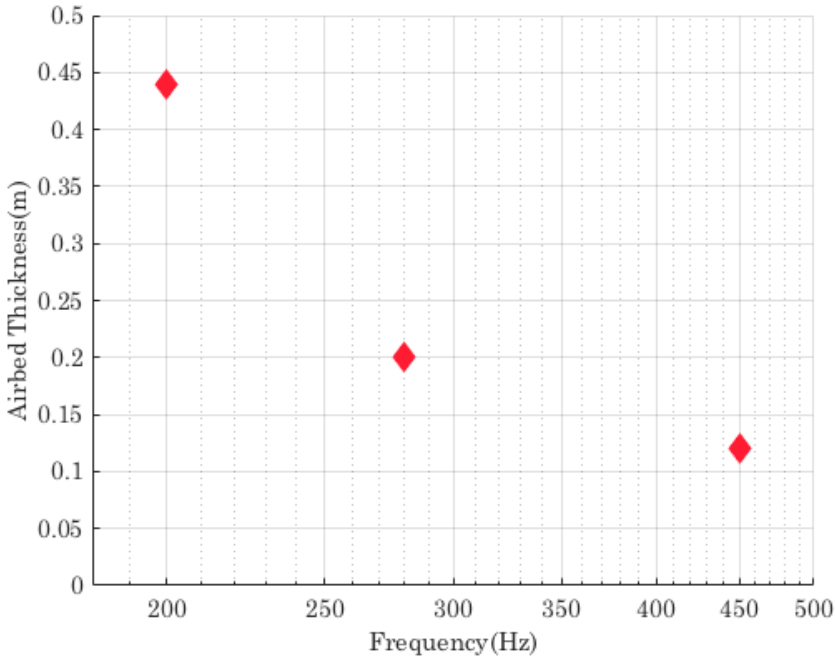

Figure 63: Frequency vs airbed thickness of the main (lowest) absorption peak for three airbeds.

The two deeper airbeds show at least one smaller peak in absorption higher up the spectrum, above 1000Hz, which correspond well to the distance between constrained portions. These vibrations will be damped more due to their curvature, which will also result in modal frequencies higher than those for a flat membrane. Lower frequency absorption, below the primary resonance, depends on airbed depth and mounting condition and is discussed below.

4.6.1.1 Effect of Pressure

To give some idea of how inflation changes the absorption characteristics of airbeds in practice, ISO 354 measurements were conducted in the reverberation room on the thicker airbed, which had been selected as the most suitable absorber for Henry Wood Hall, at different inflations. The expected use condition of the airbeds was for a single rehearsal session lasting two to four hours, so maintaining

operating pressure over time was not envisioned as an operational problem. Although the actual pressure in the airbed proved difficult to measure accurately or precisely, an estimation method was devised to explore inflation dependency in the reverberation chamber.

Figure 64: Partially inflated airbeds during inflation tests.

The large airbeds have a built-in pump, which connects to mains power and has a simple valve to ensure over inflation is not possible. This condition, where overflow air is leaking from the valve, was considered 'full inflation' and took around 2.5 minutes to achieve. Other inflation pressures of 1/2, 1/4 and 1/8 full inflation were achieved by activating the pumps for 1.25 minutes, 0.63 minutes and 0.31minutes respectively, making the simple assumption that the pumps provided a constant mass flow, and that each had near identical performance.

Thus, absorption was measured again in accordance with ISO354 at full inflation and again at 1/2, 1/4 and 1/8 full inflation, and also deflated on the floor. Given that it is a pneumatic structure, the geometry of the airbed changed significantly with inflation. While fully inflated, it presented a ribbed slab shape caused by the drop cords acting on certain small areas to constrain deformation into a near-sphere. This is the stable equilibrium shape envisioned by the designer at the form finding shape of their design. When in interim inflation stages, the shape becomes highly nonlinear, with much wrinkling, especially around the edges, but also across the face when lightly inflated (see Figure 64). The relatively unconstrained

edge of the bed, thought to contribute most to low frequency absorption, is first to become nonlinear as inflation decreases, so it was expected that low frequency performance would be best at full inflation.

Figure 65 shows the dependency on inflation. Below 315Hz, absorption increases with inflation, with a resonant peak at 200Hz becoming increasingly dominant with inflation. This peak absorption frequency appears to be unchanged by inflation pressure, indicating an overall linear response. One nonlinearity, however, is the response below 125Hz, which shows only a small amount of absorption, decreasing as frequency lowers; but as full inflation is reached, an additional absorption peak of around 0.4 at 80Hz is shown. This is believed to be due to the edge of the Livivo bed becoming completely flat in this condition and thus allowing the long, unconstrained surfaces of the sides to act as plane membranes unhindered by local crumpling and shell-like nonlinear portions associated with partial inflation.

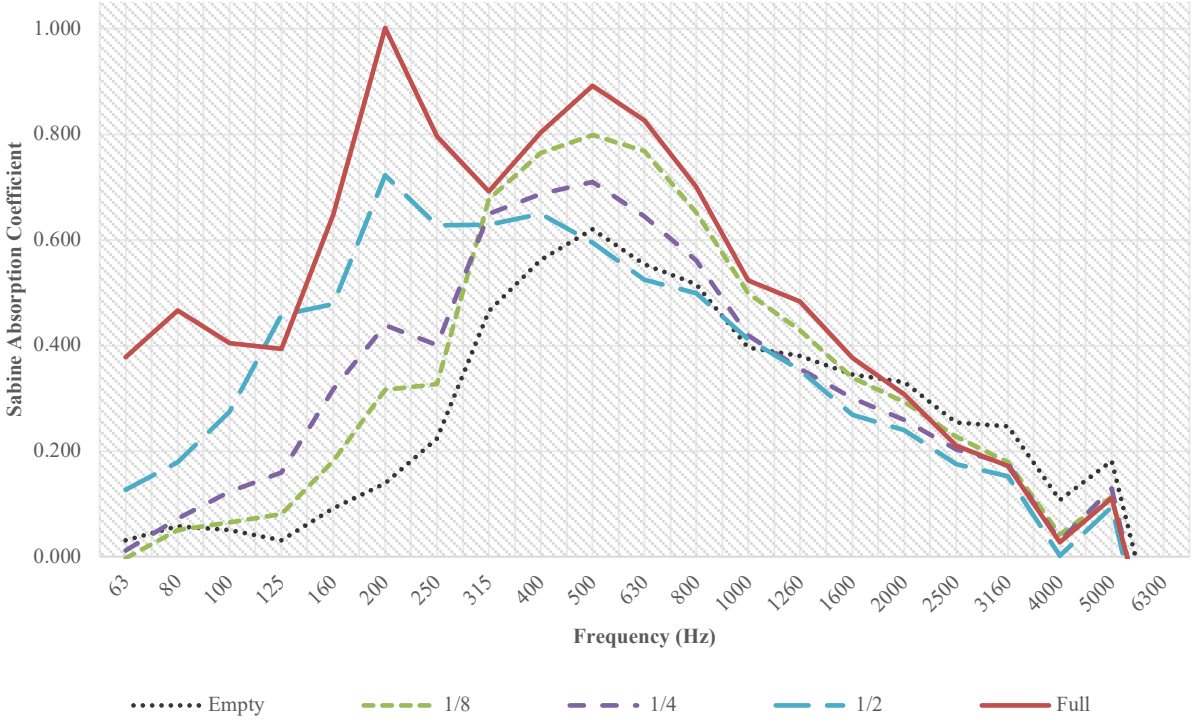

Figure 65: Dependency on inflation, 4 airbeds in reverberation chamber.

Above 315Hz, the response is not so linear; a large increase in absorption is shown as inflation increases from the empty state to 1/8 inflation. Absorption then

reduces as inflation increases to 1/4 and 1/2, before increasing again at full inflation. This is thought to be due to scattering from the semi-inflated airbed whose surfaces become curved and crinkled with partial inflation, thus scattering incident energy more efficiently. This characteristic becomes reduced at half and full inflation as the bed takes on its more regular, near-rectangular shape, and at full inflation there is again increased curvature as the bed strains against the increased internal pressure.

It is instructive when thinking about the effect of inflation, to normalise the absorption coefficients to the absorption of the deflated beds, which must be due to the material alone, as no surface is pneumatically supported in such a way as to allow membrane resonance of any kind. These modified results are presented below (see Figure 66).

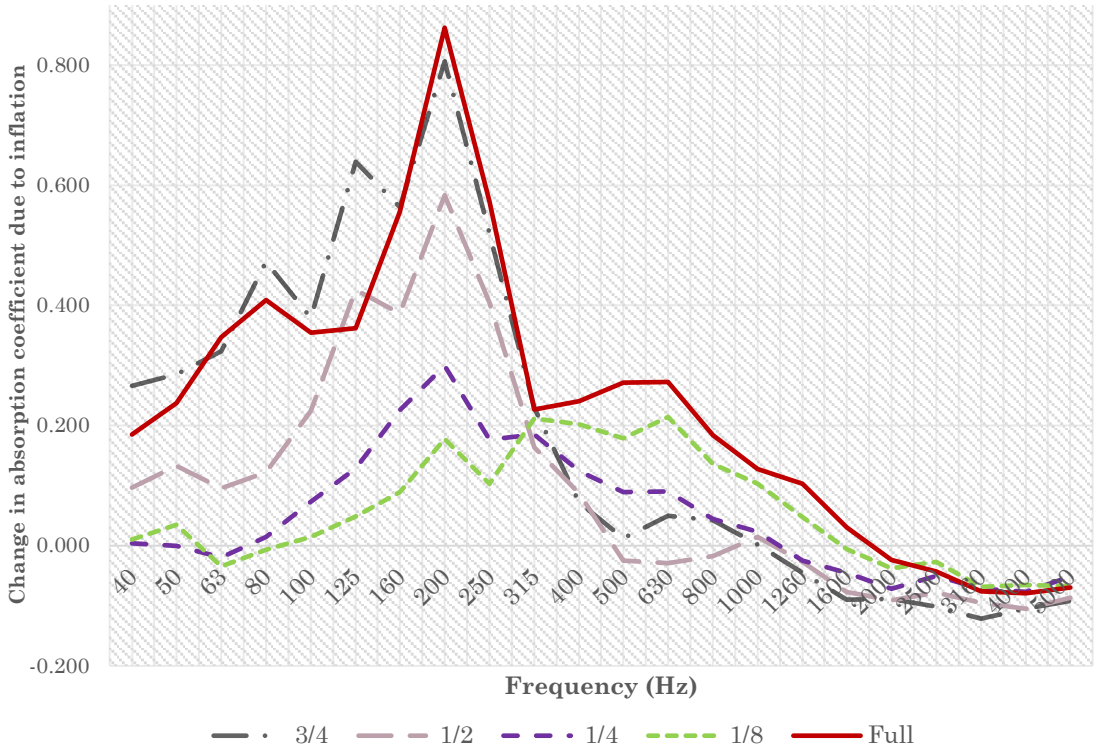

Figure 66: Normalised change in absorption coefficient due to inflation.

Also, shown in Figure 66 is the absorption at 3/4 inflation, which interestingly shows increased low frequency absorption compared to full inflation. At 1/2 and 3/4 inflation, additional absorption peaks are present below the main peak. As inflation maximises, these secondary peaks are supressed.

Figure 66 shows more clearly the effect of inflation. At and below the peak at 220Hz, absorption correlated near-linearly with inflation. Above this frequency, things were not so straightforward. At 1/8 inflation, absorption increased, in quite a broadband manner, but then reduced with increased inflation. It is thought that this is because the initial inflation lifts the membrane little, but provides little damping, so this curved, crumpled surface can move somewhat freely and absorb and scatter in complex ways. Further inflation also increases damping and tension in drop cords, so this mechanism is suppressed.

Finally, when full inflation is achieved, the front surface is uncrumpled and thus uniform in geometry, and also drop cords are taut and constrain the face in a uniform pattern. The taut cords would restrict motion of the front face, thus absorption occurs only at resonance frequencies of the portions of the face between drop-cords, as shown by the peak around 630Hz.

Interestingly, looking again at Figure 65, at half inflation, absorption has a broader bandwidth than at full inflation, with the low frequency mechanism complementing the contribution from the airbed's materials. Since precise targeting of the "boom" in the hall was not immediately possible, this was considered desirable, so hyperinflation was avoided, and the hall management were instructed not to be overly vigilant regarding maintenance of full pressure. Thus, reducing the time spent on maintenance of the proposed solution.

4.6.1.2 Installation Location

A further test was undertaken to determine the influence of mounting position on the absorption achieved, as this can be critical, as shown by Warnock [36] and by Bartel [35]. This is normally of key importance with any absorber, as it must be remembered that laying a sample in the centre of the test room in ISO 354 measurements is a standardised and easily replicable procedure. In real rooms, absorption can almost never be placed in the centre.

Mounting in other parts of the room changes absorption performance because of differing effects of scattering from edges, from different coupling at low frequencies to room modes, and from a differing amount of surface area exposed to the sound in the room if, for instance, several absorbers are mounted separately as opposed to all in a single block.

Further measurements were undertaken to compare the absorption achieved with mounting of these airbeds propped around the corners and edges of the room as opposed to standard mounting in the centre of the reverberation room, with the results showing a little more absorption at lower frequencies. However, this mechanism may be less pronounced with the beds deployed in Henry Wood Hall, as that space is suitably large to be non-modal at the frequency range of interest, whereas the reverberation room, where this test was conducted, certainly is modal.

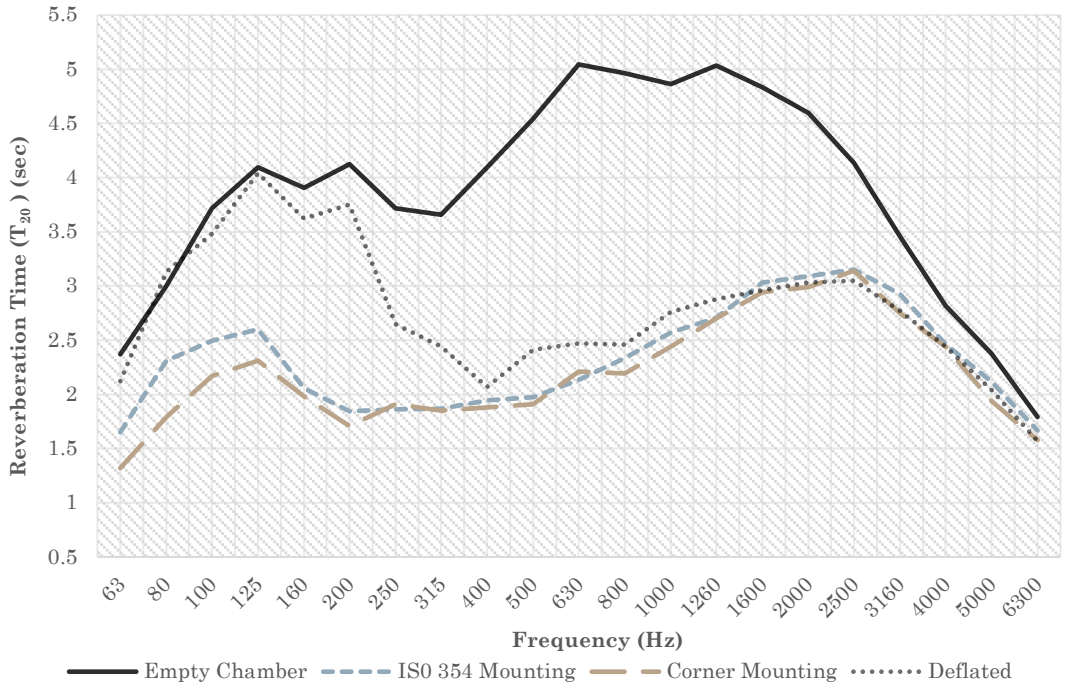

Figure 67: Dependency on mounting position within the reverberation room.

Figure 67 shows that the reverberation at low frequencies was reduced most when the airbeds were positioned in the four lower corners in the chamber compared to the normal grouped position in the centre of the room. This result demonstrated the optimal arrangement for the airbeds in their final deployment.

4.6.1.3 Spatial variation on the airbed surface

The construction of the airbed is too complex to allow generalisation about its resonant frequency; curvature, size of open area and proximity to constraints determine the dynamics of a given portion of the bed. But a further experiment was undertaken to explore this spatial dependence further. A single thick airbed was placed in the LSBU anechoic chamber (see Figure 68).

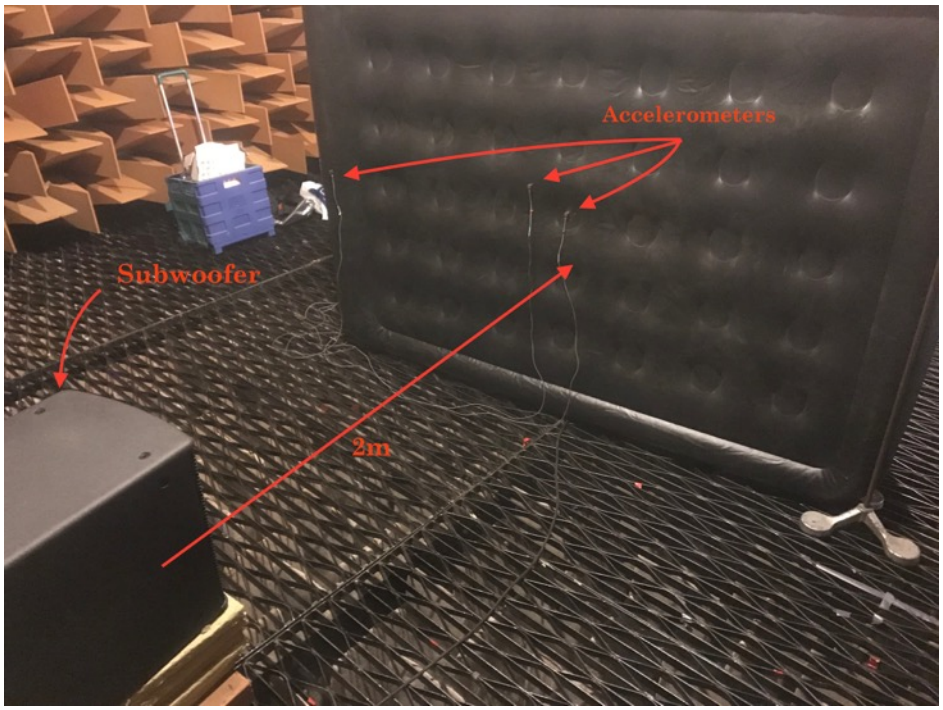

Figure 68: The Livivo airbed mounted in the LSBU anechoic chamber, with accelerometers mounted and connected to the B&K LAN-XI system.

The experiment consisted of a JBL subwoofer sound source driven by a Devine hi-fi amplifier using a pink noise source signal. The motion of the membrane was measured in several places using three accelerometers feeding a Bruel & Kjaer LAN-XI system. Three initial positions were chosen to represent key locations on the airbed

1. The main surface of the airbed, just off-centre and in-between constraints/drop cords. This section is lightly curved due to inflation. This represents the majority of the bed's surface.

2. The area above the constraint next to accelerometer 1. On this particular airbed this comprises a circular plane drop structure. The volume thus enclosed does

not appear to be part of the inflated volume, however, it is surrounded by the inflated volume and closely coupled to it.

3. The edge of the airbed, where the front surface transitions to the side face. This is a highly curved but relatively free area, relatively far from drop cords.
   The source was placed 2m from the bed, initially at normal incidence to it and opposite the centre of it. A time series measurement was taken for 5 seconds of pink noise and enough time to encompass the free decay of the airbed surface. It must be stated that ideally a plane wave source would be used; the subwoofer is not truly that but was deemed acceptably so at the frequency range of interest. It should also be noted that the airbed is not a Type 1, locally reacting absorber. Below 160 Hz the airbed was in the near field of the source: a direct consequence of the size of the chamber. Despite these shortcomings it was felt that further insight could be gained into the response of the complex structure inside the airbed.

   The results from the three accelerometers are shown in Figure 69. Both the accelerometers on the main front face of the airbed showed an identical resonance frequency around 95Hz, although the face of the constrained portion had a narrower resonance peak. This is significantly lower in frequency than the absorption peak shown in the reverberation chamber under random incidence. This could be a coupling effect which changes the resonant frequency when in a reverberant, modal sound field.

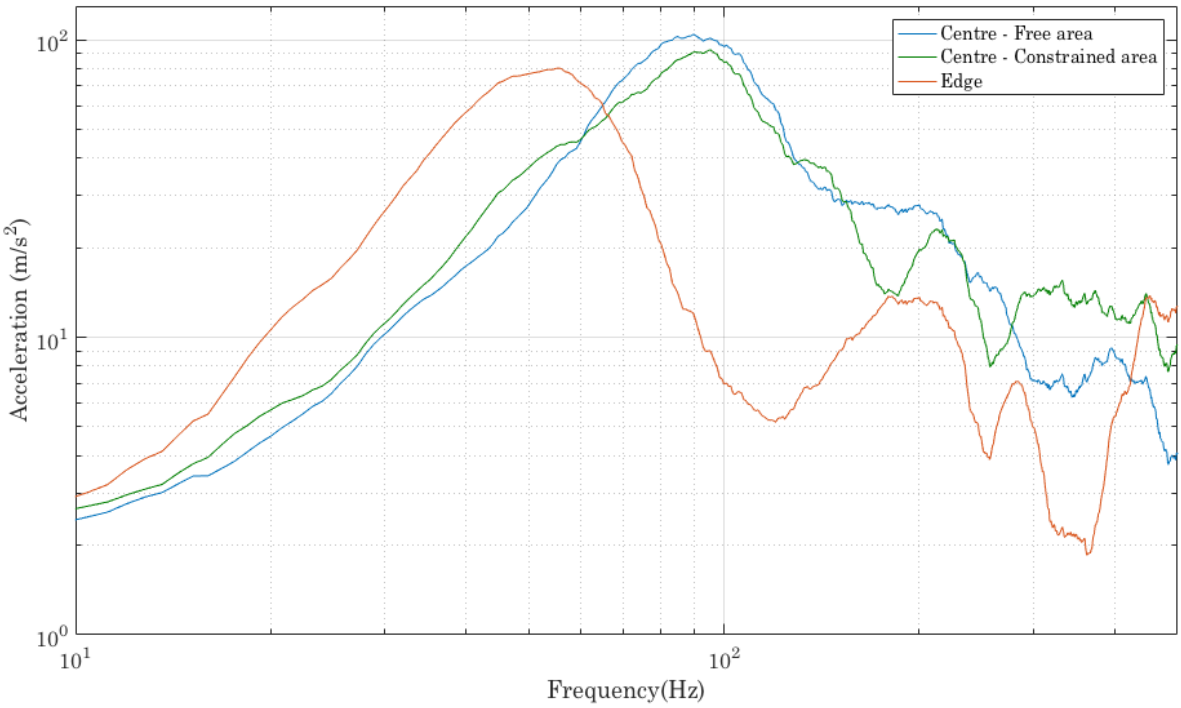

Figure 69: Frequency response of airbed at three locations on the surface in anechoic chamber.

The accelerometer on the edge of the bed, however displayed an even lower, and narrower resonance of 50Hz, most likely due to its proximity to the long, unconstrained portion of the bed around the edge. This demonstrated that the airbed did indeed react in a complex fashion which might explain how such a broad range of frequencies were absorbed in the laboratory experiments.

4.7 Installation in Henry Wood Hall

Although an affordable, portable absorber with good performance had been identified and tested, ultimately the space limitations in the hall were the constraining factor in the amount of absorption which could be achieved. The available space around the rear of the rostra and the choir stalls was calculated to accommodate 30 airbeds.

A comparison of room volumes between the reverberation chamber and Henry Wood Hall suggested that 30 airbeds in the hall was equivalent to one airbed in the reverberation room, as opposed to the four used in the ISO354 tests; therefore, it was anticipated that a modest but meaningful amount of absorption could be achieved. It should be remembered that this was a successful space already and

that this treatment should be a refinement of the existing acoustic, rather than a drastic modification.

The airbeds were installed by a team of four people within the target time of one hour. No special equipment was needed, as inflation was achieved using each airbed's built-in pump. This pump is mains-powered and had a built-in overfill valve to ensure correct inflation. With a four-way mains power block, each person could inflate four airbeds simultaneously, with each bed taking around 2.5 minutes to fully inflate (see Figure 70).

Figure 70: Airbeds upon installation in Henry Wood Hall.

4.8 In-Situ Test Results

The effect of the airbeds on the acoustic within Henry Wood Hall was tested in accordance with ISO3382-1 using a Norsonic dodecahedron loudspeaker/Norsonic Nor280 amplifier combination in two source positions, and an Earthworks M30BX measurement microphone in six receiver positions. WinMLS software running on a PC laptop was used to perform the tests and process the results.

Again, the hall was tested as found, with curtains mainly pulled back and chair and music stands set out ready for a large chamber ensemble (see Figure 70). The management explained that the musicians preferred a naturally lit hall over artificial light. The results for reverberation time measurements, before and after installation of the 30 airbeds, are shown in Figure 71.

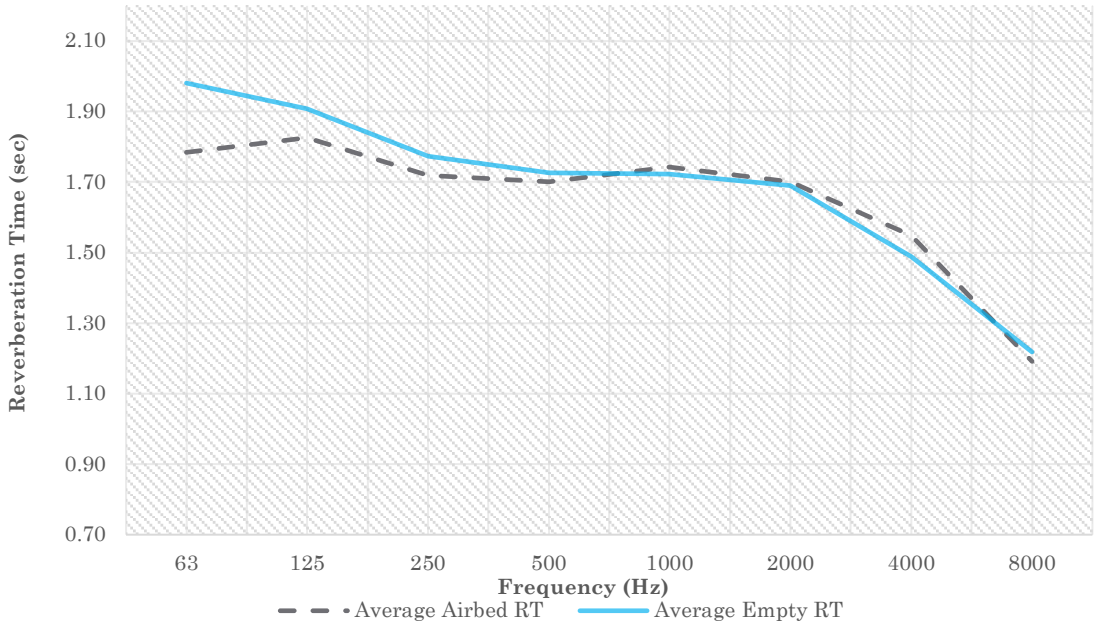

Figure 71: Measured RT with and without 30 inflated airbeds in octave bands.

As predicted, the absorption achieved was modest, but this was expected given the relatively small area available for absorption when compared with the volume of the hall. But this was considered a successful outcome, as only a subtle modification was required to improve the acoustics of the room without adversely affecting its good qualities.

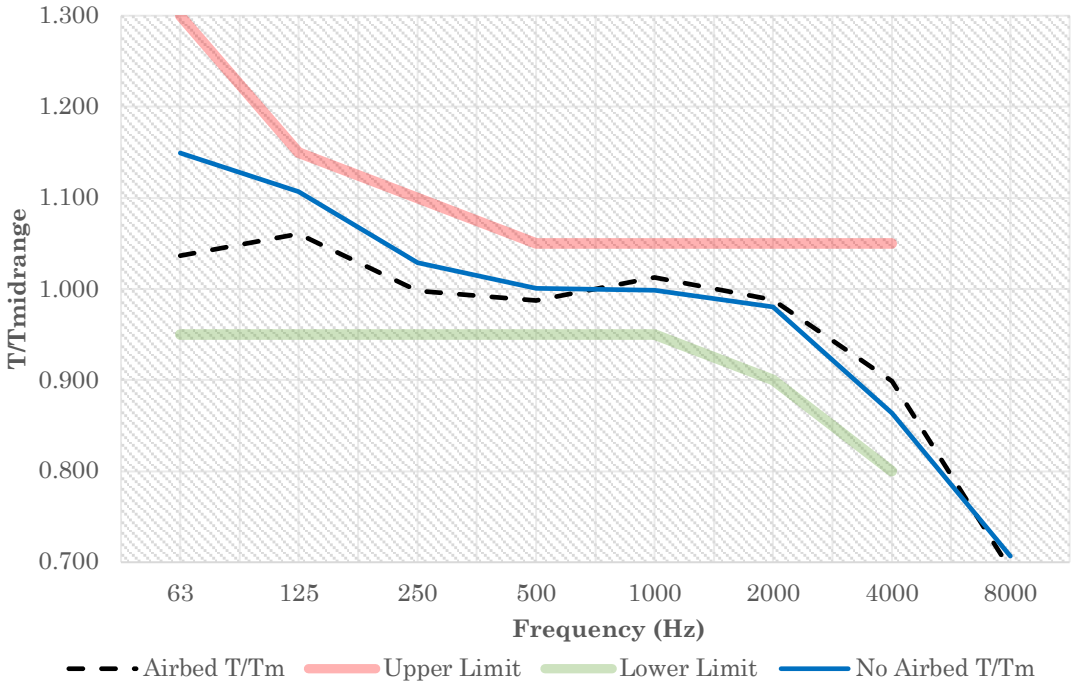

Figure 72: Airbed results with reference to NS8178 frequency dependence guidance. [62] NS8178 guidance reproduced with permission.

As discussed in section 2.5.3, Norwegian standard NS8178:2014 gives guidance for suitable frequency dependence of reverberation time in performance and rehearsal spaces. Figure 72 shows the result for reverberation time in Henry Wood Hall with 30 airbeds with reference to this guidance [62]. The most affected frequency bands were those specifically targeted, the 63-250Hz octave bands, showing that the absorption behaviour was in line with that predicted by the ISO 354 tests on these airbeds. Absorption was well spread over several of the lower octave bands, however absorption above 1kHz was minimal as required. Bass Ratio was changed from 1.07 (empty condition) to 1.03 (with 30 airbeds present). Figure 73 shows a more detailed 1/3 octave band analysis.

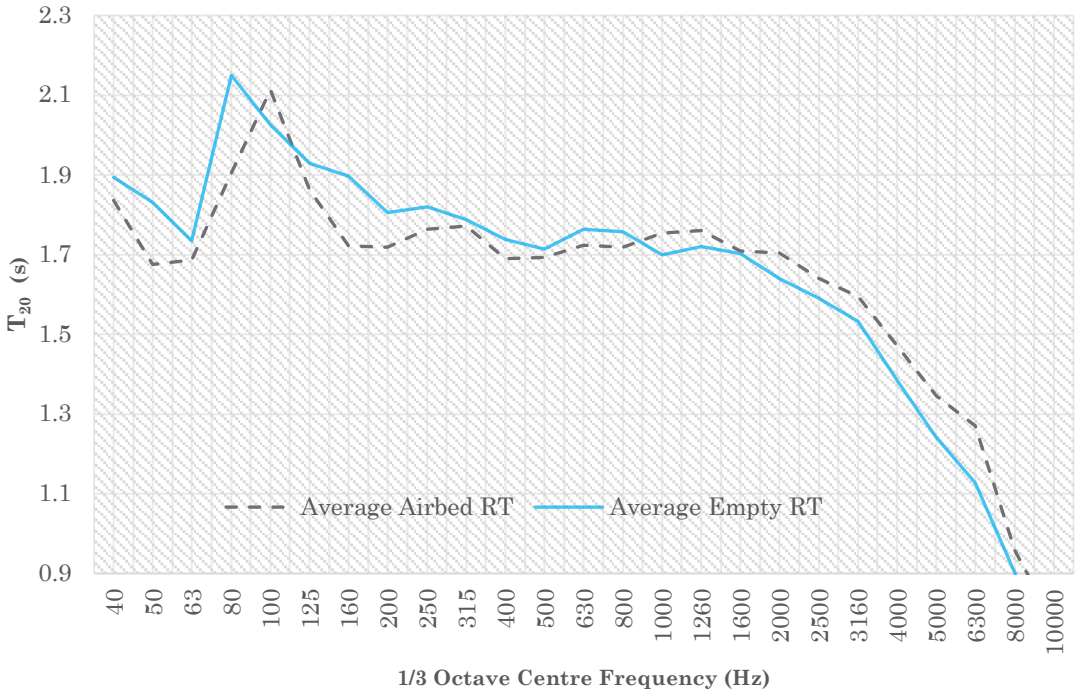

Figure 73: One-third octave ISO 3382-1 Results for 30 airbeds deployed in Henry Wood Hall.

Looking at the 1/3 octave band results (see Figure 73) it can be seen again that significant absorption has been achieved below 315Hz, although the nature of the resonant peak of the room is more apparent. The addition of the airbeds has caused the room resonance to move from the 80Hz 1/3 octave band to the 100Hz band. There are two possible contributing factors for this, first it is an effect of the coupling of the sound field in the room with the airbeds, and secondly, the presence of the airbeds effectively reduces slightly the volume of the room. This latter is only a small change, approximately 0.5% of room volume for 30 airbeds. This can also truly be taken to be the case at higher frequencies.

4.9 Subjective Performance

The response from users of the hall was positive; Robin Ticciti, the Musical Director of the Glyndebourne Opera noted that the hall was "drier in the lower register", while appreciating its discreet form "[the] solution is not visible to the orchestra or conductor". Interestingly, the Manager of the hall, Charles Strickland, mentioned that the hall seemed less harsh in *tutti* passages, "…I have to say I can hear a difference; it seems less harsh when large forces are playing all at once". This is an interesting observation as one normally associates

"harshness" with the 2-4kHz range to which humans are most sensitive – several instruments in the orchestra can sound "harsh" in this range such as violin, piccolo and E*b* clarinet. If anything, this reduction in bass frequencies might be expected to make the orchestra sound harsher in the room. However, it may, by removing energy from lower pitched, masking instruments, allow a more rounded tone in higher pitched instruments, leading to a reduction in perceived harshness.

This solution was intended to be affordable, flexible and portable, and for occasional use. However, and somewhat unexpectedly, the airbeds have remained deployed in the hall for all rehearsals since installation and appear to be popular for all repertoires.

4.10 Conclusions

Airbeds were selected for use in a music rehearsal space, with expected behaviour akin to that of a membrane absorber, albeit one with behaviour less easily predicted using analytical methods. Therefore, ISO 354 tests were undertaken to assess their effectiveness. Having selected an appropriate airbed type, and an appropriate number, they were installed and tested in accordance with ISO3382-1. The result was a small but significant reduction of reverberation time in lower frequency bands. The installation has become a permanent fixture and the acoustics have been well received by users.

This study and previous work [115] have shown that inflatable absorbers are a viable option for low frequency absorption with certain favourable characteristics such as light weight and inherent adjustability by inflation/deflation.

There appear to be three frequency regimes in an airbed-like pneumatic structure comprising an inflatable envelope constrained by drop cords or other restraints.

- Primary resonance, in the manner of a conventional membrane absorber, although existing empirical relations are insufficient due to curvature and other

nonlinearities in pneumatic structures, with the primary resonance generally being higher than predicted by Eq 70. Larsen *et al* quoted a figure of four times higher in their study of air mattresses [111], but in this study, the measured frequencies were closer to what classical theory predicts.

- Low frequency absorption, broadband and below primary resonance, this correlates well with airbed depth, or area of unconstrained side material.
- Higher frequency absorption, due to membrane-type resonance in smaller portions of the airbed face, in-between constraints.

Specialist absorbers could be designed to cause these three mechanisms to act together to give very broad and even absorption, the key being in understanding the effect of the presence of the drop cords. This is a problem which defies a simple analysis as the arrangement is sufficiently complex such that there is no archetypal geometry to form the basis of an analytical solution, and each case would require careful modelling using FEM or other numerical method.

Giving the client some agency (within certain bounds) over their acoustic solution in the form of a modular solution resulted, after a short period of experimentation, in an optimised solution which the management and users can take ownership of and benefit from.

5 Case Study C: Targeted Energy Transfer

Targeted Energy Transfer (TET) is a relatively new passive loss mechanism where energy in a vibratory system is trapped in a nonlinear attachment, thus damping the main system. A certain amount of literature is present in the physical acoustics and nonlinear dynamics fields for TET, and it was hoped to build on the relatively slim portion of that literature relating to acoustics (as opposed to vibration, which is better represented) and investigate the mechanism's suitability to architectural acoustics.

The literature in acoustics suggested that a light weight, broadband, small sized low frequency absorber was theoretically possible, which could be constructed from readily available and inexpensive materials. It was hoped to bring this to fruition, but in the end this work could not be completed for technical and logistical reasons. Therefore, this chapter briefly details the preparatory work which was undertaken, together with a few interim experimental results taken before the line of research was abandoned.

5.1 Test Rig

Cochelin *et al* [137] and Bellet *et al* [138] [120] were the first to explore TET in acoustics. The linear subsystem comprised an acoustic mode within a duct, energised by a loudspeaker at one end, and the nonlinear subsystem an elastic membrane. As a nonlinear response is required, conventional (non-elastic) membranes cannot be used as their stiffness (in the case of a plate) or tension (in the case of a membrane) do not permit large vibrations, and hence they respond in a largely linear way. Elastic membranes permit large excursions, with a cubic stiffening nonlinearity arising geometrically as resistance increases with displacement, as described by McFarland et al [136].

As a starting point to explore the Targeted Energy Transfer (TET) mechanism it was decided to create a similar rig to first recreate their simplest observations and continue from there. The rig was based on the work of Bellet *et al* [138] and comprised a loudspeaker source coupled to a 3m long pipe (see Figure 74)

terminated at a coupling volume with a clamp with which to mount the sample at its far wall (see Figure 75).

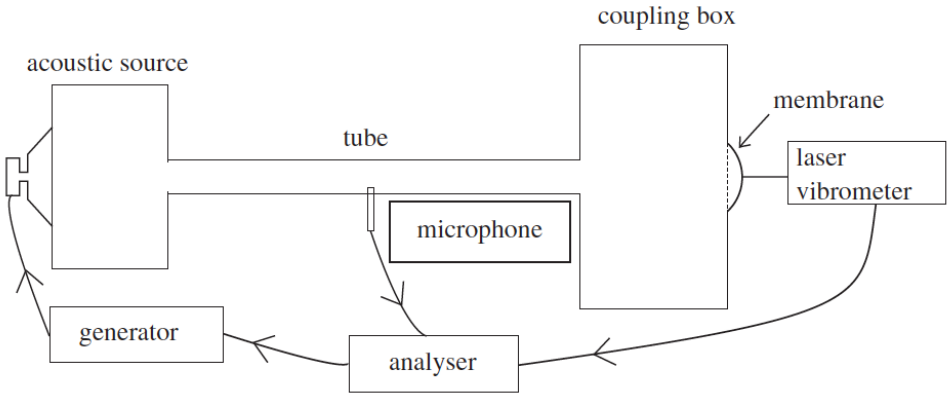

Figure 74: Arrangement of test rig from Bellet et al [138]. Reproduced with permission.

This arrangement was designed to present plane waves incident at the sample, which was mounted with fixed edges such that the majority of the sample was free to make large excursions in response to the incident wave. The coupling box was considered small enough that its modal effects are out of the frequency range of interest. It is also deep enough that nonlinear effects close to the pipe ending were considered to not affect the sample. At frequencies of interest, pressure was considered constant within the box.

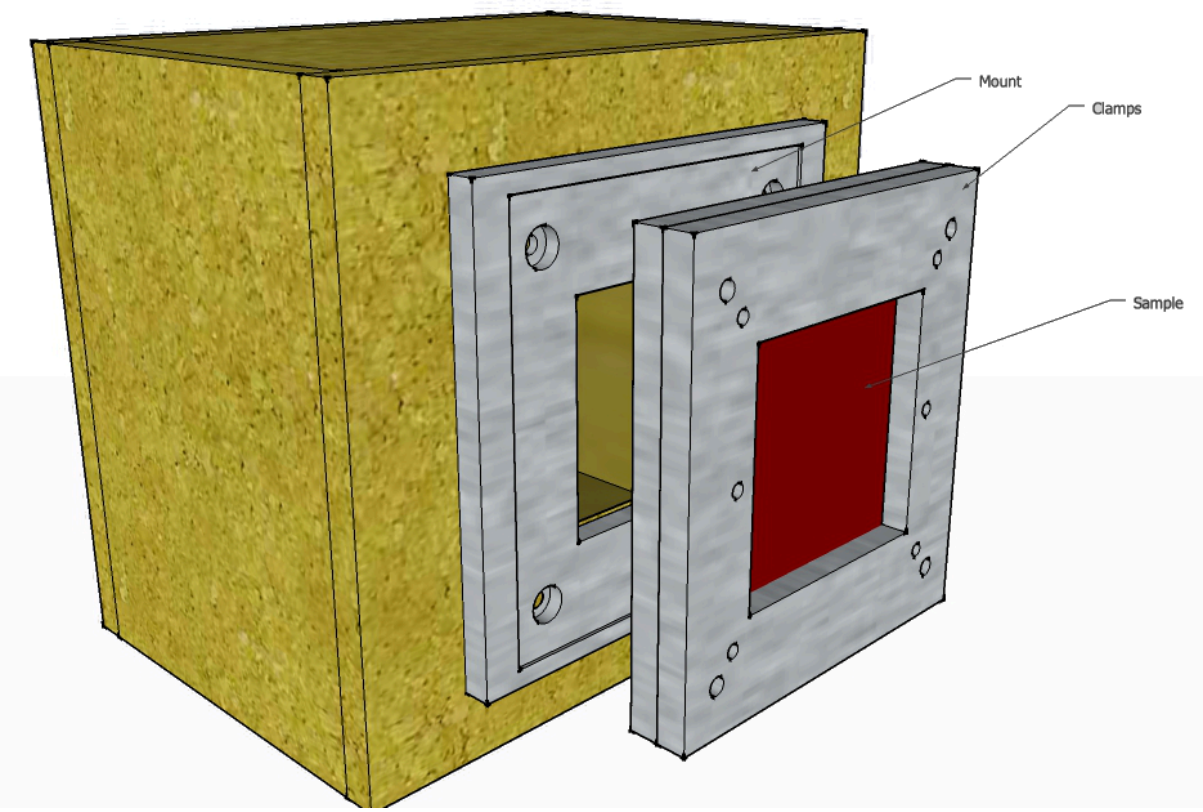

Figure 75: Conceptual drawing of the coupling box.

Both the loudspeaker and coupling boxes were constructed from 18mm thick MDF with dimensions selected to match that constructed by Bellet *et al* [138] (see Table 6).

Dimensions (in m)	***Length (m)***	***Width (m)***	***Height (m)***	***Volume (m^3)***
Speaker Box (External)	0.37	0.32	0.36	
Speaker Box (Internal)	0.33	0.28	0.32	0.029
Coupling Box (External)	0.25	0.35	0.32	
Coupling Box (Internal)	0.21	0.31	0.28	0.018

Table 6: Dimensions of speaker and coupling boxes in test rig.

The tube was 91mm in diameter and was connected to the boxes at each end via an interference fit to a pipe connector section glued with epoxy and secured with a wooden plate to each box. The resulting fit was considered not sufficiently secure, so rubber bridging rings were clamped over the joint to secure it. The boxes were isolated from each other by being mounted on separate benches and via rubber mats.

5.2 Latex Materials

Two types of hyperelastic material were trialled, one natural rubber and one silicone-based latex - neither being a specialist material. Special properties such as durability could be considered if creating a commercial product utilising the TET mechanism, but for the present study this was considered less important. Durability was considered briefly in 5.2.2.1 to ensure that the material was sufficiently stable over the duration of the testing schedule.

5.2.1 Tensile Tests

To investigate the tensile properties of the sample materials, tensile tests were undertaken in the LSBU Material Testing Lab in accordance with ISO 37:2017 [165]. Test specimens were cut out in that standard's Type 1 sample dimensions, with test length being 20mm±0.5mm. The width of the test strip was 2.0mm±0.2mm. The samples were cut out using a rotary cutter to avoid tearing.

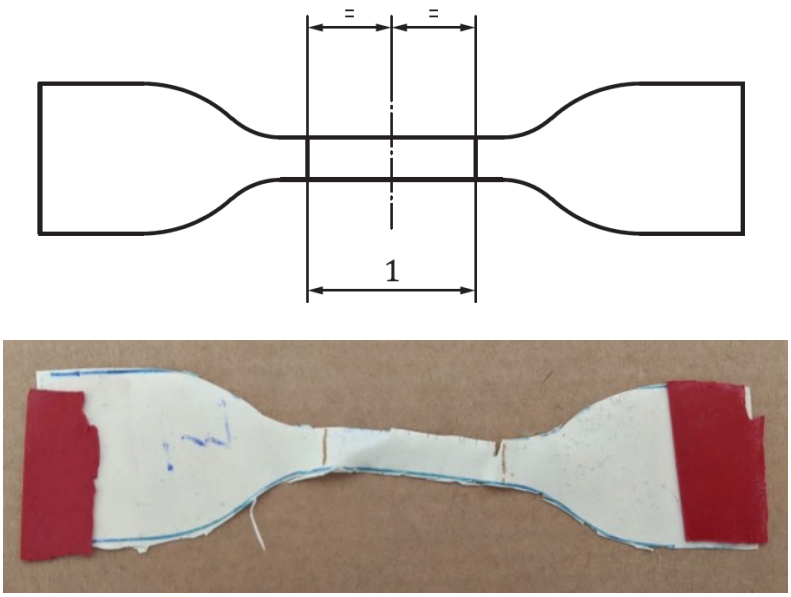

Figure 76: (Top) Standard dimensions of tensile test sample as defined in BS ISO 37:2017. For a Type 1 test piece as used here, the test length (1) was 20mm±0.5mm [165] (Bottom) Silicone test specimen after tensile test. The red portions show thicker silicone sheet used to enable a good purchase by the testing machine's grips.

The samples were mounted in a Tinius Olsen H25KS Materials Testing machine fitted with a 2.5N load cell. The initial clamp spacing was 65mm. The grips advanced slowly in 0.5mm steps for the rubber sample (0.4mm steps for the silicone sample) whereupon stress was measured. The results for both materials are shown in Figure 77 alongside 6th order polynomial fits to the data.

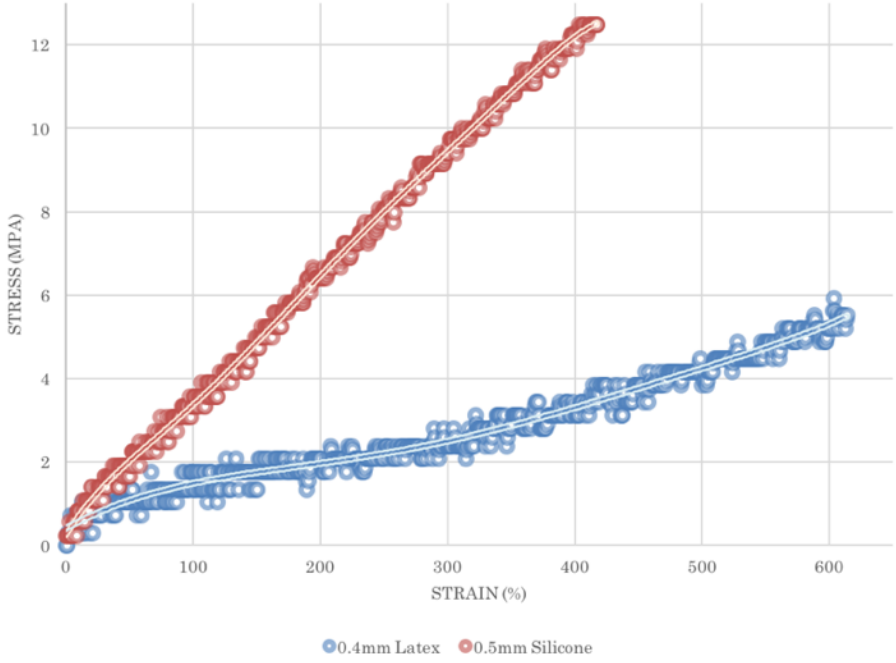

Figure 77: Tensile test results for rubber latex and silicone samples, tested in accordance with BS ISO 37:2017.

Both materials were broadly linear within the test range, with the rubber sample showing a very shallow yield point around 100% strain, but even after this point, its behaviour deviates little from the linear. The silicone sample was stiffer and showed near perfect linearity within the range of interest, with Young's Modulus calculated to be 0.03GPa.

5.2.2 Long Term Stability of Rubbers

Most rubbers and artificial latexes are not stable in the long term. The mere presence of air and sunlight triggers free radicals within the material to precipitate an autocatalytic process called autooxidation. This was originally studied by Bolland [166]. In autocatalytic processes, the result of the chemical reaction acts as a catalyst in the same reaction, thus a self-perpetuating degradation occurs. This normally propagates from the surface of the material, where brittleness and cracking may eventually occur, towards the inside. Later, Gryn'ova *et al* showed that the autooxidative process originates at structural defects in the material, such as terminal or internal double bonds, which originate at manufacture or because of degradation [167]. This improvement to Bolland's model opens the way to more durable materials being developed.

5.2.2.1 Creep Tests

While this thesis does not concern the materials themselves, as any hyperelastic membrane material may lend itself to the application, a simple stability test was undertaken to give an idea of the test materials' suitability in the long term, and even for the duration of testing.

BS ISO 899-1: 2017 gives a framework for performing creep tests on polymeric materials [168] and the test was done in accordance with this standard as closely as practicable over a two-week duration.

A test specimen was prepared, and a pre-load was applied, and then measurements of strain were taken after 30s, 60s, 2mins, 4mins, 8mins etc. in doublings of time up to 14 days. The range of loading forces were chosen to

reflect the range of loading force the specimen would experience in the test rig, allowing for the smaller cross-sectional area of the test specimens. The masses used were 17.5g, 52.5g and 105g. These had the same general geometry as those for the tensile test but were 7mm wide with a test area of 30mm.

Shao's [141] parametric study of TET indicated that there was a linear relation between operating range and membrane thickness. Therefore, for creep tests, and initial tests to identify the TET phenomenon, the thinnest available membrane was used. For creep tests, a silicone-based latex of 0.22mm was used.

Results were calculated in terms of tensile creep modulus E_t as defined in ISO 899-1.

$$E_t = \frac{\sigma}{\varepsilon_t} = \frac{F.L_0}{A.(\Delta L)_t} \qquad \text{Eq 87}$$

where σ is stress, ε_t is strain at time t, F is the applied force in Newtons, L_0 is the initial gauge length in mm, A is the initial cross-sectional area in mm^2, and $(\Delta L)_t$ is extension at time t.

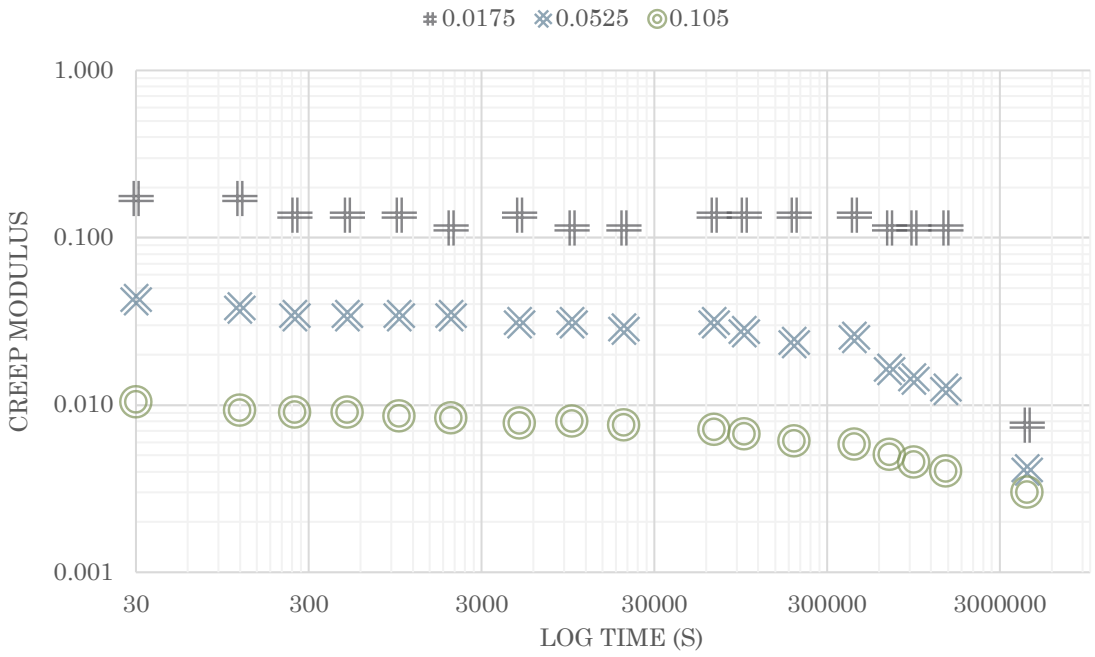

Figure 78: Creep test on 0.22mm Silicone membrane samples, under three static loads (0.0175kg, 0.0525kg and 0.105kg) over 14 days.

The results are shown in Figure 78. Creep modulus has an inverse relationship with applied load and decreases over time as the samples exhibit excess strain due to creep induced deformation. The sample with very light loading showed very little (but not zero) decrease in creep modulus over the duration of the test. The other two samples showed similar levels of decrease in creep modulus, with the rate of decrease becoming more rapid toward the end of the two-week test. This is to be expected as conventional rubber and silicone-based materials are not known for their durability. This is, however, an active area of research, notably in the medical industry as elastic materials are widely used. To be useful in a widespread manner without constant renewal, any TET-exploiting "absorber" would need to await new, durable hyperelastic materials. It can be concluded, however that samples mounted for a duration of a few days would not degrade significantly.

5.2.3 Mounting of Samples

The mounting clamp assembly was constructed from 15mm aluminium on a CNC milling machine in LSBU's Mechanical Engineering Workshop. It comprised a mount to interface the sample holder to the coupling box, and a sample holder comprising two near identical plates with an opening of the size of the sample at their centre.

- Mount: This comprises a 240 x 240mm plate with a 120 x 140mm opening for the sample in the centre. It is mounted to the coupling box via four M8 bolts, the heads of which are recessed to allow mounting of the sample clamp. A stock surface finish was applied by the workshop and this was considered sufficient for early tests, but later a 1mm thick rubber gasket was used at the clamp-mount interface. A 1mm recess in the mount helps to locate the clamp holder in the correct location over the opening (see Figure 79).

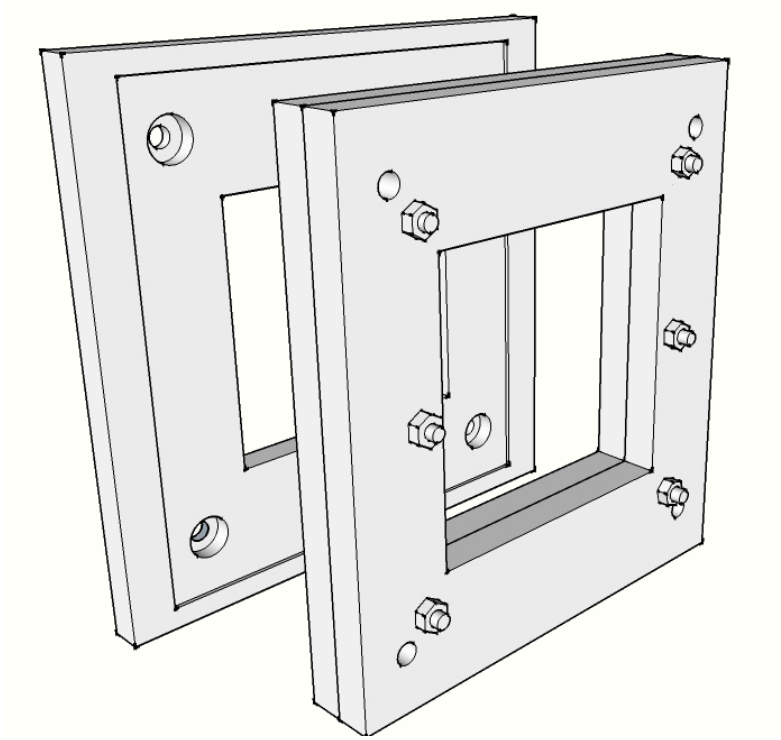

Figure 79: 3D design for clamp assembly.

- Clamps: These two flat plates support the sample and are held together via three M6 bolts on each side. Since very thin rubber sheets will be mounted here, the flatness of the inner surfaces is critical, and surface roughness (R_t) was specified to be 0.025-0.05mm. The clamps thus assembled are attached to the mount via four M8 bolts.

Pre-Stress: Samples were lightly pre-stressed and mounted using a rack made for the purpose from wood. This comprised a base with two clamps, one fixed to the base and one floating, to which a mass hanging over the edge of a bench could be attached via rope (see Figure 80). In this manner, the membrane could be held under the tension due to a known mass while it was clamped into the sample holder.

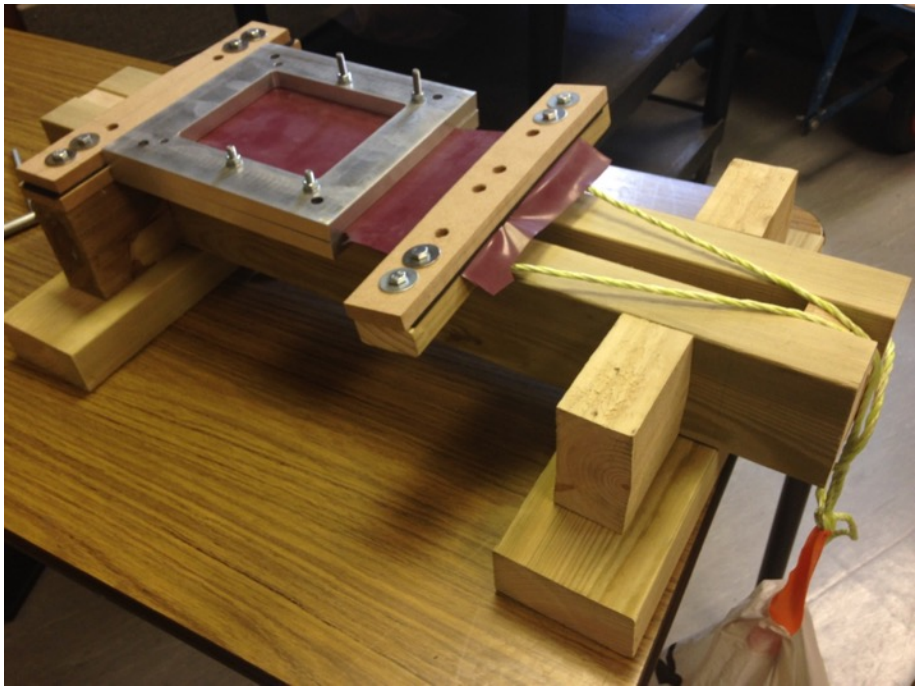

Figure 80: Rack made for pre-stressing samples.

Measurement Points: Measurements were taken at three points in the rig.

- Firstly, the voltage signal being sent to the loudspeaker was measured (scaled through a resistor) to give a reference for timing.
- Secondly, a Behringer ECM8000 Electret Capacitor measuring microphone with a ¼" capsule was mounted half-way along the pipe. It was connected to an audio preamp which provided power to the microphone and gain control.
- Lastly, a Micro-Epsilon opto NCDT1420 single point laser displacement sensor was used to measure the displacement of the membrane. This was mounted to read the centre of the membrane, where displacement at the lowest mode was greatest. This sensor is controlled via a web-based interface and can provide both digital and analogue outputs.

These measurements were captured via a BMCM USB-AD16f data logger with BMCM's proprietary NEXTview software running on a PC laptop [169], [170]. Data was exported from NEXTview in its propriety format, then edited in Delimit software to cull unwanted results and convert to .csv format [171]. These files were analysed in MATLAB code developed for the project (see 5.3.2.1).

5.3 Experiment

5.3.1 Calibration

Calibration of the pressure measurement system was performed by comparison with a Norsonic 140 sound level meter in the LSBU anechoic chamber in accordance with BS EN 60268-4:2014 [172] simultaneous comparison method. This resulted in a calibration coefficient by which the voltage values from the microphone/amp system were multiplied. In initial tests the audio preamp was used in stock condition, however sound levels were high compared to normal audio use, so gain levels were very low. Resolution on the gain potentiometer in this part of the range was poor, however, so in the name of reproducibility it was replaced by a fixed-value resistor. The pressure measurements were filtered to remove signal above 1000Hz, notably extraneous system noise (see 5.3.3).
The laser displacement sensor is factory calibrated with an analogue output of between 4mA and 20mA from minimum measurable distance (35mm) to maximum measurable distance (85mm). The sensor had a maximum sampling rate of 4kHz with an unfiltered input to the data logger, this meant accurate resolution up to 400Hz (10 data points per cycle).

The sensor works by triangulation; a light beam from a class 1 laser is emitted towards the sample, and diffuse reflections are scattered across a CMOS sensor mounted at a set angle to the emitter. The output of the sensor is linearised within the sensor and output in analogue or digital forms.

The measured output from the loudspeaker was not calibrated as it was required for timing reference only.

5.3.2 Test Signal and Analysis

The source signals for the tests comprised a series of pure tones, increasing in frequency throughout the test, and separated by silence. Each series of tones was repeated over in 3dB increments over a 20dB range to determine the nonlinear response.

A MATLAB code (TestTonePulse.m) was written to create a .WAV file of a sequence of tones for a given test. Parameters included the number of tones required, the increase in frequency between adjacent tones, the duration of each tone and the duration of the silence between adjacent tones, as well as practicalities such as sample rate and signal level.

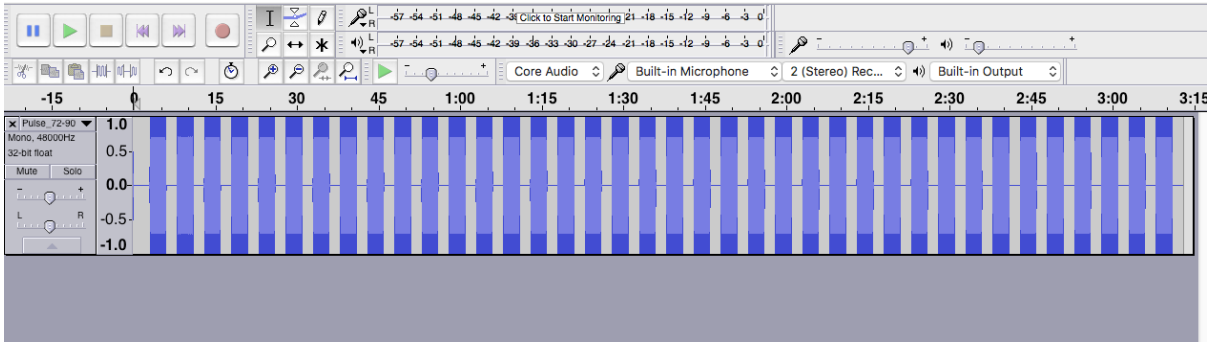

Figure 81: A complete .WAV file of pure tone bursts loaded in Audacity software ready for a test run. Tone bursts are three seconds long with a two second gap between adjacent frequencies.

After the cessation of each tone, a clean free response could be measured, and thus sufficient time between tone bursts was allowed to facilitate this. Also, each tone burst was of sufficient duration such as to be longer than the systems free response plus an additional duration. Thus, the portion of the output tone after the free response had receded but before the cessation of the input tone could be analysed as a steady state response.

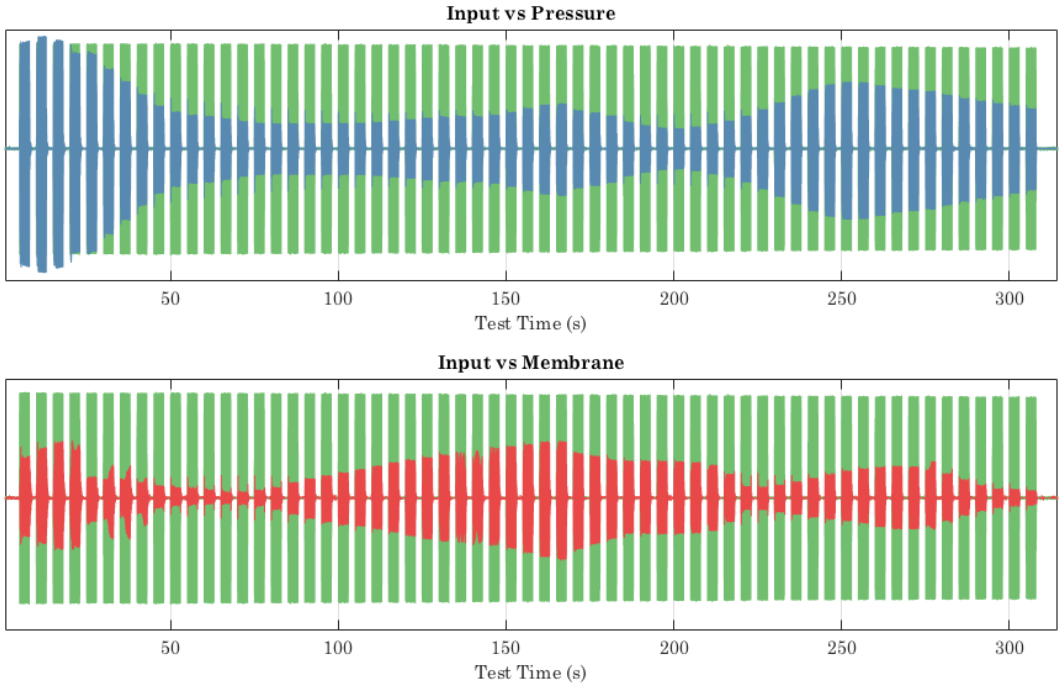

Figure 82: A test result in raw, unprocessed format, presented for qualitative assessment during the data import process only. The green time series indicates the input signal, the blue line indicates the response at

the pressure sensor, and the red line the response (displacement) of the membrane. Magnitudes of these data have been scaled to allow plotting on the same graph, so Y-axis data is in arbitrary units.

The start and end of each tone was windowed using a linear window over three wavelengths in order to reduce the broadband response associated with a sudden onset of signal level. The finished .WAV file was reproduced via Audacity audio software on a PC and connected to a hi-fi amplifier.

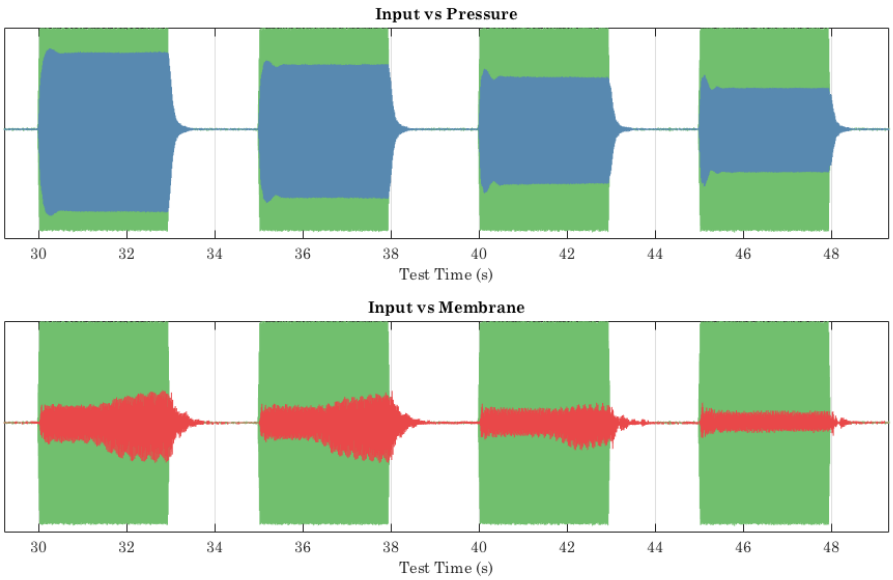

Figure 83: Zoomed in raw data output for four frequencies, showing onset, steady state and free responses. The green time series indicates the input signal, the blue line indicates the response at the pressure sensor, and the red line the response (displacement) of the membrane. Magnitudes of these data have been scaled to allow plotting on the same graph, so y-axis data is in arbitrary units and are for qualitative analysis only.

To determine the nonlinear response, the series of tones was re-run at a series of sound pressure levels of decreasing magnitude, starting at the system maximum (the level where distortion associated with the amplifier/loudspeaker system was apparent) and adjusted in 3dB increments via the gain control in the Audacity software. Therefore, each result set comprised the response to 61 pure tones for each of 6-8 sound pressure levels.

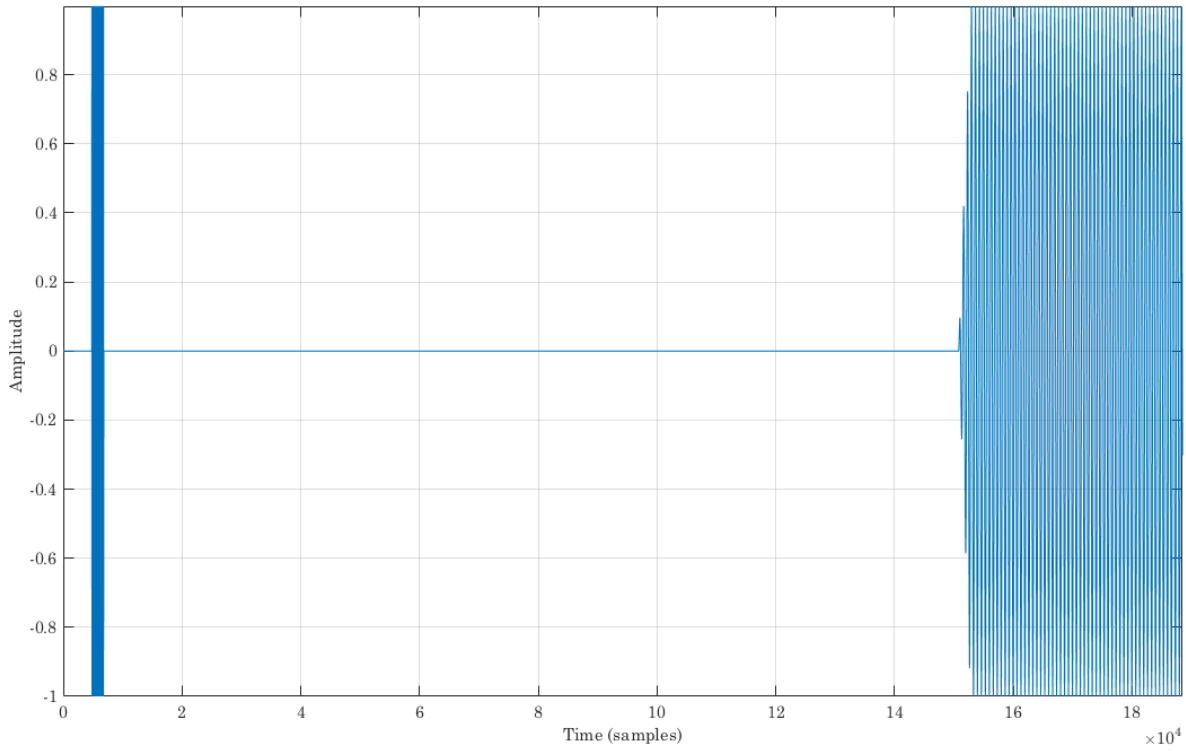

Figure 84: Test signal zoomed in to the start, showing the 1000Hz synchronisation burst (L) and the start of the first test tone burst (at 72Hz), showing windowing over three cycles.

Measured responses were recorded "wild" in NEXTview; that is, unsynchronised with the playback system. Therefore, in order to re-synchronise the separate runs recorded at different input amplitudes for analysis, reference to the loudspeaker output was planned to be sufficient. After initial tests, a brief 1kHz synchronisation tone was added before the start of the tone sequence. The MATLAB scripts for importing data incorporated a manual reference to this synchronisation tone to allow subsequent scripts to extract the free and steady state responses in the correct locations in the data. This arrangement was considered more convenient.

For most tests, a sequence of 61 tones with a 0.5 Hz resolution between 70 and 90Hz was used, with tone durations of three seconds and the silence between tones of two seconds. These parameters were determined empirically during the initial tests. The complete WAV file of the 61-tone sequence took around five minutes to run, and a series of runs over a range of 20dB took one half hour to

complete. A sampling rate of 48kHz at a bit depth of 16 bits was used in all cases.

5.3.2.1 Analysis Codes

Raw results were analysed using codes developed for the project. The codes are presented in the Appendix (see 9.4).

5.3.3 Pilot Experiments & Problems

Initial shakedown experiments were to be undertaken with the 0.22mm rubber membrane. Pre-stress was between zero and 500g. Some problems immediately became apparent. The membrane displacement signal was dirty, and characterised by a periodic, low frequency broadband spike which repeated around twice every second. It was accompanied by a strong tonal element around 600Hz, with weaker sidebands at 500 and 700Hz (see Figure 85, first panel). This was eventually improved by adjusting the exposure time of the micro-Epsilon sensor, although it was not completely eradicated. Its energy was, however significantly reduced, with a harmonic component also remaining above around 250Hz, but its repeating frequency reduced to around once every five seconds.

An intermittent broadband, low frequency component was traced to the USB connection to the laser displacement sensor (see Figure 85, panel 2). The sensor is controlled via a web-based interface running on the PC and has both digital and analogue outputs. The latter were used for measurements to facilitate simultaneous measurement of pressure data. Thus, after the device was set up, the USB connection was superfluous and could be removed. This removed the low frequency noise.

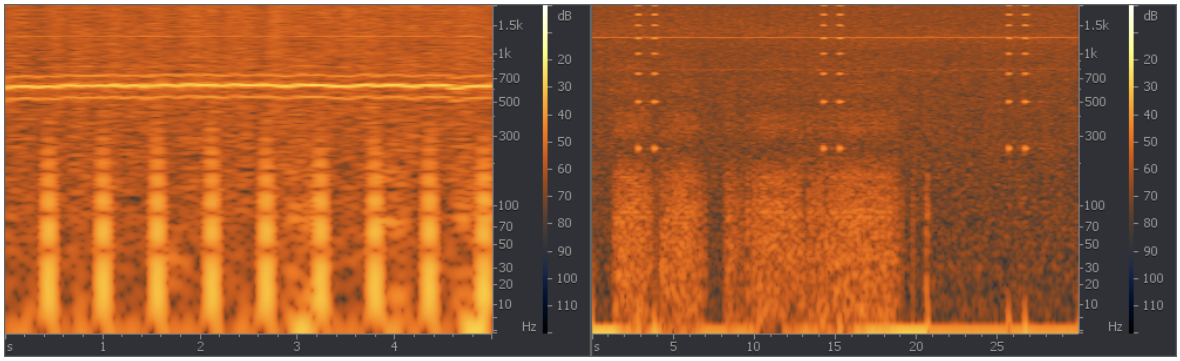

Figure 85: Spectrogram of noisy displacement data. (L) low frequency thumps improved by adjusting exposure time of sensor (R) With broadband noise caused by the sensors USB connection.

Thus, ultimately, the frequency range of interest was clear, with occasional impulsive disturbances at low frequencies prior to signal conditioning in MATLAB (Cal.m script in the Appendix 9.4.2.3) (see Figure 86).

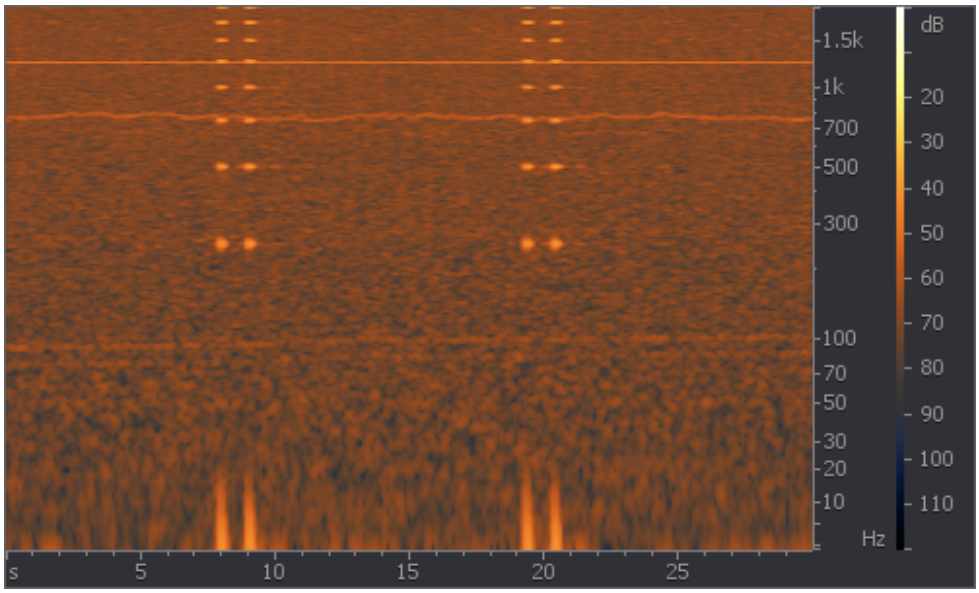

Figure 86: Improved signal, the tonal elements at 800Hz and 1.4kHz were outside the frequency range of interest and were reduced further by filtering at the import stage.

5.3.4 Measurements

Several measurement conditions were considered, starting with a rigid termination, then moving on to a number of elastic membrane conditions. Finally, some experiments with membranes enhanced with magnets subject to external magnetic fields to modify their geometrical nonlinearity were completed.

5.3.4.1 *Rigid Termination*

The first experiments involved using a rigid sample to quantify the resonant frequency of the tube/loudspeaker/amp subsystem and to define a test range of frequencies. A ceramic floor tile 10mm thick was used for this purpose.

Figure 87: Ceramic floor tile used as a rigid target.

Since this this sample should exhibit virtually no motion, the laser displacement sensor was not attached during this test.

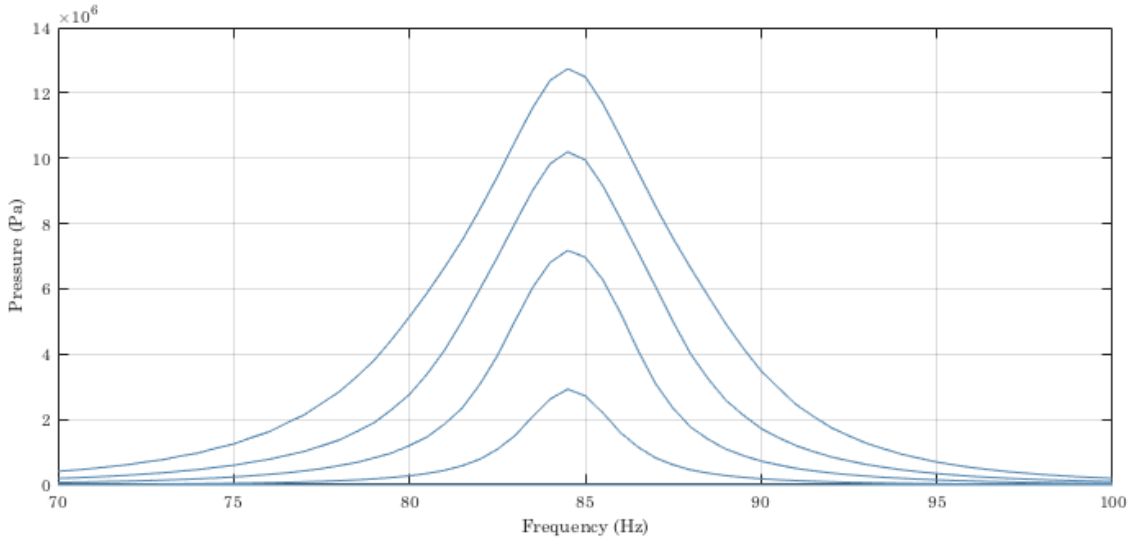

Figure 88: Frequency response of the tube system with rigid termination, pressure sensor. Each curve represents the system response to the input signal at a given sound pressure level.

The result (see Figure 88) shows the frequency response at four sound pressure levels and, since each peak reaches its maximum at the same frequency, a linear response with a peak at 84Hz can be observed. This is considered a baseline for the response of the amp/loudspeaker/tube/coupling box subsystem.

5.3.4.2 Non-elastic Membrane

Next a test involving a Mylar sample was undertaken. Mylar has a high Young's modulus and thus exhibits very low strain under tensile stress. Thus, its deformations should be small enough to be considered linear (see Figure 89).

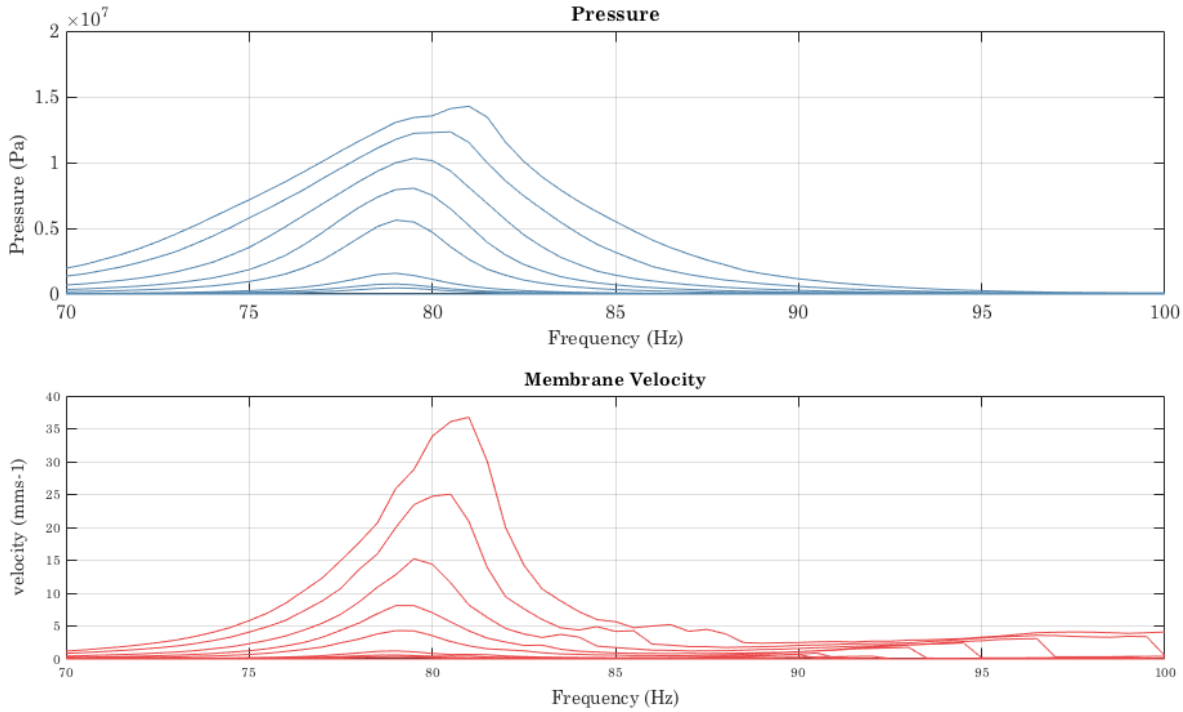

Figure 89: Frequency response for Mylar sample. Pressure in middle of tube (top), and membrane velocity (bottom).

The test showed a weak hardening nonlinearity caused by the geometry of the deformations undertaken by the sample; that is, the resonant peak increses slightly in frequency as incident sound level increases. The main resonant frequency of the system was observed to be lower; in the 78-82Hz range, rather than the 84Hz resonance observed for the rigid termination sample. This difference is due to coupling effects between the tube and the sample.

5.3.4.3 Latex Measurements

Measurements were taken with latex and silicone samples of 0.45mm and 0.22mm, but the latter proved much more liable to make large deformations, so most tests were done with these samples in the hope of observing the TET mechanism as a starting point to further research. Sadly, TET-like behaviour was elusive and only observed fleetingly (see Figure 90). This test was with a 0.22mm silicone membrane with nominal pre-stress, just enough to be pulled flat.

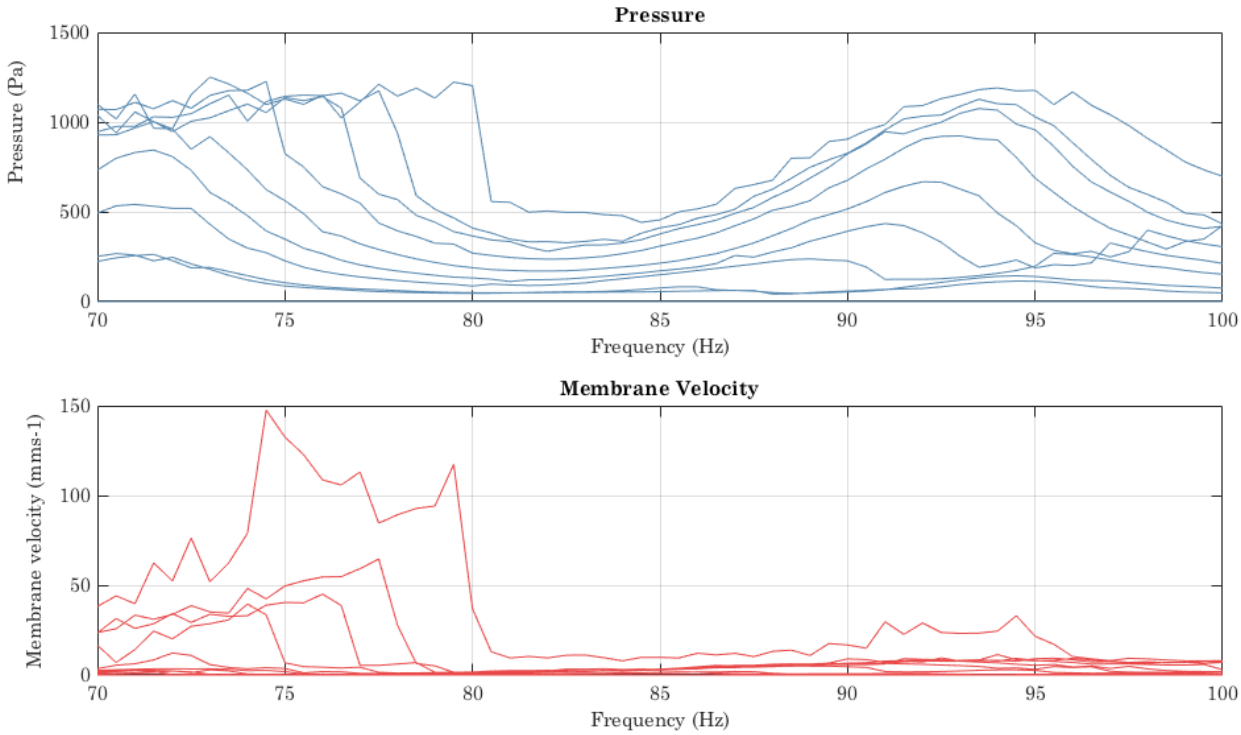

Figure 90: Nonlinear frequency response for light, slack 0.22mm membrane for pressure a centre of the tube (top) and for membrane velocity (bottom).

The main tell-tale sign for TET was the plateau in the pressure curve at high excitation levels. This is easier to visualise in a 3D plot, Frequency vs Excitation level (Run) vs Pressure (see Figure 91).

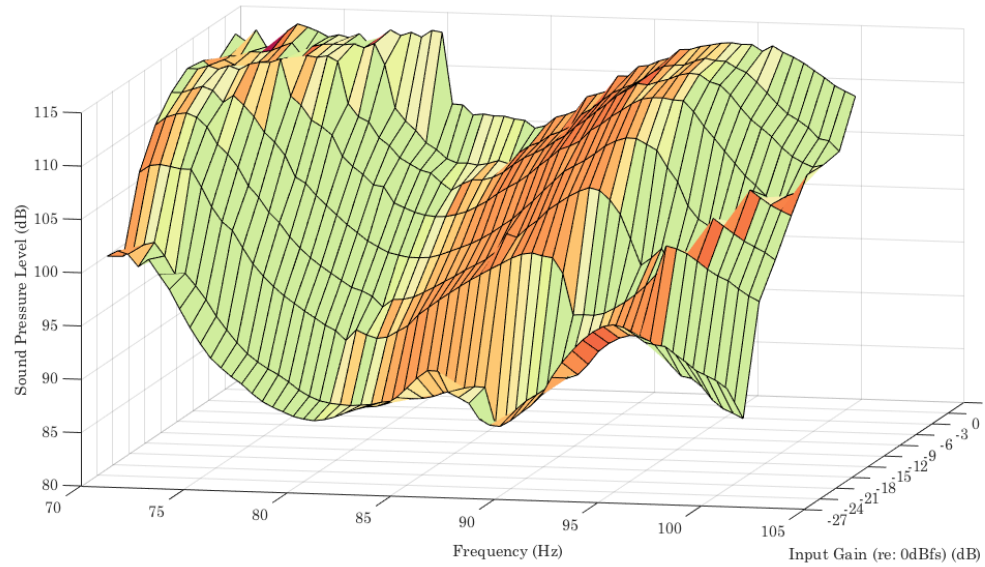

Figure 91: Nonlinear frequency response of sound pressure level measurement showing plateau between 70 and 80Hz in the response.

While this flattening of the resonant peak around 75Hz is indicative of TET, the latter is usually associated with a single resonance peak, rather than the two here, which indicates that the membrane was badly tuned, or else excitation is below that required for TET to occur. However, in this test, subharmonic behaviour akin to energy pumping was observed in the Wavelet transform spectrogram of the free response decay at cessation of excitation at the plateau frequencies (see Figure 92 and Figure 93 which compares the response at high and intermediate excitation levels).

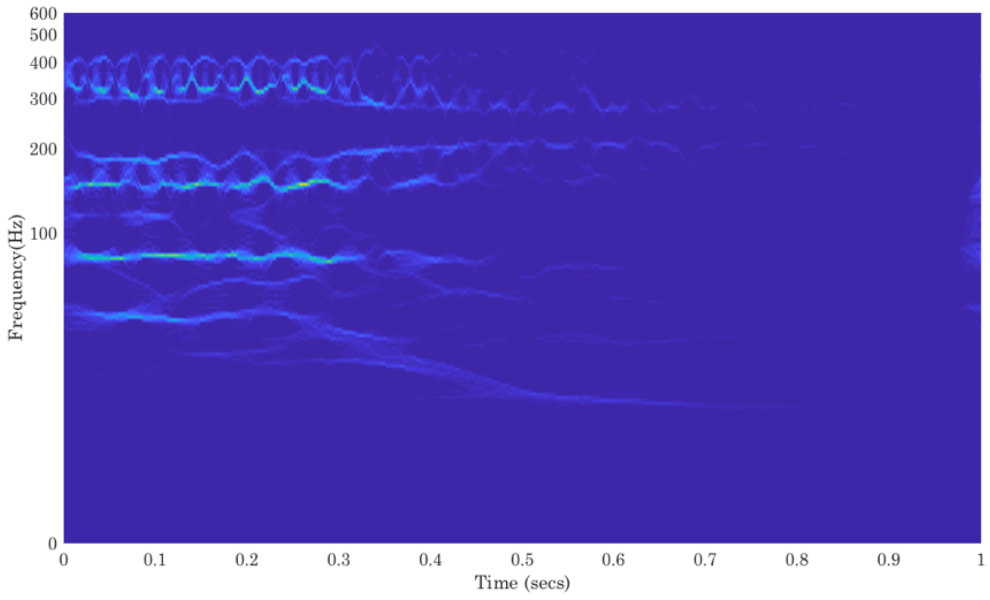

Figure 92: Synchrosqueezed wavelet transfer spectrogram showing the free response at the cessation of a 91.5Hz tone on a slack 0.22mm latex membrane with high excitation level. Subharmonic energy pumping-like behaviour below 100Hz is shown, and linear modality in higher harmonics.

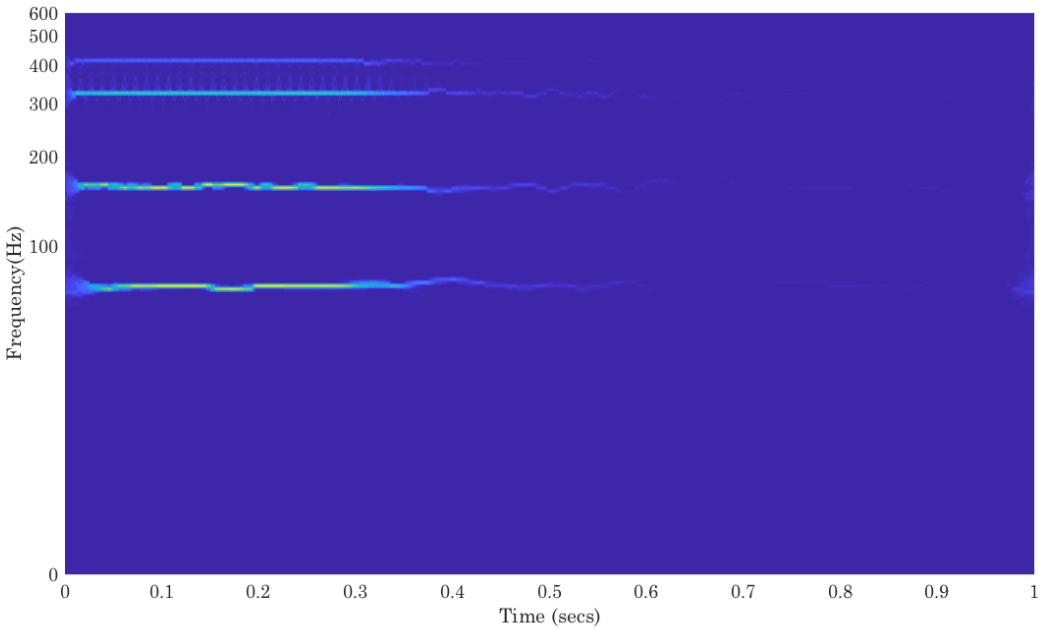

Figure 93: The same sample at low incident energy level - all modality is linear.

5.3.4.4 Magnetically Modified Membranes

Given the difficulty in obtaining the conditions for TET in a passive system, consideration was given to manipulating the nonlinearity of the membrane in some way. From McFarland *et al* [136] and Bellet *et al* [138] it was known that the nature of the nonlinearity was a (cubic) function of displacement, so a way of applying a pre-displacement to the membrane was considered. Some work along similar lines had been undertaken, in the context of pure research rather than connected with TET or indeed acoustics or vibration.

Raikher *et al* had deformed a hyperelastic membrane by electromagnetic means, embedding rare earth magnetic particles within the silicone membrane to create a *magnetoelastic* material and drawing it into a dome shape by means of a uniform electromagnetic field (see Figure 94) [173].

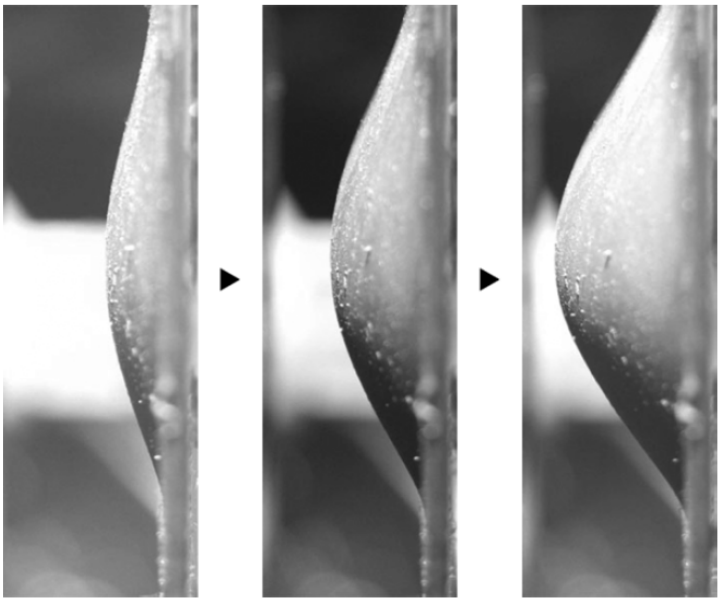

Figure 94: Deformation of a hyperelastic membrane embedded with rare earth magnetic particles by an electromagnet. From Raikher et al [173]. Reproduced with the permission of the authors.

Such a deformation would serve to manipulate the nonlinearity and hence the dynamic response of the membrane. Of course, such a deformation would also apply damping to the membrane so the attracting force must be modest.

In fact, the addition of an external magnetic force changes the nonlinearity somewhat to a bistable type, whereby two stable points were achieved, with the membrane at x=0 (plane) condition, and with the membrane in contact with the magnet, with the operating point being an unstable point between the two opposing, cubically nonlinear forces. Bistable TET has been explored in the context of vibration mitigation by Iurasov *et al* [142].

5.3.4.5 Single magnet

Several very simple explorations of concept tests were undertaken with the simple aim to prove that the dynamics of the membrane could be manipulated in this way. The first of these adding a small neodymium magnet to the centre of the membrane and attracting a stronger permanent magnet opposite it near the displacement sensor (see Figure 95).

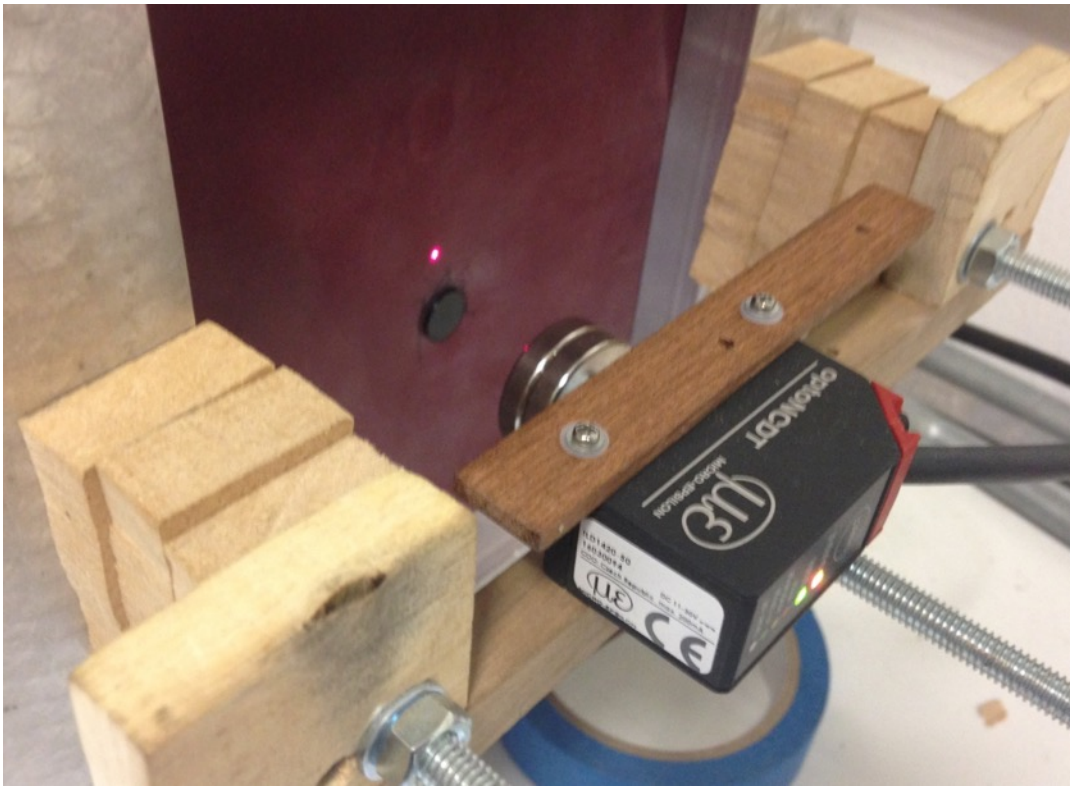

Figure 95: First pilot test of single magnet embedded in membrane, attracted by single permanent magnet. The latter was replaced by a toroidal electromagnet for measurements.

This setup produced extremely rich dynamics with strong deformations of the membranes as well as strong rotations of the membrane's magnet and strong lateral motions around the attractor magnet. The displacement measurements thus taken contained many out-of-range portions and could not be taken to be meaningful and were discarded. A second experiment used a specially constructed electromagnet to replace the permanent magnet attractor. Again, large rotations and non-axial motions were observed and were unmeasurable.

5.3.4.6 Multiple Magnets

The final experiment used an array of very small magnets attached to the membrane as an attempt to spatially distribute the magnet elements in the membrane and remove rotational motions (see Figure 96). An electromagnet was used at this stage with a view to manipulating the geometric nonlinearity of the membrane during tests (see Figure 97).

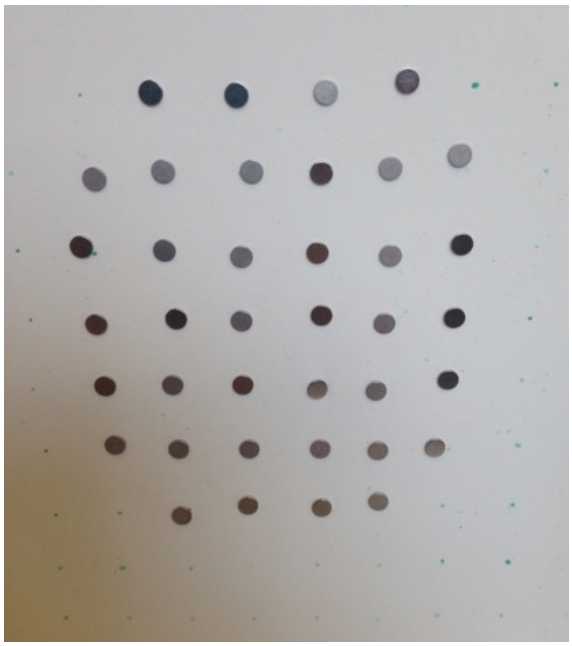

Figure 96: Close-up of membrane with array of small neodymium magnets embedded.

Figure 97: Simple electromagnet constructed for tests.

With no external magnetic field, this again resulted in very rich dynamics with large oscillations, which still exhibited some twisting and rotational components. Some subharmonic TET behaviour was observed at certain frequencies (see Figure 98). When the external electromagnet was turned on, this behaviour was much reduced, with the larger oscillations being reduced in size, and the subharmonic TET being reduced in magnitude of frequency drift (see Figure 99).

This shows that the dynamic response of the membrane, and hence TET behaviour can be manipulated by electromagnetic means.

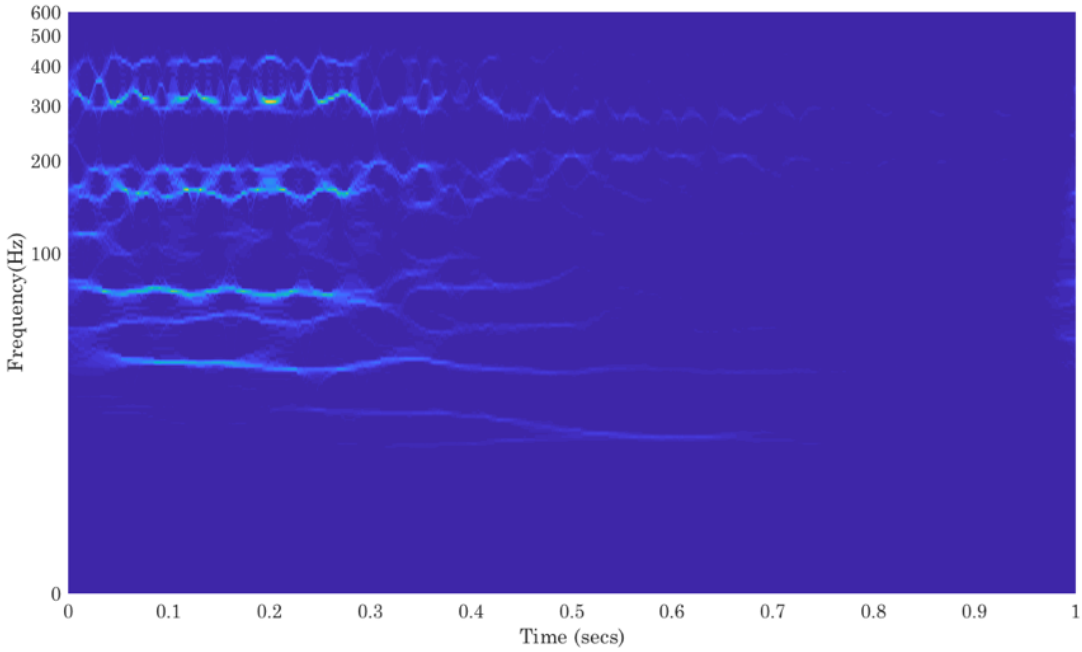

Figure 98: Synchrosqueezed wavelet transfer spectrogram for free response at cessation of 83.5Hz tone on a thin silicone sample with an array of small permanent magnets attached, but external electromagnet turned off. Excitation level was high. Large oscillations and some subharmonic TET is observed at the bottom.

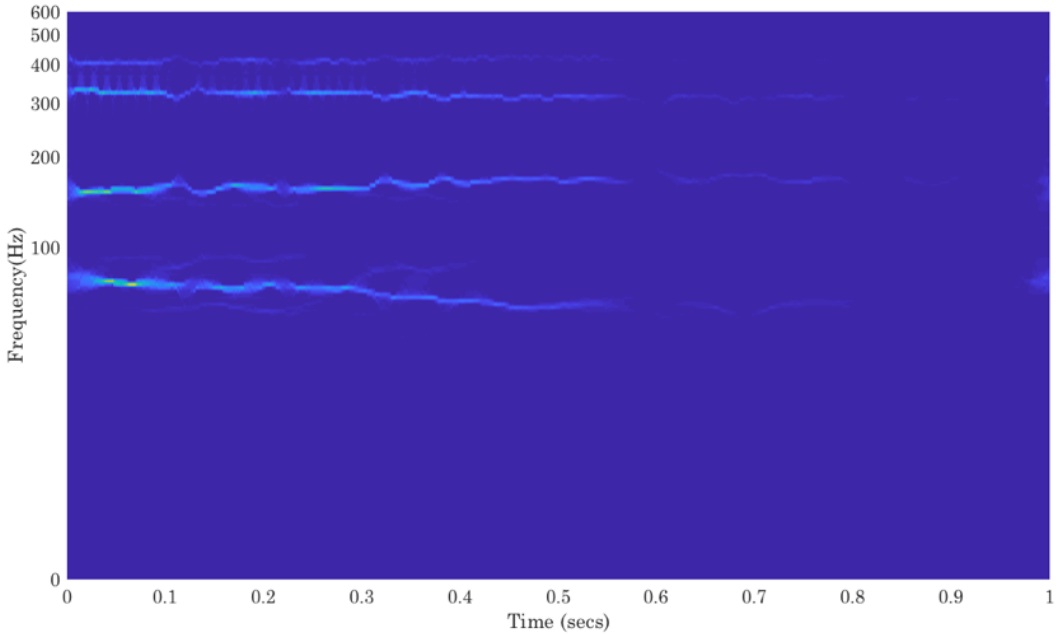

Figure 99: The same sample, frequency and excitation level, with external electromagnet switched on, showing how larger oscillations are damped and subharmonic TET tendency is reduced. This shows that the dynamics of the membrane can be manipulated by electromagnetic means.

However, viewing the corresponding pressure nonlinear frequency response indicates that the difference in response between the two states is minimal, although the inertia of the added masses, in forcing the membrane to make

larger oscillations, creates a strong stiffening nonlinearity in the response (see Figure 100). This is present from the lowest excitation levels when the electromagnet is off, (Figure 100, top) whereas with the external electromagnet switched on, the nonlinearity is reduced initially, until higher excitation causes the nonlinearity to increase strongly until the highest excitation levels are almost identical (see Figure 100). This suggests that the electromagnet had enough influence to only modify the lower-level behaviour, thus sabotaging the TET mechanism as it moves energy to lower frequencies during the key grounding phase of the decay.

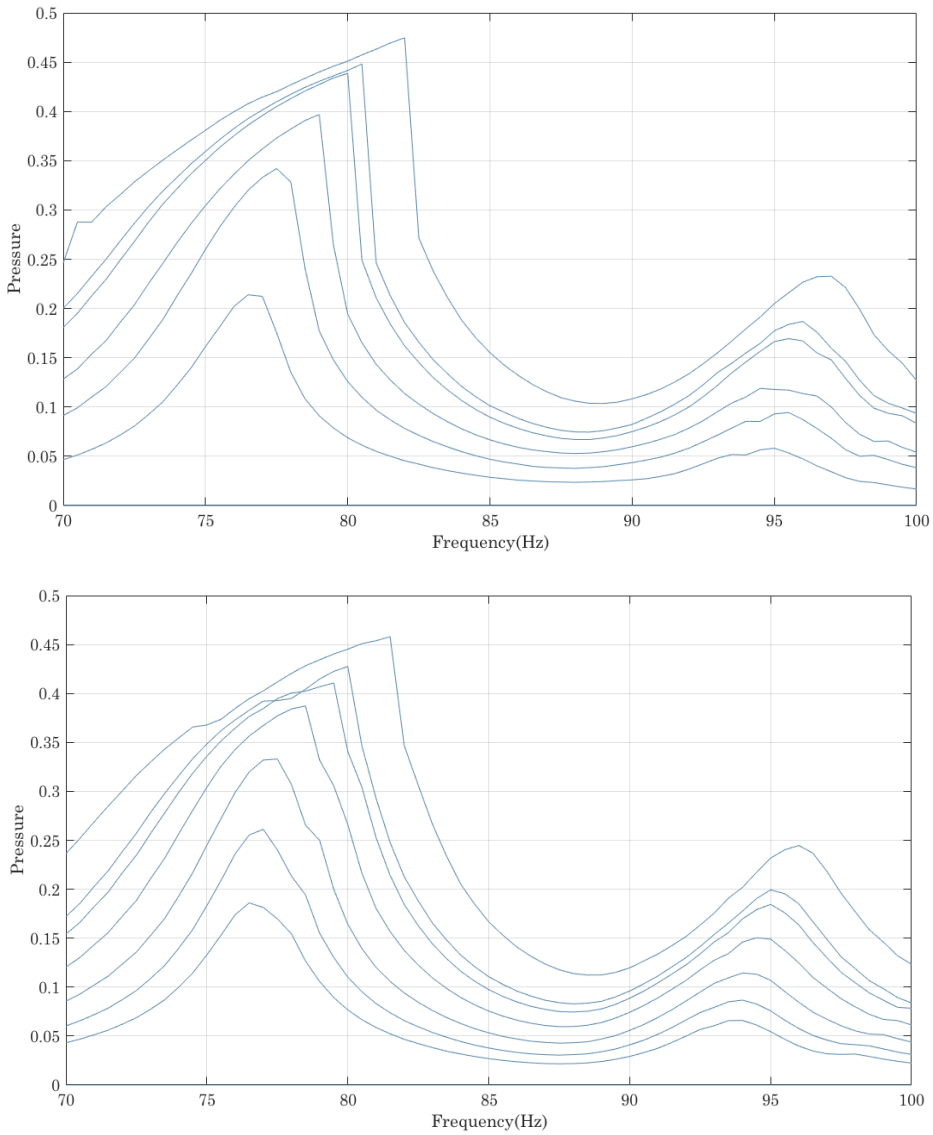

Figure 100: Pressure vs frequency nonlinear frequency response for thin silicone membrane with array of small permanent magnets six excitation levels. Top, with external electromagnet off, bottom, with it switched on. Showing only a small change in response. The added masses cause the membrane to make large excursions causing a stiffening geometrical nonlinearity.

Future work could look to the creation of lighter magnetic membranes with evenly distributed magnetic particles within the silicone matrix, potentially enabling control of the whole dynamic spectrum of the system.

5.3.5 Limitations and Constraints

Many difficulties had to be overcome in undertaking these experiments and the decision was made to cease this line of enquiry (magnets) and that of TET. This was influenced by several factors.

- Measurement equipment capable of measuring the motion of the whole of the membrane was not available. This would require a scanning laser vibrometer which would have been very expensive to acquire. Multiple measurements over the whole area of the sample could have been undertaken, but the nonlinear nature of the motion is non-deterministic and hence not necessarily comparable over multiple runs. A single test took over half an hour, so a complete sampling of the membrane surface would also be extremely time consuming.

- Apparatus to accurately measure membrane tension was not available.

- Expertise in nonlinear dynamics and TET was not available in the University and, although attempts were made to contact experts in the field (Jianwang Shao in Tongji University and Pierre-Olivier Mattei at the Universitaire de Aix-Marseille), they were unable to offer concrete help with this project.

5.4 Discussion

An ambitious attempt to harness the Targeted Energy Transfer loss mechanism for use in architectural acoustics was made. This mechanism promises broad band low frequency absorption above a threshold pressure using lightweight nonlinear materials; hyperelastic membranes making large oscillations under low frequency incident waves. A test rig was built to a design used by previous

researchers, but several technical difficulties arose and were not fully resolved. During initial experiments, ambiguous but clearly nonlinear behaviour was observed, with subharmonic TET believed to be observed.

Further experiments with membranes deflected further into the nonlinear region by electromagnets displayed rich dynamics but also much higher-level acoustic re-radiation, less useful in an absorption context, but such chaotic oscillations have been explored as a means to extend the output of acoustic and vibration energy harvesting systems.

The tentative conclusion based on these initial experiments is that TET is difficult to implement in an architectural acoustics setting, but incorporating the loss mechanism in a waveguide arrangement, and in louder music rooms (clubs, amplified gigs) might yield a lightweight, compact bass absorber, provided a durable hyperelastic material could be developed. These experiments have yielded a large amount of test data upon which to build.

6 Discussion

This thesis has considered two case studies in low frequency problems and their control in classical music rooms, along with one novel approach to low frequency control which is new to architectural acoustics.

6.1 Case Study A: Recital Hall

A recital room which was also used for teaching and occasionally lectures, with capacity of 100 was assessed following negative comments from users who considered that the room lacked music warmth. Measurements in accordance with BS3382-1 confirmed that there was a broad dip in the room frequency response around 125Hz. Curtains were available to be deployed around the sides of the room which improved the room response somewhat, and this was the condition in which the room was being used exclusively (see Figure 30). Comparison with Norwegian Standard NS8178:2014 showed that in either condition, the hall's performance fell outside of guidance for frequency dependence in the lower frequency range (see Figure 34).

Several reasons for this were explored, including the room's geometry, the materials used in its construction, and the presence of false walls either side of the entrance door. These were open to the room on two adjacent sides, leaving the space behind to act as a cavity: a quarter wave resonator. This latter aspect was explored in more detail and was found to have some effect in room measurements around 100-200Hz, but the effect was not clear in the results from a numerical simulation.

In the final analysis, the major contributor to the room's lack of bass was the extensive use of ribbed wood panelling in front of a cavity, despite the cavity being filled with Rockwool. When stock impedance figures from the literature for wood panelling were used in the FDTD model, the result echoed the real room's nature perfectly, although estimating a significantly longer reverberation time, indicating that although the panelling in the recital hall was damped, the overall balance of frequencies imposed on the room by reflected sound remained similar.

As the recital room is sited at the top of a four-storey building, weight was no doubt an issue during design. In addition, the architect chose a very wood-intensive aesthetic, with every room surface made from oak panelling; this works extremely well visually but leads to the contribution of this single material being disproportionately represented in the room response compared to a space with mixed material use. This is the case with any resonant absorber, which will exhibit an absorbent behaviour characterised by a single or multiple peaks in absorption. This will need to be carefully considered in any control measure as it would be hard to create an even response by removing energy at a single frequency, so resonant absorbers must be deployed in complementary arrays to cover a wide frequency range.

6.2 Case Study B: Pneumatic Absorbers

In case study B, an orchestral rehearsal space sited in a converted late Regency church building in South London was studied. It had been used successfully for over 30 years but with some reservations about excess bass sound by some users, despite a previous effort to damp the rostra with plastic-wrapped absorbing material. The management also desired to expand its user base to include more operatic rehearsals and the hall was assessed with these aims in mind. Measurements were taken in accordance with BS3382-1 and showed that the room has a pronounced peak in its response around 125Hz. This greater response in level and hence T_{20} at this frequency will mask adjacent frequencies causing muddiness around this area of the spectrum, often described as boominess. The source of this boominess is not obvious as the frequency range is well above the Schroeder frequency for modality. Possible candidates include the rostra, the coffered ceiling or the floor. Since access to the hall was very limited, the focus of this case study was on a control solution which would allow the hall to expand its client base to operatic rehearsal. Upon reference to Norwegian Standard NS8178 it was considered that the hall already fell broadly within the specification for a hall used to rehearse “loud” music (orchestral and operatic). The focus of the control measure proposed was concentrated on reducing the influence of the boom in the frequency response as this was the only shortcoming

in this successful room, and one which could adversely affect operatic rehearsal. The solution had to be economical and light weight and be removable by a small staff in the hour in-between sessions. Having observed FlexAcoustic's use of large-scale pneumatic absorbers in halls for rock and pop music and their success, it was proposed to use airbeds as a modular, lightweight, portable low frequency absorber. Three designs were tested in the LSBU reverberation room in accordance with ISO 354 and the largest of these was found to have the best low frequency performance. This latter airbed was also subject to a vibration test in LSBU's anechoic chamber with accelerometers attached to different parts of the surface while the whole was subject to incident low frequency pink noise. This indicated that the edge of the airbed had a different, lower vibration frequency than the main surface, indicating that the airbed, while being a membrane absorber of sorts, was much more complex in its behaviour, due to curved geometry when inflated, and due to the presence of drop cords which enable it to maintain its bed-like shape.

Locations within Henry Wood Hall were identified where airbeds might be installed discreetly, as the management did not want to impact the hall visually if possible; the space behind and to the sides of the rostra, and the choir stalls (which, although a performance location, was rarely used).

Thirty airbeds were initially installed. Measurements with and without airbeds were made in accordance with BS3382-1 and showed that a small reduction in low frequency T_{20} was achieved. Given that this was already a successful room, the fact that the existing qualities of the room were not affected was considered a success.

Now some time has passed the reaction from the room users has been positive. The management have taken advantage of the modular nature of the solution and have themselves experimented with removing some airbeds and leaving others. For instance, when the recording engineers come to record piano lead performances the airbeds were reversed. This exposed the plastic rather than the

velvet of the airbed. In this way, the hall management have gained some agency over their own acoustic. The project has also succeeded in attracting new clients to the hall.

6.3 Case Study C: Targeted Energy Transfer

A new dynamic loss mechanism, previous exploited in vibration control, was assessed as a low frequency noise control solution. A test rig was built, and materials investigated. Following some technical problems and difficulty in engaging experts in the field as advisors, the line of research was terminated after some initial, possibly ambiguous results. A great deal of data was gathered, which may be of use to investigators of this mechanism in future. Also, the rich dynamics displayed in some configurations suggest the setup might be better deployed in a field such as energy harvesting, where some similar work exists in the literature [174], [175].

6.4 Music Rooms

The music rooms studied in the first two case studies are interesting to contrast. In a way, they display opposite problems, being dominated by (low frequency) absorbing and reflecting surfaces respectively, and it is tempting to suggest that they each hold the key to the other's solution. This is true to an extent; the recital room would have benefitted from some surfaces being reflecting (concrete etc) and Henry Wood Hall's "boom" could be countered with an increased area of wood panelling.

However, the first case study was in a recently built room, whereas the second was in a listed building. This adds additional complexity. The recital hall owners, having invested in this space recently, are keen to keep the oak-panelled look of the hall, and are seeking a solution which does not affect this.

In listed buildings, such as Henry Wood Hall, the solution cannot permanently change the room and hence severely limits possible options. Under these circumstances a temporary non- fixed installation solution must be selected. The

airbeds match the criteria well although another solution was considered as a proposal; 120 Helmholtz resonators. Each resonator would target an individual frequency, hence, the need for 120 resonators. Each resonator would weigh approximately 50 kg and would need to be positioned along the bottom of three walls. This solution could not be easily adapted for the particular acoustic condition required for a recording or rehearsal of a specific piece of music. This solution would also take a significant amount of space in the hall and hence was not pursued as a solution as discussed by Dance and Hassan [156]. The idea came from a leading commercial acoustic consultancy and would have worked as a solution.

All of the proposed solutions at the very least illustrate the delicate balancing act which the designer must perform.

6.5 Application of Findings and Further Work

In this section, further applicability of the thesis' findings are discussed, along with what further investigation must be undertaken in this direction.

6.5.1 Case Study A

As Field and Fricke pointed out in [95], despite quarter wavelength resonators (QWR) being well known in acoustics, they have not found widespread use despite their simple and compact design. The example in the recital hall was interesting as rather than being one-dimensional it was two-dimensional. The analysis in this thesis assumes the QWR action in these two dimensions act orthogonally and in parallel. Eigenmode analyses using COMSOL indicated that many modes indeed seemed to exist in either x or z dimension, but also showed that many others caused excitation in two dimensions together with radial mode shapes. These were not accounted for in the analysis and future work could clarify the behaviour of this particular geometry and extend it to arbitrary two-dimensional geometries. This would require numerical methods which were not generally available during this study, COMSOL only becoming available to the

author during the writing up phase of the project, leaving little time to explore this form of modelling.

On a different scale level, resonant structures are being explored extensively in the field of metamaterials and two-dimensional Quadratic Residue Diffusers (QRD) could be utilised as a metamaterial resonant structure [176]. And this advance, being purely geometric could be scaled to lower frequency ranges, and being highly subwavelength, is also very space economical.

Nonetheless, QRDs remain a resonant structure and thus their behaviour depends strongly on the room in which they are placed and where in that room they are placed; that is to say the coupling condition is an important factor. Also, being resonators, such structures need to be deployed in arrays. This technique has been used in large scale in several concert halls including the Queen Elizabeth Hall, a large chamber hall from 1967 in London, where the side walls comprise a series of large 4x6 arrays of resonators with modular plugs whereby the aperture size can be adjusted for each resonator. Sizes are chosen to give overlapping bands to broaden the range of absorption (see Figure 101).

Figure 101: Arrays of Helmholtz resonators lining the side walls of the Queen Elizabeth Hall in London [177].

Prior to refurbishment by Ramboll UK in 2014, six of these modules were tested in the LSBU labs as part of a master's thesis by Christina Higgins [177]. This report showed that resonators also lend themselves to adjustable acoustics as Higgins also tested an acoustic curtain which could be lowered at a distance

between 0 and 200mm in front of the resonators to add mid and high frequency absorption. This solution was proposed to accommodate the wide variety of chamber ensembles and amplified ensembles, which use the hall.

Quarter wave resonators could also be deployed in arrays and could be easily built into existing walls, with the complexity involved being that they have potentially multiple (odd harmonic) resonances, albeit with generally a decreasing propensity to resonate as frequency increases. The two-dimensional QWR can at least double the power of a one-dimensional case, while taking up the same space. The false wall concept lends itself more readily to be incorporated into architectural forms. A design methodology for this more complex problem remains to be developed however, and this would require complex numerical methods.

The demand for variety was also present in both case studies, with the recital hall of case study A being used for concerts and rehearsals from soloists to medium sized chamber ensembles, as well as for lectures. Henry Wood Hall in case study B was mostly used by symphony orchestras, but solo playing and a variety of chamber rehearsals were not uncommon either.

Overall, the false wall was not considered to be the dominant mechanism causing problems in the recital hall, but this troubled hall has illuminated an interesting future path for research.

6.5.2 Case Study B: Pneumatic Absorbers

Membrane absorbers are the best option for control of the lowest part of the audio range, and this thesis has shown that simple airbeds can be put to profitable use as low cost, modular, adjustable low frequency absorbers, that can easily be removed from the room and stored when not required. As such, they fill an important gap in the designer's palette; low frequency absorbers traditionally being large and heavy and permanently installed.

Work on pneumatic absorbers has been continued with the use of inflatables in large arenas. This retrofit solution is being investigated for repurposed warehouses in Mexico that are currently being used to hold amplified music events. The inflatables, many of which would be required, would reduce the boominess of the arena, thus improving the speech intelligibility in the room and providing a more balanced acoustic. Again, here the cost and flexibility are the attractive aspects, and this is the context in which pneumatic absorbers first proved themselves. See FlexAcoustic [117] and Adelman-Larsen [178].

Experiments are now also being carried out with pneumatic seating (chairs and sofas) and how seated persons affect their absorbing properties. It is possible that seating itself could be used as a low frequency absorber.

Pneumatic absorbers lend themselves to many new applications – they could be considered ideal for sports spaces and arenas as they can be hung from the lightest of roof structures, or stored beneath seating, although placing them out of reach necessitates a method for maintaining pressure remotely, and FlexAcoustic have developed such a mechanism [117].

As previously mentioned, the use of airbeds in Henry Wood Hall came following a report by a leading commercial acoustic consultancy. The recommended large array of Helmholtz resonators to address the low frequency issue would have cost £150,000 to construct and significant time to build and install. Therefore, the airbed solution proved significantly lower in cost, at around £1200 for 30 airbeds. This is enough alone to recommend it, but more importantly, it requires no permanent change to the hall, being completely removable within an hour. In practice, something even more powerful has happened, the room's users have, over some months, experimented with different numbers of airbeds in the two locations (behind the rostra and in the choir stalls at the back of the room), to arrive at a general use configuration which is all their own.

This is a quietly revolutionary act; in acoustics, problems with a particular room, especially in the context of music, can be easy to perceive for an expert critical listener such as a sound engineer, conductor or musician; whether they can articulate the problem or not; whether the language they use to articulate it is meaningful to the designer or not. On the other hand, the designer is often faced with the problem of estimating the acoustic qualities of a space that has yet to be built or modified. Therefore, his own perceptual facilities are of no use. These are the two worlds which auralisation attempts to bridge, but this still has its own problems [179].

But allowing critical listeners who regularly use the room the time and scope to experiment puts the tools of science in the hands of creatives, and they will optimise within the scope available to them; also, giving them a sense of ownership in the solution, rather than being treated as outsiders.

Moving away from absorption, inflated pneumatic structures have a natural bulging geometry which can scatter sound. Therefore, it would seem that a hybrid low frequency absorber/high frequency diffuser could be constructed. In the context of the entertainment industry, much research has been done to enable an inflatable of almost arbitrary geometry to be made, see Skouras *et al* [180] who describe Disney's design process for inflatables design of cartoon characters, therefore an optimised scattering geometry could be made.

6.5.3 Case Study C: Targeted Energy Transfer

The Targeted Energy Transfer loss mechanism continues to be studied but mainly in vibration mitigation. The incident energy levels required make it impractical for acoustic music spaces as is, although spaces with high sound level amplified music such as clubs and music venues might be more appropriate.

The mechanism might be improved by the use of a waveguide and by an array of membranes – indeed multiple membranes were explored in one paper by Bellet

et al where they were discovered to extend the plateau of favourable operation [139].

The original team at CNRS Marseille have continued by exploring bistable TET in vibration [142], in improvement over mass law in sound insulation between rooms, and in mitigating against "wolf" tones in musical instruments [181].

Application to a musical context remains a niche application and the mainstream of this and other nonlinear dynamics-based research is in vibration, especially in space structures.

7 Conclusions

Two classical music spaces have been considered in this study; one with a difficult acoustic for performance, the second in the context of suitability for the range of ensembles and uses envisioned by the customer. Solutions have been offered through a process of extensive scientific investigations specifically in the low frequency range of room acoustics. The result of this has been new knowledge in inflatables (absorption characteristic with inflation and the absorptive mechanism) has been gained, demonstrated through empirical laboratory experiments and field trials. In addition, new knowledge in quarter wavelength resonators (absorption characteristics and the absorptive mechanism) has been gained through empirical laboratory experiments, computer simulation and a field trial.

7.1 Future Directions

This thesis has identified a number of research avenues which could be continued.

- The effect of a two-dimensional quarter-wavelength resonator in the form of a false wall open on two sides has been observed in a recital hall and in a reverberation room test. Its effect was not observed in an initial FDTD model, however, so there remains some mystery about their loss mechanism. A parametric study using a numerical method could be undertaken to explore the coupling between the room and the cavity, and the radiation characteristic of the latter, as the fact that the cavity is open on two sides in effect amounts to a spatially varying end correction.

- Pneumatic structures with panel-like geometry have been shown to provide an effective low-frequency absorber which is lightweight and cost-effective. Further work could find a predictive relation between volume, dimensions and proportion of drop cords to facilitate easier design.

- A numerical analysis of such structures can identify in close detail the dynamics of the different parts of the airbed.

- A hybrid low frequency absorber/high frequency diffuser could be developed.

- The TET loss mechanism could be harnessed for absorption in an amplified music context, probably within a waveguide structure.

7.2 Reflections

This thesis has represented almost four years' work. One scientific principle which has been applied to the letter is the Pareto Principle. Case Study C took up perhaps 80 percent of this time, and accounts for maybe 20 percent of the finished article. This reflects the challenges encountered and perhaps the underestimation of the work required.

The first part of the research consisted of reading through the literature and identifying a subject, and a lack of pragmatism at this stage led to a very difficult subject being chosen. It turned out that four years was insufficient to learn about nonlinear dynamics sufficiently (let alone linear dynamics). However, much was learned, such as gaining a good working knowledge of MATLAB, having never used it before this thesis, and in general research methodology, planning and approach.

After no small amount of time, it was decided to focus upon room acoustics of music spaces, where LSBU was already closely engaged with several conservatoires, orchestras and classical venues, including my sponsor, the Royal Academy of Music. Here, all I lacked was extended access to rooms; the spaces studied here are both extremely busy, so measurements occurred over two to three days per venue.

Nonetheless I have learned a great deal during this journey and look forward to the next challenge in acoustics.

8 Bibliography

[1] S. Donnadieu, “Mental representation of the timbre of complex sounds,” in *Analysis, synthesis, and perception of musical sounds*, Springer, 2007.

[2] P. Duarte Pestana, Z. Ma, J. D. Reiss, A. Barbosa and D. A. A. Black, “Spectral Characteristics of Popular Commercial Recordings 1950-2010,” in *135th AES Conference*, New York, NY, USA, 2013.

[3] W. C. Sabine, “Reverberation,” in *Collected Papers on Acoustics*, Boston, Mass: Harvard University Press, 1922.

[4] R. F. Norris and C. F. Andree, “An instrumental method reverberation measurement,” *Journal of the Acoustical Society of America,* April 1930.

[5] C. F. Eyring, “Reverberation time in "dead" rooms,” *Journal of the Acoustical Society of America,* January 1930.

[6] L. E. Kinsler, A. R. Frey, A. B. Coppens and J. V. Sanders, Fundamentals of Acoustics, Third Edition ed., New York, NY: John Wiley & Sons, 1982.

[7] BS 354: 2003: Measurement of sound absorption in a reverberation room, British Standards Institute, 2003.

[8] G. Millington, “A modified formula for reverberation,” *Journal of the Acoustical Society of America,* vol. 4, pp. 69-82, 1932.

[9] W. J. Sette, “A new reverberation time formula,” *Journal of the Acoustical Society of America,* vol. 4, pp. 193-210, 1933.

[10] S. M. Dance and B. M. Shield, “Modelling of sound fields in enclosed spaces with absorbent room surfaces. Part I: performance spaces,” *Applied Acoustics,* vol. 58, pp. 1-18, 1999.

[11] C.-H. Jeong, “Converting Sabine absorption coefficients to random incidence absorption coefficients,” *Journal of the Acoustical Society of America,* vol. 133, no. 6, pp. 3951-3962, June 2013.

[12] D. Fitzroy, “Reverberation formula which seems to be more accurate with non-uniform distribution of absorption,” *Journal of the Acoustical Society of America,* vol. 31, no. 7, pp. 893-897, 1959.

[13] H. Arau-Puchades, “An improved reverberation formula,” *Acustica,* vol. 65, 1988.

[14] R. O. Neubauer, “Prediction of reverberation time in rectangular rooms with non-uniformly distributed absorption using a new formula ,” in *Acustica 2000*, Madrid, 2000.

[15] L. J. Vilhelm, “Acoustical criteria for auditoriums and their relation to model techniques,” *Journal of the Acoustical Society of America,* vol. 47, no. 408, pp. 408-412, 1970.

[16] M. Barron, “Interpretation of Early Decay Times in concert auditoria,” *Acustica,* vol. 81, pp. 320-331, July 1995.

[17] D. Lee, J. v. D. Schuitman, D. Cabrera and X. Qui, “Comparison of psychoacoustic-based reverberance parameters,” *Journal of the Acoustical Society of America,* vol. 142, no. 4, pp. 1832-1840, October 2017.

[18] H. Kutruff, Room acoustics, New York, New York: John Wiley & Sons, 1973.

[19] D. A. Bies and C. H. Hansen, Engineering noise control: theory and practice, 5th Edition ed., Boca Raton: CRC Press, 2018.

[20] C.-H. Jeong, D. Lee, S. Santurette and J.-G. Ih, “Influence of impedance phase angle on sound pressures and reverberation times in a rectangular room,” *Journal of the Acoustical Society of America,* vol. 135, no. 2, pp. 712-723, February 2014.

[21] H. V. Fuchs, X. Zha and M. Pommerer, “Qualifying freefield and reverberation rooms for frequencies below 100 Hz,” *Applied Acoustics,* vol. 59, pp. 303-322, 2000.

[22] Historic England, “The Henry Wood Hall, including gate piers and railings,” [Online]. Available: https://historicengland.org.uk/listing/the-list/list-entry/1385999. [Accessed 19th February 2019].

[23] J. H. Rindel, “Modal energy analysis of nearly rectangular rooms at low frequencies,” *Acta Acustica United with Acustica,* vol. 101, pp. 1211-1221, 2015.

[24] P. M. Morse and R. H. Bolt, “Sound Waves in Rooms,” *Reviews of Modern Physics,* vol. 16, no. 2, pp. 69-150, 1st 4 1944.

[25] M. R. Schroeder, “The “Schroeder frequency” revisited,” *Journal of the Acoustical Society of America,* vol. 99, no. 5, pp. 3240-3241, May 1996.

[26] S. M. Dance and G. van Buuren, “Effects of damping on the low-frequency acoustics of listening rooms based on an analytical model,” *Journal of Sound and Vibration,* vol. 332, pp. 6891-6904, 2013.

[27] M. R. Schroeder, “Die statistischen parameter der frequenzkurven von grossen räumen.,” *Acustica,* vol. 4, 1954.

[28] H. Fletcher and W. A. Munson, "Loudness, its definition, measurement and calculation," *Journal of the Acoustical Society of America,* pp. 377-430, October 1933.

[29] B. Fazenda and M. Wankling, "Optimal modal spacing and density for critical listening," in *125th AES Convention, San Francisco*, 2008.

[30] S. E. Olive, P. L. Schuck, J. G. Ryan, S. L. Sally and M. E. Bonneville, "The detection thresholds of resonances at low frequencies," *Journal of the Audio Engineering Society,* vol. 45, no. 3, pp. 116-128, 1997.

[31] B. M. Fazenda, M. Stephenson and A. Goldberg, "Perceptual thresholds for the effects of room modes as a function of modal decay," *Journal of the Acoustical Society of America,* vol. 137, no. 3, pp. 1088-1098, March 2015.

[32] BS 10534-1: 2001: Determination of sound absorption coefficient and impedance in impedance tubes — Part 1: Method using standing wave ratio, British Standards Institute, London, 2001.

[33] BS 10534-2: 2001: Determination of sound absorption coefficient and impedance in impedance tubes - Part 2: Transfer-function method, BSI, London, 2001.

[34] P. E. Sabine, "Measurement of sound absorption coefficients from the viewpoint of the testing laboratory," *Journal of the Acoustical Society of America,* vol. 11, pp. 41-44, July 1939.

[35] T. W. Bartel, "Effect of absorber geometry on apparent absorption coefficients as measured in a reverberation chamber," *Journal of the Acoustical Society of America,* vol. 69, pp. 1065-1074, 1980.

[36] A. C. C. Warnock, "Some practical aspects of absorption measurements in reverberation rooms," *Jounal of the Acoustical Society of America,* vol. 74, no. 5, pp. 1422-1432, November 1983.

[37] BS 1793-5: 2016: Road traffic noise reducing devices - Test method for determining the acoustic performance: Part 5: Intrinsic characteristics - In situ values of sound reflection under direct sound field conditions, British Standards Institute, London, 2016.

[38] K. Attenborough, K. M. Li and K. Horoshenkov, Predicting outdoor sound, London: Taylor & Francis, 2007.

[39] L. N. Bolen and H. E. Bass, "Effects of ground cover on the propagation of sound through the atmosphere," *Journal of the Acoustical Society of America,* vol. 69, no. 4, pp. 950-954, 1981.

[40] E. Mommertz, "Angle-dependent in-situ measurements of reflection coefficients using a subtraction technique," *Applied Acoustics,* vol. 46, pp. 251-263, 1995.

[41] S.-I. Thomasson, "TRITA-TAK 8201: Theory and experiments on the sound absorption as a function of area.," Stockholm, 1982.

[42] F. J. Fahy, Sound Intensity, London: Elsevier, 1989.

[43] F. Jacobsen and H.-E. de Bree, "A comparison of two different sound intensity measurement principles," *Journal of the Acoustical Society of America,* vol. 118, no. 3 Pt 1, pp. 1510-1517, September 2005.

[44] E. Tijs and E. Druyvesteyn, "Spatial variation of impedance and intensity measured close to a sample in the near field of a spherical sound source," in *SAPEM 2011*, 2011.

[45] X. Zha, H. V. Fuchs, C. Nocke and X. Han, "Measurement of an effective absorption coefficient below 100 Hz," *Acoustics Bulletin,* vol. 24, no. 1, pp. 5-10, january/February 1999.

[46] F. Jacobsen, "Decay rates and wall absorption," *Journal of Sound and Vibration,* vol. 81, no. 3, pp. 405-412, 1982.

[47] E. D. Daniel, "On the dependence of absorption coefficients upon the area of the absorbent material," *Journal of the Acoustical Society of America,* vol. 35, pp. 571-573, 1963.

[48] H. D. Harwood, K. E. Randall and K. F. L. Landsdowne, "RD 1978/27: The variation of absorption coefficient of absorber modules with ambient conditions," BBC Research Department, Tadworth, 1978.

[49] R. V. Waterhouse, "Interference patterns in reverberant sound fields.," *Journal of the Acoustical Society of America,* vol. 27, no. 2, March 1955.

[50] R. V. Waterhouse and R. K. Cook, "Interference patterns in reverberant sound fields. II," *Journal of the Acoustical Society of America,* vol. 37, no. 3, March 1965.

[51] A. Prato, F. Casassa and A. Schiavi, "Reverberation time measurements in non-diffuse acoustic field by the modal reverberation time," *Applied Acoustics,* vol. 110, pp. 160-169, 24 March 2016.

[52] Y. Zhang, Z. Kuang, W. Ming and J. Yang, "In-situ measurement of sound absorbing properties using plane-wave sound field reproduced by virtual loudspeaker array," *Building and Environment,* vol. 94, pp. 883-890, 2015.

[53] B. Castagnede, A. Moussatov, D. LaFarge and M. Saeid, "Low frequency in situ metrology of absorption and dispersion of sound absorbing porous materials based on high power ultrasonic non-linearly demodulated waves," *Applied Acoustics,* vol. 69, pp. 634-648, 2008.

[54] M. Barron, "Bass sound in concert auditoria," *Journal of the Acoustical Society of America,* vol. 97, no. 2, pp. 1088-1098, February 1995.

[55] A. H. Marshall, "Levels of reflection masking on concert halls," *Journal of Sound and Vibration,* vol. 7, no. 1, pp. 116-118, 1968.

[56] Z. Schärer-Kalkandjiev and S. Weinzierl, "Room acoustics viewed from the stage: Solo performers' adjustments to the acoustical environment," in *International Symposium on Room Acoustics*, Toronta, 2013.

[57] N. G. Patrick and C. R. Boner, "Acoustics of school-band rehearsal rooms," *Journal of the Acoustical Society of America,* vol. 41, pp. 215-219, 1967.

[58] R. Osman, "Designing small music practice rooms for sound quality," in *20th International Conference on Acoustics*, Sydney, 2010.

[59] R. Walker, "RD 1993/8: Optimum Dimension Ratios for Studios, Control Rooms and Listening Rooms," BBC Research Department, Tadworth, 1993.

[60] BB86: Music accomodation in secondary schools, The Stationary Office, London, 1997.

[61] BB93: Acoustic Design of Schools, Department for Education and Skills.

[62] NS8178:2014: Acoustic criteria for rooms and spaces for music rehearsal and performance, Standard Norge, Lysaker, 2014, Figure 1 and figure 2c from NS 8178:2014 is reproduced by Douglas Shearer for use in 'Case Studies in the Absorption of Low Frequency Sound in Music Rooms' under licence from Standard Online AS April 2021. © All rights are reserved. Standard Online .

[63] BS 3382-1: 2009: Measurement of room acoustic parameters: Part 1: Performance spaces, BSI, 2009.

[64] A. C. Gade, "Acoustics for symphony orchestras; status after three decades of experimental research," *Building Acoustics,* vol. 18, no. 3, pp. 181-206, 2011.

[65] EBU, "Tech 3276: Listening conditions for the assessment of sound programme material: monophonic and two-channel stereophonic,," European Broadcasting Union, Geneva, 1998.

[66] M. Barron, Auditorium acoustics and architectural design, 2nd ed., London & New York: Spon Press, 2010, p. 30.

[67] EBU, "Tech 3276-E: Listening conditions for the assessment of sound programme material: supplement 1: multichannel sound," European Broadcasting Union, Geneva, 2004.

[68] R. Walker, *WHP021: Acoustic criteria and specification,* London: British Broadcasting Corporation, 2002.

[69] T. J. Cox and P. D'Antonio, Acoustic absorbers and diffusers: theory, design and application, Second Edition ed., London, New York: Taylor & Francis, 2009.

[70] M. E. Delaney and E. N. Bazley, "Acoustical properties of fibrous absorbent materials," *Applied Acoustics,* vol. 3, pp. 105-116, 1970.

[71] Y. Miki, "Acoustical properties of porous materials - Modifications of Delany-Bazley models," *Journal of the Acoustical Society of Japan,* vol. (E) 11, no. 1, pp. 19-24, 1990.

[72] P. Newell, Recording studio design, 3rd Edition ed., Focal Press.

[73] S. Torres-Guijarro, A. Pena, A. Rodriguez-Molares and N. Degara-Quintel, "A study of wideband absorbers in a non-environment control room: characterisation of the sound field by means of p-p probe measurements," *Acta Acustica with Acustica,* vol. 97, pp. 1-11, 2011.

[74] J. N. Wincentz, J. Martinez-Villalba Garcia and C.-H. Jeong, "Sound field characterisation and absorption measurement of wideband absorbers.," in *Inter-Noise*, Hamburg, 2016.

[75] I. P. Dunn and W. A. Davern, "Calculation of acoustic impedance of multi-layer absorbers," *Applied Acoustics,* vol. 19, pp. 321-334, 1986.

[76] J. Xu, J. Nannariello and F. R. Fricke, "Optimising flat-walled multi-layered anechoic linings using evolutionary algorithms," *Applied Acoustics,* vol. 65 , pp. 1009-10026, 2004.

[77] P. M. Morse and K. U. Ingard, Theoretical acoustics, New York: McGraw-Hill Book Company, 1968.

[78] L. Cremer and H. A. Müller, Principles and applications of room acoustics, Volume 2, vol. 2, London & New York: Applied Science Publishers, 1978.

[79] H. von Helmholtz, Theorie der luftschwingungen in röhren mit offenen enden, Berlin: Verlag von Wilhelm Engelmann, 1859.

[80] U. Ackermann, H. Fuchs and N. Rambausek, "Sound Absorbers of a Novel Membrane Construction," *Applied Acoustics,* vol. 25, pp. 197-215, 1988.

[81] BBC Engineering, "Guide to acoustic practice," BBC, London, 1990.

[82] D.-Y. Maa, "Theory and design of microperforated panel sound absorbing constructions," *Scientia Sinica,* vol. 18, pp. 55-71, 1975.

[83] H. V. Fuchs, Applied Acoustics: Concepts, Absorbers, and Silencers for Acoustical Comfort and Noise Control, London: Springer, 2013.

[84] R. D. Ford and M. A. McCormick, "Panel sound absorbers," *Journal of Sound and Vibration,* vol. 10, no. 3, pp. 411-423, 1969.

[85] K. Sakagami, M. Kiyama, M. Morimoto and D. Takahashi, "Sound absorption of a cavity-backed membrane: a step towards design method for membrane-type absorbers.," *Applied Acoustics,* vol. 49, pp. 237-247, 1996.

[86] K. Sakagami, D. Takahashi, H. Gen and M. Morimoto, "Acoustic properties of an infinite elastic plate with a back cavity," *Acustica,* vol. 78, pp. 288-295, 1993.

[87] Kirkegaard Associates, "Selected Project: Concert Halls - Royal Festival Hall," [Online]. Available: https://www.kirkegaard.com/arts/concert-halls. [Accessed 6th April 2020].

[88] S. J. Elliott and P. A. Nelson, "The active control of sound," *Electronics and Communication Engineering Journal,* pp. 127-136, August 1990.

[89] P. Lueg, "Process of Silencing Sound Oscillations". USA 9th June 1936.

[90] W. B. Conover, "Fighting noise with noise," *Noise Control,* vol. 2, pp. 78-82, 1956.

[91] A. J. Fleming, D. Niederberger, S. O. Reza Moheimani and M. Morari, "Control of resonant acoustic sound fields by electrical shunting of a loudspeaker," *IEEE Transactions of Control Systems Technology,* vol. 15, no. 4, July 2007.

[92] H. F. Olson and E. G. May, "Electronic Sound Absorber," *Journal of the Acoustical Society of America,* vol. 25, no. 6, pp. 1130-1136, November 1953.

[93] A. Pittet and D. Strobino, "Low frequency absorption by velocity control through acoustic resistance," in *AES Swiss section 135th meeting*, Yverdon, 2015.

[94] D. Taczycz, "Investigation of the effectiveness of acoustic velocity absorbers on low frequency sounds," 2018.

[95] C. D. Field and F. R. Fricke, "Theory and applications of quarter-wave resonators: A prelude to their use for attenuating noise entering buildings through ventilation openings," *Applied Acoustics,* vol. 53, no. 1-3, pp. 117-132, 1998.

[96] E. H. Dowell and H. M. Voss, "The effect of a cavity on panel vibrations," *AIAA Journal,* vol. 1, pp. 476-477, 1963.

[97] F. Fahy, Sound and structural vibration, Academic Press, 1987.

[98] J. Pan and D. A. Bies, "The effect of fluid–structural coupling on acoustical decays in a reverberation room in the high-frequency range," *Journal of the Acoustical Society of America,* vol. 87, no. 2, pp. 718-727, February 1990.

[99] J. Pan and D. A. Bies, "The effect of fluid–structural coupling on sound waves in an enclosure—theoretical part," *Journal of the Acoustical Society of America,* vol. 87, pp. 691-707, 1990.

[100] R. B. Davis, "A simplified approach for predicting interaction between flexible structures and acoustic enclosures," *Journal of Fluids and Structures,* vol. 70, pp. 276-294, 2017.

[101] Y. Y. Lee, "Structural-acoustic coupling effect on the nonlinear natural frequency of a rectangular box with one flexible plate," *Applied Acoustics,* vol. 63, pp. 1157-1175, 2002.

[102] J. Y. Chi and R. M. Pauletti, "An outline of the evolution of pneumatic structures," in *Il Simposio Latinoamericano de Tensoestructuras*, Caracas, 2005.

[103] A. Tedeschi, AAD - Algorithms aided design, Second Edition ed., Potenza: Le Penseur, 2018.

[104] S. Francis, Bubbletecture: inflatable architectiure and design, London: Phaidon, 2019.

[105] A. V. Gorkavyy, "On inflating closed mylar shells," *Comptes Rendus Mechanique,* vol. 338, pp. 656-662, 15th September 2010.

[106] R. Wagner, "On the design process of tensile structures," in *Textile composites and inflateable structures*, vol. 1, Dordrecht, Springer.

[107] R. N. Dent, Principles of pneumatic architecture, London: The Architectural Press, 1971.

[108] T. Herzog, Pneumatic structures: a handbook for the architect and engineer, Crosby Lockwood Staples, 1977.

[109] J. J. Kim, J. H. Jeong and J. Y. Sohn, "Sound absorption characteristics of PTFE membrane Material and their application to a multi-purpose stadium," *Building Services Engineering Research and Technology,* vol. 30, no. 3, pp. 213-226, 2009.

[110] G. H. McComb Jr, "A linear theory for inflatable plates of arbitrary shape," NASA, 1961.

[111] N. W. Larsen, E. R. Thompson and A. C. Gade, "Variable low-frequency absorber for multi purpose concert halls," in *Forum Acusticum*, Budapest, 2005.

[112] N. W. Adelman-Larsen, "Method, device and system for altering the reverberation time of a room.". USA Patent 7905323, 15th March 2011.

[113] N. W. Adelman-Larsen, "Method, device and system for altering the reverberation time of a room". Europe Patent EP 1 779 375 B1, 16th February 2006.

[114] N. W. Adelman-Larsen, "Method, device and system for altering the reverberation time of a room". Japan Patent JP 2008510408.

[115] N. W. Adelman-Larsen, E. R. Thompson and A. C. Gade, "The flexible bass absorber," in *122nd Conference of the Audio Engineering Society*, Vienna, 2007.

[116] W. Soedel, Vibrations of shells and plates, Third Edition ed., New York: Marcel Dekker, 2005.

[117] Flex Acoustics, "Flex Acoustics," [Online]. Available: http://flexac.com/. [Accessed 26th February 2019].

[118] A. D. Pierce, Acoustics An introduction to Its physical principles and applications, Third Edition ed., ASA Press/Springer Verlag, 2019.

[119] B. S. Massey, Mechanics of fluids, 3rd Edition ed., New York: Van Norstrand Reinhold, 1975.

[120] R. Bellet, "Vers une nouvelle technique de controle pasif du bruit: Absorbeur dynamique non lineare et pompage energetique," 2010.

[121] R. Rosenberg, "On nonlinear vibrationsof systems with many degrees of freedom," *Advances in Applied Mechanics,* 1966.

[122] A. F. Vakakis, "Non-similar normal oscillations in a strongly non-linear discrete system," *Journal of Sound and Vibration,* vol. 159, pp. 341-361, 1992.

[123] S. W. Shaw and C. Pierre, "Non-linear normal modes and invariant manifolds," *Journal of Sound and Vibration,* vol. 150, pp. 170-173, 1991.

[124] G. Kerschen, M. Peeters, J. C. Golinval and A. F. Vakakis, "Nonlinear normal modes, part 1: a useful framework for the structural dynamicist," *Mechanical Systems and Signal Processing,* vol. 23, no. 1, 2009.

[125] M. Peeters, R. Viguie, G. Serandour, G. Kerschen and J.-C. Golinval, "Nonlinear normal modes part II: toward a practical computation using numerical continuation techniques," *Mechanical Systems and Signal Processing,* vol. 23, pp. 195-216, 2009.

[126] A. H. Nayfeh and C.-M. Chin, "Nonlinear interactions in a parametrically excited system with widely spaced frequencies.," *Journal of Nonlinear Dynamics,* vol. 7, pp. 195-216, 1995.

[127] A. G. Haddow and S. M. Hasan, "Nonlinear oscillations of a flexible cantilever: experimental results," in *Proceedings of the Second Conference on Nonlinear Vibrations, Stability, and Dynamics of Structures and Mechanisms*, Blacksburg, VA, 1988.

[128] C. Hayashi, Nonlinear oscillations in physical systems, Princeton: Princeton University Press, 1985.

[129] N. E. Huang, Z. Shen, S. R. Long, M. C. Wu, H. H. Shih, Q. Zheng, N.-C. Yen, C. C. Tung and H. H. Liu, "The empirical mode decomposition and the Hilbert spectrum for nonlinear and non-stationary time series analysis," *Proceedings of the Royal Society of London A,* pp. 903-995, 1998.

[130] I. Daubechies, J. Lu and H.-T. Wu, "Synchrosqueezed wavelet transforms: An empirical mode decomposition-like tool," *Applied and Computational Harmonic Analysis,* vol. 30, pp. 243-261, 2011.

[131] O. V. Gendelman, "Transition of energy to a nonlinear localized mode in a highly asymmetric system of two oscillators," *Nonlinear Dynamics,* vol. 25, pp. 237-253, 2001.

[132] O. Gendelman, L. I. Manevitch, A. F. Vakakis and R. M'Closkey, "Energy pumping in nonlinear mechanical oscillators- Part I—Dynamics of the underlying hamiltonian systems," *Journal of Applied Mechanics,* vol. 68, no. 1, pp. 34-41, 2001.

[133] A. F. Vakakis and O. Gendelman, "Energy pumping in nonlinear mechanical oscillators: Part II—Resonance capture," *Journal of Applied Mechanics,* vol. 68, no. 1, pp. 42-48, January 2001.

[134] R. H. Rand and D. D. Quinn, "Resonant capture in a system of two coupled homoclinic oscillators," *Journal of Vibration and Control,* vol. 1, no. 1, pp. 41-56, 1995.

[135] G. Kerschen, Y. S. Lee, A. F. Vakakis, D. M. McFarland and L. A. Bergman, "Irreversible passive energy transfer in coupled oscillators with essential nonlinearity," *SIAM Journal of Applied Mathematics ,* vol. 66, no. 2, pp. 648-679, 6th January 2006.

[136] D. M. McFarland, L. A. Bergman and A. F. Vakakis, "Experimental study of non-linear energy pumping occurring at a single fast frequency," *International Journal of Non-Linear Mechanics,* vol. 40, pp. 891-899, 2005.

[137] B. Cochelin, P. Herzog and P.-O. Mattei, “Experimental evidence of energy pumping in acoustics,” *Comptes Rendus Mechanique,* vol. 334, September 2006.

[138] R. Bellet, B. Cochelin, P. Herzog and P.-O. Mattei, “Experimental study of targeted energy transferfrom an acoustic system to a nonlinear membrane absorber,” *Journal of Sound and Vibration,* vol. 329, pp. 2768-2791, 18th February 2010.

[139] R. Bellet, B. Cochelin, R. Cote and P.-O. Mattei, “Enhancing the dynamic range of targeted energy transfer in acoustics using several nonlinear membrane absorbers ,” *Journal of Sound and Vibration,* vol. 331, pp. 5657-5668, 2012.

[140] J. Shao and B. Cochelin, “Theoretical and numerical study of targeted energy transfer inside an acoustic cavity by a non-linear membrane absorber ,” *International Journal of Nonlinear Mechanics,* vol. 64, pp. 85-92, 2014.

[141] J. Shao and X. Wu, “Parameters design of a nonlinear membrane absorber applied to an acoustic cavity,” in *Inter-Noise 2014*, Melbourne, 2014.

[142] V. Iurasov, “Control pasif en vibroacousticqueavec aborbeur dynamique bistable,” 2018, 2018.

[143] BS 3382-1: 2009: Measurement of room acoustic parameters: part 1: performance spaces, British Standards Institute, London, 2009.

[144] F. Jacobsen, “The sound field in a reverberation room,” Technical University of Denmark.

[145] COMSOL Inc, “COMSOL,” COMSOL Inc, 2019. [Online]. Available: https://uk.comsol.com/. [Accessed 14th August 2019].

[146] COMSOL Inc, “Eigenmodes of a room,” 2020. [Online]. Available: https://www.comsol.com/model/eigenmodes-of-a-room-63. [Accessed 9th May 2020].

[147] S. Davidson, “Grasshopper; Algorithmic modelling for Rhino,” 2019. [Online]. Available: https://www.grasshopper3d.com/. [Accessed 14 August 2019].

[148] Robert McNeel & Associates, “Rhinoceros 3D,” Robert McNeel & Associates, 2019. [Online]. Available: https://www.rhino3d.com/. [Accessed 14th August 2019].

[149] F. P. Mechel, Formulas of acoustics, Berlin: Springer.

[150] University of Edinburgh, “University of Edinburgh Acoustics & Audio Group: Dr Brian Hamilton,” [Online]. Available: http://www.acoustics.ed.ac.uk/group-members/brian-hamilton/. [Accessed 16th April 2020].

[151] Roomerical, “Roomerical: Wave-based room acoustic simulation in the cloud.,” 2019. [Online]. Available: https://www.roomerical.com/. [Accessed 18th March 2020].

[152] Institute of Tecnical Acoustics, Aachen, “ITA Toolbox,” [Online]. Available: http://www.ita-toolbox.org/index.php. [Accessed 20th August 2019].

[153] H. Tahvanainen, A. Haapaniemi and T. Lokki, “Perceptual significance of seat-dip effect related direct sound coloration in concert halls,” *Journal of the Acoustical Society of America,* vol. 141, no. 3, pp. 1560-1570, 2017.

[154] A. Novak, P. Lotton and L. Simon, “Synchronized swept-sine: theory, application and implementation,” *Journal of the Audio Engineering Society,* vol. 63, no. 10, October 2015.

[155] P. H. Parkin and K. Morgan, “"Assisted resonance" in the Royal Festival Hall, London,” *Journal of Sound and Vibration,* vol. 2, no. 1, pp. 74-85, 1965.

[156] S. Dance, J. Bernays and S. Liu, “Singing and Loudness: A short study at the Royal Opera House,” in *Proc. Institute of Acoustics*, 2018.

[157] V. Välimäki, J. D. Parker, L. Savioja, J. O. Smith and J. S. Abel, “More than fifty years of artificial reverberation,” in *Audio Engineering Society*, Leuven, 2016.

[158] American Institute of Physics, “Leo Beranek: Interview by Jack Purcell,” 26th February 1989. [Online]. Available: https://www.aip.org/history-programs/niels-bohr-library/oral-histories/5191. [Accessed 6th April 2020].

[159] Standard Norge, “Lydklasser for bygningstyper: NS8175:2012,” 2012.

[160] Microflown Technologies, “FAQ: Impedance,” Microflown Technologies, 2010-12. [Online]. Available: http://www.microflown.com/support/faq/faq-impedance.html. [Accessed 21st January 2016].

[161] S. Dance, Interviewee, *In-situ absorption measurements in Henry Wood Hall in 2014.* [Interview]. 2020.

[162] J. Schira, “Enhancement of bass frequency absorption in fabric-based absorbers,” in *Auditorium Acoustics Hamburg 2018*, 2018.

[163] Arup Acoustics, “Acoustic Treatment of Henry Wood Hall,” 2009.

[164] S. Dance and S. Hassan, "Henry Wood Hall: An acoustic assessment of a proposed solution: Full width curtain," 2014.

[165] BS 37:2017; Rubber, vulcanised or thermoplastic - Determination of tensile stress-strain properties., British Standards Institute.

[166] J. L. Bolland, "Kinetic studies in the chemistry of rubber and related materials.," *Proceedings of the Royal Society,* vol. 186, 1946.

[167] G. Gryn'ova, J. L. Hodgson and M. L. Coote, "Revising the mechanism of polymer autooxidation," *Organic and Biomolecular Chemistry,* vol. 9, p. 480, 2011.

[168] BS 899-1: 2017; Plastics-Determination of creep behaviour: Part 1: Tensile creep, BSI, London, 2017.

[169] BMC Messsysteme GmbH, "Products: USB-AD16f," [Online]. Available: https://www.bmcm.de/external-daq-systems/usb-ad16f.html. [Accessed 19th April 2020].

[170] BMC Messsysteme GmbH, "Products: Nextview," [Online]. Available: https://www.bmcm.de/nextview-5-en.html. [Accessed 19th April 2020].

[171] Delimitware, "Delimit," [Online]. Available: http://delimitware.com/. [Accessed 19th April 2020].

[172] BS 60268-4: 2014: Sound system equipment: Part 4; microphones, British Standards Institute, 2014.

[173] Y. L. Raikher, O. V. Stolbov and G. V. Stepanov, "Shape instability of a magnetic elastomer membrane," *Journal of physics D: Applied Physics,* vol. 41, 2008.

[174] F. U. Khan and Izhar, "Electromagnetic energy harvester for harvesting acoustic energy," *Indian Academy of Sciences,* vol. 41, no. 4, 20 April 2016.

[175] B. Li, A. J. Laviage, H. Y. Jeong and Y.-J. Kim, "Harvesting low-frequency acoustic energy using multiple PVDF beam arrays in quarter-wavelength acoustic resonator," *Applied Acoustics,* vol. 74, 2013.

[176] E. Ballestero, N. Jiménez, J.-P. Groby, S. Dance, H. Aygun and V. Romero-Garcia, "Experimental validation of deepsubwavelength diffusion by acoustic metadiffusers," *Applied Physics Letters,* vol. 115, p. 081901, 2019.

[177] C. Higgins, "An investigation into the helmholtz resonators of the Queen Elizabeth Hall, London," 2014.

[178] N. W. Adelman-Larsen, Rock and Pop Venues, Berlin: Springer.

[179] M. Vorländer, Auralisation: fundamentals of acoustics, modelling, simulation, algorithms and acoustic virtual reality, Berlin: Springer, 2008.

[180] M. Skouras, B. Thomaszewski, P. Kaufmann, A. Garg, B. Bickel, E. Grinspun and M. Gross, "Designing inflatable structures," 10 August 2014. [Online]. Available: https://la.disneyresearch.com/publication/designing-inflatable-structures/. [Accessed 3 May 2020].

[181] P.-O. Mattei, *Private correspondance,* 2019.

[182] J. Luo, "Numerical differentiation based on wavelet transforms," 14 Feb 2007. [Online]. Available: https://uk.mathworks.com/matlabcentral/fileexchange/13948-numerical-differentiation-based-on-wavelet-transforms. [Accessed 9 Feb 2018].

[183] J. C. Lansey, "Beautiful and distinguishable line colors + colormap," 16 Sept 2015. [Online]. Available: https://uk.mathworks.com/matlabcentral/fileexchange/42673-beautiful-and-distinguishable-line-colors-colormap. [Accessed 1 Apr 2018].

9 Appendix

9.1 T_{20} Presented Spatially for Recital Hall FDTD Model Result

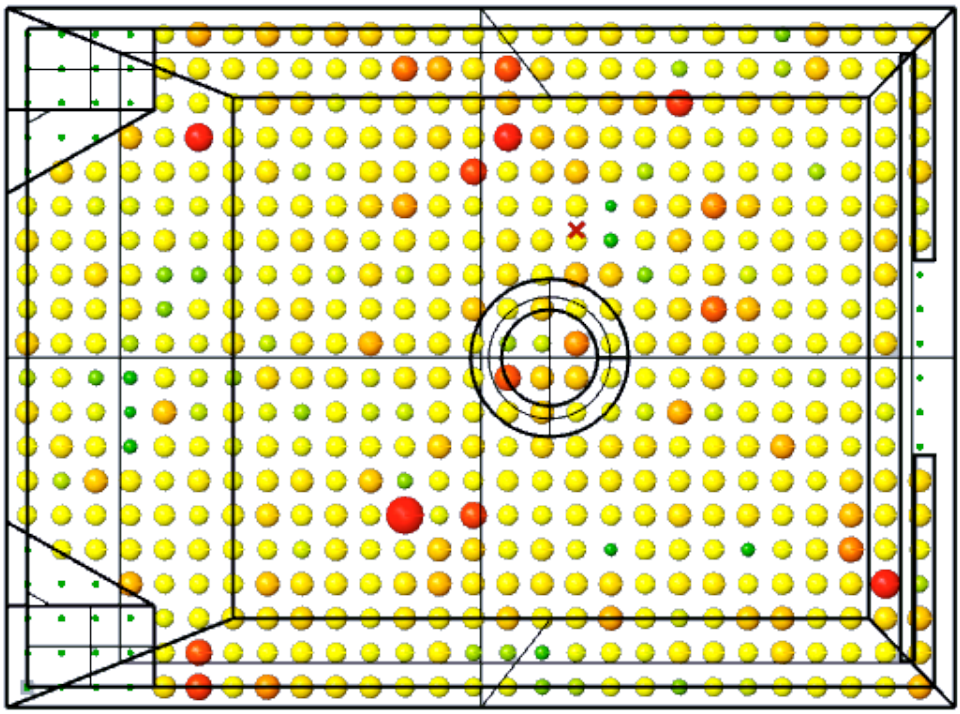

Figure 102: T_{20} FDTD model results at 125Hz throughout the recital hall with cavity wall. T_{20} indicated both by colour (green to red) and by size of sphere at receiver

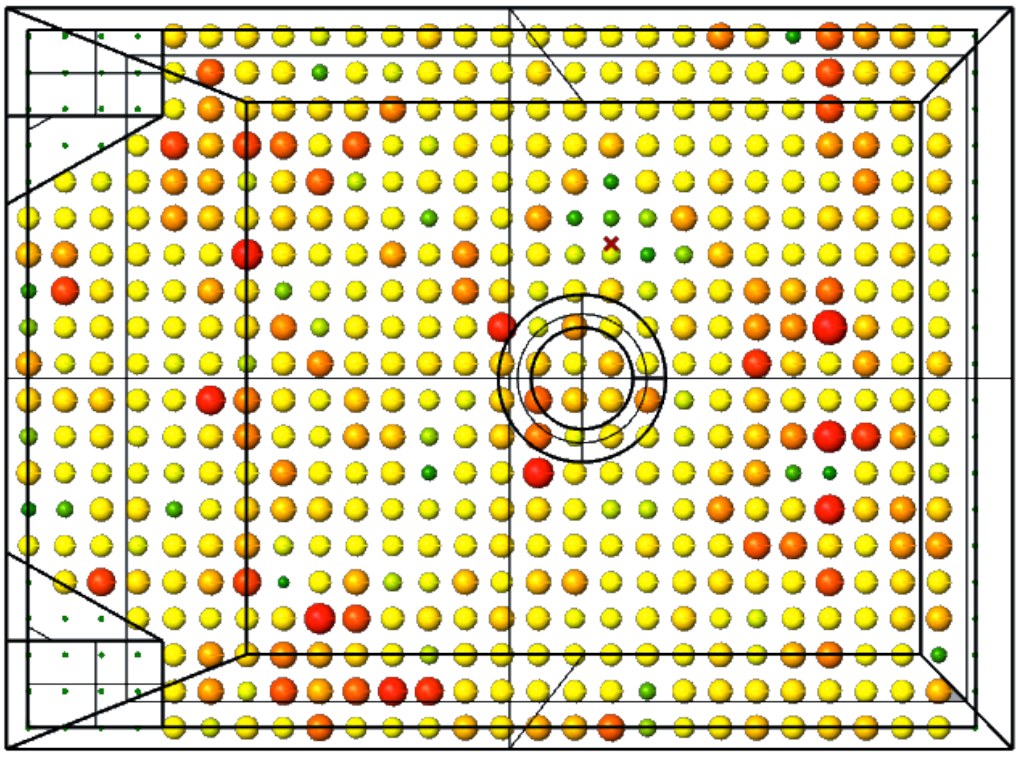

Figure 103: T_{20} FDTD model results at 125Hz throughout the recital hall with plain back wall. T_{20} indicated both by colour (green to red) and by size of sphere at receiver

9.2 Code for Analysing Performance Room Measurements Using ITA Toolbox

ReadRIR_ITA.m: This is a launch code which imports room impulse response data from .mat file formats and outputs result matrices in octave and 1/3 octave bands, calling on functions within the ITA Toolbox developed by Aachen Technical University [152]. Near identical codes were created for reading data from .WAV files.

```
%% CLEAR A SPACE FOR YOUR WORK
clear
clc

% SET SCALE FACTOR
scale=1;

%% SELECT THE IMPULSES YOU WANT TO LOOK AT
% THEN PUTTING THE IMPULSE DATA INTO A MATRIX CALLED T
[filenames, pathname, filterindex] = uigetfile( '*.mat', 'MAT-files (*.mat)', 'Pick
a file', 'MultiSelect', 'on');
for R=1:length (filenames)
    thisfullname = fullfile(pathname, filenames{R});
    load(thisfullname,'H','fs','f1','f2')  % TAKE IR, SAMP RATE, HI AND LOW FREQ
FROM FILE
    T(:,:,R) = H;
    Fs = fs;
    % APPLY SCALING FACTOR
    Fs=Fs/scale;
    f1_sc=f1/scale;
    f2_sc=f2/scale;
    clear H SR
end

clear S R

%% Creating ITA Audio Object and importing RIR data into it
for  count=1:length (filenames)  % RECIEVER NUMBER
       IR = T(:,count);
       RIR1 = itaAudio;
       RIR1.samplingRate = Fs(:,1);
       RIR1.time = IR;

       RIR_extract = ita_extract_dat(RIR1);
       PAR = ita_roomacoustics_parameters('getAvailableParameters');
       RES = ita_roomacoustics(RIR_extract,'freqRange',[f1_sc
       f2_sc],'T20','EDT','EDC','C80','D50','PSNR_Lundeby','PSPNR_Lundeby','Interse
       ction_Time_Lundeby','T_Lundeby');

       % PUT THE RESULT IN MATRICES WHICH COMPILE ALL MEASUREMENTS TOGETHER
       rezF(:)=RES.EDT.freqVector;
       rezE(count,:)=RES.EDT.freqData;

       rezT(count,:)=RES.T20.freqData;
       rezTL(count ,:)=RES.T_Lundeby.freqData;% THIS IS THE RT YOU ARE LOOKING FOR
end

%% THESE ARE THE AVERAGES YOU ARE LOOKING FOR
rezTL_Av=mean(rezTL,1);
rezE_Av=mean(rezE,1);
```

```
% MAKE A NEW AVERAGE RESULT STRUCTURE FOR THE AVERAGE RESULTS
RES_Av = ita_roomacoustics(RIR_extract,'freqRange',[f1_sc
f2_sc],'T20','EDT','EDC','C80','D50','PSNR_Lundeby','PSPNR_Lundeby','Intersection_T
ime_Lundeby','T_Lundeby');
RES_Av.T_Lundeby.freqData = rezTL_Av';
RES_Av.T_Lundeby.freq = rezTL_Av';
RES_Av.T_Lundeby.bar;

RES_Av.EDT.freqData = rezE_Av';
RES_Av.EDT.freq = rezE_Av';
RES_Av.EDT.bar;
```

9.3 Codes for Calculation of Quarter Wave Resonator impedance

QWRLaunch.m. This code launches the impedance calculation, calling on the later two functions QWR.m (which is the main quarter wave calculation) and zCombo.m (which combines the two parallel impedances in the width and height directions.

```
% LAUNCHES QWR CALCULATIONS USING FUNCTIONS
% QWR.m and zCombo.m

% FREQ RANGE
f1=20;
f2=1000;
freq=linspace(f1,f2,100000);

% CAVITY X DIRECTION
depthX=3;
widthX=0.26;
heightX=4;
roomSizeX=6.35;

% CAVITY Z DIRECTION
depthZ=4;
widthZ=0.26;
heightZ=3;
roomSizeZ=4.3;

% X DIRECTION
% PARAMS (f1,f2,length,cavWidth, roomWidth,cavHeight)
xx=QWT(f1,f2,depthX,widthX,roomSizeX,heightZ);

% DOUBLE FOR 2x CAVITIES
xxxx=xx.*2;

% Z DIRECTION
zz=QWT(f1,f2,4,0.26,6,3);

% DOUBLE FOR 2x CAVITIES
zzzz=zz.*2

% COMBINE AXES IN PARALLEL
% PARAMS (Z1,Z2,freq)
dddd=zCombo(xxxx,zzzz,freq)
% NORMALISE TO IMP OF AIR
rho=1.204;       % DENSITY AIR
c0=343.15;
Zair=rho*c0;
ddddNorm=dddd-Zair;
```

```
% PLOT
plot(freq,xxxx)
hold on
plot(freq, zzzz)
grid on
xlabel('Frequency(Hz)')
ylabel('Impedance(Pa s m-1)')
set(gca,'FontSize',14)
set(gca,'FontName','Century Schoolbook')
hold off

figure
plot(freq,ddddNorm)
grid on
xlabel('Frequency(Hz)')
ylabel('Normalised Impedance (z/z0)')
set(gca,'FontSize',14)
set(gca,'FontName','Century Schoolbook')
```

QWT.m

This function calculates the impedance of a quarter wave resonator.

```
function Zqwt=QWT(f1,f2,length,apGap,roomDim,apHeight)
%
%
% CALCULATES IMPEDANCE OF QWT
% FROM BIES & HANSEN CH8
% f1-f2 IS FREQ RANGE OF INTEREST
% Length IS LENGTH OF CAVITY
% apGap IS WIDTH OF CAVITY
% roomDim IS WIDTH OF ROOM
% apHeight IS HEIGHT OF CAVITY

% IMPEDANCE OF QWT
% RESISTANCE
% RANGE OF INTEREST
freq=linspace(f1,f2,100000)';
omeg=freq.*(2*pi);
c0=343.15;
k=omeg./c0;

% QWT STUFF
% length=3;    % PHYSICAL LENGTH
% smallDim=0.205;    % APERTUDE WIDTH
% largeDim= 9.5  ;      % room dimension
betaa=apGap/roomDim;
S=apHeight*apGap;
P=(apHeight*2)+(apGap*2);  % X-SECT PERIMETER
eRAD=0.106;       % EDGE RADIUS h IN BIES HANSE Eq 8-33
eps=0.5;         % RADIATION CONST - INTO FREE SPACE UNFLANGED

% SOME VARIABLES
rho=1.204;       % DENSITY AIR
squig=1.4;     % RATIO OF SPECIFIC HEATS
mu=18.25e-6;    % DYNAMIC VISCOSITY AIR
tBL=sqrt((2*mu)./(rho.*omeg));
M=0;            % MACH NUMBER OF FLOW

% BIG RESISTANCE EQUATION
rMult=(rho*c0)/S;
rMult2=(k.*tBL*P*length)./(2*S);
rT1a=rMult2;
```

```
rT1b=rMult2*(squig-1)*(sqrt(5/(3*squig)));
rT2=(0.288.*k.*tBL).*(log10((4*S/pi*eRAD^2)));
rT3=eps.*((S.*k)/(2*pi));
rT4=0.7*M;
Rqwt=rMult.*(rT1a+rT1b++rT2+rT3+rT4);

% END CORRECTION
deltal=(apGap/pi)*(1-log(4*betaa));
leff=length+deltal;

% IMPEDANCE EQN
zMult1=(-1i*rho*c0)/S;
zMult2=(k.*leff.*(1-M));
Zqwt=abs((zMult1*cot(zMult2))+Rqwt);

end
```

zCombo.m

```
function Ztot=zCombo(Z1,Z2,freq)

Znum=Z1+Z2;
Zden=Z1.*Z2;
Ztot=Znum./Zden;

plot(freq, abs(Ztot))

end
```

9.4 MATLAB Codes for analysis of TET test rig results

9.4.1 Creation of Test Tone Sequence for TET Rig Tests

9.4.1.1 TestTonePulse.m

This script creates bespoke .wav file of required number of ascending tones starting and ending at frequencies set by the user. Other parameters include sample rate, pulse duration, inter-pulse gap duration and amplitude.

```
% SCRIPT TO MAKE SINE PULSE TEST RUN FILE
% FORMAT IS PULSE ON (DURATION) AND OFF (GAP DURATION)

plopAmp=1;    % Set plop amplitude
plopF=1000;     % Set plop frequency

% SET DEFAULT VALUES
pulDef={'48000','3','2','72','90','0.5','1'};

% DIALOGUE BOX ASKS FOR SETTINGS
prompt={'Sample rate (samples/sec)','Pulse Duration (s)','Gap Duration (s)','Lowest
Frequency (Hz)','Highest Frequency (Hz)','Frequency Increment(Hz)','Amplitude'};
dlgtitle='Settings';
num_lines=1;
answerset=inputdlg(prompt,dlgtitle,num_lines,pulDef);

% MAKE INPUTS INTO VARIABLES
Fs=str2double(answerset{1});
pulT=str2double(answerset{2});
pulGap=str2double(answerset{3});
freqLo=str2double(answerset{4});
freqHi=str2double(answerset{5});
freqInc=str2double(answerset{6});
ampPul=str2double(answerset{7});

% DERIVED VARIABLES
Ts=1/Fs;
if freqInc>=1
     numPuls=round((freqHi-freqLo+1)/freqInc);

elseif freqInc<1
     numPuls=round((freqHi-freqLo+1)/freqInc)-((1/freqInc)-1);

end

% MAKE MATRIX TO BASE SIN WAVE ON
pulMat=0:Ts:pulT;
pulZeros=0:Ts:pulGap;

% MAKE FADEIN/OUT ENVELOPE.
numCyc=3;        % Number of cycles in fade in/out
fadeTi=numCyc/freqLo;
fIn=linspace(0,1,(fadeTi*Fs));
% fIn=(0:1/(abs(fadeTi*Fs)):1);
% fIn(abs(fadeTi*Fs))=[];
fOut=fliplr(fIn);

% LOOP
% freqN=1;
freqCnt=freqLo;
pulsOut=zeros(1,Fs);
```

```
for  freqN=1:numPuls

    % SINEWAVE
    sinPul = ( ampPul * sin(2 * pi * freqCnt * pulMat));

    % APPLY FADE IN/OUT
    bodWin=ones(1,(length(sinPul)-round((2*fadeTi*Fs))));
    winPul=[fIn bodWin fOut];
    sinPul = sinPul.*winPul;

    % ADD SILENCE AFTER
    sinPul=[sinPul (0 * sin(2 * pi * freqCnt * pulZeros))];

    % ADD TO OUTPUT MATRIX
    pulsOut=[pulsOut sinPul];

    % COUNT STUFF
    freqN=freqN+1;
    freqCnt=freqCnt+freqInc;

end

% ADD SYNC PLOP OF 1/24s STARTING 2s BEFORE FIRST MOD
plopT=Fs/24;
plopDat=0:Ts:plopT/Fs;
plop = (plopAmp * sin(2 * pi * plopF .* plopDat));

% SILENCE AFTER PLOP
plopSil=zeros(1,2*Fs);

% BIT OF SILENCE AT START
plopIntro=zeros(1,0.1*Fs);

% ADJUST SO PLOP + SILENCE = 2s
ploL=length(plop);
ploSilL=length(plopSil);
plopSil((ploSilL-ploL):(ploL))=[];

% PUT IT ALL TOGETHER
plop=[plopIntro plop plopSil];
pulsOut=[plop pulsOut];

% OUTPUT FILE
[file,path] = uiputfile('*.wav','Save file');
audiowrite([path file], pulsOut,Fs);

% GRAPH IT!
plot(pulsOut)
grid on
xlabel('Time (samples)')
ylabel('Amplitude')
set(gca,'FontSize',14)
set(gca,'FontName','Century Schoolbook')
set(gcf, 'color', 'w')


% CLEAR UP VARIABLES
clear freqN freqCnt lamLo lamHi pulMat pulZeros ampPul winPul plop...
plopSil plopIntro plopDat plopT plopAmp bodWin numCyc num_lines plopF ...
Ts Fs numPuls prompt sinPul
```

9.4.2 Data Import Codes for TET Rig Measurements.

9.4.2.1 Settings.m

Applies basic settings for import and analysis of data, including sample rate, format of the test tone sequence used.

```
% THIS SCRIPT INITIALISES THE WORKSPACE READY FOR MEASUREMENTS
% INPUT IS SAMPLE RATE AND TEST RUN FORMAT
clear
% Defaults
defSet={'4000','3','2','1.9','61','70','100','0.5','3'};

% Make dialogue box asking for settings
prompt={'Sample rate (samples/sec)','Pulse Duration (s)','Gap Duration (s)'...
    ,'Decay Duration (s)','Number of Pulses in Test','Lowest Frequency (Hz)',...
    'Highest Frequency (Hz)','Frequency Increment(Hz)','Plop Leadin(s)'};
dlgtitle='Settings';
num_lines=1;
answerset=inputdlg(prompt,dlgtitle,num_lines,defSet);

% Take inputs and save as variables
Fs=str2num(answerset{1});
impT=str2num(answerset{2});
impGap=str2num(answerset{3});
impDec=str2num(answerset{4});
Runs=str2num(answerset{5});
loFreq=str2num(answerset{6});
hiFreq=str2num(answerset{7});
incFreq=str2num(answerset{8});
plopLI=str2num(answerset{9});
fudgeFactor=15;       % FUDGE FACTOR TO ADD TO TOTAL TEST TIME JUST TO BE SAFE
freqRng=(loFreq:incFreq:hiFreq);
totTestDur=(((hiFreq-loFreq)*(impT+impGap)/incFreq)+plopLI+fudgeFactor)*Fs;

% STARTS AND END FOR DECAYS
[starts, steddys]=RangesF(impT,impGap,Runs,plopLI);

% CREATE MATRIX FOR SYNCHED RESULTS
noCSV = dir([pwd, '/*.csv']);
csvSize=size(noCSV);
setts=csvSize(1);
rezRaw=zeros(totTestDur,5,setts);
% rawRez=zeros(  ((((impT+impGap).*Runs)+3+5).*Fs),4,length(noCSV));
```

9.4.2.2 ImpPcsv.m

This script imports raw data from .csv files, calls the calibration script Cal.m to apply calibration and signal conditioning and, in conjunction with Summ.m and Cutout.m, places raw calibrated data in a result matrix.

```
% THIS SCRIPT IMPORTS THE RAW MEASUREMENT DATA FROM FREQ-STEPPING PULSE
% TESTS (IN CSV FORM) THIS IS THE FIRST STEP TO ANALYSIS:
% IT IMPORTS TIME, PRESSURE, AMP VOLTAGE AND MEMBRANE DISPLACEMENT
% DATA, APPLIES CALIBRATION ADJUSTMENTS AND PRESENTS A GENERIC SET
% OF PLOTS. DATA IS SAVED FOR FURTHER ANALYSIS
% EXTERNAL FUNCTIONS REQUIRED ARE...

%       Cal.m (Calibration of results and filtering,
%       impl.m (Imports .csv),
%       plo.m (Plotting),
```

```
%       Ranges.m (Works out segments to cut out),
%       Snips.m (cuts out)


% SELECT REQUIRED DATA
filename=uigetfile('.csv','CSV-files (*.csv)', 'Multiselect','on');
startRow=4;
endRow=inf;

% READ FILE
% load filename
rez=impl(filename, startRow, endRow);

% SOME PARAMETERS
T=1/Fs;
L=length(rez);
t=rez(:,1);
p=rez(:,2);
a=rez(:,3);
m=rez(:,4);

% CALIBRATE!
[rezcal]=Cal(t,p,a,m,Fs);
% pdB= sqrt (mean (p .^2) );
% pdB=real(20*(log10(p/0.00002)));
% plopID=a(1:Fs*6);

% ADD MEMBRANE VELOCITY TO REZCAL
rezcal(:,5)=dsdx(rezcal(:,4),'spl',2,1,1);
biggy=size(rezcal);
channs=biggy(2);

% GET plo.m TO PLOT
plo(rezcal)
```

9.4.2.3 Cal.m

This script applies calibration and signal conditioning to the raw data prior to analysis.

```
function [rezcal] = Cal(t,p,a,m,Fs)

% APPLIES CALIBRATION AND FILTERING TO RAW DATA

% PRESSURE DATA
p=46.*p;      % 24 for 30Ohm , 46 for 15Ohm %
[HPb, HPa]=butter(5,0.0031,'high');
p=FiltFiltM(HPb,HPa,p,1);

% MEMBRANE FILTER AND CALIBRATION
[HPb, HPa]=butter(5,0.00314,'high');
% freqz(HPb,HPa);
[LPb, LPa]=butter(5,0.2,'low');

m=FiltFiltM(HPb,HPa,m,1) ;
m=FiltFiltM(LPb,LPa,m,1) ;

m=m/163.2;   % Membrane: zero offset, cal and filter
m=m*1000;

% AMP SIGNAL FILTER
[LPb2, LPa2]=butter(5,0.1,'low');
a=FiltFiltM (LPb2,LPa2,a,1) ;
[HP2b, HP2a]=butter(4,0.01,'high');
a=FiltFiltM (HP2b,HP2a,a,1);

% ENTER INTO A NEW TABLE AND OUTPUT
```

```
rezcal=[t,p,a,m];

%   take out the trash
clear freqP freqS LfreqP LfreqS LFPn LFSn FSn FPn LfreqPee LfreqSee LFSnee LFPnee

end
```

9.4.2.4 impl.m

Contains format information for retrieving data from raw result .csv files. This was auto-generated in MATLAB's File import function.

```
function R31 = importfile(filename, startRow, endRow)
%IMPORTFILE Import numeric data from a text file as a matrix.
%   R31 = IMPORTFILE(FILENAME) Reads data from text file FILENAME for the
%   default selection.
%
%   R31 = IMPORTFILE(FILENAME, STARTROW, ENDROW) Reads data from rows
%   STARTROW through ENDROW of text file FILENAME.
%
% Example:
%   R31 = importfile('191217R3-1.csv', 2, 800001);
%
%    See also TEXTSCAN.

% Auto-generated by MATLAB on 2018/03/12 15:17:15

%% Initialize variables.
delimiter = ';';
if nargin<=2
    startRow = 2;
    endRow = inf;
end

%% Format for each line of text:
%   column1: double (%f)
%   column2: double (%f)
%   column3: double (%f)
%   column4: double (%f)
% For more information, see the TEXTSCAN documentation.
formatSpec = '%f%f%f%f%[^\n\r]';

%% Open the text file.
fileID = fopen(filename,'r');

%% Read columns of data according to the format.
% This call is based on the structure of the file used to generate this
% code. If an error occurs for a different file, try regenerating the code
% from the Import Tool.
dataArray = textscan(fileID, formatSpec, endRow(1)-startRow(1)+1,...
    'Delimiter', delimiter, 'TextType', 'string', 'EmptyValue', ...
    NaN, 'HeaderLines', startRow(1)-1, 'ReturnOnError', false, ...
    'EndOfLine', '\r\n');
for block=2:length(startRow)
    frewind(fileID);
    dataArrayBlock = textscan(fileID, formatSpec, endRow(block)-startRow(block)+1,
'Delimiter', delimiter, 'TextType', 'string', 'EmptyValue', NaN, 'HeaderLines',
startRow(block)-1, 'ReturnOnError', false, 'EndOfLine', '\r\n');
    for col=1:length(dataArray)
        dataArray{col} = [dataArray{col};dataArrayBlock{col}];
    end
end
```

```
%% Close the text file.
fclose(fileID);

%% Post processing for unimportable data.
% No unimportable data rules were applied during the import, so no post
% processing code is included. To generate code which works for
% unimportable data, select unimportable cells in a file and regenerate the
% script.

%% Create output variable
R31 = [dataArray{1:end-1}];
```

9.4.2.5 dsdx.m

This script reformats data for the dx_dwt function by Jianwen Luo. This is a toolbox for wavelet-based differentiation of continuous data. [182] This is used to calculate membrane velocity from measured displacement.

```
function oot=dsdx(u,wTyp,lev,dx,flaag)
% THIS FUNCITON FLIPS INPUT TO dx_dwt
%
% OTHERWISE OPERATION IS LIKE dx_dwt SO INPUTS ARE
%
%   oot=differential of input
%   u=DATA IN, AS COLUMN VECTOR
%   wTyp - WAVELET TYPE ('haar' or 'spl')
%   lev - SMOOTHING LEVEL (1-10)
%   dx - SAMPLING INTERVAL (DEFAULT=1)
%   flaag - TRANSLATION/ROTATION, DEFAULT 1
%

u=u';
oot=dx_dwt(u,wTyp,lev,dx,flaag);
oot=oot';
end
```

9.4.2.6 plo.m

This function takes input from ImpPcsv.m and plots a time series plot for the data in two subplots, one for pressure data, one for membrane velocity. This script uses linspecer.m, a script which creates a distinguishable palette of colours for plots which are separated in perceptual space rather than RGB space, resulting in more pleasing and viewable plots. It is © Jonathan C Lansey 2015. [183]

```
function plo(rezcal)

% THIS FUNCTION TAKES VALUES FROM ImpPcsv.m AND PRESENTS A
% QUALITATIVE PLOT OF THE DATA. DATA IS SCALED TO APPEAR ON
% THE SAME GRAPH VISBLY SO MAGNITUDE MEASUREMENTS SHOULD NOT BE TAKEN
% VISUALLY FROM THE GRAPHS

% COLOURS
colormap(linspecer);
plocol = linspecer(4);
```

```
%make variables from table
t=rezcal(:,1);
p=rezcal(:,2);
a=rezcal(:,3);
m=rezcal(:,4);
% mv=rezcal(:,5);

%scale for graph
sm=m*4;
sp=p*0.1;
sa=a*10;
% smv=mv*400;

%basic plot of pressure & membrane velocity with input
% figure
ax(1)=subplot(2,1,1);
plot(t,sa,'color',plocol(3,:));
title('Raw test results: Pressure')
xlabel('Test Time (s)')
grid on
hold on
plot(t,sp,'color',plocol(1,:));
grid on
title('Input vs Pressure')
hold off
ax(2)=subplot(2,1,2);
title('Raw test results: Membrane Displacement')
xlabel('Test Time (s)')
plot(t,sa,'color',plocol(3,:));
grid on
hold on
% plot(t,smv,'r');
plot(t,sm,'color',plocol(2,:));
grid on
hold on
% plot(t,smv);
title('Input vs Membrane')
linkaxes([ax(1),ax(2)],'xy');

hold off

% TAKE OUT THE TRASH
clear sp sm sa smv
```

9.4.2.7 Cutout.m

When a set of measurements are imported using ImpPcsv.m, the resulting data is inpected visually for the first modulated sample value. This will be the start of the 1000Hz sync pulse at the start. This sample value is entered into Cutout.m which then removes the data before this point. Using this reference start point, which is the same for all runs, decay and steady state response data for each frequency is extracted and stored in a results matrix named rezRaw.

```
% THIS SCRIPT ASKS FOR INPUT OF THE FIRST MODULATED
% SAMPLE (SYNC PULSE) AND TAKES THIS AND THE DURATION OF PULSE SILENCE
% AND DECAY TO DECIDE WHERE TO CUT OUT DECAYS.
% RESULTING DECAYS ARE STORED IN A TABLE

prompt={'Time of first modulation (s)'};
```

```
dlgtitle='First Mod';
num_lines=1;
answerset=inputdlg(prompt,dlgtitle,num_lines);
mod1=str2double(answerset{1});
mod1FS=mod1*Fs

% if moddy=1
% defV=mod1
% end

thisRezRaw=rezcal((round(mod1FS)):end,:);
```

9.4.2.8 Summ.m

This script calculates the total energy in each decay and stores it in a large result matrix rezRaw.mat.

```
% SUMM
% CALCULATES THE TOTAL ENERGY IN A DECAY AND SAVES TO TABLE FOR COLLATING
prompt={'Which Run is This Again?'};
dlgtitle='Forgetful';
num_lines=1;
answerset=inputdlg(prompt,dlgtitle,num_lines);
thisSett=str2double(answerset{1});

thisSize=size(thisRezRaw);
thisSizeLen=thisSize(1);

% VARIABLES
cnt=1;
cnt2=1;

% CALC POWERS AND ADD TO MATRIX
while cnt<=Runs

    % ADD RAW DATA TO 3D MATRIX TO SAVE FOR LATER
    rezRaw((1:thisSizeLen),:,thisSett)=thisRezRaw;
    cnt = cnt+1;

end


%% COMPUTES THE RMS VOLTAGE FOR EACH RUN FOR REFERENCE
Araw=rezRaw(:,3,thisSett);
Astarts=starts-2.9;
AstartsSam=(Astarts.*Fs);
StartsSamps=(starts.*Fs)-100;
for N=1:Runs
    A_N(:,N)=Araw(AstartsSam(N):StartsSamps(N));
    A_Nrms(N)=rms(A_N(:,N));
    A_Nrms=A_Nrms';
end

aveRMS(thisSett)=mean(A_Nrms);
aveRMS=aveRMS';


% PRINT HELPFUL MESSAGES
filename
thisSett
fprintf('Remember to Save the Five Output Matrices at the End!!!!')
```

9.4.3 Analysis Scripts

9.4.3.1 RangesF.m

This script takes the start point of each frequency run and defines start and end points of steady state and free response decays for analysis and plotting.

```
function [Dst, Sst]=RangesF(impT,impGap,Runs,plopLI)

% FUNCTION TO READ STARTPOINT OF DATA IN TEST RUN
% THEN ADD TIMES TO THIS TO DEFINE RANGES

% INITIALISATION
count=1;
N=Runs+1;
Dst=zeros(N,1);
% Ren=zeros(N,1);

% LOOP TO GENERATE INDEXES
 for count=1:N

    % GET DECAY STARTS
    Dst(count,1)=plopLI+(impT*count)+(impGap*(count-1));

    % GET STEADY STATES
    Sst(count,1)=Dst(count,1)-1;
    % THIS LATTER NUMBER IS THE STEADY STATE DURATION
    % IN SECONDS BEFORE DECAY

end
```

9.4.3.2 dsNLFR.m

This script calls on RangesF.m to define start and end of decays for plotting, then plots them in a Nonlinear Frequency Response plot for pressure (top) and membrane velocity (bottom). This script also uses linspecer.m by Jonathan C Lansey [183].

```
% % GET RANGES
[starts, steddys]=RangesF(impT,impGap,Runs,plopLI);

% STARTS
stsec=starts/Fs;
sssec=steddys/Fs;
startsamps=starts.*Fs;

% DIMENSIONS OF RESULTS DATA
ipSize=size(rezRaw);
rezSetts=ipSize(3);
rezChanns=ipSize(2);
rezLeng=ipSize(1);

% CUT OUT DECAYS FROM 1 SET
[allDecs]=getDecs(rezRaw,Runs,impDec,startsamps,Fs);
adSize=size(allDecs);
bum=adSize(1);
Sqa=zeros(bum,Runs,rezChanns,rezSetts);
allDecsPow=zeros(1,Runs,rezChanns,rezSetts);

for S=1:rezSetts
    for C=1:rezChanns
        for D=1:Runs
```

```
            Sqa(:,D,C,S)=allDecs(:,D,C,S).^2;
            allDecsPow(1,D,C,S)=sum(Sqa(:,D,C,S));

        end
    end
end

NLFRplotP=zeros(Runs,rezSetts);
NLFRplotMV=zeros(Runs,rezSetts);

for P=1:rezSetts
    for Z=1:Runs
    NLFRplotP(Z,P)=allDecsPow(1,Z,2,P);
    NLFRplotMV(Z,P)=allDecsPow(1,Z,5,P);
    NLFRplotM(Z,P)=allDecsPow(1,Z,4,P);
    end
end

NLFRplotProot=sqrt(NLFRplotP)./impDec; % RETURNS P TO
%                                      PRESSURE PER SECOND

% COLOUR
colormap(linspecer);
NLFRcol = linspecer(4);

% PLOT!
subplot(2,1,1);
plot(freqRng,NLFRplotProot,'color',NLFRcol(1,:))
grid on
title('Pressure')
xlabel('Frequency (Hz)')
ylabel('Energy')

% MEMBRANE VELOCITY
subplot(2,1,2)
plot(freqRng,NLFRplotMV,'color',NLFRcol(2,:))
grid on
title('Membrane Velocity')
xlabel('Frequency (Hz)')
ylabel('Energy')

% GETTING READY FOR SAVING NLFR MATRIX
N1=size(NLFRplotP);
N11=N1(1);
N22=N1(2);

% SAVING NLFR MATRIX
NLFRout=zeros(N11, N22, 3);
NLFRout(:,:,1)=[NLFRplotP];
NLFRout(:,:,2)=[NLFRplotM];
NLFRout(:,:,3)=[NLFRplotMV];
fprintf  ('Remember to Save the NLFR Matrix "NLFRout"')

clear N1 N11 N12 NLFRplotP NLFRplotM NLFRplotMV S C D P
```

ds3DFR.m

This script creates a 3D surface plot for the nonlinear response of pressure decays. This script also uses linspecer.m by Jonathan C Lansey [183].

```
% MAKES 3D PLOT OF NLFR
% FOR P, M and A

% % GET RANGES
```

```
[starts, steddys]=RangesF(impT,impGap,Runs,plopLI);

% STARTS
startsamps=starts.*Fs;
steddysamps=steddys.*Fs;

% DIMENSIONS OF RESULTS DATA
ipSize=size(rezRaw);
rezSetts=ipSize(3);
rezChanns=ipSize(2);
rezLeng=ipSize(1);

% MAGNITUDE OF INPUT
rmsIns=zeros(rezSetts,1);

% CUT OUT DECAYS FROM 1 SET
[allDecs]=getDecs(rezRaw,Runs,impDec,startsamps,Fs);
adSize=size(allDecs);
bum=adSize(1);
Sqa=zeros(bum,Runs,rezChanns,rezSetts);
allDecsPow=zeros(1,Runs,rezChanns,rezSetts);

% CUT OUT INPUTS FOR REFERENCE
% DO THIS LATER

for S=1:rezSetts
    for C=1:rezChanns
        for D=1:Runs
            Sqa(:,D,C,S)=allDecs(:,D,C,S).^2;
            allDecsPow(1,D,C,S)=sum(Sqa(:,D,C,S));

        end
    end
end

% INITILISE MATRICES
NLFRplotP=zeros(Runs,rezSetts);
NLFRplotMV=zeros(Runs,rezSetts);
NLFRplotM=zeros(Runs,rezSetts);
NLFRplotA=zeros(Runs,rezSetts);

for P=1:rezSetts
    for Z=1:Runs
    NLFRplotP(Z,P)=allDecsPow(1,Z,2,P);
    NLFRplotMV(Z,P)=allDecsPow(1,Z,5,P);
    NLFRplotM(Z,P)=allDecsPow(1,Z,4,P);
    NLFRplotA(Z,P)=allDecsPow(1,Z,3,P);
    end
end


NLFRplotPdB=10.*log10(NLFRplotP./0.000020); % RETURNS P TO
%                                       dBs

% COLOUR
colormap(linspecer);
NLFRcol = linspecer(4);

% PLOT
surfl(NLFRplotPdB)
% figure
% surfl(NLFRplotMV)
% hold on
% surfl(NLFRplotM)
% figure
% surfl(NLFRplotA)

% GETTING READY FOR SAVING NLFR MATRIX
```

```
N1=size(NLFRplotP);
N11=N1(1);
N22=N1(2);

% SAVING NLFR MATRIX
NLFRout=zeros(N11, N22, 3);
NLFRout(:,:,1)=(NLFRplotP);
NLFRout(:,:,2)=(NLFRplotM);
NLFRout(:,:,3)=(NLFRplotMV);
fprintf  ('Remember to Save the NLFR Matrix "NLFRout"')

clear N1 N11 N12 NLFRplotP NLFRplotM NLFRplotMV S C D P Z
```